A study on non-canonical autophagy signalling

Cansu Karabiyik

UNIVERSITY OF CAMBRIDGE

Pembroke College

February 2021

This thesis is submitted for the degree of Doctor of Philosophy

Dedicated to

my parents Hatice & Raif Karabiyik

and

grandmothers Fatma Yildirim & Esma Karabiyik

Preface

This thesis is the result of my own work and includes nothing which is the outcome of work done in collaboration except as declared in the preface and specified in the text.

It is not substantially the same as any that I have submitted, or, is being concurrently submitted for a degree, diploma or other qualification at the University of Cambridge or any other University or similar institution except as declared in the Preface and specified in the text.

I further state that no substantial part of my dissertation has already been submitted, or, is being concurrently submitted for any such degree, diploma or other qualification at the University of Cambridge or any other University of similar institution except as declared in the Preface and specified in the text

It does not exceed the prescribed word limit of 60,000 words.

A study on non-canonical autophagy signalling - Cansu Karabiyik

Summary

An essential requirement for cell viability is the ability to restore energy supplies to avoid exhaustion of all resources upon nutrient depletion. Autophagy is an essential catabolic process induced to provide cellular energy sources in response to nutrient limitation through the engulfment of intracellular content in double-membrane vesicles known as autophagosomes, which fuse with lysosomes for the degradation and recycling of the autophagic cargo. Nutrient starvation leads to the induction of autophagy by activating the master regulator AMP-activated protein kinase (AMPK). AMPK activates multiple downstream regulators such as ULK1, which in the canonical pathway is known to activate the VPS34 complex, resulting in the formation of PI(3)P-containing autophagosomes.

A failure to induce functional autophagy has been implicated in a range of neurodegenerative diseases, in which the aggregation of toxic proteins and organelles cause neuronal loss. Since studies suggest that canonical PI(3)P-dependent autophagy is impaired in many neurodegenerative diseases, the potential of upregulating non-canonical autophagy holds great therapeutic value. As earlier research showed that autophagy can be upregulated in a VPS34-independent, PI(5)P-dependent manner upon glucose starvation, in this thesis I elucidated the mechanism leading to upregulation of PI(5)P-dependent autophagy.

Here, a new role has been revealed for ULK1. ULK1 activated by AMPK during glucose starvation phosphorylates the lipid kinase PIKfyve on amino acid S1548, thereby increasing its kinase activity and the synthesis of the phospholipid PI(5)P without changing the levels of $PI(3,5)P_2$. ULK1-mediated activation of PIKfyve enhances the formation of PI(5)P-containing autophagosomes upon glucose starvation, resulting in an increase in autophagy flux. Phospho-mimic PIKfyve S1548D drives autophagy upregulation and lowers autophagy substrate levels such as the neurodegeneration-associated mutant polyQ-huntingtin. This study has identified how ULK1 upregulates autophagy upon glucose starvation and induces the formation of PI(5)P-containing autophagosomes by activating PIKfyve, revealing a novel mechanism by which autophagy is induced.

Acknowledgements

I would like to express my gratitude to Professor David Rubinsztein for his supervision and guidance and for offering me the opportunity to undertake my scientific training in his lab. I am grateful that he became both a supervisor and a mentor for me throughout this time and always offered his support when I needed it.

I would like to acknowledge the financial support I received from the Gates Cambridge Scholarship and thank the Gates Cambridge Trust for creating an environment that allow scholars to develop their personal and professional skills.

I am grateful to Mariella Vicinanza for her guidance and for critically reviewing this thesis. I would further like to thank other DCR lab members that played a great role in my scientific training: Farah Siddiqi for training me in working with mice and Fiona Menzies who became a mentor to me even after she left the lab. In addition, I am grateful to members of the Cambridge Institute for Medical Research Core Proteomics, Robin Antrobus and Jack Houghton for performing the mass spectrometry, microscopy facility members, Matthew Gratian and Mark Bowen for training me in confocal microscopy and to John Clarke at the Drug Discovery Institute for his scientific input. Special thanks to our lab manager Victoria Barratt for all her support through the years and to Sung Min Son for help with experiments. I am also thankful to members of the Hyslop lab, Seema Qamar and William Meadows for offering their technical knowledge.

Furthermore, I would like to sincerely thank my friends and fellow DCR lab members Lidia Wrobel, Sandra Malmgren-Hill and Sojung Park for their valuable scientific input and friendships throughout my PhD and for always allowing me to invade their spaces and seek answers to my many questions. They never objected to me ruining lunch or afternoon coffee time with my relentless need to discuss experiments, projects, and career prospects. They truly are the best friends/colleagues one could ask for. Additional thanks to Lidia and Sandra for their critical input on parts of this thesis.

The more than five years I spent in the DCR lab was a profound time in my life and the people I met both in the lab, in the Gates community and in Pembroke College have added a tremendous value to my life. Some of the people who made life in the lab enjoyable were Ting (Xiaoting) Wu, Mariana Pavel, Floriana Licitra, Rebecca Frake, Rany (Hyeran) Won, Carla Bento, Ye Zhu and Swati Keshri. Special thanks to Eliska Zlamalova for her kindness and friendship these last few years. Thanks to all current lab members for the good times and birthday cakes. Living through a pandemic has made it obvious how precious these times were. I wish my final time in Cambridge had not been as somber as it has, but I have years of great memories that I will carry with me.

I have had the great fortune of meeting amazing people outside of the lab who have truly made my time in Cambridge special: Paulo Savaget, Rebecca Love, Parvathi Subbiah, Nick O'Connor, Zach Fitzpatrick, Melisa Basol, Samuel Kebede, Alex L'Hereux, Matt Malone, June Park and Sridhar Sriram. A special thanks to my dear

friends Michael Pashkevich, Jack Myhre and Isabella Ferreira for having been my lifelines during this pandemic.

I would also like to thank my friends Nazia Abbas, Mette Jorgensen and Sumia Naz back in Denmark who have always managed to schedule time for me on my visits home.

A very special thanks to my parents and my brothers Sinan, Hasan and Sergen for their unwavering support and for always encouraging me in all my endeavors. While the physical distance between us has become increasingly great throughout my education, their emotional support and love have kept us as close as ever and have allowed me to strive to be a better version of myself.

Cansu Karabiyik

“I don't feel that it is necessary to know exactly what I am. The main interest in life and work is to become someone else that you were not in the beginning.”

— Michel Foucault

Table of Contents (abbreviated)

Table of Contents (detailed)

1 Introduction

A fundamental requirement for cell viability is the maintenance of cell metabolism, organelle biogenesis and stress adaptation through regulation of the protein homeostasis (proteostasis) network. Most proteins must fold into well-defined three-dimensional structures to exert their biological functions. The proteostasis network prevents protein misfolding and accumulation and ensures the stoichiometric balance of the proteome in a spatiotemporal manner. Impaired proteostasis leads to a variety of proteinopathies caused by the accumulation of unfolded, misfolded or damaged proteins that disrupt cellular functions and has been linked to aging and age-related diseases (Menzies et al., 2017).

1.1 Protein degradation pathways

The cellular proteome is maintained by careful regulation of protein synthesis and degradation. Damaged or unused proteins as well as organelles are removed in eukaryotic cells by two main systems: the ubiquitin-proteasome system (UPS) and the autophagosomal–lysosomal pathway (Ciechanover, 2017; Rubinsztein et al., 2010).

1.1.1 Ubiquitin-proteasome system

The primary proteolysis of misfolded or damaged short-lived proteins is undertaken by the UPS and is responsible for degradation of 80-90% of intracellular proteins (Rajeshwary Ghosh, Vishaka Vinod, 2020). Protein degradation by the UPS is a multistage process that involves the small regulatory protein ubiquitin, three classes of enzymes and the proteasome.

Protein degradation is initiated with the targeting of proteins with a chain of ubiquitin monomers. Ubiquitin is a polypeptide consisting of 76 amino acids. The conjugation of ubiquitin is an ATP-dependent cascade event catalysed by three types of enzymes: E1 (ubiquitin-activating enzyme), E2 (ubiquitin-conjugating enzyme) and E3 (ubiquitin ligases) (Pickart, 2001).

First, E1 adenylates and activates a molecule of ubiquitin (Ub). Next, E1 transfers the activated Ub to E2. Finally, E3, which is a substrate-binding enzyme, binds the E2-Ub complex and transfers Ub from E2 onto the substrate protein, thus marking it for

degradation by covalently attaching Ub to a specific lysine residue on the targeted protein (Hershko et al., 1983).

Ubiquitin contains seven lysine residues, which can all subsequently become ubiquitinated until a polyubiquitin chain is formed, although lysine 48 (K48), 11 (K11) and 68 (K68) are the most commonly ubiquitinated residues. Proteins poly-ubiquitinated on K48 are usually degraded by the 26S proteasome (Grice and Nathan, 2016), while K63-linked chains seem to be involved in a number of different cellular processes, such as endocytosis and DNA repair (Duncan et al., 2006; Hofmann and Pickart, 1999). K11-linked substrates are involved in the endoplasmic reticulum-associated degradation (ERAD) (Xu et al., 2009), in addition to their roles in cell cycle regulation and cell adaptation to stressful stimuli (Akutsu et al., 2016).

The 26S proteasome complex consists of the catalytic 20S core particle and the regulatory 19S particle. The 19S proteins are responsible for the identification and binding of targeted substrates, deubiquitination, substrate unfolding and translocation of substrates into the hollow barrel cavity of 20S core. In the 20S core, the proteins are degraded by three distinct catalytic activities (trypsin-like, chymotrypsin-like and caspase-like) (Livneh et al., 2016).

Due to the narrow barrel structure of the 20S subunit, substrates must be unfolded before entering the core structure, rendering oligomers and aggregates of toxic proteins inaccessible for proteasomal degradation. The degradation of such long-lived and accumulated proteins involves K63-polyubiquitination and is undertaken by the larger system: the autophagosomal–lysosomal degradation system (Nathan et al., 2013).

1.1.2 Macroautophagy

Autophagy is subcategorized into three groups – chaperone-mediated autophagy (CMA), microautophagy and macroautophagy. The three pathways coexist in most mammalian cells and differ in their delivery of cytoplasmic cargo to the lysosomal compartments. In brief, microautophagy involves direct delivery of cytosolic components to the lysosome by invagination of the lysosomal membrane (Cai et al., 2012a), while CMA involves selective translocation of cytoplasmic proteins with a KFERQ peptide motif into lysosomal lumens for degradation (Cuervo, 2009).

Macroautophagy (hereafter called autophagy) is the most widely studied autophagic pathway and the subject of this study.

Autophagy is an evolutionary conserved process characterized by sequestration and engulfment of cytoplasmic cargo by the phagophore, a double-membraned cup-shaped transient structure. Expansion and closure of this structure results in a vesicle known as the autophagosome, which subsequently fuses with the lysosome leading to degradation of autophagosomal content. Autophagy exists both in a selective and non-selective form and maintains degradation of cargo material such as aggregate-prone proteins (aggrephagy), pathogens (xenophagy) and damaged organelles, such as mitochondria, endoplasmic reticulum (ER), peroxisomes or ribosomes (mitophagy, reticulophagy, pexophagy, ribophagy) (Stolz et al., 2014).

The term autophagy (Greek for self-eating) was first coined by Christian de Duve during his work on lysosomes (Duve and Wattiaux, 1965). Until the 1990s, autophagy remained poorly understood, until a genetic screen by Yoshinori Ohsumi led to the isolation of autophagy-related genes (ATG proteins) (Tsukada and Ohsumi, 1993).

The physiological relevance of autophagy has since been extensively shown and its critical roles in a variety of biological processes ranging from development to aging has been established (Hansen et al., 2018). Autophagy is an essential process that maintains cellular health and becomes activated as a response to environmental stress factors, such as nutrient starvation and oxidative stress. Defects in autophagy has been implicated in a variety of proteinopathies, as mutations underlying various neurodegenerative diseases that manifest with accumulations of aggregate-prone, intra-cytoplasmic proteins have been shown to affect the clearance of these substrates by compromising autophagy (Menzies et al., 2017).

1.2 The autophagic machinery

In early yeast screens, more than 30 different ATG proteins were identified (Tsukada and Ohsumi, 1993). Their mammalian orthologues have since been characterized and a plethora of other proteins have been shown to play a role in autophagy, in addition to other cellular functions. Autophagy can be split into four main stages with different proteins operating at each stage: initiation, elongation, maturation, and fusion with the lysosomes (Ravikumar et al., 2010a; schematic in **Figure 1.1**).

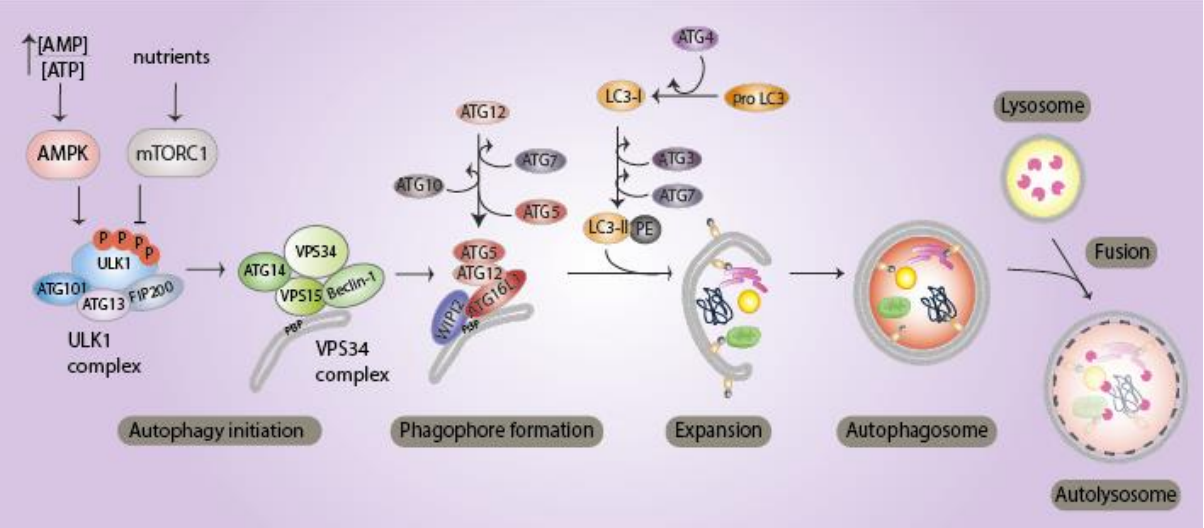

Figure 1.1 | Overview of the autophagy pathway

During glucose deprivation, AMPK activates the ULK complex, which in nutrient replete conditions is inhibited by the mTORC1 complex. The activated ULK complex phosphorylates the VPS34 complex, resulting in PI(3)P synthesis on the nascent autophagosomes. PI(3)P recruits WIPI2 and assists in the recruitment of the ATG12–ATG5–ATG16L1 complex, which is essential for the conjugation of LC3-I to PE, resulting in membrane elongation and engulfment of cytosolic contents. These include aggregate-prone proteins and damaged organelles that are ultimately degraded in the lysosome after fusion with autophagosomes.

1.2.1 Initiation

Autophagosome precursors, named phagophores, are the first structures associated with autophagy. The concerted action of ATG and other autophagy-related proteins result in the reorganization of membranes for the formation of phagophores.

Multiple sources have been suggested to supply membranes to the elongating phagophore (Ravikumar et al., 2010a). Some studies have shown that autophagosomes are formed near the ER and that this organelle provides the membrane sources (Axe et al., 2008; Hayashi-Nishino et al., 2009; Ylä-Anttila et al., 2009). Inhibition of autophagosome maturation showed an accumulation of nascent autophagosomes on the ER (Axe et al., 2008). However, other reports have suggested the plasma membrane (Ravikumar et al., 2010b), ER–Golgi intermediate compartment (ERGIC) (Ge et al., 2013), the Golgi apparatus (Ohashi and Munro, 2010), mitochondria (Cook et al., 2014) and the recycling endosomes (Knaevelsrud et al.,

2013; Puri et al., 2018) as direct contributors to the formation of phagophores. RAB11A, a core component of recycling endosomes, is involved in recruiting autophagy proteins to phagophores on the recycling endosomes. RAB11A-positive membranes provide a direct primary platform for autophagosome formation. Loss of RAB11A impaired recruitment and assembly of the autophagic machinery (Puri et al., 2018).

The conserved transmembrane protein ATG9 is essential for the nucleation of the phagophore and has been found on forming autophagosomes in both yeast and mammalian cells (Noda et al., 2000; Ohashi and Munro, 2010). A study in plant cells also showed an impairment of autophagosome formation upon ATG9 downregulation (Zhuang et al., 2017). ATG9 appears to be involved in the supply of lipid bilayers, as Atg9 in yeast is one of the first components associating with the pre-autophagosomal structures (Kraft and Martens, 2012). In mammalian cells, trafficking of ATG9 from the plasma membrane in clathrin-coated pits to the recycling endosome was shown to be important for autophagosome formation (Puri et al., 2013).

Autophagy is induced as a response to various stimuli, including the primordial stimulus of nutrient starvation. Upon autophagy induction, two distinct kinase complexes are activated for vesicle nucleation – the ULK complex and phosphatidylinositol 3-kinase complex.

In nutrient-rich conditions, the presence of nutrients, growth factors and the AMP/ATP levels are sensed by the Ragulator complex and tyrosine kinase receptors, causing activation of the primordial negative autophagy regulator, mammalian target of rapamycin complex 1 (mTORC1). Active mTORC1 inhibits the ULK complex comprised of the unc-51 like autophagy activating kinase (ULK1/2), ATG13, ATG101 and the focal adhesion kinase family interacting protein of 200 kDa (FIP200) through phosphorylation of ULK1/2 and ATG13. The inhibition of the ULK complex results in suppression of autophagosome formation (Ganley et al., 2009; Hosokawa et al., 2009; Kim et al., 2011a). The upstream signalling regulating autophagy through mTORC1 or AMPK is described in detail in **1.4**.

Upon cellular starvation, mTORC1 is no longer activated and dissociates from the ULK complex. This results in the dephosphorylation and activation of the ULK complex,

which leads to the subsequent activation of a second complex that consists of the class III phosphatidylinositol 3-kinase (PI3K), VPS34. VPS34 is the catalytic component of the core VPS34 complex, which also includes the regulatory subunit VPS15, required for the kinase activity and the tumour suppressor Beclin-1 (Baskaran et al., 2014). The VPS34 complex generates phosphatidylinositol 3-phosphate (PI(3)P) lipids, which recruit downstream effectors. Additionally, the VPS34 complex can be activated by proteins that interact with Beclin-1, which regulates both autophagosome synthesis and autophagosome maturation by forming multiple complexes with VPS34 and VPS15 (Matsunaga et al., 2009). Beclin-1 recruits either ATG14 or UVRAG to the VPS34 complex and forms two distinct complexes, the ATG14-containing complex, which is involved in the initiation of autophagosomes or the UVRAG-containing complex, which is involved in maturation/degradation of autophagosomes (Itakura et al., 2008; Liang et al., 2006, 2008; Matsunaga et al., 2009; Wu et al., 2018). By sensing highly curved membranes, ATG14 targets the VPS34 complex to the phagophore initiation site (Fan et al., 2011), while UVRAG competes with ATG14 for binding to Beclin-1 and enhances VPS34 activity during autophagosome membrane expansion, inducing membrane curvature by recruiting Bif1-endophilin1 (BAR-domain-containing protein) (Takahashi et al., 2007). In addition to its role in autophagosome formation with VPS34 and Beclin-1, UVRAG has been implicated in endosome maturation and lysosome fusion (Itakura et al., 2008; Jiang et al., 2014a; Lee et al., 2018; Liang et al., 2008).

PI(3)P on nascent autophagosomes leads to the recruitment of PI(3)P-binding proteins, such as the double FYVE-containing protein 1 (DFCP1) and WD repeat domain phosphoinositide-interacting (WIPI) proteins WIPI1 and WIPI2, which localise to the autophagosomes upon autophagy induction and are crucial for recruitment of downstream effectors for the elongation of the phagophore (Axe et al., 2008; Backer, 2008; Dooley et al., 2014; Proikas-Cezanne et al., 2004; Russell et al., 2014). WIPI2 directly binds ATG16L1 and leads to the recruitment of downstream ATG proteins (Hanada et al., 2007).

1.2.2 Elongation

Phagophore elongation is mediated by two specialized ubiquitin-like conjugation-systems (Mizushima et al., 2001).

The first system involves a conjugation reaction between ATG12 and ATG5 mediated by the E1 and E2-like enzymes ATG7 and ATG10, respectively. First, ATG12 becomes activated by ATG7 and is transferred onto ATG10, which catalyses the binding between the C-terminal glycine of ATG12 and the lysine 130 of ATG5 (Mizushima et al., 1998). Next, the ATG12-ATG5 binds non-covalently to ATG16L1, which enables the final 800-kDa complex (ATG16L1 complex) to associate with pre-autophagosomal membranes by binding WIPI proteins (Itakura and Mizushima, 2010). ATG16L1 is required for the correct localisation of the ATG12-ATG5 conjugate to the pre-autophagosomal structures (Fujita et al., 2008a; Suzuki et al., 2001). The assembly of this complex is required for the formation of autophagosomes through the recruitment of relevant proteins involved in the second system of phagophore elongation.

The second system involves the lipidation of the microtubule-associated protein 1 light chain3 (MAP1-LC3/LC3), which is an orthologue of the yeast Atg8 family of ubiquitin-like proteins. Mammalian Atg8 proteins can be divided into two subgroups, LC3 and GABARAP subfamilies (Nguyen et al., 2016). Atg8 proteins are lipidated through conjugation of a phosphatidylethanolamine (PE) lipid (Ichimura et al., 2000). First, LC3 is cleaved at its C terminal by ATG4B resulting in the cytosolic form LC3-I (Tanida et al., 2004a), which has an exposed glycine residue onto which PE is conjugated (Fujita et al., 2008b; Hemelaar et al., 2003; Kabeya et al., 2000) in a reaction mediated by ATG7 (E1-like) and ATG3 (E2-like), resulting in formation of LC3-II. ATG3-LC3 bound intermediates are recruited to phagophores through a direct interaction with ATG12 (Metlagel et al., 2013; Mizushima et al., 2001; Noda et al., 2013). LC3-II can be found both on the inner and outer surfaces of the autophagosome (Kabeya et al., 2000; Tanida et al., 2004b), unlike the ATG16L1 complex, which dissociates from mature autophagosomes. LC3-II acts as a widely used autophagy marker as it remains bound to the outer membrane after lysosomal fusion. Following lysosomal fusion, LC3-II on the outer membranes of autolysosomes eventually become delipidated by ATG4B (Tanida et al., 2004a).

The two ubiquitin-like systems are interconnected in a manner that is not yet fully elucidated. The ATG16L1 complex have been shown to facilitate LC3-I conjugation to PE, thus acting like an E3 ubiquitin ligase (Hanada et al., 2007). Similarly, ATG10 can

interact with LC3 and facilitate LC3 conjugation to PE (Nemoto et al., 2003), while ATG3 can interact with ATG12 resulting in ATG5-ATG12 conjugation (Hanada et al., 2007), as well as LC3 lipidation (Metlagel et al., 2013).

Although the exact mechanism by which autophagosomes are sealed remains elusive, several studies suggest that core autophagy proteins play an active role in this. In ATG conjugation–deficient cells (ATG3, ATG5 or ATG7 KO), degradation of the inner autophagosomal membrane was disrupted and autophagic activity was strongly suppressed (Tsuboyama et al., 2016). Additionally, silencing of ATG2A and ATG2B led to impaired autophagic flux and accumulation of unclosed autophagic structures (Velikkakath et al., 2012). A recent study shows that the yeast Atg2 possesses a hydrophobic cavity that accommodates phospholipid acyl chains and supplies phagophores with phospholipids for autophagosome formation (Osawa et al., 2019). These findings were corroborated in mammalian cells (Maeda et al., 2019; Valverde et al., 2019). ATG2A was shown to mediate lipid transfer between PI(3)P-containing vesicles. This has been suggested to be mediated by WIPI4 and WIPI1 (Maeda et al., 2019). In mammalian cells, TRAPPC11, a member of the TRAPP family of multisubunit complexes implicated in membrane trafficking, recruits the ATG2-WIPI4 complex onto phagophores depending on ATG9 function, and its loss of function causes an autophagosome-closure defect (Stanga et al., 2019). Furthermore, LC3 has been implicated in the sealing of the elongated autophagosome, as overexpression of an inactive form of ATG4B impaired maturation of autophagosomes without affecting the formation of phagophores (Fujita et al., 2008b). Similarly, accumulation of elongated phagophores and impairment of autophagosome closure was observed in *ATG3* knockout (KO) mice, in which LC3 lipidation is eliminated (Sou et al., 2018).

1.2.3 Maturation and fusion

Once an autophagosome has been sealed and has no ATG proteins on its surface, it is characterised as a mature autophagosome. The mechanism behind autophagosome closure is not fully understood yet, although the process has been proposed to be similar to the endosomal sorting complex required for transport (ESCRT)-mediated membrane scission in multivesicular bodies (MVBs) (Knorr et al., 2015). Mutation or loss of proteins in the ESCRT complex leads to impairment of autophagic degradation (Filimonenko et al., 2007; Lee et al., 2007; Rusten et al.,

2007a). In a study in yeast, Atg17, the yeast orthologue of FIP200 recruits the ESCRT complex to autophagosomes. Depletion of subunits from ESCRT complex, such as Snf7 and Vps4 leads to accumulation of open autophagosomes and late autophagy defects (Zhou et al., 2019).

Mature autophagosomes are transported towards the lysosomal compartment by utilizing microtubules and dynein in what is known as the microtubule organizing center (MTOC) (Kimura et al., 2008). Accordingly, loss of dynein function caused impaired autophagosome-lysosome fusion (Jahreiss et al., 2008; Ravikumar et al., 2005). Furthermore, disruption of the microtubules and the lysosomal positioning influences the autophagosome–lysosome fusion rates (Korolchuk et al., 2011).

The formation of the autolysosome involves various proteins that are involved in tethering the autophagosome to the lysosome and subsequently the fusion of the autophagosome and lysosome. Autophagosomes are also able to fuse with late endosomes, forming the intermediate structure called an amphisome, which subsequently fuses with lysosomes (Filimonenko et al., 2007; Razi et al., 2009). This includes SNAREs (e.g. syntaxin 17 - STX17), Rab7, and the class C vacuolar protein sorting (VPS) proteins (Noda et al., 2009).

UVRAG has been implicated in the late stages of autophagy as it is involved in recruiting the fusion machinery to the autophagosomes. UVRAG recruits the class C VPS proteins and through this interaction activates Rab7, which links autophagosomes to microtubule motors through FYVE and coiled-coil domain-containing protein 1 (FYCO1), thereby mediating kinesin-driven movement towards the cell periphery (Pankiv et al., 2010), resulting in autophagosome fusion with late endosomes and lysosomes (Liang et al., 2008). STX17 interacts with components of the homotypic fusion and protein sorting (HOPS)–tethering complex. Knockdown of VPS33A, VPS16, or VPS39 of the HOPS complex blocked autophagic flux and caused accumulation of STX17- and LC3–positive autophagosomes (Jiang et al., 2014a). Furthermore, oligomeric forms of ATG14 promote membrane tethering by binding STX17, which stabilises the interaction of the STX17-containing SNARE complex with the autophagosome, leading to enhanced endo-lysosomal fusion (Diao et al., 2015).

Lysosomal fusion results in the degradation of the inner autophagosomal membrane and the autophagosomal content by lysosomal acid hydrolases. The acidification of autolysosomes is maintained by a proton pump assembled on the lysosomal membrane, vacuolar [H^+] ATPase (v-ATPase) (Yoshimori et al., 1991). The v-ATPase is a multisubunit protein complex composed of a cytosolic V1 sector and a lysosomal membrane-anchored V0-sector. The acidification of lysosomes is crucial for activating acid hydrolases such as cathepsins to obtain an effective degradation of substrates (Luzio et al., 2007). Prevention of lysosomal acidification by inhibition of the v-ATPase with the macrolide antibiotic Bafilomycin A1 prevents autophagosome-lysosome fusion (Yoshimori et al., 1991).

1.2.4 Transcriptional regulation of autophagy

The expression of autophagosomal and lysosomal genes is controlled by transcription factors, including transcription factor EB (TFEB), which is negatively regulated by mTORC1 (Palmieri et al., 2011). TFEB is a member of the microphthalmia/transcription factor E (MiT/TFE) family of transcription factors (TFs), which also includes MITF, TFE3, and TFEC proteins (Hemesath et al., 1994). In nutrient-rich conditions, TFEB becomes phosphorylated by mTORC1, resulting in TFEB interaction with 14-3-3 proteins, thereby promoting the cytoplasmic retention of TFEB. Upon nutrient and energy deprivation, TFEB becomes dephosphorylated and translocates to the nucleus, enabling its transcriptional activity and leading to increased autophagosome formation and autophagosome-lysosome fusion (Roczniak-Ferguson et al., 2012; Sardiello et al., 2009). Other transcription factors implicated in regulation of autophagy and lysosomal biogenesis include TFE3 and MITF (Martina et al., 2014; Ploper et al., 2015).

1.3 Autophagy in health and disease

Autophagy is essential for maintaining neuronal homeostasis because of the susceptibility of neurons to accumulate defective organelles and proteins due to their post-mitotic nature. The importance of autophagy for the nervous system was demonstrated in studies in which suppression of autophagy in *Atg5* and *Atg7*-deficient mice led to phenotypes similar to those observed in neurodegenerative diseases, such as progressive motor impairment and inclusion bodies (Hara et al., 2006; Komatsu et al., 2006). Polymorphisms in autophagy genes have been implicated in age-related

neurodegeneration, suggesting that defects in the autophagy pathway may contribute to age-related pathologies (Menzies et al., 2017). Indeed, many late-onset neurodegenerative disorders, including Parkinson's disease (PD), Huntington's disease (HD) and Alzheimer's disease (AD) possess genetic components that underlie the presence of toxic intracellular protein aggregates in the brain through impairment of the autophagic machinery. Therefore, autophagy has in recent years been extensively studied for its potential as a treatment against age-related diseases. Below, I will present the evidence of autophagy association with aging and age-related disorders.

1.3.1 Aging

There is increasing evidence suggesting that autophagy declines during aging in many organisms and that this reduction plays a role in the functional deterioration of biological functions with age (Hansen et al., 2008).

In multiple studies, autophagy gene transcripts decreased with age in the brain and muscle of *Drosophila melanogaster* (*D. Melanogaster*; Demontis and Perrimon, 2010; Sarkis et al., 1988; Simonsen et al., 2008a). A study by Lipinski et al. (2010) showed transcriptional downregulation of *ATG5*, *ATG7* and *BECN1* with age in post-mortem human brains. This correlates with the age-related decrease in autophagy proteins in the mouse hypothalamus (Kaushik et al., 2012) and human muscle (Carnio et al., 2014), as well as lysosomal proteins in rat livers (Cuervo and Dice, 2000). In a spatiotemporal analysis of autophagy in *Caenorhabditis elegans (C. elegans),* an age-dependent decrease was observed in longevity models (Chang et al., 2017). Electron microscopy analysis have shown an accumulation of autophagic vacuoles and decreased ability to clear autophagic vesicles in mouse and rat livers with age (Del Roso et al., 2003).

Additionally, studies have shown a correlation between autophagy and lifespan. In *C. elegans*, decreased expression of orthologues of the mammalian *ATG1, ATG7, ATG12, BECN1* and *ATG18* led to shortened lifespan (Meléndez et al., 2003). Deletion of core autophagy genes such as *Atg7* in flies reduced life-span and caused accumulation of aggregated proteins in degenerating neurons (Juhász et al., 2007), which was supported by findings revealing reduced lifespan in mutant flies with reduced *Atg1* and *Atg8* expression (Simonsen et al., 2008). A study in senescence-

accelerated mouse-prone 8 (SAMP8) mice, a rodent model with accelerated aging, showed an accumulation of autophagic vesicles in hippocampal neurons along with deficits in learning and memory with increasing age (Ma et al., 2011). The age-dependent decline in autophagic function and lysosomal degradation was prevented with dietary restriction (Cavallini et al., 2001; Donati, 2006).

Overexpression of specific autophagy genes was found to extend lifespan in flies and mice (Bai et al., 2013; Pyo et al., 2013; Simonsen et al., 2008a). Additionally, overexpression of the TFEB orthologue, helix–loop–helix transcription factor *hlh-30* in *C. elegans* extends lifespan in an autophagy-dependent manner (Lapierre et al., 2013).

In an attempt to corroborate these findings, I used our mRFP-GFP-LC3 transgenic mice (Pavel et al., 2016) to investigate changes in autophagic flux in 2, 12, 18 and 24 months old mice. This assay allows the characterization of LC3-II vesicles and discrimination between autophagosomes or non-acidified lysosomes, and acidified autolysosomes. This tool takes advantage of the different pKa values of the two LC3 tags (<4.5 for mRFP and around 6 for GFP), allowing the GFP signal to become rapidly quenched by the acidic lysosomal environment, while the mRFP-tagged LC3 persists. I found a profound decrease in numbers of autophagosomes and autolysosomes with age, thus showing *in vivo* evidence of decreased autophagic flux in aged mice (**Figure 1.2**; Park et al., in preparation).

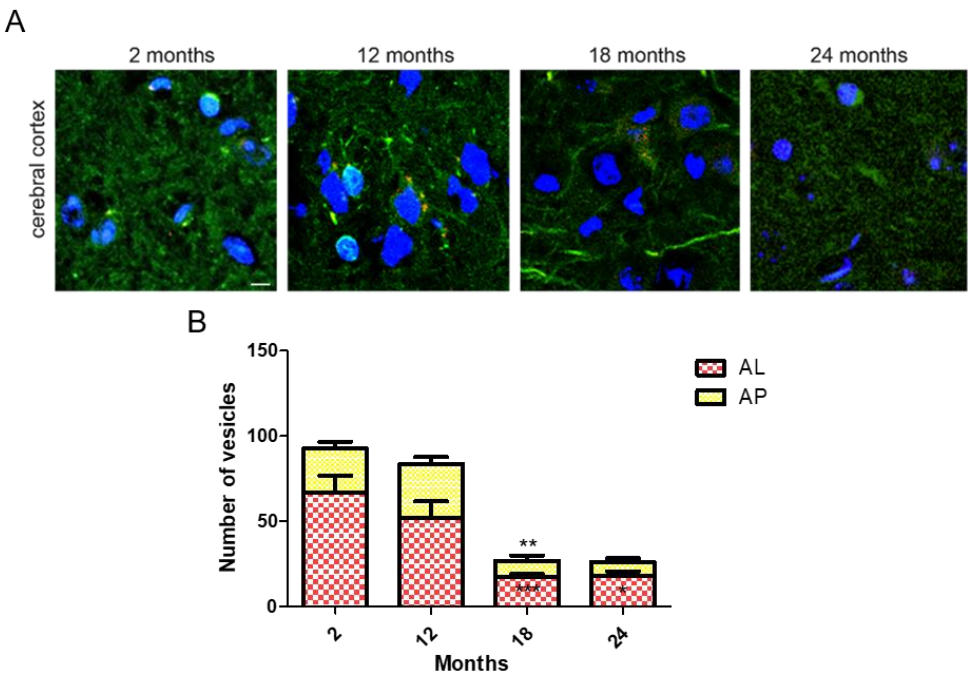

Figure 1.2 | Number of autophagic vesicles decrease in aged mice

(A) Representative images of cerebral cortex from 2, 12, 18 and 24 months old mRFP-GFP-LC3 transgenic mice. **(B)** Number of autolysosomes (AL) and autophagosomes (AP) in the motor cortex of 2 (n = 12), 12 (n = 9), 18 (n = 8) and 20-24 (n = 5) months old GFP-RFP-LC3 mice (mean ± SEM; ***P < 0.001; **P < 0.01; *P < 0.05; two-tailed t-test).

1.3.2 Neurodegeneration and autophagy modulation

Studies of post-mortem brains of aged individuals, who were not diagnosed with neurological conditions, showed the presence of amyloid plaques, neurofibrillary tangles, Lewy bodies, synaptic dystrophy and neuronal loss supporting the notion that the integrities of degradative pathways are challenged with age (Elobeid et al., 2016).

It is evident that the progressive loss of the degradative capacity can lead to an accumulation of toxic proteins, as autophagy gradually decreases with age. This can have a detrimental impact on neuronal health and may play a role in manifestation of neurodegenerative diseases.

Since most aggregate-prone, neurodegenerative disease-associated proteins are autophagy substrates (Menzies et al., 2015), autophagy upregulation has great therapeutic value as a treatment for neurodegeneration. A lot of work has focused on

the identification of autophagy modulators and their therapeutic potentials (Fleming et al., 2011). These compounds are currently categorised into two distinct groups based on their mechanisms of action — mTOR-dependent compounds such as rapamycin and its analogues or mTOR-independent compounds, including the disaccharide trehalose and L-type Ca^{2+}-channel antagonists like felodipine and rilmenidine. In the section below, I will describe the evidence of autophagy defects in neurodegenerative diseases and the effects of autophagy modulators on disease progression. A description of the modes of action of mTOR-dependent and independent autophagy modulation is included in 1.4.

Huntington's Disease

HD is a hereditary neurodegenerative disease resulting from abnormally long CAG trinucleotide expansions in the huntingtin *(HTT)* gene, leading to the translation of polyglutamine (PolyQ) tracts (MacDonald et al., 1993). Mutant HTT (mHTT) accumulates in cells and forms toxic oligomeric species and aggregates. Although mHTT is an autophagy substrate and can be cleared with autophagy inducers, like rapamycin, which specifically inhibits the mTOR kinase (Berger et al., 2006; Ravikumar et al., 2004), when not cleared, they appear to disrupt the autophagic machinery, contributing to accumulation of aggregate-prone proteins and toxicity (Menzies et al., 2011).

It is well-established that the autophagy flux is impaired in HD. Increase in autophagic vacuoles have been seen in cells across a range of HD models and in patients (Davies et al., 1997; Heng et al., 2010; Sapp et al., 1997). Studies in *in vivo* and *in vitro* HD models showed that autophagic vacuoles form and are adequately eliminated by lysosomes, but fail to efficiently trap cytosolic cargo in their lumen (Vicente et al., 2010). Expansions of PolyQ tracts impair autophagy, resulting in the accumulation of toxic accumulates (Ashkenazi et al., 2017).

Furthermore, PolyQ-expanded proteins may cause defects in vesicular trafficking. In neurons, pathogenic PolyQ-proteins impair axonal transport (Gunawardena et al., 2003). Mutations of the dynein machinery, which as mentioned above is responsible for autophagosome movement, exacerbated the progression of Huntington disease in fly and mouse models (Kimura et al., 2008; Ravikumar et al., 2005).

A range of autophagy modulation strategies alleviate the pathogenesis of HD. Other than rapamycin, trehalose was found to improve motor dysfunction and extend lifespan in a transgenic mouse model of Huntington disease (Tanaka et al., 2004). The L-type Ca^{2+}-channel antagonists felodipine reduces mHTT toxicity in zebrafish and mouse models of HD (Siddiqi et al., 2019a). Other mTOR-independent autophagy inducers like SMER10, SMER18, and SMER28 reduce mHTT toxicity in cells and *D. melanogaster* (Sarkar et al., 2007a). The toxic aggregation of mHTT is ameliorated in cells treated with rilmenidine in an autophagy-dependent manner (Rose et al., 2010) and in cells and zebrafish models treated with verapamil, clonidine, and calpastatin (Fleming et al., 2011).

Alzheimer's disease

AD is characterized by the intracellular accumulation of neurofibrillary tangles that consist of hyperphosphorylated tau, a microtubule-associated protein and extracellular deposits of amyloid-β (Aβ) plaques, derived from defective proteolysis of amyloid precursor protein (APP). Mutations in APP and presenilin (PS1), which is involved in APP to Aβ proteolysis, cause rare autosomal dominant forms of familial Alzheimer disease (FAD) (Alison Goate et al., 1991).

The accumulation of autophagosomes is a prominent feature of AD (Boland et al., 2008). Autophagosomes in AD mouse models show an increased presence of APP, Aβ and PS1 (Haung Yu et al., 2005), suggesting decreased clearance of autophagic vesicles.

However, it has also been postulated that autophagosome formation is affected in AD, as brain samples from patients appeared to have reduced levels of *BECN1* mRNA expression and protein levels (Rohn et al., 2011). Genetic deletion of *BECN1* in mice led to decrease in autophagy and resulted in neurodegeneration (Pickford et al., 2008). This correlates with earlier studies showing an association between a reduction in Beclin-1 levels and neurodegeneration (Shibata et al., 2006). The reduction in Beclin-1 levels has been linked to increased caspase-3 activation in brains of AD patients (Rohn et al., 2011), as a previous study showed that Beclin-1 is a substrate for Caspase-3 and that the proteolytic cleavage of Beclin-1 reduces autophagy in AD (Luo and Rubinsztein, 2010). Another possibility is that autophagy is inactivated by

mTORC1 signalling, as Aβ increases mTORC1 signalling, which was alleviated upon treatment with rapamycin causing a reduction in Aβ levels and tau pathology through autophagy upregulation (Caccamo et al., 2010). However, mTOR-independent autophagy modulation with trehalose has also been shown to reduce tau aggregation (Krüger et al., 2012) and Aβ aggregates (Liu et al., 2005).

Genome-wide association studies have implicated phosphatidylinositol-binding clathrin assembly protein (PICALM) as a genetic risk factor in AD (Harold et al., 2009). Reduced levels of PICALM, which is required for endocytosis of SNARE proteins were found in brains of AD patients (Ando et al., 2013). Loss of this function inhibits autophagy at multiple steps, including early autophagosome formation and maturation of autophagosomes leading to tau accumulation (Moreau et al., 2014).

Mutations in PS1 is associated with FAD. Other than its function of processing APP, PS1 functions as an ER chaperone for the lysosomal v-ATPase. Interestingly, FAD-associated mutations in PS1 result in reduced maturation of the lysosomal v-ATPase, leading to increased lysosomal pH (Coffey et al., 2014; Lee et al., 2010a; Wolfe et al., 2013). As mentioned above, the maintenance of the lysosomal pH is important for successful fusion events. Thus, the effects on lysosomal pH arising from mutations in PS1 could explain the impaired clearance of autophagic vesicles.

Treatment with rapamycin and its analog, temsirolimus increased the autophagic clearance of hyperphosphorylated tau in AD mice and alleviated the disease pathology (Jiang et al., 2014b; Ozcelik et al., 2013). Rapamycin also reduced toxicity in *D. melanogaster* expressing wild-type or mutant (R406W) forms of tau, which was attributed to an autophagic clearance of insoluble tau (Berger et al., 2006).

Treatment with mTOR-independent autophagy modulators such as trehalose led to enhanced autophagic clearance of tau aggregates and increased neuronal survival in an AD mouse model (Schaeffer et al., 2012) and in a mouse model of tau overexpression with Parkinsonism (Rodríguez-Navarro et al., 2010). Treatment of zebrafish expressing mutant tau with clonidine and rilmenidine increased clearance of mutant tau and ameliorated the abnormal morphological and motor defects observed in the vehicle control (Lopez et al., 2017). Furthermore, felodipine and verapamil reduced levels of insoluble tau species in transgenic zebrafish expressing mutant tau

in an autophagy-dependent manner, resulting in the amelioration of the abnormal phenotype (Siddiqi et al., 2019b)

Parkinson's Disease

PD is the most common neurodegenerative movement disorder. It is characterized by the presence of intraneuronal inclusions known as Lewy bodies (LBs) and Lewy neurites enriched with filamentous forms of α-synuclein (α-syn) (Spillantini et al., 1997), which is encoded by the synuclein (*SNCA*) gene. Multiplications of the *SNCA* locus cause autosomal dominant forms of PD. Levels of α-syn correlates with disease severity (Ross et al., 1998). Studies suggest that both autophagosome biogenesis and fusion with lysosome are compromised in PD (Karabiyik et al., 2017).

The presence of inclusion bodies containing α-syn affects autophagosome maturation and fusion with lysosomes, resulting in decreased protein degradation (Tanik et al., 2013). Overexpression of α-syn *in vitro* and *in vivo* results in compromised autophagosome biogenesis through the inhibition of Rab1, causing mislocalisation of ATG9 (Winslow et al., 2010). A mutation in *VPS35*, encoding a component of the retromer complex, in an autosomal dominant form of PD impairs autophagy, causing ATG9 mislocalisation and inhibition of autophagosome formation (Zavodszky et al., 2014).

Lysosomal impairment has been shown to cause accumulation of α-syn aggregates in the nervous system (Qiao et al., 2008). There is increasing evidence of lysosomal defects in PD. Autosomal dominant mutations in the *LRRK2* gene appear to affect endosome-to-lysosome trafficking. Overexpression of mutant lrrk, analogous to the most common PD causing mutation in human LRRK2 (G2019S), led to defective lysosomal positioning mediated by Rab7 and enlarged lysosomes containing undigested content (Dodson et al., 2012).

Heterozygous mutations in the gene encoding the lysosomal enzyme glucocerebrosidase (GBA) are the most commonly known genetic risk factors for PD. Induced pluripotent stem cells (iPSC)-derived neurons from PD patients with *GBA* mutations showed increased α-syn levels, as well as autophagic and lysosomal defects (Schöndorf et al., 2014).

Furthermore, the PD-associated genes *ATP13A2* and *SYT11* regulate autophagy through a pathway mediated by TFEB (Bento et al., 2016). Depletion of ATP13A2 *in vitro* led to a decrease in the levels of SYT11. The decrease in SYT11 can account for the lysosomal dysfunction and impaired autophagosome degradation resulting from ATP13A2 deficiency, since SYT11 overexpression in ATP13A2 knockdown cells was able to rescue the autophagy defects in these cells (Bento et al., 2016).

Rapamycin increases the clearance of WT and PD-related mutant forms of α-syn in PC12 cells (Webb et al., 2003) and ameliorates toxicity in animal models of PD (Crews et al., 2010; Malagelada et al., 2010). Upon treatment with trehalose, autophagy was induced and enhanced clearance of α-syn both *in vitro* (Sarkar et al., 2007b) and *in vivo* (Tanji et al., 2015). Additionally, felodipine decreased the levels of the PD-causing A53T mutant α-syn in a mouse model of PD (Siddiqi et al., 2019a).

1.4 Signalling pathways involved in autophagy regulation

Autophagy is regulated by multiple upstream signalling pathways, the main pathways involving the serine/threonine kinase mTOR, which inhibits autophagy and the autophagy regulator AMPK. Since various disease-related mutations have been shown to affect different stages of the autophagic machinery, the strategy of upregulating autophagy as a treatment for neurodegenerative diseases requires the unravelling of the interactomes involved in each stage. Therefore, in this study I focus on the upstream signalling mechanisms that lead to autophagy upregulation.

Cells are fundamentally required to manage their energy levels by balancing ATP consumption and generation depending on the availability of nutrients and must, therefore, be capable of restoring their energy supplies to avoid exhausting all their resources upon nutrient depletion. The capacity to sense the energy status of the cells is one that makes mTOR and AMPK major regulators that coordinates cell growth and metabolism by switching between anabolic and catabolic pathways to recycle organic material, according to the availability of nutrients.

1.4.1 mTORC1 signalling

1.4.1.1 mTORC1-dependent autophagy

The mTOR pathway is the most studied pathway in the context of autophagy. mTORC1 is activated by growth factors, amino acids, and cellular energy status to regulate autophagy in addition to protein synthesis, mitochondrial function and glucose homeostasis. In conditions that promote autophagy upregulation, such as nutrient deprivation, the absence of stimulatory inputs inactivates mTORC1 and allows the induction of autophagy (Laplante and Sabatini, 2012).

The mTOR pathway involves two functional complexes: a rapamycin-sensitive mTOR complex 1 (mTORC1), which regulates autophagy and mTOR complex 2 (mTORC2)

Both complexes contain the catalytic mTOR subunit and the G protein β-subunit like protein (GβL) (Jacinto et al., 2004; Kim et al., 2003), the DEP domain containing mTOR-interacting protein (DEPTOR) (Peterson et al., 2009), and the Tti1/Tel2 complex (Kaizuka et al., 2010).

In addition, mTORC1 complex contains the regulatory-associated protein of mammalian target of rapamycin (Raptor), which also plays an important role in the regulation of autophagy and proline-rich Akt substrate 40 kDa (PRAS40), which inhibits the mTORC1 activity (Haar et al., 2007), while the mTORC2 complex contains the rapamycin-insensitive companion of mTOR (rictor), mammalian stress-activated map kinase-interacting protein 1 (mSin1), and protein observed with rictor 1 and 2 (Protor) (Laplante and Sabatini, 2012).

Phosphorylation of mTOR on T2446, S2448 and S2481 within the kinase domain (KIN) domain of mTOR increases mTOR activity which leads to downregulation of autophagy. Rapamycin binds the intracellular 12-kDa FK506-binding protein (FKBP12) protein on the rapamycin-binding domain (FRB), causing FKBP12 to directly interact with and inhibit mTOR when it is part of the mTORC1 complex but not mTORC2 (Laplante and Sabatini, 2012). Induction of autophagy, such as starvation and binding of rapamycin to FKBP12 disturbs the interaction between mTOR and Raptor, thus impairing mTOR activity (Sabatini et al., 1994).

In its active state, mTORC1 is recruited to the lysosomal membranes by the trimeric Ragulator complex where it interacts directly with the GTPase Ras homolog enriched in brain (Rheb) in its GTP-bound form (Sancak et al., 2008), leading to Rheb-mediated stimulation of the kinase activity of mTORC1. This interaction is regulated by another key upstream regulator of autophagy, the heterodimer consisting of tuberous sclerosis 1 (TSC1) and TSC2. The TSC complex responds to and integrates a range of stimuli upstream of mTORC1, including removal of amino acids or growth factors, upon which the TSC complex translocates to the lysosome where it interacts with Rheb (Demetriades et al., 2016). TSCs GTPase-activation protein (GAP) activity converts Rheb into its inactive GDP-bound state (Rabanal-Ruiz and Korolchuk, 2018). Inactivation of Rheb by the TSC complex suppresses the Rheb-mediated activation of mTORC1 (Inoki et al., 2003a).

Another key regulator of autophagy is protein kinase B (Akt/PKB). In response to growth factors, Akt becomes catalytically active. Moreover, growth factors activate Ras, which stimulates a cascade involving ERK1/2. Both Akt and ERK1/2 can phosphorylate one of two subunits of the TSC complex, and Akt can phosphorylate Raptor, causing the dissociation of PRAS40, an mTORC1 inhibitor, from Raptor, thus activating mTORC1 and inhibiting autophagy (Haar et al., 2007; Inoki et al., 2002; Ma et al., 2005; Sancak et al., 2007).

Removal of amino acids from culture media was shown to potently suppress mTORC1 signalling in mammalian cells and yeast (Boya et al., 2005). Amino acids activate mTORC1 through Rag GTPases independently of the TSC complex (Jewell et al., 2013; Sancak et al., 2008; Smith et al., 2005). The four Rag proteins in mammalian cells form obligate heterodimers that consist of RagA/B or RagC/D. The GDP/GTP binding of these two heterodimers are inversely correlated in that when RagA/B is bound to GTP, RagC/D is bound to GDP and *vice versa*. Amino acids promote the loading of RagA/B with GTP, which enables the heterodimer to interact with Raptor (Jewell et al., 2013; Sancak et al., 2008). Of the amino acids knowns to regulate mTORC1 activity, leucine (Leu) has been widely studied (Jewell et al., 2013). Sestrin2, a GATOR2-interacting protein that inhibits mTORC1 was reported as an intracellular Leu sensor for mTORC1 pathway (Chantranupong et al., 2014; Parmigiani et al., 2014; Saxton et al., 2016). Another proposed Leu sensor is the leucyl-tRNA synthetase

(LRS), which was shown to act as a GAP on Rag proteins (Han et al., 2012; He et al., 2018). In a recent study, the Leu metabolite acetyl-coenzyme A (Acetyl-CoA) positively regulated mTORC1 activity by EP300-mediated acetylation of Raptor on K1097 and appears to be a major pathway for direct mTORC1 regulation in most cell lines. In fasting mice, acetylation of Raptor decreased in brain, liver and muscle tissues. In accordance with the observations made in cells, accompanying inhibitions of mTORC1 and EP300 activities were observed in the studied mouse tissues (Son et al., 2019).

As previously mentioned, mTORC1 inhibits autophagy in nutrient and energy replete conditions by hyperphosphorylating ATG13, which prevents its binding to ULK1 and therefore inhibits the downstream activity of ULK1 in the autophagic initiation process (Kamada et al., 2010).

Unlike mTORC1, little is known about the mTORC2 pathway. While rapamycin acutely and specifically inhibits mTORC1, its effects on mTORC2 are more variable and generally require prolonged treatment (Sarbassov et al., 2006). While induction of Akt signalling by the insulin-like growth factor (IGF-1) leads to activation of mTORC1, it has also been implicated in mTORC2 regulation. Depletion of the IGF-1 receptor in zebrafish and mice models inhibits mTORC2, which reduces the activity of protein kinase C (PKCα/β). This decreases the rate of clathrin-dependent endocytosis, which negatively impacts autophagosome precursor formation, suggesting that mTORC2 is required for autophagy. Indeed, depletion of rictor, a critical component of mTORC2, leads to a decrease in autophagy (Renna et al., 2013). In contrast, a study in *C. elegans* suggest that inactivation of mTORC2 and its target serum-and glucocorticoid-inducible kinase 1 (SGK-1) induces mitophagy (Aspernig et al., 2019). However, in a study of the role of mTORC2 in longevity in *C. elegans*, it was found that upon different experimental conditions, mTORC2 either promoted lifespan or reduced it (Mizunuma et al., 2014). Since autophagy has been widely implicated in promoting longevity as described earlier, the temporal effects of mTORC2 on longevity could explain the conflicting findings on the role of mTORC2 in autophagy regulation.

1.4.1.2 mTORC1-independent autophagy

In the mammalian system, autophagy can be regulated in a mTORC1-independent manner.

Intracellular inositol and inositol 1,4,5-trisphosphate (IP_3) levels negatively regulate autophagy. Treatment of cells with lithium and sodium valproate was shown to induce autophagy through inhibition of inositol monophosphatase and led to an increase in free inositol depletion, relieving the negative regulation of IP_3 on autophagy (Sarkar et al., 2005; Shaltiel et al., 2004; Williams et al., 2002).

L-type Ca^{2+} channel antagonists, the K^+ ATP channel opener minoxidil, and the imidazoline-1 receptor (I1R) agonists like clonidine and rilmenidine induce autophagy by reducing cAMP levels, which regulates IP_3 levels (Williams et al., 2008). These activators prevent the influx of Ca^{2+}, which leads to inhibition of Ca^{2+}-dependent cysteine proteases called calpains and the induction of autophagy via regulation of intracellular IP_3. Pharmacological inhibition of calpains and knockdown of calpain induces autophagy by reducing cAMP levels (Renna et al., 2010).

Additionally, trehalose has been shown to induce autophagy in a mTOR-independent manner in several studies through activation of AMPK (Mizunoe et al., 2018; Rodríguez-Navarro et al., 2010; Sarkar et al., 2007b).

1.4.2 AMPK signalling

AMPK signalling is a key regulatory system that maintains the balance between energy consumption and production. AMPK is a heterotrimeric complex that comprises the catalytic (α) and regulatory (β and γ) subunits and responds to reduced glucose levels by inducing autophagy to recycle cytoplasmic content. Since AMPK is an important subject in this thesis, details of AMPK activation and regulation of the autophagic machinery is described below, as summarized in schematic **Figure 1.3**.

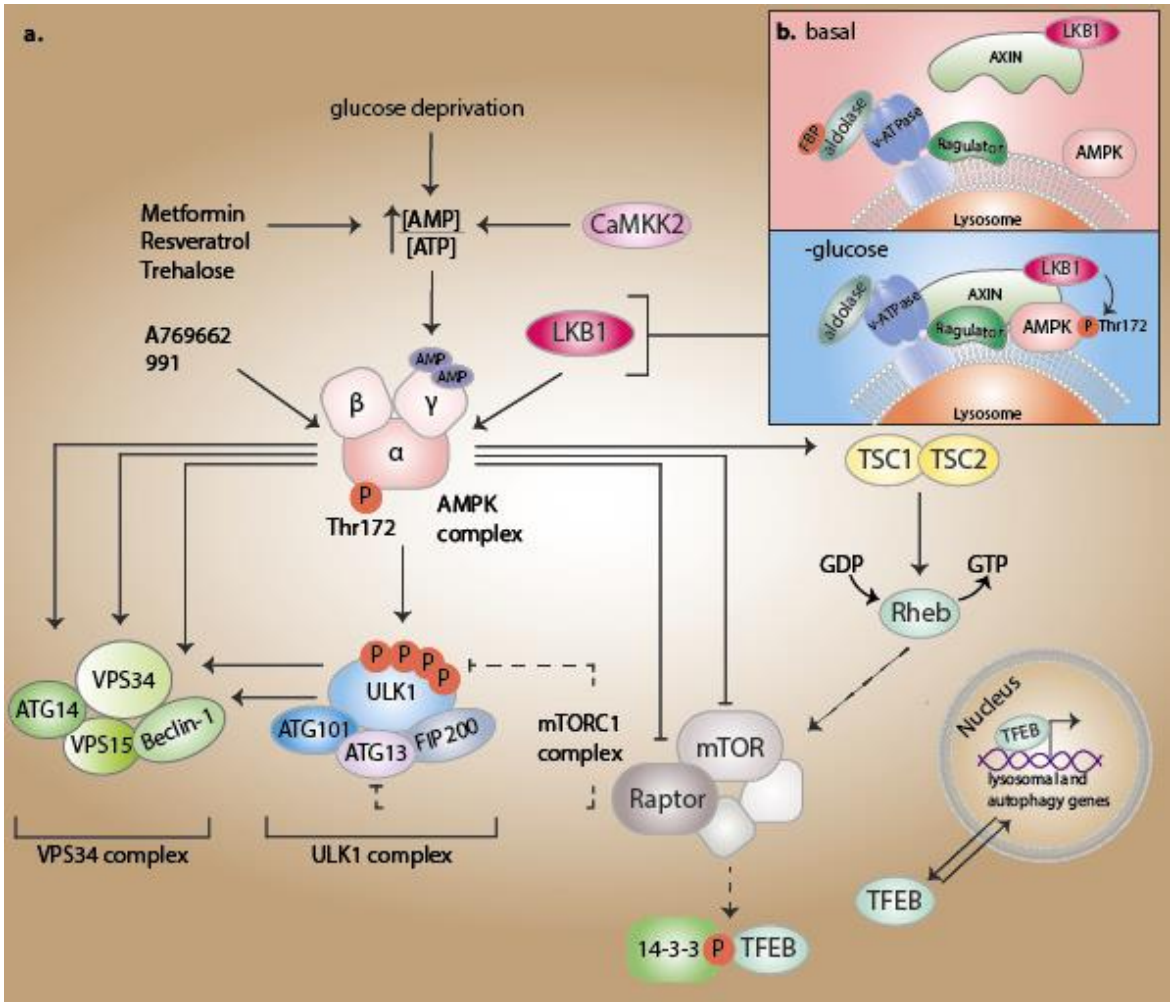

Figure 1.3 | Overview of AMPK and mTORC1 signalling

(A) During glucose deprivation, AMPK becomes activated by AMP binding to the regulatory γ subunit and LKB1 or CAMKII phosphorylation of the T172 residue on the catalytic α subunit. Many different compounds can activate AMPK directly or indirectly by acting either on the allosteric ADaM site or by increasing the [AMP/ATP] ratio. Upon activation, the AMPK complex phosphorylates and activates components of the ULK complex, which in nutrient replete conditions is inhibited by the mTORC1 complex (dashed arrows). In the presence of sufficient nutrients, the mTORC1 complex, which is activated by Rheb, prevents TFEB from translocating to the nucleus. In glucose deprivation, AMPK activates TSC1/TSC2 which inhibits Rheb, thus allowing TFEB to translocate to the nucleus to induce transcription of lysosomal and autophagy genes. Dashed arrow, mTOR signalling in basal conditions. **(B)** In glucose deprivation, the AMPK complex becomes activated on the lysosomal surface. The dissociation of FBP from aldolase causes a conformational change that allows the vATPase-Ragulator complex to bind AMPK and the AXIN-LKB1 complex, which subsequently leads to the phosphorylation of AMPK by LKB1.

1.4.2.1 AMPK structure and activation

AMPK is an obligate heterotrimeric complex that consists of a catalytic α subunit and two regulatory subunits, β and γ. Mammals possess two genes encoding the α subunits, α1 (*PRKAA1)* and α2 (*PRKAA2),* two genes encoding the β subunits, β1 (*PRKAB1)* and β2 (*PRKAB2)* and three genes encoding the γ subunits, γ1 (*PRKAG1)*, γ2 (*PRKAG2)* and γ3 (*PRKAG3)* (Hardie, 2007). An AMPK complex is composed of a α, β and γ subunit, giving rise to twelve different possible complex combinations. Only three combinations, α1β2γ1, α2β2γ1 and α2β2γ3 have been implicated in the AMPK activity in tissues. The activities of the different complexes appear to be specific to cellular function (Birk and Wojtaszewski, 2006).

The α subunit contains a N-terminal protein kinase domain (KD) with the critical residue T172 located in the activation loop, which is phosphorylated by upstream kinases (Stein et al., 2000). Upon phosphorylation of the α subunit, its kinase activity increases 100-fold. The key upstream kinase phosphorylating T172 is the tumor suppressor kinase liver kinase B1 (LKB1), a component of the heterotrimeric complex with the pseudokinase STRAD, and the scaffold protein MO25 (Hawley et al., 2003; Woods et al., 2003). AMPK activation is abrogated in mouse liver depleted of LKB1 (Shaw et al., 2004). Furthermore, the T172 site can be phosphorylated by calmodulin-dependent kinase kinases (CaMKKs) (Hawley et al., 2005; Hurley et al., 2005; Woods et al., 2005) in what is considered a Ca^{2+}-dependent pathway (different from the AMP-dependent pathway).

The β subunit contains a myristoylated N-terminal region (Mitchelhill et al., 1997; Oakhill et al., 2010), a central carbohydrate-binding module (β-CBM) and a C-terminal domain (β-CTD). The β-CBM has been suggested to have a role in localizing AMPK to late endosomal glycogen particles (Hudson et al., 2003; Polekhina et al., 2003), and for AMPK activation. The cleft between the β-CBM and the N lobe of the α-KD is referred to as the allosteric drug and metabolite (ADaM) site, as it is the binding site for many AMPK activators (Langendorf and Kemp, 2015), as discussed below. It has been proposed that the ADaM site is bound by a metabolite yet to be discovered (Lin and Hardie, 2018). Interactions between the phosphorylated S108 residue on β-CTD and K40/K42 in α1 or K29/K31 in α2 are stabilized when this site is unoccupied, resulting in activation of AMPK (Li et al., 2015).

The γ subunit is composed of four tandem repeats of a cystathionine-β-synthase (CBS) domain and contains the regulatory adenine-nucleotide-binding sites that allow the binding of adenine nucleotides, thus allowing AMPK to respond to changes in AMP:ATP ratio (Adams et al., 2004). AMPK activity is stimulated upon binding of AMP and to some extent ADP (Ross et al., 2016). AMP binding activates AMPK by three mechanisms:

(i) AMP binding promotes LKB1-induced T172 phosphorylation. Some studies have suggested that the AMP binding also promotes activation through CaMKIIB (Oakhill et al., 2010, 2011). However, this has yet to be corroborated by others (Gowans et al., 2013).

(ii) AMP binding leads to a conformational change that prevents the dephosphorylation of T172 by protein phosphatases (Davies et al., 1995; Gowans et al., 2013).

(iii) AMP causes allosteric activation of AMPK already phosphorylated on T172 (Gowans et al., 2013; Suter et al., 2006).

AMPK senses changes in the AMP:ATP and ADP:ATP ratios through the competitive binding of nucleotides to the γ subunit, rather than the total number of nucleotides and responds accordingly by activating downstream effectors, including important components of the autophagic machinery.

An AMP-independent mechanism for AMPK activation has been proposed that involves the AMPK interactor AXIN and LKB1 and the translocation of AMPK to the lysosomal compartment where it is phosphorylated by LKB1 (further described below) (Zhang et al., 2014, 2017). A recent study suggests that different compartmentalized pools of AMPK are activated depending on the cellular AMP levels. As a response to low glucose levels, AMPK can be activated through an AMP-independent, AXIN-dependent pathway on lysosomes, while upon moderate increases in cytosolic AMP, AMPK is activated in an AXIN-dependent manner. However, during conditions that resemble severe starvation, all pools of AMPK are activated independently of AXIN (Zong et al., 2019) **(Figure 1.3B)**.

1.4.3 mTOR-AMPK-ULK1 signalling

1.4.3.1 AMPK and the regulation of ULK1

The interaction between AMPK and ULK1 was identified by two separate groups through proteomics and co-immunoprecipitation (co-IP) studies (Behrends et al., 2010; Lee et al., 2010b). AMPK binds the P/S-rich domain of ULK1. This interaction is required for ULK1-mediated autophagy upregulation in U2OS cells (Lee et al., 2010b). Subsequently, studies have shown that AMPK phosphorylates ULK1 upon glucose starvation or pharmacological AMPK activation. However, the findings in these studies are contentious. According to Egan et al., AMPK phosphorylates ULK1 on S555, T574 and S637 following treatment with the AMPK activator phenformin. Mutation of these sites led to defective autophagy and increased cell death upon nutrient deprivation (Egan et al., 2015). According to Kim et al., upon four hours of glucose starvation, AMPK phosphorylates ULK1 on S317 and S777. The ULK1-mediated upregulation of autophagy during glucose starvation was shown to be regulated by AMPK signalling, since dominant-negative kinase-dead AMPK abrogated the ULK1 phosphorylation and autophagy upregulation. Similarly, autophagy upregulation upon glucose starvation was prevented when these sites on ULK1 were mutated (Kim et al., 2011b).

Different studies have implicated different residues for AMPK phosphorylation. While a study by Bach et al., (2011) confirmed the S555 site as an AMPK phosphorylation site, Shang et al. (2011) found that S638 (S637 in human cells) was dephosphorylated under starvation conditions. This contradicts the function of this site as an AMPK phosphorylation site proposed by Egan et al., (2015). Furthermore, Shang et al. (2011) found that the dephosphorylation of this site was necessary for ULK1-AMPK association and for autophagy upregulation. A study suggested that the AMPK activation and phosphorylation of ULK1 inhibits autophagy following starvation (Nwadike et al., 2018). However, this has yet to be corroborated by others. Moreover, a study found that ULK1 also phosphorylates AMPK on the β subunit on S108 and proposed that AMPK initially stimulates ULK1 (e.g. S555 phosphorylation) and once activated, ULK1 phosphorylates β S108, sensitizing AMPK to drugs/metabolites acting at the ADaM site (Dite et al., 2017).

Although various studies identified different phosphorylation sites, these are all located in the S/T-rich region. Despite of the varying details, there seems to be a strong

consensus that AMPK interacts with and phosphorylates ULK1 upon glucose starvation. It is noteworthy that the starvation approaches used by the various groups differ, which could explain the discrepancies in their results. The contention between studies implies that the AMPK-mediated regulation ULK1 upon glucose starvation is transient and tightly controlled. It has been reported that ULK1 negatively feeds back to AMPK during starvation by phosphorylating all three AMPK subunits, leading to inactivation of AMPK. The study showed an increased phosphorylation of AMPK on T172 in ULK1 knockdown cells (Löffler et al., 2011), suggesting that the activation of ULK1 by AMPK cannot be sustained during prolonged treatments.

AMPK-ULK1 signalling has additionally been shown to play a role in mitophagy. Replacement of endogenous ULK with kinase-deficient or phospho-mutant forms of ULK1 resulted in elevated levels of mitochondria with abnormal morphology and reduced membrane potential upon glucose starvation, indicating a defect in mitophagy (Egan et al., 2011). Oxidative stress and hypoxia result in ULK1 recruitment to mitochondria and initiation of mitophagy mediated by CaMKK2 phosphorylation of AMPK, causing activation of ULK1 (Sinha et al., 2015) through phosphorylation of the ULK1 S555 residue (Laker et al., 2017; Tian et al., 2015).

As previously mentioned, ULK1 is inactivated after phosphorylation by mTORC1. In energy replete conditions, mTORC1 phosphorylates ULK1 S757 (S758 in mice) and disrupts the interaction between ULK1 and AMPK. Overexpression of the mTORC1 activator, Rheb, promoted this phosphorylation event, while treatment with the mTORC1 inhibitor rapamycin prevented it (Kim et al., 2011a). Conversely, Shang et al. suggested that the AMPK-ULK1 association was only relevant during basal conditions and reported impaired interaction between AMPK-ULK1 in cells expressing a S758A mutant form of ULK1 (Shang et al., 2011). Based on these findings, it was proposed that the dephosphorylation of S758 during starvation leads to dissociation of AMPK and ULK1, resulting in increased autophagy induction (Shang et al., 2011). This hypothesis was corroborated in a study in which treatment of skeletal muscle cells with the AMPK activator AICAR (5-amino-4-imidazolecarboxamide riboside) or glucose starvation for three hours resulted in ULK1-AMPK complex dissociation. After a six hour treatment, the dissociation was found to be complete (Sanchez et al., 2012).

These findings highlight the importance of considering the transiency of AMPK and ULK1 signalling when dissecting the mechanistic details of this pathway.

1.4.3.2 AMPK and the regulation of mTOR

In addition to regulating autophagy through ULK1 phosphorylation, AMPK causes autophagy upregulation by inhibiting the mTORC1 pathway. AMPK partly regulates mTORC1 activity by phosphorylating TSC2 on T1227 and S1345 upon glucose starvation (Corradetti et al., 2004a; Inoki et al., 2003b). This modification activates TSCs GAP activity, converting Rheb into its inactive GDP-bound state, thus suppressing Rheb-mediated activation of mTORC1 (Inoki et al., 2003a). The observation that mTORC1 is inhibited by AMPK activators in TSC2-null MEFs and the fact that regulation of mTORC1 by AMPK upon glucose deprivation is found across all eukaryotes, including in species missing a TSC2 orthologue, such as *C. elegans* and *Saccharomyces cerevisiae (S. cerevisiae)*, led to the investigation of additional mechanisms of mTORC1 regulation during glucose deprivation. Raptor was identified as a direct substrate of AMPK. Phosphorylation of Raptor on S722 and S792 leads to recruitment and binding of 14-3-3 proteins and mTORC1 inhibition (Gwinn et al., 2008a).

As both mTOR and AMPK are regulated on the lysosome, this further underlines the crosstalk between the two pathways. The AMPK interactor AXIN translocates with LKB1 to the lysosome where it binds LAMTOR, a component of the Ragulator complex. Ragulator, as mentioned earlier, is involved in mTORC1 activation by interacting with Rags in response to nutrients (Bar-Peled et al., 2012; Sancak et al., 2008). After translocation to the lysosome, AXIN forms a complex with Ragulator, the v-ATPase, LKB1 and AMPK, leading to LKB1-induced AMPK activation (Zhang et al., 2017) to turn on catabolic processes, while it turns off anabolic processes by inhibiting the GEF activity of Ragulator, causing mTORC1 to dissociate from the lysosome and become inactivated (Zhang et al., 2014). In AXIN KO MEFs, formation of the complex, including phosphorylation and activation of AMPK was abolished in response to glucose starvation. Furthermore, depletion of AXIN slowed down the dissociation of mTOR from the lysosome, suggesting that mTOR remains active (Zhang et al., 2014).

Interestingly, reducing glucose levels to below 5 mM from the 25 mM glucose concentration in basal media led to activation of AMPK although no changes in the

cellular AMP/ATP or ADP/ATP ratios were observed suggesting an entirely AMP/ADP-independent mechanism for glucose sensing (Zhang et al., 2017; Zong et al., 2019). In the presence of glucose, the glycolytic enzyme aldolase, which associates with v-ATPase and Ragulator on the lysosomal membrane has fructose-1,6-bisphosphate (FBP) bound, preventing the interaction of the v-ATPase-Ragulator with the Axin-LKB1 complex. Since glucose deprivation leads to a decrease in glycolysis and therefore FBP, aldolase becomes unoccupied by FBP, which causes a conformational change in Ragulator and leads to recruitment of the AXIN-LKB1 complex to the Ragulator, thus allowing LKB1 to phosphorylate and activate AMPK (Zhang et al., 2017).

Recent studies have revealed that lysosomal damage induces autophagy in a process that involves galectins. During nutrient replete conditions, active mTOR and its regulators are localized with the glycosylated lysosomal transmembrane protein SLC38A9 on the lysosome close to galectin 8 (Gal8). Following lysosomal damage, Gal8 moves towards SLC38A9 and components of Ragulator and away from mTOR, as mTOR becomes inactivated and leaves the lysosomal membrane and translocates to the cytosol. AMPK was found to be activated during lysosomal damage and interacted with galectin 9 (Gal9), which was involved in the activation of AMPK in response to lysosomal damage (Jia et al., 2018, 2020).

The AMPK α1-subunit can be inhibited by Akt by phosphorylation of S487 (Hawley et al., 2014). In the context of autophagy, Akt is best known for its role in activating mTORC1 and inhibiting autophagy (Huang and Manning, 2009). In cells with hyperactive Akt, AMPK was resistant towards chemically-induced activation (Hawley et al., 2014). Interestingly, Akt also phosphorylates and inactivates both ULK1 (Bach et al., 2011) and Beclin-1, causing autophagy inhibition (Wang et al., 2012). These findings imply the presence of reciprocal regulation of autophagy by AMPK and Akt.

In AMPK KO embryonic stem cells, lysosomal gene expression was decreased due to TFEB hyperphosphorylation and impaired TFEB translocation to the nucleus (Young et al., 2016). As mentioned earlier, mTORC1 phosphorylates TFEB and prevents it from translocating to the nucleus, thus inhibiting its transcriptional function. However, AMPK activation results in dephosphorylation and nuclear translocation of TFEB in a manner that appears to be independent of mTORC1 (Collodet et al., 2019), although the exact mechanism has yet to be elucidated.

1.4.3.3 AMPK and the regulation of other autophagy proteins

AMPK has been shown to act directly on other components of the autophagic machinery to positively regulate autophagy.

AMPK exerts a dual regulation on VPS34 complexes, either by activating complexes involved in autophagy (VPS34 in complex with ATG14 or UVRAG), or by inhibiting complexes unrelated to autophagy (hereafter referred to as non-autophagic complexes, such as VPS34 complexes free of ATG14 and UVRAG) (Kim et al., 2013). AMPK phosphorylates the catalytic subunit of VPS34 on T163 and S165 in the non-autophagic complexes, which leads to a decrease in overall PI(3)P production and thus suppresses vesicle trafficking, which helps preserve cellular energy for survival during starvation. In contrast, AMPK phosphorylation of Beclin-1 on S90, S93 and T388 in the ATG14- or UVRAG-containing VPS34 complexes increases PI(3)P and induces autophagy (Kim et al., 2013; Zhang et al., 2016). Interestingly, ATG14 is critical in directing AMPK activity towards Beclin-1 and in suppressing AMPK-mediated phosphorylation of VPS34, which results in the activation of the ATG14-containing VPS34 complex and inhibition of the non-autophagic complex. Activation of ATG14 by AMPK does not depend on its localisation on autophagosomes, as mutants of ATG14 missing the membrane-targeting domain BATS retain the ability to induce Beclin-1 phosphorylation (Kim et al., 2013). It has been proposed that ATG14 binding to the core complex may induce conformational changes that reduce the accessibility of T163 and S165 on VPS34, thus preventing the inhibitory phosphorylation and promoting the availability of S91 and S94 in Beclin-1 towards activating phosphorylation by AMPK. *In vitro* studies suggest that UVRAG might play a similar role in promoting AMPK activity towards the activation of the UVRAG-containing VPS34 complex (Kim et al., 2013). AMPK-dependent phosphorylation of Beclin-1 on T388 stabilizes the Beclin-1–containing VPS34/ATG14 complex and dramatically decreases the affinity of Beclin-1 for the anti-apoptotic protein BCL2, while increasing the interaction of Beclin-1 with VPS34 and ATG14 (Zhang et al., 2016). Additional studies proposed that AMPK might boost VPS34 activity during glucose starvation by also phosphorylating the scaffold protein PAQR3, a constitutive component of the ATG14-containing VPS34 complex that increases the Beclin-1 phosphorylation on S93 (Xu et al., 2016). The details of the role of AMPK phosphorylation on the Beclin-

1 engagement with complexes related to autophagy or non-autophagic complexes remains to be addressed.

Upon hypoxic stress, AMPK-dependent phosphorylation of S761 on the C-terminus of ATG9 creates a docking site for 14-3-3ζ, which increases the ability of ATG9 to redistribute to autophagosomes. In the absence of phosphorylation and 14-3-3ζ binding, ATG9 fails to properly mobilize in response to autophagic signals (Weerasekara et al., 2014).

AMPK also phosphorylates death-associated protein kinase 2 (DAPK2) on S289, increasing its catalytic activity (Shiloh et al., 2018). DAPK2 has previously been shown to inhibit mTORC1 (Ber et al., 2015) and induce autophagy (Chi et al., 2016; Soussi et al., 2015). Activation of DAPK2 leads to phosphorylation of Beclin-1, thus causing it to dissociate from its inhibitor Bcl-XL, resulting in an increase in autophagy (Shiloh et al., 2018). While DAPK1 has also been shown to induce autophagy by phosphorylating Beclin-1 (Singh et al., 2016), its regulation appears to be independent of AMPK (Shiloh et al., 2018). An overview of the phosphorylation sites involved in a cross-talk between AMPK, ULK1, mTORC1 and other autophagy-related proteins is shown in **Table 1**.

Table 1 | Overview of the phosphorylation sites involved in the signalling between AMPK, ULK1, mTORC1 and other autophagy-related proteins.

Kinase	Substrate	Phosphorylation site(s)	Reference(s)
AMPK	ULK1	S637/S638	(Egan et al., 2011; Shang et al., 2011)
		S748, T764	(Yu et al., 2011)
		S555	(Egan et al., 2011; Laker et al., 2017; Shang et al., 2011; Tian et al., 2015)
		S467, T574	(Egan et al., 2011)
		S317, S777	(Kim et al., 2011a)
	Raptor	S722, S792	(Gwinn et al., 2008a)
	TSC2	T1227	(Corradetti et al., 2004b; Inoki et al., 2003b)
		S1345	(Inoki et al., 2003b)
	AKT	S487	(Hawley et al., 2014)
	DAPK2	S289	(Shiloh et al., 2018)

	Beclin-1	S90/91, S93/94	(Kim et al., 2013; Xinxin Song et al., 2018)
		T388	(Zhang et al., 2016)
		S96	(Xinxin Song et al., 2018)
	mATG9	S761	(Weerasekara et al., 2014)
ULK1	ULK1 (autophosphorylation)	S1047	(Dorsey et al., 2009)
	Raptor	S696, T706, S792, S855, S859, S863, S877	(Dunlop et al., 2011)
	AMPK	α-subunit: S360/T368, S397, S486/T488 β-subunit: S38, T39, S68, S173 γ-subunit: S260/T262, S269	(Löffler et al., 2011)
		S108	(Dite et al., 2017)
	ATG13	Unknown	(Hosokawa et al., 2009; Hwa Jung et al., 2009)
	AKT	S774	(Bach et al., 2011)
mTORC1	ULK1	S757/S758	(Kim et al., 2011a; Shang et al., 2011; Yu et al., 2011)
	ATG13	Unknown	(Ganley et al., 2009; Hosokawa et al., 2009; Hwa Jung et al., 2009)

1.4.3.4 AMPK activators and their effects on neurodegeneration

AMPK has been the target of extensive drug development efforts as a therapeutic strategy for treating metabolic diseases, as well as cancer and inflammatory diseases. AMPK activators also hold a yet unexplored potential for the treatment of neurodegenerative diseases through the upregulation of the autophagic machinery. Below, I describe the different types of AMPK activators and evidence of their therapeutic benefits through the upregulation of autophagy.

AMPK activators are divided into three classes according to their mechanisms of action:

Indirect activators reduce ATP production through the inhibition of components of the respiratory chain, leading to an increase the AMP:ATP and ADP:ATP ratios, thus resulting in activation of AMPK.

In cells expressing a mutant form of the AMPK γ subunit (R531G), which is unable to bind AMP on its activation site, compounds such as the antidiabetic drug metformin, the glycolytic inhibitor 2-deoxyglucose, resveratrol, berberine, and galegine, activate AMPK by increasing AMP levels (Hawley et al., 2010).

Metformin, used in diabetes therapy since 1957, gained popularity after studies showed that its ability to decrease glucose production and increase glucose consumption in skeletal muscle was mediated through AMPK (Musi et al., 2002). Since epidemiological evidence suggests that diabetes mellitus is associated with a higher risk of cognitive impairment, dementia and AD (Leibson et al., 1997), multiple studies have assessed the therapeutic efficacy of metformin on neurodegenerative diseases. In an *in vitro* neuronal insulin-resistant model that displayed AD-like phenotypes, treatment with metformin was found to reduce Aβ protein aggregates (Gupta et al., 2011). Metformin had beneficial effects on clearance of hyperphosphorylated tau and Aβ in AD models in multiple studies (Chiang et al., 2016; Li et al., 2012; Ou et al., 2018). In a recent study, metformin treatment increased autophagic clearance of hyperphosphorylated tau in the brains of diabetic mice through activation of AMPK, resulting in attenuation of cognitive impairment (Chen et al., 2019). These findings are consistent with a study showing that treatment of cells with cilostazol, an antiplatelet medication known to increase intracellular cyclic AMP levels, activated AMPK leading to an increase in autophagy and a decrease in Aβ levels (Park et al., 2016).

Additionally, metformin treatment was applied to animal HD models leading to reduced mHTT accumulations and an improvement in the behavioural aberrations associated with HD (Arnoux et al., 2018).

The naturally occurring compound, resveratrol, which induces autophagy (Fleming et al., 2011) has been shown to recruit AMPK through activation of CaMKK2, causing an increase in autophagy, resulting in reduced Aβ levels in

N2a cells and neurons (Vingtdeux et al., 2010) and the elimination of mHTT and Aβ in animal models of HD and AD, respectively (Parker et al., 2005; Vingtdeux et al., 2011).

Other indirect AMPK activators, such as nilotinib and bosutinib known to increase autophagy (Yu et al., 2013) have shown beneficial effects in AD mouse models (Lonskaya et al., 2014, 2015). As mentioned above, trehalose has been shown to reduce tau, α-syn and mHTT aggregation in animal models of AD, PD and HD by upregulating autophagy (Rodríguez-Navarro et al., 2010; Sarkar et al., 2007b; Schaeffer et al., 2012; Tanaka et al., 2004). This has been shown to be mediated through AMPK activation (Tang et al., 2017).

AMP analogues, such as 5-aminoimidazole-4-carboxamide ribonucleoside (AICAR) are taken up by cells by adenosine transporters and converted into the equivalent nucleotide ZMP (Gadalla et al., 2004). ZMP binds to AMPK and mimics all three effects of AMP. Additional AMP analogues include 5-(5-hydroxyl-isoxazol-3-yl)-furan-2-phosphonic acid or C2 and were found to be 100-fold more potent than AMP and over 1,000-fold more potent than ZMP in cell-free assays and appear to have fewer off-targets.

The therapeutic efficacy of AICAR has been widely studied in recent years. AICAR was shown to reduce Aβ levels in cellular and animal models of AD (Cai et al., 2012b; Li et al., 2018; Won et al., 2010) and tau phosphorylation in cellular models of AD (Greco et al., 2009).

The mode of which AICAR acts remains uncertain. AICAR treatment (1-2 hours) was shown to induce autophagy in MEFs, hepatocytes, HeLa and HEK 293T cells (Lee et al., 2010b; Meley et al., 2006; Zhang et al., 2016). However in primary rat hepatocytes, AICAR was shown to inhibit autophagy (Samari and Seglen, 1998). Multiple studies showed that prolonged treatment (>four hours) with AICAR blocks proteolysis (Liu et al., 2014a; Viana et al., 2008), which was proposed to be due to an inhibition of PI3K causing impaired formation of a functional VPS34 complex (Viana et al., 2008).

Direct AMPK activators such as salicylate and the thienopyridone A769662 bind the CBM domain of the β subunit in the ADaM site, causing allosteric

activation of AMPK. Mutations in K29 and K31 residues in the ADaM site in α-KD decreased the affinity of A769662 to AMPK and prevented AMPK activation (Xiao et al., 2013). Since A769662 is able to activate AMPK in AMP-insensitive R531G mutant cells, this implies that it acts in an AMP-independent manner (Hawley et al., 2010). The effects of AMP binding to AMPK are mimicked upon treatment with A769662 and T172 dephosphorylation is prevented (Göransson et al., 2007; Sanders et al., 2007). Additional compounds in this category include 991 and MT-63-78, which both appear to act selectively through the β subunits by causing phosphorylation of S108 on the β1 subunit, hence mimicking the effects of ULK1 on AMPK (Dite et al., 2017). Treatment with 991 increases phosphorylation of Acetyl-CoA carboxylase, which is an AMPK substrate, with only minor increases in T172 phosphorylation (Willows et al., 2017). Additionally, allosteric activation with A769662 increased AMP levels. The need for β1-S108 and α-T172 phosphorylation for AMPK activation was entirely bypassed and led to a >1,000-fold activation of AMPK (Scott et al., 2014). Although these findings suggest that allosteric activation of AMPK could bypass the requirements of various phosphorylation events involved in AMPK activation during physiological conditions, ULK1 phosphorylation of AMPK on β1-S108 was shown to increase the potency of A769662 (Dite et al., 2017). The exact modes of action of these activators, including the roles of β1-S108 and α-T172 phosphorylation in their potencies remains unclear.

Treatment of striatal progenitor cells expressing mHTT with A769662 caused an increase in autophagy markers and reduced mHTT-containing aggregates (Walter et al., 2016).

Although their therapeutic efficacies have yet to be elucidated, these compounds appear to have fewer off-targets (Collodet et al., 2019), which raises their profiles as potential therapeutic targets.

These findings suggest that AMPK activation is protective against neurodegeneration through the upregulation of autophagy. Although, contentious outcomes have been reported, these could be explained by the variations in cell types, treatment durations and types of AMPK modulation used. Given the transiency and sensitivity of AMPK signalling, there is great demand on future studies dissecting the exact mechanisms

by which AMPK is involved in autophagy through the regulation of ULK1 and its role in autophagy-related pathologies.

1.5 Non-canonical autophagy signalling

There is increasing evidence that autophagy can be upregulated in a non-canonical manner, in particular independently of VPS34 and Beclin-1 (Codogno et al., 2011).

While canonical autophagy is considered to be PI(3)P-dependent, there is evidence showing the existence of non-canonical VPS34-independent autophagy, in which conventional steps of autophagosome formation is bypassed (Codogno et al., 2011; Devereaux et al., 2013). This was evident in an *in vivo* study showing the presence of LC3-positive autophagosomes in VPS34-null sensory neurons (Zhou et al., 2010). In autophagy induced by glucose starvation, PI(3)P is not required to initiate autophagy (Mcalpine et al., 2013a). Furthermore, Beclin-1-independent autophagy upregulation was reported upon treatment of human breast cancer cells with resveratrol (Scarlatti et al., 2008). Resveratrol-mediated autophagy was shown to induce autophagic degradation independently of VPS34 but dependent on ATG7 and ATG5 (Mauthe et al., 2011).

In accordance with this, an *in vitro* study showed that PI(5)P synthesized by the phosphatidylinositol 5-kinase, PIKfyve, could upregulate autophagosome synthesis and induce autophagy. This became evident when the compromised autophagosome formation caused by inactivation of VPS34 *in vitro* was rescued upon treatment with exogenous PI(5)P (Vicinanza et al., 2015).

The removal of PI(5)P is maintained by type II PI(5)P kinases (phosphatidylinositol 5-phosphate 4-kinases, PIP4K2s), which converts PI(5)P to PI(4,5)P_2 (Clarke et al., 2010). The mammalian genome contains three genes encoding three isoforms of PIP4Ks – PIP4K2α, PIPK2β, PIP4K2γ. Silencing of the three PIP4K2s increased cellular PI(5)P levels and led to increased autophagosome formation (Vicinanza et al., 2015).

Furthermore, the PI(5)P-containing autophagosomal structures recruited downstream effectors such as WIPI2 and DFCP1 similar to PI(3)P-containing autophagosomes

(Vicinanza et al., 2015). The mechanism behind upregulation of VPS34-independent, PI(5)P-dependent autophagy remains to be elucidated.

Understanding this pathway holds great potential, as canonical Beclin-1/VPS34-dependent autophagy signalling dysfunction is common in numerous neurodegenerative diseases as mentioned earlier (Mealer et al., 2014; Pickford et al., 2008). Indeed, lentiviral delivery of Beclin-1 into PD and AD mouse models reduced protein deposits and ameliorated the neuropathology (Pickford et al., 2008; Spencer et al., 2010).

Thus, overcoming Beclin-1/VPS34-dependent autophagy downregulation by upregulating autophagy in a VPS34-independent manner could evade the involvement of functionally impaired proteins and open a new avenue for therapeutic interventions.

1.5.1 PIKfyve activity and regulation

Phosphoinositides (PIs) are essential and versatile membrane-anchored signals that in addition to autophagy control various cellular processes, such as intracellular membrane trafficking, signalling, cytoskeletal reorganization, DNA synthesis and cell cycle (Shisheva, 2001).

An important actor in PI signalling is PIKfyve, an evolutionarily conserved protein of ~230 kDa and a product of a single-copy gene across species, first found as *Fab1* in yeast. It is known to associate with membrane PIs and PI(3)P through its FYVE finger domain and for synthesizing PI(3,5)P_2 and PI(5)P (Shisheva et al., 1999).

PIKfyve phosphorylates the D-5 position in PI and PI(3)P to generate PI(5)P and PI(3,5)P_2, respectively (Sbrissa et al., 1999a). Genetic manipulation of *PIKfyve* in several mammalian cell types has shown correlating changes in levels of ^{32}P-PI(3,5)P_2 (Ikonomov et al., 2001; Sbrissa and Shisheva, 2005). Similarly, the mass levels of PI(5)P were higher in a HEK 293T cell line stably expressing PIKfyve WT and lower in a HEK 293T cell line stably expressing the dominant-negative kinase-deficient PIKfyve K1831E mutant (Sbrissa et al., 2002). Finally, in a PIKfyve KO mouse model and in a PIKfyve hypomorph mouse model, it was shown that PIKfyve was responsible for production of both PI(3,5)P_2 and PI(5)P (Ikonomov et al., 2011; Zolov et al., 2012).

PIKfyve is best known for its role in the endosomal/endocytic system. In cell lines expressing the mutant PIKfyve K1831E, vacuolation of early endosomal vesicles was induced (Ikonomov et al., 2001). This was suggested to be the result of the decrease in $PI(3,5)P_2$, as microinjection of $PI(3,5)P_2$ (but not PI(5)P) into vacuolated COS cells reversed the defective phenotype (Ikonomov et al., 2002). In a number of cellular studies, mutant PIKfyve led to enlargement of compartments along the endo-lysosomal system in *S. cerevisiae*, *C. elegans* and *D. melanogaster* (Nicot et al., 2006; Rusten et al., 2007b). These findings suggest that suppression of PIKfyve-generated $PI(3,5)P_2$ synthesis in mammalian cells induces an imbalance in endosomal membrane trafficking, resulting in endosome enlargement and vacuolation. PIKfyve triggers maturation of transport intermediates from early endosomes and initiates reformation of lysosomes from endo-lysosomes, suggesting that PIKfyve through $PI(3,5)P_2$ synthesis regulates membrane remodelling and dynamics of late endocytic compartments by regulating the reformation of terminal storage lysosomes (Bissig et al., 2017; Ikonomov et al., 2006; Min et al., 2015; Sbrissa et al., 2007a; Sultana et al., 2019).

Complete loss of PIKfyve function is associated with developmental defects and embryonic lethality, as well as defects in endo-lysosomal maturation in *C. elegans* and *D. melanogaster* (Nicot et al., 2006; Rusten et al., 2007b).

Due to its low abundance (5% of cellular PI) and the poor chromatographic separation from other PIs, PI(5)P was the last PI to be identified and has remained enigmatic (Rameh et al., 1997). It has been implicated to have a role in immune responses, platelet aggregation, glucose uptake and cytoskeletal remodelling (Poli et al., 2019).

Although earlier studies suggested that PI(5)P is a result of dephosphorylation of $PI(3,5)P_2$ by myotubularins (Michell et al., 2006; Walker et al., 2001), it has in recent years become evident that PIKfyve is an important contributor to maintaining steady-state levels of PI(5)P in mammalian cells. Acute inhibition of PIKfyve at low doses with the PIKfyve inhibitor YM201636 reduces intracellular PI(5)P by 71% – 62% (Sbrissa et al., 2012).

PIKfyve forms a complex with the adaptor protein ArPIKfyve (Vac14 in yeast) (Bonangelino et al., 2002; Sbrissa et al., 2004) and the phosphatase Fig4 (Sac3 in

yeast), which specifically dephosphorylates $PI(3,5)P_2$ on D-5. ArPIKfyve depletion leads to a decrease in both $PI(3,5)P_2$ and PI(5)P levels, while overexpression of ArPIKfyve leads to an increase in said lipids (Sbrissa et al., 2004).

PIKfyve has been implicated in the autophagosomal-lysosomal pathway through its role in maintaining lysosomal function. Inhibition of PIKfyve with YM206136 and depletion of PIKfyve with siRNA, leads to vacuolation and a block in autophagic flux due to impaired lysosomal maturation (de Lartigue et al., 2009; Martin et al., 2013; Sano et al., 2016). Interestingly, PIKfyve inhibition with YM206136 prevents autophagosome formation in cells (Vicinanza et al., 2015).

Furthermore, PIKfyve has in recent years been proposed to have a role in mTORC1 activity and TFEB regulation. However, the exact role of PIKfyve in this pathway remains elusive. In a recent study of autophagy in bacterial infections (xenophagy), treatment of infected macrophages with trehalose led to upregulation of xenophagy. The treatment led to a PIKfyve-mediated increase in $PI(3,5)P_2$, which activated mucolipin 1 (MCOLN1) and led to Ca^{2+} release from the lysosomal lumen (Sharma et al., 2020). The release of Ca^{2+} activates calcineurin, which dephosphorylates and activates TFEB, leading to nuclear translocation of TFEB (Medina et al., 2016). Additionally, PIKfyve was shown to activate MCOLN1 in the context of phagosome acidification (Isobe et al., 2018). Although additional studies have supported the role of PIKfyve in TFEB localisation through $PI(3,5)P_2$ synthesis, their findings appear contentious. It was reported that nutrient deprivation, which conventionally causes nuclear TFEB translocation, leads to a decrease in $PI(3,5)P_2$ levels (Li et al., 2013). In another study, $PI(3,5)P_2$ appears to play a role in the activation and localisation of mTORC1 caused by insulin and amino acids, mediated by an interaction of $PI(3,5)P_2$ with Raptor (Bridges et al., 2012). However, inhibition of PIKfyve has been shown to cause nuclear accumulation of TFEB without affecting mTORC1 activity and cause impaired autophagic clearance (Gayle et al., 2017; Wang et al., 2015).

In addition to mTORC1, PIKfyve has been shown to be regulated by the mTORC1 activator Akt (PKB) in numerous studies (Er et al., 2014; Munoz et al., 2013). Upon insulin stimulation, Akt phosphorylates PIKfyve on S318, which leads to translocation of the glucose transporter GLUT4 from intracellular vesicles to the plasma membrane in 3T3 L1 adipocytes (Berwick et al., 2004; Hill et al., 2010). Mice with *PIKfyve* deletion

in striated muscles developed systemic glucose intolerance, which suggests that PIKfyve signalling is required for systemic glucose homeostasis (Ikonomov et al., 2013).

Mutations in *PIKfyve* are associated with François-Neetens Mouchétee corneal fleck dystrophy (CFD), which is a rare, autosomal dominant corneal dystrophy characterized by numerous small white flecks scattered in the stroma (Boisset et al., 2008; Li et al., 2005). Although, there is no direct link between PIKfyve and neurodegeneration, there is increasing association of the PIKfyve complex and $PI(3,5)P_2$ with neurodegenerative diseases. Mutations identified in the *FIG4* gene lead to neurodegeneration in humans including Charcot-Marie-Tooth syndrome type 4J (CMT4J) and Amyotrophic Lateral Sclerosis (ALS) (Chow et al., 2007, 2009). Furthermore, *ArPIKfyve* KO mice displayed reduced levels of $PI(3,5)P_2$ and profound neurodegeneration (Zhang et al., 2007). Additionally, studies show that PIKfyve interacts with APP, which as mentioned above plays a central role in AD. Overexpression of APP increased the number of $PI(3,5)P_2$ positive vesicles in multiple cell lines. Conversely, knockdown of APP reduced the number of $PI(3,5)P_2$ positive vesicles, suggesting that APP is able to stimulate PIKfyve activity. Interestingly, deletion of APP led to vacuolation in cells, suggesting that PIKfyve dysfunction, albeit not a causal factor, could be involved in exacerbation of neurodegenerative pathologies (Currinn et al., 2016).

1.5.2 PIKfyve and AMPK intersection

In addition to its role in upregulating autophagy, AMPK plays a role in activating catabolic energy-releasing pathways in response to physical exercise, leading to contraction-mediated glucose uptake in skeletal muscles. Similar to the inverse effect of Akt on autophagy, upon insulin signalling Akt activates anabolic pathways that promotes storage of energy substrates, thus counteracting the effects of AMPK.

In 2013, Liu et al. showed that PIKfyve interacts with AMPK and is phosphorylated by AMPK on S307. This led to an increase in PIKfyve activity and $PI(3,5)P_2$ synthesis, which was shown to be involved in contraction-induced glucose uptake in skeletal muscle (Liu et al., 2013).

While it remains unknown whether the interaction between PIKfyve and AMPK may have a role in autophagy, two recent studies link AMPK-mediated PIKfyve activation to maintaining lysosomal function through $PI(3,5)P_2$ synthesis. AMPK activates PIKfyve, causing an increase in $PI(3,5)P_2$, which leads to increased activation of MCOLN1, thus proposing a role for AMPK in lysosomal catabolism (Fernandez-Mosquera et al., 2019). In a study focused on scaffolding complexes that regulate endosome sizes, such as the biogenesis of lysosome-related organelles complex 1 (BLOC-1) and the late endosomal/lysosomal BLOC-1-related complex (BORC), deletion of components of the BORC complex led to an increase in $PI(3,5)P_2$ levels (Yordanov et al., 2019). The increase in lipids were abrogated upon AMPK inhibition with Compound C also known as dorsomorphin, which led the authors to propose that the BORC complex regulates PIKfyve activity by acting on AMPK for lysosomal reformation. The exact mechanism behind this function remains to be elucidated.

PIKfyve is involved in the endo-lysosomal system through its synthesis of $PI(3,5)P_2$. However, the physiological importance of PI(5)P has yet to be dissected. Furthermore, the abovementioned evidence suggests that PIKfyve is activated by AMPK upon stimuli that activates catabolic processes. This raises the question of whether the increase in PI(5)P-containing phagophores observed by Vicinanza et al. (2015) upon glucose starvation could be due to an AMPK-mediated activation of PIKfyve and play a role in the well-known AMPK-mediated autophagy upregulation upon energy depletion.

1.6 Research objectives

Since studies suggest that canonical autophagy is impaired in many neurodegenerative diseases, the potential of upregulating non-canonical autophagy holds great therapeutic value. As earlier research showed that autophagy can be upregulated in a VPS34-independent, PI(5)P-dependent manner upon glucose starvation, in the present study I sought to elucidate the mechanism leading to upregulation of PI(5)P-dependent autophagy.

Given that AMPK is a master regulator of autophagy, activated as a response to low energy levels and since PI(5)P signalling has been shown to play a role in the autophagy response upon glucose starvation, I explored the link between AMPK and PIKfyve signalling in the context of autophagy upregulation as a response to glucose starvation.

In the present study, I aimed to first investigate the importance of AMPK for activating the PI(5)P-dependent autophagic machinery using genetic and pharmacological manipulations in cellular systems and next to define the PIKfyve interactome involved in autophagosome formation.

2 Materials and Methods

2.1 Materials

2.1.1 Antibodies

The list of primary antibodies used in this study and their corresponding dilutions are shown below.

Table 2 | Primary antibodies used in this study

Antibodies	Host	Dilution	Source	Identifier
anti-P-ACC (S79)	rabbit	WB 1:1000	Cell Signaling	#11818S RRID:AB_2687505
anti-ACC	rabbit	WB 1:1000	Cell Signaling	#4190 RRID:AB_10547752
anti-actin	rabbit	WB 1:5000	Sigma-Aldrich	A2066 RRID:AB_476693
anti-AMPKα	rabbit	WB 1:1000	Cell Signaling	#2532 RRID:AB_330331
anti-ATG16L1	rabbit	WB 1:1000	Cell Signaling	#D6D5 RRID:AB_10950320
anti-CD63	mouse	IF 1:200	Abcam	#ab8219 RRID:AB_306364
anti-FLAG	rabbit	WB 1:1000	Sigma-Aldrich	F7425 RRID:AB_439687
anti-FLAG M2	mouse	IF 1:400	Sigma-Aldrich	F3165 RRID:AB_259529
anti-GAPDH	mouse	WB 1:5000	Abcam	#ab8245 RRID:AB_2107448
anti-GFP	rabbit	WB 1:1000	Abcam	#ab6556 RRID:AB_305564
anti-GST antibody [3G10/1B3]	mouse	WB 1:1000	Abcam	#ab92 RRID:AB_307067
anti-HA.11 clone 16B12	mouse	WB 1:1000	Covance	#MMS-101P RRID:AB_10064068
Normal IgG	rabbit	IP 1 µg	Cell Signaling	#2729S RRID:AB_1031062
anti-LC3B	rabbit	WB 1:2000	Abcam	#ab192890 RRID:AB_2827794
anti-myc 9E10 tag	mouse	WB 1:1000	Abcam	#ab206486 RRID:AB_2861226
anti-P-PIKfyve (S307)	rabbit	WB 1:1000	Abcam	#ab62467 RRID:AB_946301
anti-PIKfyve	rabbit	WB 1:1000 IP 5 µg	Abcam	#ab137907

anti-ULK1	rabbit	WB 1:1000	Cell Signaling	#4773S RRID:AB_2288252
anti-p70 S6K1	rabbit	WB 1:1000	Cell Signaling	#9202 RRID: AB_331676
anti-P-p70 S6K1 (T389)	rabbit	WB 1:1000	Cell Signaling	#9204 RRID: AB_2269803
anti-ULK1	rabbit	IF 1:200	Proteintech	#20986-1-AP RRID:AB_2878783
anti-V5 tag	mouse	WB 1:1000	Thermofisher	#R960-25 RRID:AB_2556564
anti-WIPI1	rabbit	WB 1:1000	Abcam	#ab128901 RRID:AB_11145255

The secondary antibodies used for immunofluorescence were conjugated to Alexa Fluor 488 or 555 (Invitrogen). Secondary antibodies used for western blot analysis included anti-mouse and anti-rabbit HRP-conjugated antibodies from GE Healthcare and anti-mouse 800 and anti-rabbit 680 LI-COR antibodies.

2.1.2 Plasmids, oligonucleotides and siRNAs

The list of plasmids, oligonucleotides and siRNAs used are shown below.

Table 3 | Plasmids used in this study

Recombinant DNA	Source	Identifier
pAMPK α2 WT	Addgene	#15991
pAMPK α2 K45R	Addgene	#15992
pcDNA3-FLAG-LKB1	Addgene	#8590
pRK5 mULK1	Addgene	#31960
pRK5 mULK1 M92A	Addgene	#31962
pEGFP-C1	Clontech	N/A
pcDNA3.1-myc-DDK	Invitrogen	N/A
pcDNA3.1-HA	Invitrogen	N/A
GFP-PHD3x	Gift by B. Payrastre	N/A
GFP-MLN1	Gift by H. Xu	N/A
Myc-PIKfyve WT	Gift by A. Shisheva	N/A
Myc-PIKfyve K1831E	Gift by A. Shisheva	N/A
pCMV5-HA-PIKfyve WT	Gift by A. Shisheva	N/A
pCMV5-HA-PIKfyve ΔFYVE	Gift by A. Shisheva	N/A
pCMV5-HA-PIKfyve ΔCpn	Gift by A. Shisheva	N/A
pCMV5-HA-PIKfyve 199-1421	Gift by A. Shisheva	N/A
pCMV5-HA-PIKfyve 1-1435	Gift by A. Shisheva	N/A
GFP-PIKfyve WT	Gift by J. Tavare	N/A
GFP-PIKfyve S307A	Gift by J. Tavare	N/A
pLJM1-FLAG-Raptor-RHEB15	Addgene	#26634
pcDNA3-HA ULK1 WT	Gift by H.G. Wang	N/A
pcDNA3-HA ULK1 1-828	Gift by H.G. Wang	N/A
pcDNA3-HA ULK1 278-828	Gift by H.G. Wang	N/A
pcDNA3-HA ULK1 654-828	Gift by H.G. Wang	N/A
EGFP-HTT(Q74) was previously characterized Ashkenazi et al., 2017		
FLAG-ATG4BC74A has been described elsewhere Cadwell et al., 2008		
mRFP-GFP-LC3 has been described elsewhere Kimura et al., 2007		

Table 4 | Oligonucleotides used in this study

Plasmid	Primer sequence	Source
PIKfyve S307A (myc)	sense: 5'-CAGTGACAGATTAGTAATGGCGGCTGATCTGTTTCGAGCA-3'	Thermofisher
	antisense:5'-TGCTCGAAACAGATCAGCCGCCATTACTAATCTGTCACTG-3'	Thermofisher
PIKfyve T309A (HA)	sense: 5' GATCCAGTGACAGATTAGCAATGCTGGCTGATCTGTT-3'	Thermofisher
	antisense: 5'-AACAGATCAGCCAGCATTGCTAATCTGTCACTGGATC-3'	Thermofisher
PIKfyve S327A (HA)	sense: 5'-GCCTGGGGACTGACAGCTGTCTCATATGAAGGA-3'	Thermofisher
	antisense: 5'-TCCTTCATATGAGACAGCTGTCAGTCCCCAGGC-3'	Thermofisher
PIKfyve S710A (HA)	sense: 5'-TTCTCTATAGAGATACTCAATAGCACACTTCAACAGAAGGATTTTGG-3'	Thermofisher
	antisense: 5'-CCAAAATCCTTCTGTTGAAGTGTGCTATTGAGTATCTCTATATGAGAA-3'	Thermofisher
PIKfyve S1548A (HA)	sense: 5' GAAGTCCTGGAGCAATATTCCTTGGAGATGTGTCC-3’	Thermofisher
	antisense: 5'-GGACACATCTCCAAGGAATATTGCTCCAGGACTTC-3’	Thermofisher
PIKfyve S1548D (HA)	sense: 5’-TGTGAAGTCCTGGATCAATATTCCTTGGAGATGTGTCCATTGC-3’	Thermofisher
	antisense: 5’-GCAATGGACACATCTCCAAGGAATATTGATCCAGGACTTCACA-3’	Thermofisher
PIKfyve S1862A (HA)	sense: 5'-AAAGCAGCTCCTGCCTTGCCTCCCCGG-3’	Thermofisher
	antisense: 5'-CCGGGGAGGCAAGGCAGGAGCTGCTTT-3’	Thermofisher
PIKfyve K2000E (myc)	sense: 5'-TTCACAACCATCTCAAGCTCTTTGTCCCATGTAAATGTTCGAATGTAATCT-3'	Thermofisher
	antisense: 5'-AGATTACATTCGAACATTTACATGGGACAAAGAGCTTGAGATGGTTGTGAA-3'	Thermofisher

2.1.3 Reagents

The list of reagents used are shown below and described in 2.2.5.

Table 5 | Reagents used in this study

Chemicals, Peptides, and Recombinant Proteins	Target	Concentration/Time	Source	Identifier
Bafilomycin A1	Lysosomal inhibitor	400 nM, 4 hours	Enzo	#BML-CM110
991	AMPK activator	10 µM, 1 hour	Glixx Labs Inc	#AOB8150
AICAR	AMPK activator	10 µM, 1 hour	Sigma Aldrich	#A9978
A769662	AMPK activator	10 µM, 1 hour	Cambridge Bioscience	#SM08-10
SBI-0206965	ULK1 inhibitor	5 µM, 4 hours	Sigma Aldrich	#SML1540
Compound C	AMPK inhibitor	60 µM, 6 hours	Merck	#171260
Rapamycin	mTORC1 inhibitor	200 nM, 48 hours	LC Laboratories	#R-5000
YM206136	PIKfyve inhibitor	100 nM, 1 hour	Merck	#524611
NIH-12848	PIP5K2C inhibitor	0.5 -1 µm, 48 hours	Cambridge Drug Discovery Institute	NA
Torin1	mTOR inhibitor	1 µm, 4 hours	Tocris	#4247/10
PI(5)PdiC16		In vitro kinase assay: 100 – 6 µM Cell treatment: 400 µM, 48 hours	Echelon	# P-5016
PIdiC16, PI(3)PdiC16, PI(3,5)P_2diC16		100 µM	Echelon	#P-0016 #P-3016 #P-3516
Recombinant Human ULK1		10 ng	Thermofisher	#PV6430
Recombinant Human-ING2		10 nM	Creative Biomart	#5130H
Purified VPS34		10 ng	Purified in lab	
LysoTracker Red DND-99		1 µM, 5 minutes	Molecular Probes.	#L7528

2.2 Methods

2.2.1 Cell Culture

Human cervical cancer (HeLa) cells, human embryonic kidney 293 (HEK 293T) cells, striatal progenitor cells (SPC) and mouse embryonic fibroblasts (MEFs) were cultured in basal media: Dulbecco's Modified Eagles Medium (DMEM; Sigma D6546), supplemented with 10% fetal bovine serum (FBS; Sigma F7524), 100 units/ml penicillin-streptomycin (Sigma P0781) and 2 mM L-glutamine (Sigma G7513) at 37°C, 5% CO_2. SPCs were incubated in 33°C. AMPK α1/α2 double knock-out (dKO) MEFs were a gift from Prof. Benoit Viollet. BECN KO HeLa cells were a gift from W. Wei (Peking University). All cell lines were routinely tested for mycoplasma contamination.

Cells were passaged when reaching approximately 90% confluency in T75 (75 cm^2 area) flasks (Corning). Cells were passaged by pre-washing with 10 ml phosphate buffered saline (PBS) once to remove FBS and then digested with 2 ml Trypsin-EDTA solution (Sigma-Aldrich) at 37°C for 5 minutes. The trypsin was inactivated by adding 8 ml complete basal media to the flask and cells were collected into a 15 ml tube and seeded onto plates, as per experimental requirement.

For glucose starvation, cells were washed twice with PBS and cultured in glucose-free, sodium pyruvate free and L-glutamine free DMEM (Gibco, #A1443001) supplemented with serum (Invitrogen), for 1 hour. Cell transfection was performed with TransIT 2020 (Mirus) in Gibco™Opti-MEM I Reduced Medium (Gibco, #11524456) using the manufacturers' protocols. HEK 293T cells were seeded onto plates pre-coated with poly-D-lysine for 1 hour and washed twice with PBS before being equilibrated with basal media. HEK Expi293F suspension cells were grown in Expi293 Expression Medium (Gibco, #A1435101) in flasks (Corning Erlenmeyer sterile polycarbonate with 0.2 μm ventilated caps) on a shaker platform (125 rpm) in a humidified, CO_2 cell culture incubator.

2.2.2 Primary cultures

Primary neuronal cortical cells were dissected from the cortices of wildtype mouse embryos. The pregnant mice were sacrificed at day 16.5 of pregnancy (E16.5) by cervical dislocation and the embryos were removed from the placenta using small-

sized scissors and tweezers. Embryos were transferred to a petri dish containing cold Hanks Balanced Salt Solution (HBSS) (Gibco). The brains were isolated from the heads and transferred to another petri dish containing HBSS. The two hemispheres were separated by cutting down through the midline of the brain. The meninges was removed under a magnifier and the cortex was separated from the striatum, hippocampus and cerebellum. The cortices were transferred to a small petri dish with cold HBSS on ice. After dissection of the brains, the cortices were transferred to a 15 ml tube. Next, 10 ml pre-warmed 0.25% Trypsin-EDTA (Gibco) and 150 µl 0.1% DNase (2000 Units/mg) (Sigma-Aldrich) were added per eight embryo cortices. The cortices were incubated at 37°C in a water bath for 15 minutes. The trypsin was discarded and 10 ml pre-warmed HBSS with 10% FBS was added to the cortices to inactivate the trypsin. After turning the tube upside down three times and waiting for the cells to sink to the bottom of the tube, the media was discarded and 10 ml pre-warmed HBSS was added and the tube was turned upside down three times to wash the solution to prevent growth of glial cells. After removing the HBSS, 5 ml pre-warmed Neurobasal medium (Life Technologies) with GlutaMAX 100X supplement (1X; Life Technologies), Sodium pyruvate 100X (1X; Life Technologies), B27 supplement (200 mM; Life Technologies), and Pen/Strep (50 mg/ml; Sigma-Aldrich) were added to the tube and mechanical dissociation of the tissue was performed by pressing the pipette tip against the bottom of the tube and resuspending. The solution now containing cells was filtered in a 50 ml tube using a 70 µm cell strainer (Falcon). The cells were seeded on 12-well plates. The plates had been pre-treated with PDL 50 mg/ml overnight and washed three times with H_2O and then equilibrated with Neurobasal medium for 5 minutes before adding the cells. Cells obtained from each embryo yielded one plate. After 2 hours, the media was replaced with fresh media. After 3 days, half of the media was collected and stored in 4°C as conditioned medium and fresh neurobasal medium was added to the wells. Cells were used after 7 days *in vitro* (DIV).

2.2.3 Plasmid production and transfection

Plasmid production was achieved using high-efficiency DH5α competent *Escherichia coli* (Bioline US Inc). The transformation was performed by mixing 100 ng purified plasmid DNA and 20-50 µl competent cells thawed on ice. The mixture was incubated on ice for 30 minutes, before being subjected to 40-60 seconds heat shock and then placed in 42°C for 1 minute using a water bath and incubated on ice again for 2

minutes. The cells were cultured in 1 ml Luria Broth (LB) medium in 37°C incubator for 45 minutes. Next, 200 µl suspension was distributed evenly onto a 10 cm LB agar plate with the appropriate antibiotic for selection. The plates were cultured at 37°C overnight. Colonies obtained from the agar plates were inoculated in 200 ml LB supplemented with antibiotic and incubated at 37°C, after which plasmid isolation was performed using a Maxi Prep isolation kit (Life technologies #K210017). First, cells were spun down at 8000 rpm for 30 minutes and DNA was isolated per manufacturer's protocol. The concentration was measured with a spectrophotometer (NanoDrop1000, Thermo Scientific) using solvent as blank.

Transfections were performed either on cells seeded on 6-well plates with or without glass coverslips depending on the purpose of the experiment or on 140 mm dishes using TransIT 2020 (Mirus Bio #MIR5400). For each well, DNA plasmid constructs were added to 100 µl pre-warmed OPTIMEM reduced-serum medium (Gibco) in a sterile tube. Mirus (DNA:Mirus ratio of 1:3) was added to 100 µl OPTIMEM and incubated for 5 minutes. The two tubes were mixed and then incubated for 20-30 minutes. The DNA-Mirus mixture was gently transferred to the wells containing 800 ml complete medium. The media was replaced the following day. For transfection of cells seeded on 140 mm dishes, the amounts used were scaled up.

HEK Expi293F cells at 95% viability were transfected with PEI Max (Polysciences, #24765–1). Following day, 3.3 mM valproic acid (Sigma Aldrich) and 10 mg/mL Penicillin/Streptomycin (Sigma Aldrich) was added to the media.

2.2.4 Site-directed mutagenesis

Site-directed mutagenesis is a method used to introduce targeted mutations in a double-stranded DNA. Point mutations were introduced into myc-PIKfyve or HA-PIKfyve constructs using the QuikChange Multi Site-Directed Mutagenesis kit (Agilent, #200515) according to the manufacturer's instructions. Primers (Table 4) were designed using the Agilent primer design tool

(https://www.agilent.com/store/primerDesignProgram.jsp).

The PCR mixture (1×QuikChange Multi reaction buffer, QuikSolution (0.75 µl/reaction), DNA template (100 ng), sense and antisense primers (100 ng/primer),

dNTP mix (1 µl/reaction), QuikChange Multi enzyme blend (1 µl/reaction)) was assembled. A PCR reaction used in a reaction with the followed cycling parameters:

Table 6 | The PCR conditions used for site-directed mutagenesis

Segment	Cycles	Step	Temperature	Time
1	1	Initial denaturation	95ºC	1 minute
2	30	Denaturation	95ºC	1 minute
		Annealing	55ºC	1 minute
		Extension	65ºC	2 minutes/kb – total 23 minutes

Next the PCR mixture was treated with 10 U/µl DpnI restriction enzyme at 37°C for 2 hours to digest the parental, non-mutated dsDNA. Obtained vectors were transformed into *E. Coli* as mentioned above

2.2.5 Cell treatments

For glucose starvation, cells were washed twice with PBS and cultured in DMEM free from glucose (Gibco, #A1443001), sodium pyruvate and L-glutamine for 1 hour (Invitrogen).

Cells were treated with compounds in the concentrations and time points listed in **Table 5**. The compounds were dissolved in DMSO, which was used as a vehicle control in equivalent volumes.

Bafilomycin A1 (BafA1; Sigma-Aldrich) treatment was started 4 hours before lysis of cells at a final concentration of 400 nM to inhibit autophagosome-lysosome fusion in experiments assessing autophagy flux by western blot analysis. An equivalent volume of DMSO was used as control in these experiments.

Primary neuronal cultures were treated with PIP4K2γ inhibitor (provided by the Cambridge Drug Discovery Institute) for 48 hours at final concentrations between 0.5-1 µM. Media with compounds was replenished every 24 hours with fresh medium with compounds.

To visualise lysosomes, 1 μM LysoTracker Red was added to cells 5 minutes prior to fixation with 4% PFA.

2.2.5.1 Treatment with exogenous lipid

Unlabeled PI(5)P and carrier (Echelon) were reconstituted in H_2O:tert-BuOH (9:1) solution. After 1 minute bath sonication and vortex for 1 minute, carrier and lipids were combined at a 1:1 ratio for 10 minutes at room temperature. The mixture of lipids and carrier was diluted in HBSS in a final concentration of 10 μM and transferred to wells containing primary cultures in the presence and absence of BafA1. Carrier only was used as a negative control.

2.2.6 Immunofluorescence

For general immunofluorescence, cells seeded on glass coverslips were fixed with 4% paraformaldehyde (PFA) in PBS for 10 minutes. All steps were carried out at room temperature. Cells were next washed with 0.1% glycine in PBS for 1 minutes and permeabilised with 0.1% Triton X-100 in PBS for 10 minutes. Next, the cells were blocked with 1% BSA in PBS (blocking buffer) for 30 minutes, before incubation with primary antibody in blocking buffer for 1 hour followed by three washes with PBS for 5 minutes. Cells were then probed with secondary antibody in blocking buffer for 1 hour and washed three times with PBS for 5 minutes and once with H_2O, after which the coverslips were mounted with a drop of ProLong Gold Antifade Reagent (Molecular Probes) and stored at 4°C in the dark.

The experiments visualising mRFP-GFP-LC3 were fixed for 5 minutes. Coverslips were mounted with a drop of ProLong Gold Antifade Reagent (Molecular Probes).

2.2.7 Cell and tissue lysis and western blot analysis

Cells seeded on 6-well plates were washed with ice-cold PBS and lysed with 200 μl 2X Laemmli sample buffer (62.5 mM Tris pH 6.8, 2% w/v SDS, 10% glycerol, 50 mM DTT, 0.01% w/v bromophenol blue) supplemented with protease (Roche) and phosphatase inhibitors cocktails (Sigma Aldrich) and boiled for 10 minutes at 100°C.

Mice tissue samples were lysed in RIPA buffer (50 mM Tris-HCl pH 7.4, 150 mM NaCl, 1% Triton X-100, 0.5% sodium deoxycholatemonohydrate, 0.1% SDS), The

homogenate was centrifuged at 13400 rpm for 15 minutes at 4°C to pellet the debris and the protein concentration of supernatants was determined using a DC Protein Assay (Bio-Rad).

Tissue and cell lysates were loaded onto freshly prepared 7-15% acrylamide gels, depending on the size of the protein of interest and separated by SDS-PAGE in Tris-Glycine running buffer (25 mM Tris, 192 mM glycine, 0.05% SDS). SeeBlue Plus2 Prestained Protein Standard (ThermoFisher LC5925) was used as molecular weight marker. Proteins were transferred onto pre-activated (with methanol) PVDF or nitrocellulose membranes (Millipore) in Tris-Glycine buffer with 20% methanol for 45-70 minutes, depending on the size of the protein of interest (Immobilon-FL for LiCor detection, Immobilon-P for ECL detection; Merck-Millipore IPFL00010 and IPVH00010, respectively). Membranes were incubated first in either 5% milk in PBS with 0.01% Tween (PBS-T) or 5% bovine serum albumin (BSA) in TBS with 0.01% Tween (TBS-T), as per manufacturers' directions. After 1 hour blocking at room temperature, membranes were probed with primary antibody in blocking buffer overnight at 4°C on a shaker. Next, the membranes were washed three times with PBS-T/TBS-T. Membranes were then probed with secondary antibody in blocking buffer for 1 hour at room temperature. Membranes were next washed three times with PBS-T/TBS-T and once with PBS/TBS. The proteins were commonly visualized using fluorescent dye-labelled secondary antibodies and infrared fluorescence detection on an Odyssey Imager (LI-COR). This method enabled quantification of protein levels (relative to loading control) using Image Studio Lite software (LICOR). For some protein targets, horseradish peroxidase-linked secondary antibodies (Amersham Biosciences) were used in conjunction with enhanced chemiluminescence detection reagents (GE Healthcare) and X-ray film exposure to visualize the proteins. The protein levels were then quantified using ImageJ.

2.2.8 Immunoprecipitation

HEK 293T cells in 140 mm dishes were washed with PBS and lysed in ice-cold buffer. Cells were lysed in lysis buffer (0.5% NP-40, 10 mM Tris pH 7.5, 150 mM NaCl, 0.5 mM EDTA, protease inhibitors (Roche) and phosphatase inhibitors (Sigma Aldrich)). Lysates were incubated for 30 minutes on ice, followed by centrifugation at 16,100g for 10 minutes at 4°C and the post-nuclear supernatant were incubated with 20 µl pre-

washed GFP-Trap (ChromoTek# gtma-100) or myc-Trap (ChromoTek#ytma-100) Dynabeads per tube for 30 minutes at 4°C on a rotating wheel. GFP-Trap and myc-Trap Dynabeads were washed using lysis buffer three times.

Immunoprecipitation of endogenous proteins were performed using specific antibodies listed in **Table 2**. Supernatants were incubated with primary antibodies overnight at 4°C, followed by incubation with pre-washed Dynabeads™ Protein A or G (Invitrogen) for 2 hours at 4°C. Bound material was washed three times with lysis buffer, followed by a single wash with detergent-free buffer.

Dynabead-bound proteins were resuspended in 30 µl 1x Laemmli buffer and boiled for 10 minutes to detach the protein from the beads. Samples were analysed by Western blotting. Proteins were resolved by SDS-PAGE.

2.2.9 Lambda phosphatase treatment

Prior to treatment with Lambda phosphatase, the protein concentration was determined as described previously. Lambda phosphatase treatment was performed by incubating cell lysates with 100 Units of lambda phosphatase complemented with $MnCl_2$ per 125 ug lysates. Lysates were incubated in 30°C for 1 hour before immunoprecipitation was performed. For this experiment, phosphatase inhibitors were not added to the lysis buffer.

2.2.10 Protein purification

HEK Expi293F suspension cells (total of 1 L containing 2.5 billion cells) were transfected with HA-PIKfyve as described above. Cells were collected and lysed by homogenization in 50 mM HEPES (4-(2-hydroxyethyl)piperazine-1-ethanesulfonic acid) pH 8.0, 200 mM NaCl, 5% glycerol, protease inhibitors (buffer A) in a glass homogenizer. Lysates were cleared by centrifugation at 100,000xg for 20 minutes and incubated with 1 ml packed agarose HA resin (Sigma Aldrich) for 2 hours at 4°C. Resin was transferred to a gravity flow column and washed 10x with buffer A and twice with 50 mM NaCl. Resin-bound HA-PIKfyve was used in *in vitro* kinase assays. To optimise this protocol, 25 mL suspension containing $2.5x10^6$ ml^{-1} cells were transfected with HA-PIKfyve. Each day for 5 days, 1 mL cell suspension was collected and lysed.

Lysates from each day were loaded on a western blot to determine the optimum transfection.

2.2.11 *In vitro* kinase assay

In vitro kinase assay was performed using the Universal Kinase Activity Kit (R&D systems) according to manufacturer's instructions. A substrate mix containing resin-bound PIKfyve (15 µl of 1 ml) or VPS34 (10 ng) and ATP were mixed with recombinant ULK1 (10 ng) mixed with the nucleotidase CD39L2. The kinase reaction was performed in a 96-well microplate and the reaction was incubated for 15 minutes at room temperature. CD39L2 is used to selectively release a phosphate from ADP. Inorganic phosphates were detected with Malachite green for 20 minutes and measured using a microplate reader at 620 nm. The OD of the negative control was subtracted.

2.2.12 In vitro lipid kinase assay

An *in vitro* lipid kinase assay was performed as depicted in **Figure 2.1** based on the method described by Dowler et al. (2002). HA-PIKfyve was overexpressed in HEK 293T cells and immunoprecipitated as mentioned above. Dynabead-bound HA-PIKfyve immunoprecipitates were washed three times with RIPA buffer, twice with 50 mM HEPES, pH 7.4, 1 mM EDTA, 150 mM NaCl, three times with 100 mM Tris-HCl pH 7.5, 500 mM LiCl, twice with 10 mM Tris-HCl pH 7.5, 100 mM NaCl, 1 mM EDTA and twice with assay buffer (25 mM HEPES pH7.4, 120 mM NaCl, 2.5 mM $MgCl_2$, 2.5 mM $MnCl_2$, 5 mM β-glycerophosphate, 1 mM DTT). PI and PI(5)P (Echelon) were reconstituted to 1 mM stock in a 1:1 solution of methanol and chloroform. Reconstituted PI were dried in a glass tube before being reconstituted in lipid buffer (20 mM HEPES pH 7.5, 1 mM EDTA) and bath sonicated twice for 30 seconds. A kinase reaction was prepared including HA-PIKfyve, recombinant ULK1 and ATP for 15 minutes at 37°C in assay buffer with 50 µM ATP and 100 µM PIs. The reaction was stopped with 200 µL 1N HCL. Lipids were extracted with 1:1 chloroform:methanol, vortexed and centrifuged at 10,000g for 2 minutes. Upper layer was removed, lower layer was washed twice with 100 µl of 1:1 of methanol:1N HCL. The resulting layer was applied to a nitrocellulose membrane. PI(5)P was diluted in a 2:1:0.8 solution of methanol:chloroform:water in 5 serial dilutions starting with 100 µM and spotted on the same nitrocellulose membrane as standards. The membrane was air-dried at room

temperature for 1 hour. The membrane was incubated in blocking buffer (50 mM Tris-HCl pH 7.5, 150 mM NaCl, 0.1 % Tween-20, 2 mg/ml BSA) for 1 hour at room temperature and incubated overnight at 4°C with 10 nM GST-ING2 protein in 0.2% BSA in TBS-T. The following day, the membrane was washed 10 times over 50 minutes in TBS-T. Next, the membrane was incubated in a 1:2000 dilution of anti-GST monocolonal antibody in blocking buffer for 1 hour at room temperature, washed 10 times over 50 minutes in TBS-T. The membrane was next incubated for 1 hour with a 1:5000 dilution of DyLight Fluors-conjugated (Invitrogen) secondary antibody in TBS-T and washed 12 times over 1 hour in TBS-T. Immunoreactive bands were visualized with direct infrared fluorescence detection using LICOR-Odyssey apparatus. Densitometric analysis on the immunoblots was performed using IMAGE STUDIO Lite software.

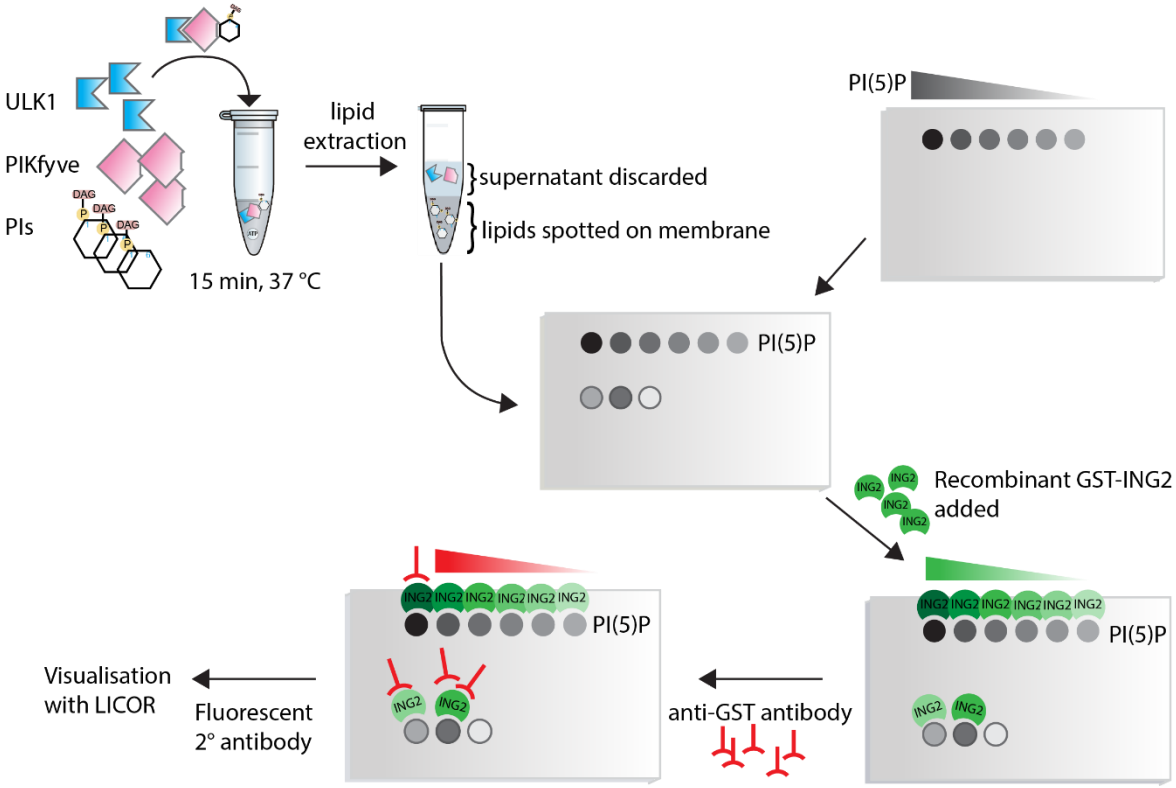

Figure 2.1 | The key steps of the lipid protein overlay assay

A schematic showing the principles of the lipid protein overlay assay.

2.2.13 Mass spectrometry

To identify possible phosphorylations of PIKfyve, samples were resolved using a pre-cast 4-12% Bis-Tris polyacrylamide gel (Invitrogen), stained using SimplyBlue SafeStain (Thermo Fischer Scientific) and the region expected to contain PIKFYVE excised. Proteins in the gel slice were reduced, alkylated and digested using trypsin and extracted for LC-MSMS analysis on an Orbitrap Fusion Lumos (Thermo Fischer Scientific) with an EASYspray source coupled to an RSLC nanoUPLC (Thermo Fischer Scientific). Peptides were fractionated using a 50 cm C18 PepMap EASYspray column using a gradient rising from 5% solvent B (80% MeCN, 0.1% formic acid) to 40% solvent B over 85 minutes. Solvent flow rate was 300 nl/minute and column temperature was 40°C. MS spectra were acquired between m/z 350 and 1500 with MSMS switching in a DDA fashion. HCD fragmentation at 30% collision energy was used with fragments scanned in the Orbitrap at 30,000 fwhm.

Raw files were processed using PEAKS Studio (version X, Bioinformatics Solutions Inc.) with the following parameters: Parent Mass Error Tolerance 15.0 ppm; Fragment Mass Error Tolerance 0.5 Da; Trypsin digestion; Human database (UniProt reference proteome downloaded 18 Dec 2018 containing 21066 proteins) with additional contaminant database (containing 246 common contaminants); oxidation (M), carbamidomethylation (C), phosphorylation (STY) as variable modifications at the PEAKS DB stage, 481 PEAKS built-in modifications at the PEAKS PTM stage; amino acid mutations identification enabled at the SPIDER stage; Modification Ascore confidence threshold >= 20.

2.2.14 Animals

In this study, WT and mRFP-GFP-LC3 mice were used under the jurisdiction of appropriate Home Office Project with local Ethics Committee approval. The mRFP-GFP-LC3 mice were generated in house by Dr. Fiona Menzies and Dr. Farah Siddiqi (Pavel et al., 2016). Both WT littermates and mRFP-GFP-LC3 mice were used after 2, 12, 18 and 24 months of age for various purposes. The mRFP-GFP-LC3 mice were perfused, as described below and the tails were collected for genotyping.

2.2.14.1 Perfusion

Mice were anesthetized by intraperitoneal Euthatal injections (0.100 ml/mice). The

paw and tail reflexes were checked to ensure that the mice were fully anesthetized. A perfusion system was used to fix the brains for cryostat sectioning. First, the abdominal skin was cut along the diaphragm with scissor. The tip of the sternum was grasped with forceps and an incision was made down the midline of the sternum to expose the heart. The syringe was placed in the apex of the left ventricle. Perfusion with 10 ml PBS buffer was initiated and the right auricle was cut to allow perfusion of the circulation. Next, 40 ml 4% PFA was connected to the system. Perfusion was done at a rate of 4 ml/minute. Muscle contractions and blanching of liver was indicative of successful fixation. The brain was removed from the skull and placed in a 10 ml tube with 4% PFA. After 3-4 hours, the PFA was removed and 30% sucrose in deionized H_2O was added. The brains in sucrose were placed in 4°C until the brains sank to the bottom of the tube. The two hemispheres were separated by cutting through the midline of the brain and each hemisphere was placed in cryo-embedding moulds in embedding media Optimal Cutting Temperature (OCT) (ThermoScientific), frozen on dry ice and stored at -80°C until sectioning.

2.2.14.2 Brain sectioning

The fixed brains were sectioned sagittally into 8 µm thick sections on a cryostat (Leica CM3050S). Sections were collected on Superfrost slides (ThermoScientific) and either air-dried for 1-2 hours for staining or stored at -80°C until further use.

2.2.15 Confocal Microscopy and Image Processing

Cells were imaged with a 63x objective with the LSM880 or LSM780 confocal microscope (Zeiss). For each condition, 3-5 images with a mean of 20 cells were taken. Exposure settings were unchanged throughout acquisition. Images were transformed into a tiff image. The scale bar for each image is 5 or 10 µm.

2.2.15.1 Quantification of puncta on brain slides

The brain sections from mRFP-GFP-LC3 expressing mice were imaged with a 63x objective with the LSM710 confocal microscope. For each mouse, 5 images were taken of the motor cortex and autophagosomes (mRFP-GFP) and autolysosomes (mRFP) were counted manually.

2.2.15.2 Quantification of puncta

For quantification of puncta, the intensity was set in control condition and maintained for each experiment. Micrographs were analysed using the Analyze Particles function on ImageJ for quantification of puncta per cell. GFP-PHD3x+ ATG16L1 puncta and mRFP-GFP-LC3 puncta were counted manually as described above. At least, 10-20 cells were counted per condition depending on the cell lines used and their transfection efficiencies.

2.2.15.3 Quantification of EGFP-HTT(Q74) aggregates

HeLa cells grown on coverslips in triplicates/condition were transfected with EGFP-HTT(Q74) using TransIT-2020 (Mirus) 48 hours before fixation, as previously described. The proportion of cells with at least one visible aggregate of EGFP-HTT(Q74) was scored out of the total number of the transfected cells counted. At least 250 cells were counted per coverslip in triplicates in three independent experiments, a method previously described in (Ravikumar et al., 2002).

2.2.16 Clustal Omega alignment

A multiple sequence alignment of PIKfyve across multiple species (human, mouse, rat, chicken, bovine, *C. elegans, Arabidopsis thaliana, S. cerevisiae*) was performed with the Clustal Omega tool provided by the EMBL-EBI. The highlighted green residue shows the PIKfyve S1548. These symbols are used to indicate amino acids aligned at the sites marked with the symbol.

"*****" indicates perfect alignment.

":" indicates a site belonging to group exhibiting strong similarity.

"." indicates a site belonging to a group exhibiting weak similarity.

2.2.17 Statistical analysis

For western blot analysis, the densitometry of bands was performed using either Image Studio (LI-COR) or ImageJ (for ECL protein revealing). The images analysed by ImageJ, were converted to an 8-bit format, inverted and the background was subtracted before measuring band intensity. The graphs depicting protein levels in cells show the mean from three independent experiments done in triplicates unless otherwise stated. To quantify the significant difference in levels between two groups, the P values were determined with two-tailed/one-tailed student's t-test in GraphPad

(Prism). If three independent experiments were combined, the controls were set to 1. In that case a paired two-tailed/one-tailed t-test was performed. For comparison between multiple treatment conditions in experiments with 3 or more conditions, a one-way ANOVA with a Tukey's post hoc test was performed in GraphPad with a confidence interval of 95%.

The error bar for each graph is the standard error of mean (SEM). *P $\leq$ 0.05, **P $\leq$ 0.01, ***P $\leq$ 0.001.

3 AMPK upregulates PI(5)P-dependent autophagy through PIKfyve activation

Autophagy was conventionally considered a PI(3)P-dependent pathway until studies reported the existence of non-canonical VPS34-independent autophagy pathways (Mcalpine et al., 2013a; Scarlatti et al., 2008; Vicinanza et al., 2015; Zhou et al., 2010). The mechanistic details of these non-conventional forms of autophagy remain yet to be elucidated.

The phosphoinositide PI(5)P has been implicated in upregulating autophagy upon glucose starvation in a VPS34-independent manner (Vicinanza et al., 2015).

PI(5)P is synthesized by the lipid kinase PIKfyve, which is an evolutionarily conserved protein. PIKfyve phosphorylates the D-5 position in PI and PI(3)P to make PI(5)P and PI(3,5)P_2, respectively (Sbrissa et al., 1999a) (schematic shown in **Figure 3.1**). PIKfyve has mainly been studied for its synthesis of PI(3,5)P_2 in the context of the endosomal/endocytic system, ever since it was found that a kinase-deficient PIKfyve mutant caused cytoplasmic vacuolation in multiple cell types (Ikonomov et al., 2001).

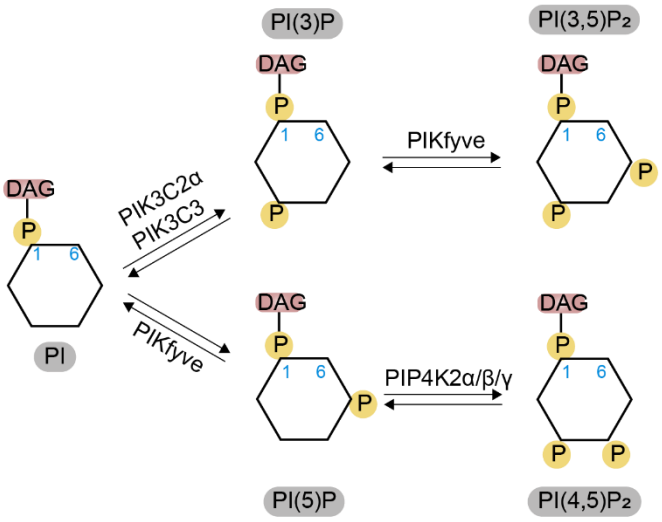

Figure 3.1 | Phosphoinositide conversion

Schematic of phosphoinositides (PI) and kinases involved in their metabolism. PIs have a glycerol backbone esterified to two fatty acid chains (DAG) and a phosphate on D1. DAG – diacylglycerol.

In 2013, Liu et al. showed that PIKfyve interacts with AMPK (Liu et al., 2013). The study showed that PIKfyve is phosphorylated by AMPK on S307. This led to an increase in PIKfyve activity and $PI(3,5)P_2$ synthesis, which was involved in contraction-induced glucose uptake in skeletal muscle (Liu et al., 2013). Since AMPK is a master regulator of autophagy, activated as a response to low energy levels (Hardie, 2011) and PI(5)P signalling was shown to play a role in the autophagy response upon glucose starvation (Vicinanza et al., 2015), I sought to study the link between AMPK and PIKfyve signalling in the context of autophagy upregulation.

3.1 Glucose starvation and AMPK activators induce autophagy

It is well-established that glucose starvation increases AMPK signalling and leads to an increase in autophagy (Ha et al., 2015). As I was interested in studying the role of AMPK in PI(5)P signalling in the context of glucose starvation-induced autophagy, I first determined the optimal starvation protocol and the effects of various AMPK activators on autophagy.

AMPK is a heterotrimer consisting of three subunits, α, β, γ. Upon phosphorylation of the α-subunit on T172 in the kinase domain by upstream kinases, such as LKB1 and binding of AMP to the γ-subunit, AMPK becomes activated (Adams et al., 2004). There are three types of AMPK activators, as described earlier – indirect activators, AMP analogues and direct activators. I decided to use direct activators and AMP analogues to minimise observations caused by off-target effects. To inhibit AMPK activity, I used the AMPK inhibitor Compound C (CC), also known as dorsomorphin. Although CC is effective in inhibiting AMPK, it also appears to have multiple off targets (Liu et al., 2014). This caveat was overcome by using genetic tools and AMPK-null cells later in this chapter.

3.1.1 Glucose starvation and AMPK activators induce AMPK activation

Prior to testing their effects on autophagy, I tested the effects of AMPK modulators and various durations of glucose starvation on AMPK activity to determine the optimal conditions in which to conduct experiments. I used glucose-free medium without sodium pyruvate and L-glutamine supplemented with serum. AMPK activity is monitored by the phosphorylation state of its substrate Acetyl-CoA carboxylase (ACC) on serine 79 (S79). I used immortalized SPCs derived from mice (Trettel et al., 2000;

Wheeler et al., 2000), since the AMPK activator A769662 was able to induce autophagy and ameliorate HD pathogenesis in these cells (Walter et al., 2016). I found that a time course of glucose starvation up to 2 hours increased AMPK activity after only 30 minutes **(Figure 3.2A-B)**. I also tested concentrations between 0.5-10 µm 991 for 1, 2 and 4 hours (data not shown) and found that 1 hour of 10 µm 991 was sufficient to induce AMPK activity **(Figure 3.2C-D**).

I then tested the selected conditions of glucose starvation and 991 treatment in HEK 293T cells to ensure that the observed changes in AMPK activity were consistent across multiple cell lines as various cell lines are used throughout this study for different purposes. Additionally, I treated the cells with the AMPK activators AICAR and A769662, and the AMPK inhibitor CC. The activation of AMPK was most efficient upon 991 treatment. The increase in AMPK activity upon glucose starvation was prevented by CC treatment **(Figure 3.2E-F)**.

Next, I confirmed that glucose starvation-mediated AMPK activation is abrogated in *AMPK α1/α2* dKO MEF cells (Laderoute et al., 2006) **(Figure 3.3)**.

Since 991 had the most consistent and profound effect on AMPK activity and it is known to have fewer off-targets than other AMPK modulators (Collodet et al., 2019), I mainly used this compound to induce AMPK activation throughout this study.

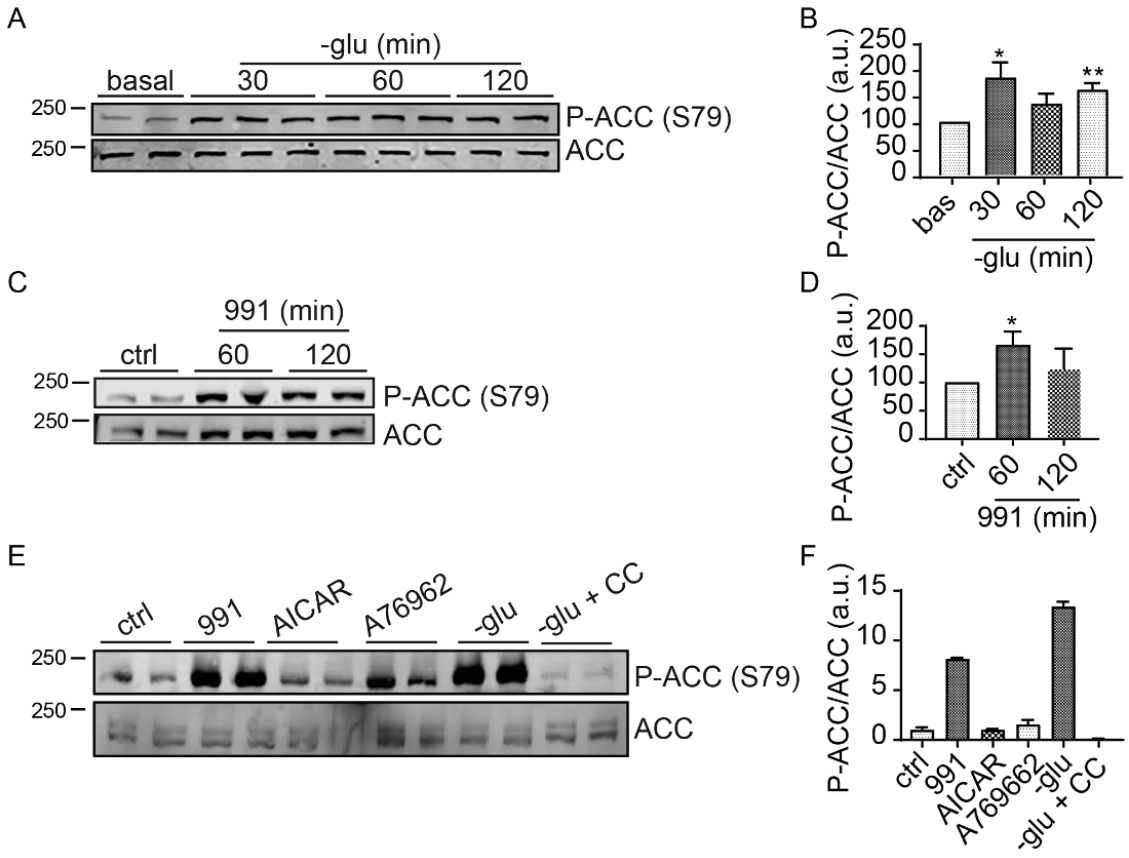

Figure 3.2 | AMPK is activated by glucose starvation and AMPK activators in SPCs and HEK 293T cells

AMPK activity is evaluated by assessing the phosphorylation of its substrate ACC on S79 by western blotting. **(A, B)** Total ACC and P-ACC (S79) immunoblots in SPCs. Cells were incubated in basal or glucose-free media (-glu) for 30, 60 or 120 minutes. Representative immunoblots are shown for triplicate experiments throughout the results chapters. Data show relative changes in P-ACC (S79) normalised to total ACC (n = 3). **(C, D)** Total ACC and P-ACC (S79) immunoblots in SPCs treated with the AMPK activator 991 or DMSO (ctrl) at 10 µM for 60 or 120 minutes. Data show relative changes in P-ACC (S79) normalised to total ACC (n = 3). **(E, F)** Total ACC and P-ACC (S79) immunoblots in HEK 293T cells treated with the AMPK activators 991, AICAR, A769662 (10 µM) or glucose-free media ± AMPK inhibitor Compound C (CC) for 1 hour. CC was added to cells 5 hours prior to glucose starvation (60 µM). Data show relative changes in P-ACC (S79) normalised to total ACC (mean ± SD of duplicate samples).
DMSO was used as vehicle control. Data are represented as mean ± SEM, unless otherwise stated (**P < 0.01, *P < 0.05; ANOVA with Tukey's post hoc test).

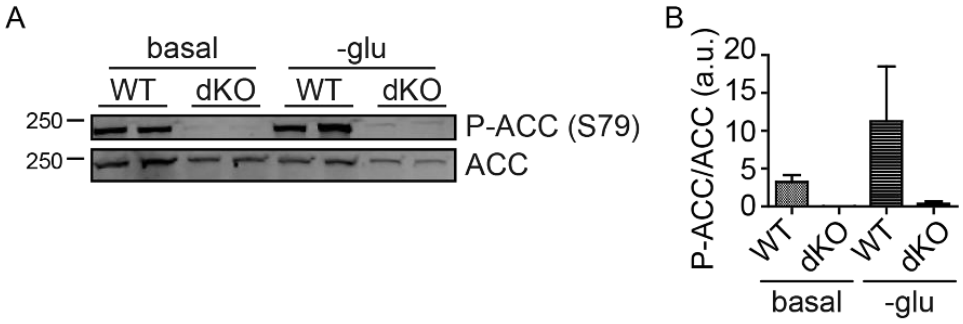

Figure 3.3 | ACC phosphorylation upon glucose starvation is impaired in AMPK dKO cells

(A) P-ACC (S79) and ACC immunoblots in AMPK dKO and WT MEFs incubated with basal or glucose-free media (-glu) for 1 hour. **(B)** Data show relative changes in P-ACC (S79) normalised to total ACC **(A)** represented as mean ± SD of duplicate samples. WT: wildtype; dKO: double knockout.

3.1.2 Glucose starvation and AMPK activation increases autophagic flux

Next, I assessed whether the selected AMPK activity-inducing conditions promoted autophagy. To assess autophagy flux upon glucose starvation and AMPK activation, I first determined the appropriate conditions in which to study glucose starvation and pharmacological AMPK activation in SPCs.

SPCs were transfected with the tandem tagged mRFP-GFP-LC3 reporter. As explained earlier, this construct allows the visualisation of autophagosomes and autolysosomes. The vesicles that emit both red and green signals are autophagosomes, while vesicles that emit only the red are acidic autolysosomes (Kimura et al., 2007). I found that upon 1 hour of glucose starvation and treatment with 991, the number of autophagosomes and autolysosomes increased in SPCs. The increase in autophagic vesicles upon glucose starvation was prevented with CC **(Figure 3.4).**

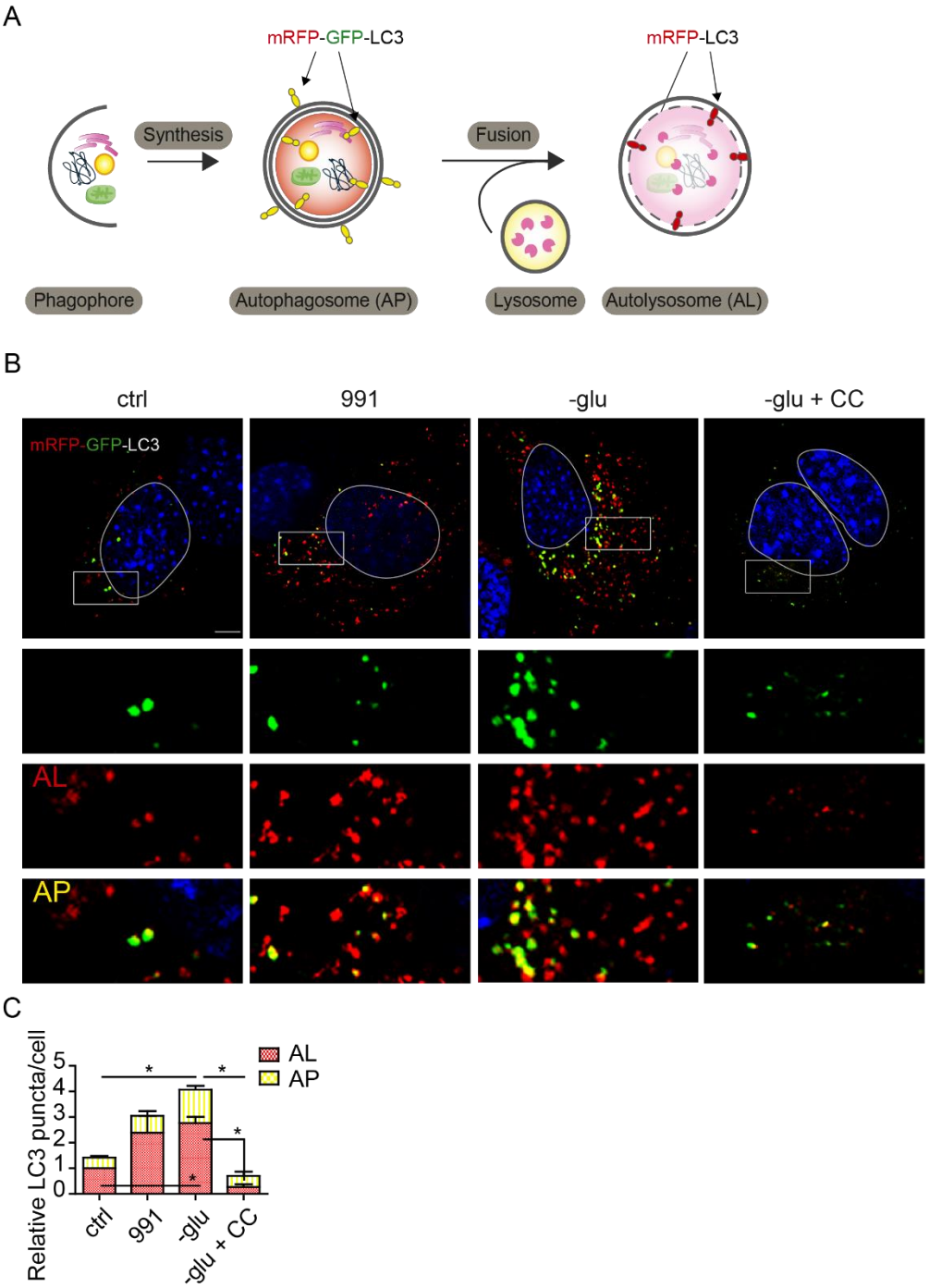

Figure 3.4 | Glucose starvation and AMPK activation increases autophagic flux

(A) Schematic model depicting the transient transfection of cells with mRFP-GFP-LC3. Due to the different pKa of the fluorescent tags (<4.5 for mRFP and ~6 for GFP), the autophagosomes (AP) emit both red (mRFP) and green (GFP) fluorescence, while the autolysosomes (AL) lose the GFP signal as it becomes quenched by the acidic lysosomal compartment and are visualised as red-only vesicles by microscopy. **(B)** SPCs transfected with mRFP-GFP-LC3 treated with 991 (10 µM, 1 hour) or glucose-free media (-glu, 1 hour) with CC (60 µM, 6 hours). DMSO was used as vehicle control. Representative micrographs shown. Scale bar, 5 µm. **(C)** Data show relative changes in autophagosomes (yellow dots) and autolysosomes (red dots) for experiment in **(B)**

normalised to AL in control represented as mean ± SEM (n = 3, 15-20 cells/condition, *P < 0.05; ANOVA with Tukey's post hoc test).

I next tested the effects of glucose starvation and AMPK activation on autophagy flux by western blotting. Autophagic flux was assessed by measuring LC3-II levels, which is a common marker of autophagosome abundance. During autophagy, cytosolic LC3 is cleaved by ATG4 to form LC3-I, which is then conjugated to phosphatidylethanolamine to form LC3-II localized on inner and outer autophagosome membranes (Kabeya et al., 2000). LC3-II levels positively correlate with the number and volume of autophagosomes in the cells. An increase in LC3-II on a western blot between control and treatment conditions could be due to increased autophagosome formation and/or impaired degradation (Klionsky et al., 2016; Tanida et al., 2005). In order to differentiate between these scenarios, LC3-II/autophagosome degradation can be blocked using a saturating concentration of Bafilomycin-A1 (BafA1), a potent inhibitor of the lysosomal V-ATPase, which impairs autophagosome degradation (see schematic in **Figure 3.5A**). Thus, increased levels of LC3-II in the presence of BafA1 correlates with increased autophagosome formation, while decreased levels indicate a reduction in autophagosome synthesis.

I observed a significant increase in LC3-II levels in both presence and absence of BafA1 upon glucose starvation in SPCs **(Figure 3.5B-C)** as expected based on previous findings (Endo et al., 2018; Maruyama et al., 2008; Williams et al., 2009). LC3 staining of SPCs showed an increase in LC3 puncta upon glucose starvation and 991 treatment **(Figure 3.5D-E)**. The AMPK inhibitor CC prevented the increase in LC3 puncta upon glucose starvation **(Figure 3.5D-E)**. Furthermore, I confirmed that LC3 puncta levels increased in HEK 293T cells upon glucose starvation, as these cells were used for immunoprecipitation experiments throughout this study **(Figure 3.5F-G)**.

I also tested the effects of glucose starvation and AMPK activation on WIPI1 levels. In conventional autophagy, increases in PI(3)P recruits WIPI proteins to phagophores and recruits downstream autophagy proteins (Backer, 2008; Dooley et al., 2014; Russell et al., 2014). WIPI1 and WIPI2 both localize to autophagosomes as a response to starvation (Dooley et al., 2014; Proikas-Cezanne et al., 2004). WIPI1

appears to be a reliable marker for autophagy levels, as it responds robustly to autophagy induction using rapamycin and starvation in a variety of cell lines (Proikas-Cezanne et al., 2007). I found that upon glucose starvation and treatment with AMPK activators, there was an increase in WIPI1 puncta in HeLa cells. The increase observed upon glucose starvation was prevented with AMPK inhibition **(Figure 3.6)**.

These findings confirm that pharmacological activation of AMPK and glucose starvation induces autophagy.

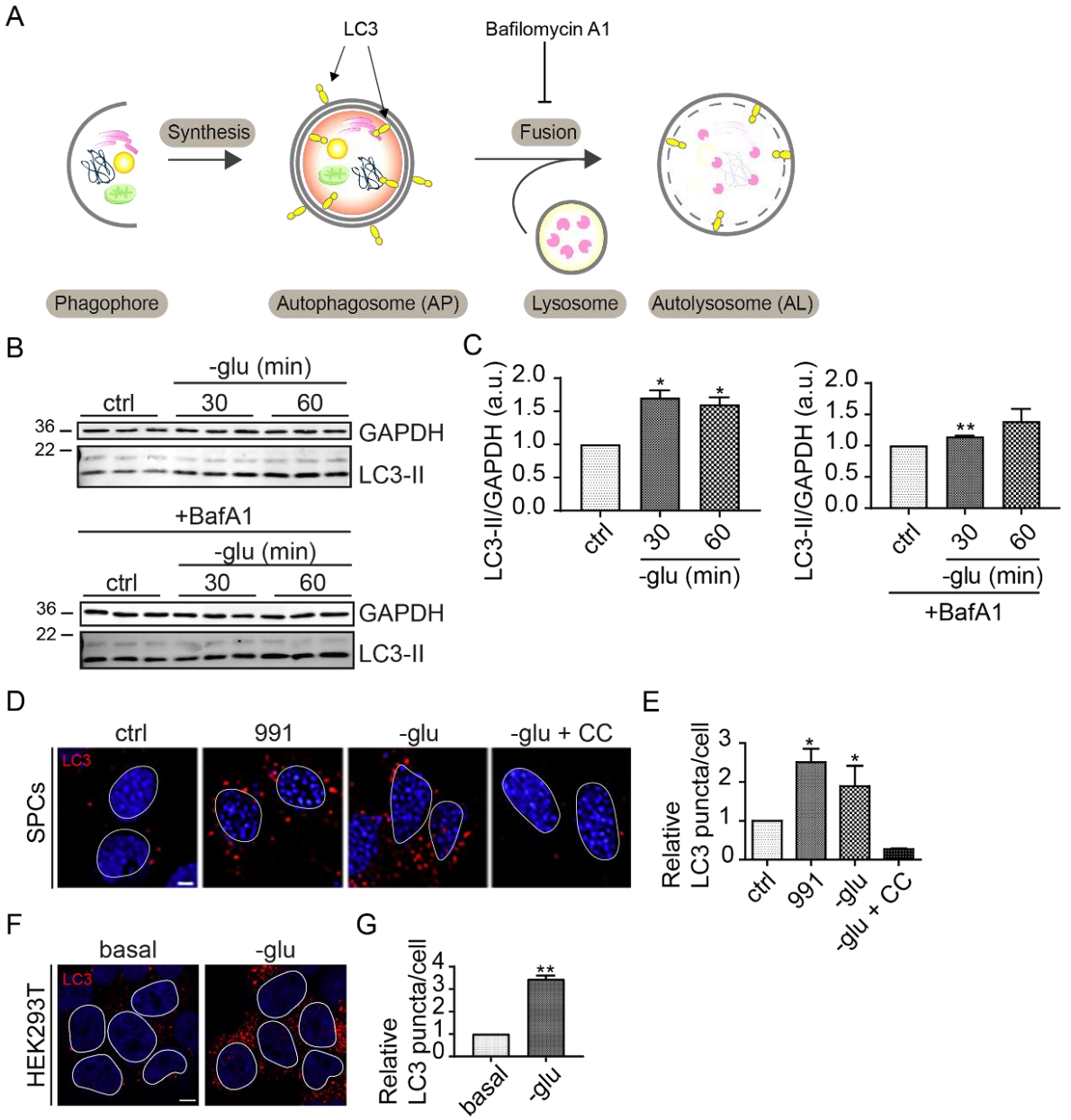

Figure 3.5 | Glucose starvation and AMPK activation increases LC3 levels

(A) Schematic depicting the autophagosome biogenesis and degradation. Bafilomycin A1 (BafA1) blocks autophagosome-lysosome fusion. **(B, C)** LC3-II immunoblots in SPCs incubated in glucose-free media (-glu) for 30 or 60 minutes ± BafA1 (400 nM), added to the cells 3 or 3.5 hours prior to glucose starvation for a total of 4 hours. GAPDH was used as loading control. Data show relative changes in LC3-II normalised to GAPDH (n = 3). **(D, E)** LC3 immunostaining (Alexa 555: rabbit) in SPCs treated with 991 (10 µM) or glucose-free media for 1 hour ± CC (60 µM, 6 hours). DMSO was used as vehicle control. Data show relative changes in LC3 puncta/cell normalised to control (n = 3, 30 cells/condition). **(F, G)** LC3 immunostaining (Alexa 555: rabbit) in HEK 293T cells in basal or glucose-free media (1 hour). Data show relative changes in LC3 puncta/cell normalised to basal (n = 3, 30 cells/condition; *P < 0.05; two-tailed, paired student's t-test).

Representative micrographs shown. Scale bar, 5 µm. Data are represented as mean ± SEM (**P < 0.01, *P < 0.05; ANOVA with Tukey's post hoc test, unless otherwise stated).

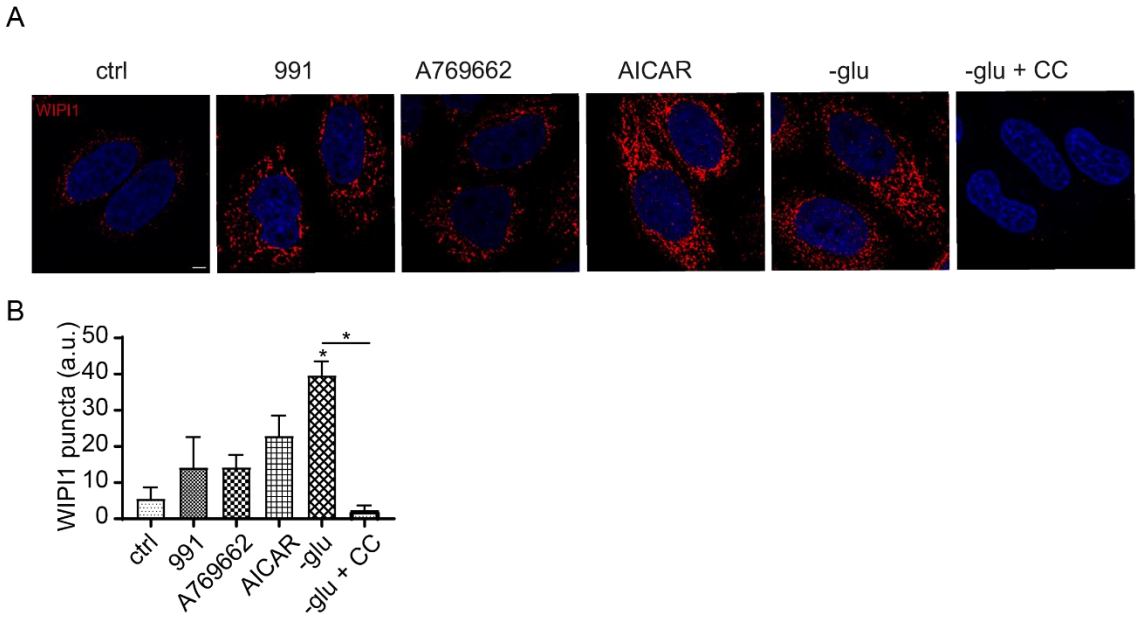

Figure 3.6 | Glucose starvation and AMPK activation increases WIPI1 puncta

(A) WIPI1 immunostaining (Alexa 555: rabbit) in HeLa cells transfected with FLAG-LKB1 and treated with 991, AICAR, A769662 (10 µM) or glucose-free media (-glu) ± CC (60 µM) for 1 hour. CC was added to cells 5 hours prior to glucose starvation for a total of 6 hours. DMSO was used as vehicle control. Representative images shown. Scale bar, 5 µm. **(B)** Data show relative changes in LC3 puncta/cell for experiment in **(A)** normalised to control represented as mean ± SEM (n = 3, 30 cells/condition, *P < 0.05; ANOVA with Tukey's post hoc test).

3.2 An increase in PI(5)P levels induces autophagy

Since a study from our lab showed that increased levels of PI(5)P in HeLa cells resulted in an increase in autophagy (Vicinanza et al., 2015), I first decided to replicate these findings in primary cortical neurons by subjecting primary cortical neurons to increased levels of PI(5)P and assessing changes in autophagy.

3.2.1 Treatment of primary cortical neurons with exogenous PI(5)P increases LC3-II levels

Upon addition of exogenous PI(5)P di-C16 to primary cortical neurons at DIV7, I observed a significant increase in LC3-II levels in both presence and absence of BafA1 suggesting that the increase in PI(5)P levels leads to an increase in autophagosome formation **(Figure 3.7)**, as shown by Vicinanza et al. (2015) in HeLa cells.

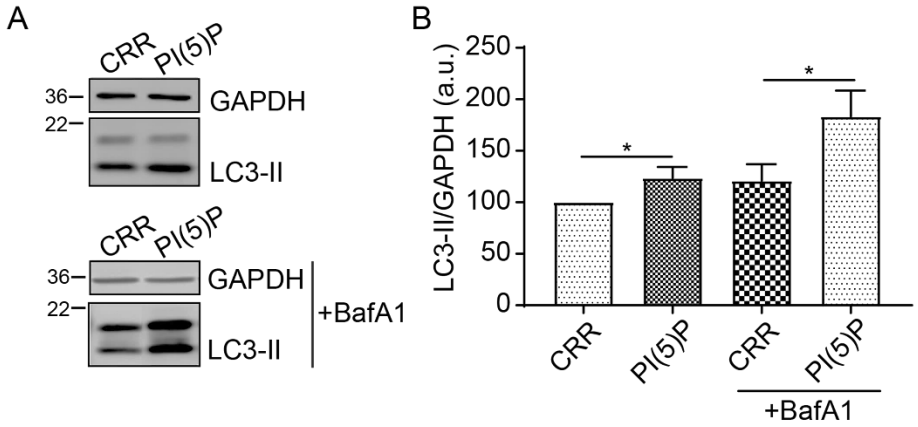

Figure 3.7 | Exogenous PI(5)P increase LC3-II levels in primary cortical neurons

(A) LC3-II immunoblots in primary cortical neurons DIV7 treated with exogenous PI(5)P (400 µM) or carrier (CRR) for 2 hours ± BafA1 (400 nM, 4 hours). GAPDH was used as loading control. **(B)** Data show relative changes in LC3-II normalised to GAPDH for experiment in **(A)** (n = 4; **P < 0.01; *P < 0.05; ANOVA with Tukey's post hoc test).

3.2.2 Inhibiting the conversion of PI(5)P to PI(4,5)P2 increases LC3-II levels

The removal of PI(5)P is maintained by type II PI(5)P kinases (phosphatidylinositol 5-phosphate 4-kinases, PIP4K2s), which converts PI(5)P to $PI(4,5)P_2$ (Clarke et al., 2010; Viaud et al., 2014). The mammalian genome contains three genes encoding three isoforms of PIP4Ks – PIP4K2α, PIPK2β, PIP4K2γ. It was shown that silencing the three PIP4K2 increased autophagy. The increase in autophagy was attributed to the impaired turnover of PI(5)P. Of the three isoforms, PIP4K2γ appeared to have the most convincing effect on autophagy (Vicinanza et al., 2015).

I, therefore, treated primary cortical neurons with NIH-12848, a PIP4K2γ inhibitor (Clarke et al., 2015). Western blots assessing changes in LC3-II levels showed that inhibition of PIP4K2γ led to an increase in autophagy **(Figure 3.8)**, thus corroborating previous findings (Vicinanza et al., 2015).

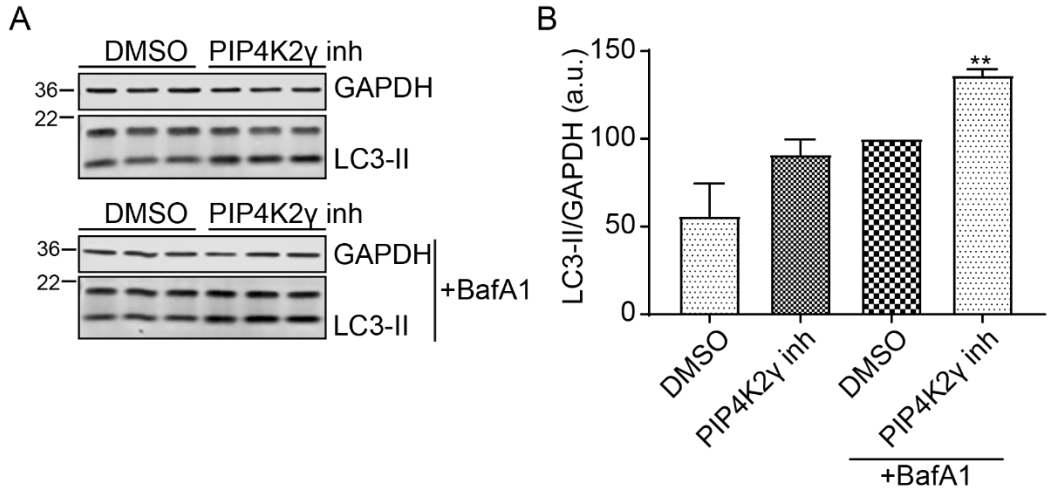

Figure 3.8 | PIP4K2γ inhibition increases LC3-II levels

(A) LC3-II immunoblots in primary cortical neurons at DIV7 treated with NIH compound PIP5K2γ inhibitor (1 µM, 48 hours) or DMSO. BafA1 (400 nM) was added 4 hours prior to finishing the experiment. GAPDH was used as loading control. **(B)** Data show relative changes in LC3-II normalised to GAPDH for experiment in **(A)** (n = 3; **P < 0.01; ANOVA with Tukey's post hoc test).

3.2.3 Glucose starvation and AMPK activation increase formation of PI(5)P-containing phagophores

To study the role of PI(5)P in glucose starvation-induced AMPK-mediated autophagy upregulation and the formation of PI(5)P-containing autophagosomal structures, I first assessed the effects of glucose starvation and AMPK activation on levels of PI(5)P-containing phagophores. As PI(5)P levels are difficult to detect, even with chromatography, I studied endogenous PI(5)P using a GFP-tagged bio-probe that contains the plant homeodomain (PHD) of ING2, as this domain has been shown to have a strong preference for PI(5)P (Bua et al., 2013; Gozani et al., 2003) and has been used to study the intracellular localization and manipulation of PI(5)P (Viaud et al., 2014). It has, however, not been determined whether this bio-probe might bind other lipids. With this caveat in mind, I transfected cells with GFP-PHD3x (three tandem repeats of PHD of ING2). Since I was interested in PI(5)P localised on autophagic structures, cells were also transfected with the proteolytic activity-deficient mutant of ATG4B (ATG4BC74A – referred to as ATG4B mutant), which freezes phagophores by preventing LC3 lipidation and autophagosome completion, thus ensuring PI(5)P visualisation on nascent autophagosomes (Fujita et al., 2008b).

Using this approach and staining cells for ATG16L1, I found that glucose starvation or direct AMPK activation with 991 increased the total numbers of phagophores (ATG16L1-containing vesicles) and the numbers of PI(5)P-containing ATG16L1-positive puncta (hereafter referred to as PI(5)P-containing phagophores) in SPCs. The effects of glucose starvation on PI(5)P-containing phagophores were prevented by CC. These findings indicate that AMPK plays a role in the upregulation of PI(5)P-containing phagophore formation **(Figure 3.9)**.

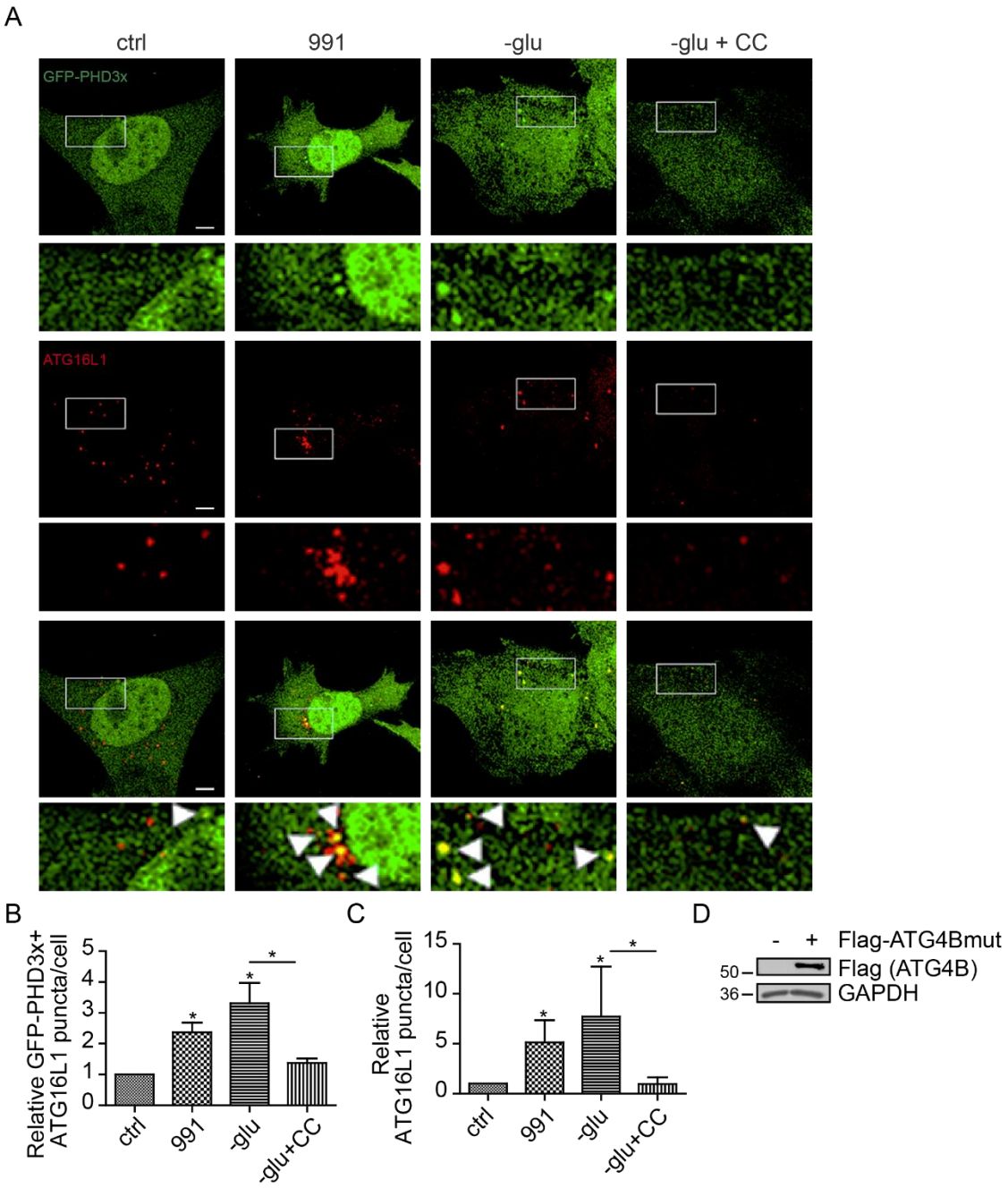

Figure 3.9 | Glucose starvation and AMPK activation increase numbers of PI(5)P-containing phagophores

(A) SPCs transfected with GFP-PHD3x and proteolytic dead FLAG-ATG4B mutant (ATG4BC74A) were treated with 991 (10 µM) or glucose-free media (-glu) for 1 hour ± CC (60 µM, 6 hours) and immunostained for ATG16L1 (Alexa 555: rabbit). The arrows indicate puncta positive for GFP-PHD3x (PI(5)P probe) and ATG16L1. DMSO was used as vehicle control. Representative micrographs shown. Scale bar, 5 µm. **(B)** Data show relative changes in GFP-PHD3x+ ATG16L1 and **(C)** total ATG16L1 puncta experiment in **(A)** normalised to control represented as mean ± SEM (n = 3, 20 cells/condition; *P < 0.05; ANOVA with Tukey's post hoc test). **(D)** Immunoblot probed

with FLAG and GAPDH antibodies showing expression of mutant FLAG-ATG4B in HeLa cells.

3.2.4 LKB1 is necessary for AMPK activation and increase in PI(5)P-containing phagophores

The principal upstream activator of AMPK is considered to be the tumour suppressor kinase LKB1 (Hawley et al., 2003; Woods et al., 2003). LKB1 phosphorylates AMPK on T172 on the α-subunit. This site can also be phosphorylated by CaMKKs in what is considered a Ca^{2+}-dependent pathway (different from the AMP-dependent pathway) (Hawley et al., 2005; Hurley et al., 2005; Woods et al., 2005).

Many human tumour cell lines, such as HeLa cells, carry deletions or loss-of-function mutations in *STK11*, the gene encoding LKB1. In HeLa cells, the activation of AMPK is attributed to CaMKK2 signalling (Fogarty et al., 2016).

To examine the role of LKB1 in PI(5)P-dependent autophagy upregulation, I tested whether glucose starvation and 991 treatment would affect formation of PI(5)P-containing phagophores in HeLa cells. I found that 991 treatment increased numbers of PI(5)P-containing phagophore as expected, since it is a direct activator of AMPK that acts through the ADaM site, while glucose starvation did not. I then transfected HeLa cells with LKB1 and found a significant increase in PI(5)P-containing phagophores in both basal conditions and upon glucose starvation and 991 treatment **(Figure 3.10A-D)**. This is in line with a study showing that treatment of HeLa cells with multiple AMPK activators was unable to activate AMPK until cells were transfected with LKB1 (Hawley et al., 2003). Our study confirms that LKB1 plays a role in AMPK activation, resulting in upregulation of PI(5)P signalling upon glucose starvation. Due to this fact, when using HeLa cells in any subsequent experiment, cells were always transiently transfected with LKB1.

Additionally, I tested the AMPK activators A769662 and AICAR in HeLa cells and found an increase in PI(5)P-containing phagophores. I also found that the increase in these structures as a response to glucose starvation was prevented using CC **(Figure 3.10E-G)**. This correlated with an increase in LC3 puncta in these conditions **(Figure 3.10H-I)**. These findings show that once LKB1 is transfected into HeLa cells, these cells respond to glucose starvation and AMPK activation in a similar fashion to SPCs.

Due to the low transfection efficiencies of SPCs, most experiments involving immunofluorescence were performed in LKB1+ HeLa cells. This includes experiments performed in HeLa cells presented earlier in **Figure 3.6**.

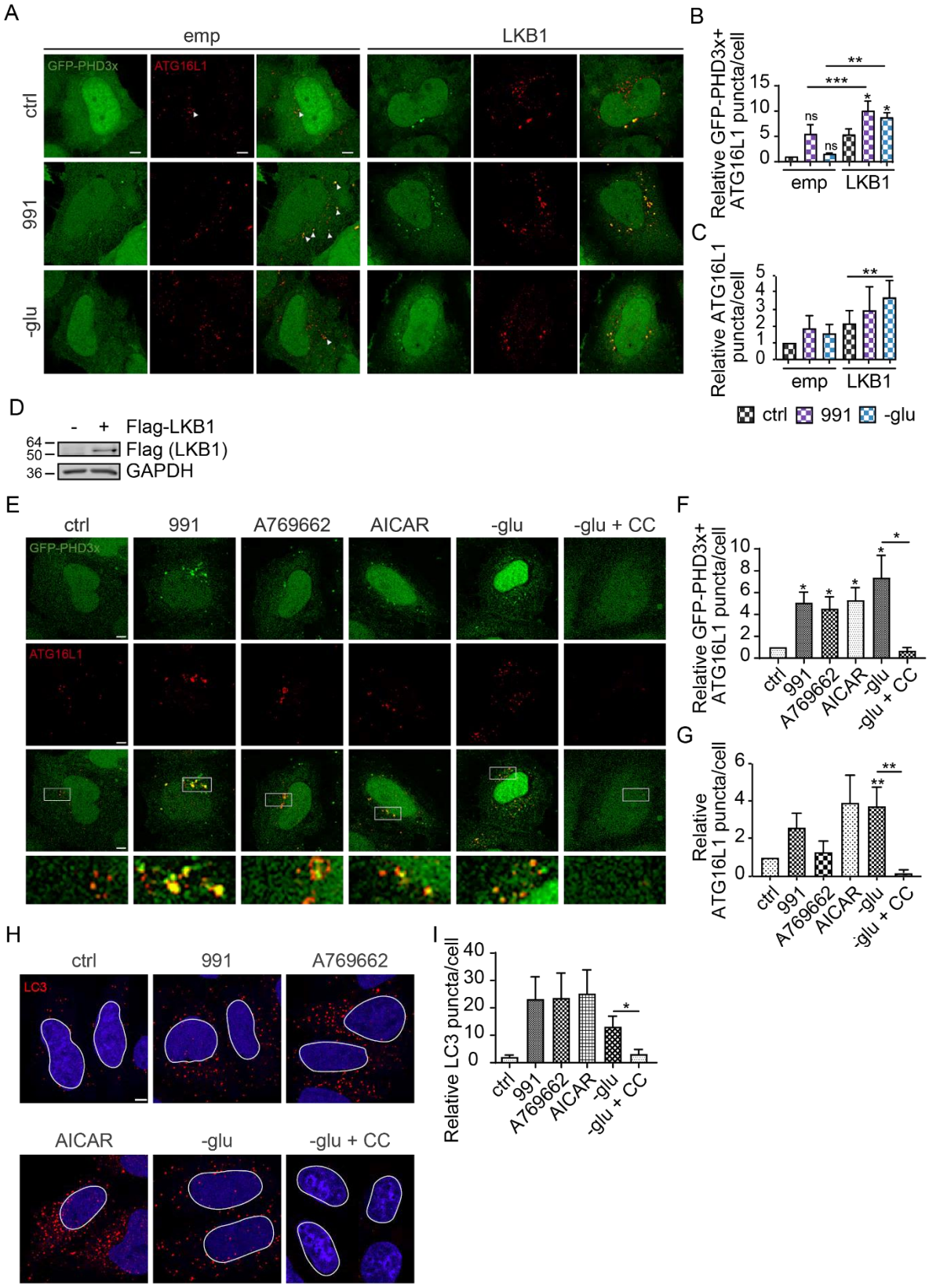

Figure 3.10 | LKB1 is required for PI(5)P-containing phagophore formation in HeLa cells

(A) HeLa cells transfected with FLAG-LKB1, GFP-PHD3x and FLAG-ATG4B mutant were treated with 991 (10 µM) or glucose-free media (-glu) for 1 hour and immunostained for ATG16L1 (Alexa 555: rabbit). The arrows indicate puncta positive for GFP-PHD3x and ATG16L1. Empty vector was used as negative control. **(B)** Data show relative changes in GFP-PHD3x+ ATG16L1 and **(C)** total ATG16L1 puncta for experiment in **(A)** normalised to control (n = 3, 20 cells/condition). **(D)** Immunoblot probed with FLAG and GAPDH antibodies showing expression of mutant FLAG-ATG4B in HeLa cells. **(E)** HeLa cells transfected with FLAG-LKB1, GFP-PHD3x and FLAG-ATG4B mutant treated with 991, AICAR, A769662 (10 µM) or glucose-free media for 1 hour ± CC (60 µM, 6 hours) were immunostained for ATG16L1 (Alexa 555: rabbit). **(F)** Data show relative changes in GFP-PHD3x+ ATG16L1 and **(G)** total ATG16L1 puncta for experiment in **(E)** normalised to control (n = 3, 20 cells/condition). **(H, I)** LC3 immunostaining (Alexa 555: rabbit) in HeLa cells transfected with FLAG-LKB1 and treated with 991, AICAR, A769662 (10 µM) or glucose-free media for 1 hour ± CC (60 µM, 6 hours). Data show relative changes in LC3 puncta/cell normalised to control (n = 3, 30 cells/condition).
DMSO was used as vehicle control. Representative micrographs shown. Scale bar, 5 µm. Data are represented as mean ± SEM (***P < 0.001, **P < 0.01, *P < 0.05; ANOVA with Tukey's post hoc test).

3.2.5 Formation of PI(5)P-containing phagophores upon glucose starvation and AMPK activation is abolished in AMPK dKO cells

Since our findings suggest that AMPK activated by glucose starvation leads to an increase in PI(5)P-dependent autophagy upregulation, I tested whether glucose starvation would increase PI(5)P-containing phagophore formation in AMPK α1/α2 dKO cells (Laderoute et al., 2006). While WT MEF cells responded to glucose starvation and 991 treatment similarly to SPCs, I found no effect on numbers of PI(5)P-containing and total numbers of phagophores in AMPK dKO cells upon treatment **(Figure 3.11)**.

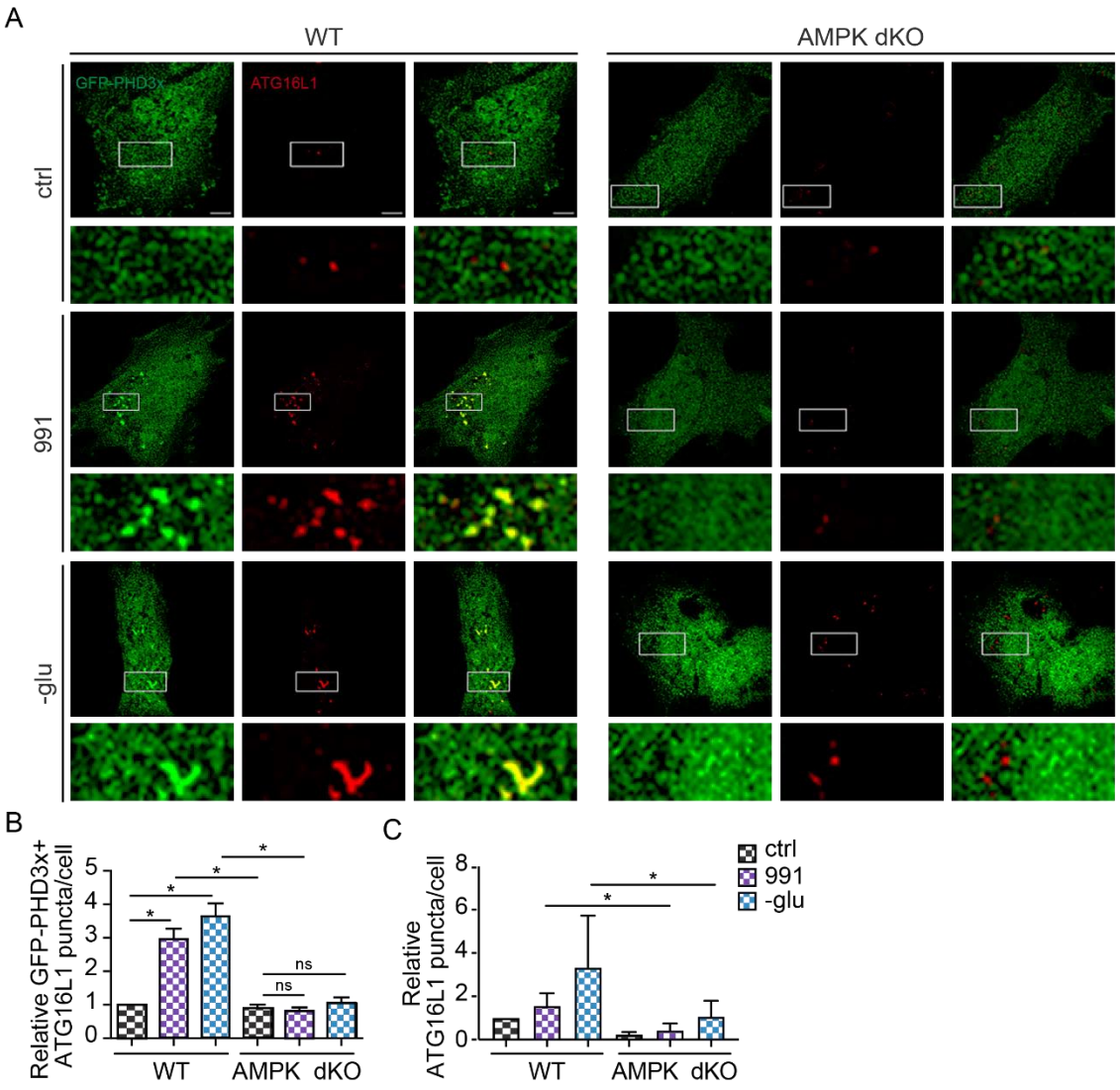

Figure 3.11 | The increase in formation of PI(5)P-containing phagophores upon glucose starvation and AMPK activation is abrogated in AMPK dKO cells

(A) WT and AMPK α1/α2 double knock-out (dKO) MEFs transfected with GFP-PHD3x and FLAG-ATG4B mutant were treated with 991 (10 µM) or glucose-free media (-glu) for 1 hour and immunostained for ATG16L1 (Alexa 555: rabbit). DMSO was used as vehicle control. Representative micrographs shown. Scale bar, 5 µm. **(B)** Data show relative changes in GFP-PHD3x+ ATG16L1 and **(C)** total ATG16L1 puncta for experiment in **(A)** normalised to control are represented as mean ± SEM (n = 3, 20 cells/condition; *P < 0.05; ANOVA with Tukey's post hoc test).

3.2.6 AMPK reconstitution in AMPK dKOs rescues the increase in PI(5)P-containing phagophores following glucose starvation and AMPK activation

Next, AMPK was reconstituted in the AMPK dKO cells. First, I tested whether the AMPK α1 or α2 catalytic subunits could rescue the formation of PI(5)P-containing phagophores, since studies have suggested that the α2 subunit plays a major role in glucose sensing (Claret et al., 2007; Viollet et al., 2003). In accordance with this, reconstitution of AMPK dKO cells with the α1 subunit did not rescue formation of PI(5)P-containing phagophores **(Figure 3.12)**, while reconstitution of AMPK α2 in AMPK dKO cells rescued the increased formation of PI(5)P-containing and total numbers of phagophores upon glucose starvation and 991 treatment **(Figure 3.13)**. This rescue was abrogated when reconstituting dominant-negative kinase-dead K45R AMPK α2 instead of WT AMPK α2 (Mu et al., 2001). This confirms that AMPK activity is required for the formation of PI(5)P-containing phagophores.

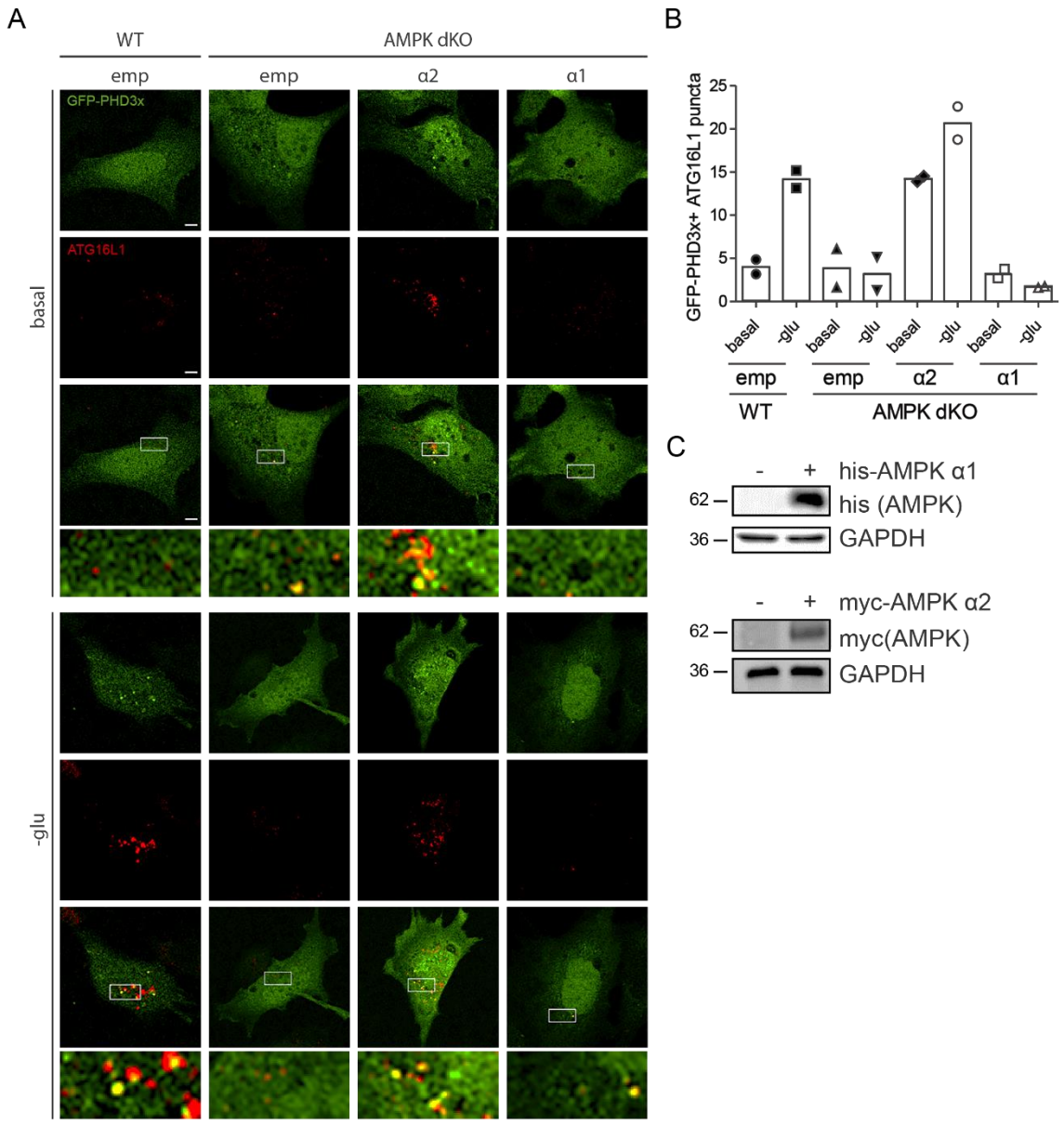

Figure 3.12 | AMPK α1 reconstitution does not rescue formation of PI(5)P-containing phagophore in AMPK DKO cells

(A) AMPK dKO MEFs transfected with GFP-PHD3x, FLAG-ATG4B mutant, AMPK α1 or α2 were incubated in basal or glucose-free media (-glu) for 1 hour and immunostained for ATG16L1 (Alexa 555: rabbit). WT MEFs were used for comparison. Empty vector was used as negative control. Representative micrographs shown. Scale bar, 5 µm. **(B)** Data show average number of GFP-PHD3x+ ATG16L1 puncta for the experiment in **(A)** from two biological replicates (n = 2, 20 cells/condition). **(C)** Immunoblot probed with his-tag (top), myc (bottom) and GAPDH antibodies showing expression of his-AMPK α1 or myc-AMPK α2 in AMPK dKO MEF cells.

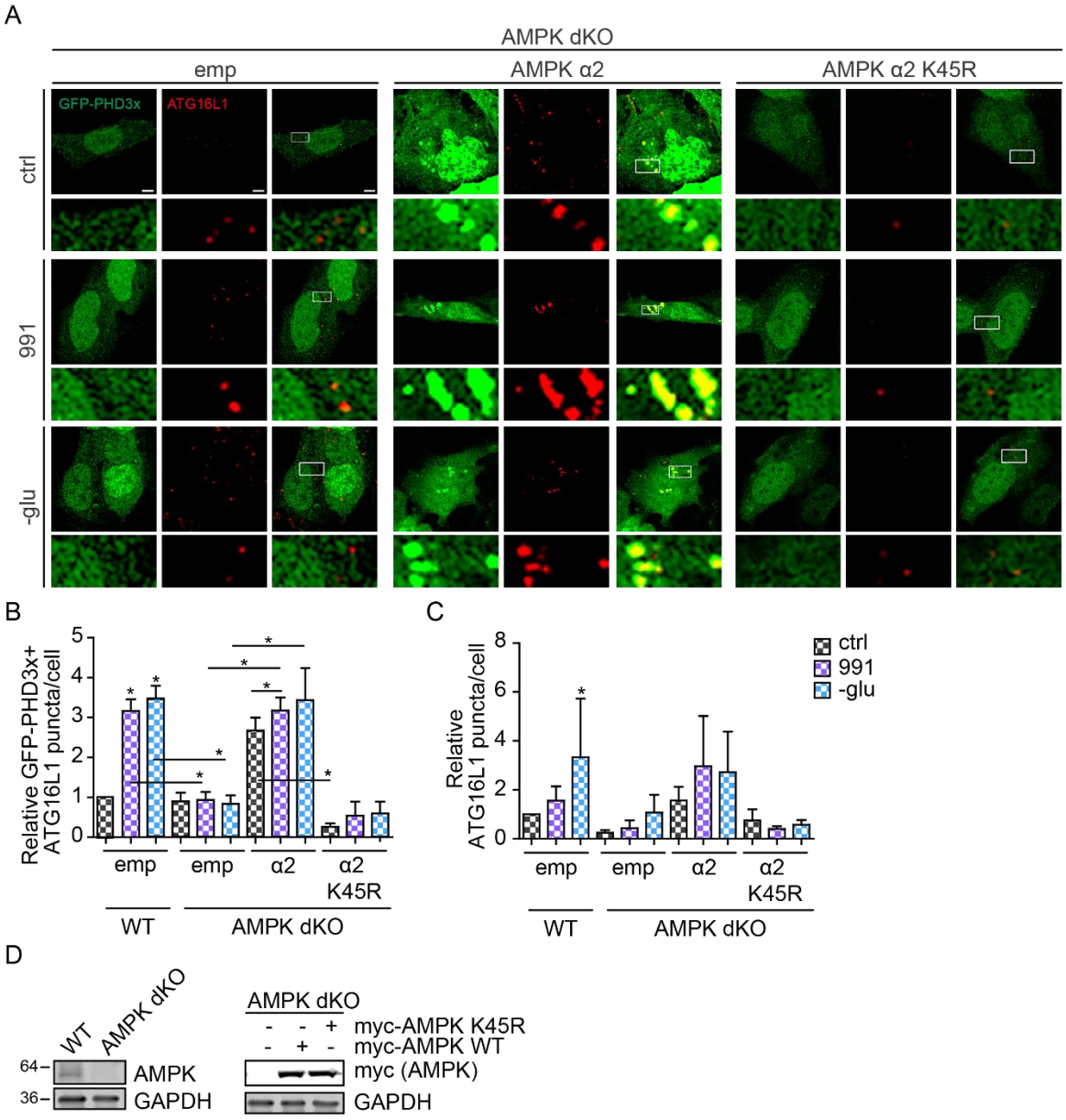

Figure 3.13 | AMPK reconstitution rescues PI(5)P-containing phagophore levels upon glucose starvation and AMPK activation in AMPK dKO cells

(A) AMPK dKO MEFs transfected with GFP-PHD3x, FLAG-ATG4B mutant and empty-myc, AMPK α2 or catalytic-dead dominant-negative AMPK α2 K45R were treated with 991 (10 μM) or glucose-free media (-glu) for 1 hour and immunostained for ATG16L1 (Alexa 555: rabbit). DMSO was used as vehicle control. Empty vector was used as negative control. Representative micrographs shown. Scale bar, 5 μm. **(B)** Data show relative changes in GFP-PHD3x+ ATG16L1 puncta and **(C)** total ATG16L1 puncta for experiment in **(A)** normalised to empty control represented as mean ± SEM. WT MEF cells are shown in **Figure 3.11** (n = 3, 20 cells/condition; *P < 0.05; ANOVA with Tukey's post hoc test). **(D)** Immunoblots probed with myc and GAPDH antibodies showing expression of myc-AMPK α2 WT or K45R in AMPK dKO MEF cells. AMPK antibody was used to validate the AMPK deletion in WT and AMPK dKO cells.

3.2.7 The increase in PI(5)P-containing phagophores following glucose starvation and AMPK activation is independent of Beclin-1

During conventional autophagy upregulation, the VPS34 complex is activated by the ULK complex. VPS34 is the catalytic component of a core complex that includes the regulatory subunit VPS15, required for the kinase activity, and the tumour suppressor Beclin-1 (BECN1) (Baskaran et al., 2014). The VPS34 complex generates PI(3)P, which was considered an essential lipid component of autophagosomes. However, in recent years, VPS34 complex-independent autophagy has been reported in multiple studies (Mcalpine et al., 2013b; Scarlatti et al., 2008; Zhou et al., 2010). In cells pre-treated with the VPS34 inhibitor Wortmannin, an increase in PI(5)P was able to induce autophagy (Vicinanza et al., 2015).

To assess whether glucose starvation and AMPK activation could increase formation of PI(5)P-containing phagophores in the absence of a functional VPS34 complex, I tested these conditions on BECN KO HeLa cells (He et al., 2015). I found that BECN KO cells had a higher baseline of PI(5)P-containing autophagosomal structures suggesting activation of PI(3)P-independent autophagy in the absence of a functional VPS34 complex for maintenance of basal autophagy. Furthermore, glucose starvation and AMPK activation using 991 was able to increase numbers of PI(5)P-containing phagophores in BECN KO cells **(Figure 3.14)**, confirming that glucose starvation-induced AMPK activity on PI(5)P-mediated autophagy is independent of the Beclin-1/VPS34 complex, as previously proposed (Vicinanza et al., 2015).

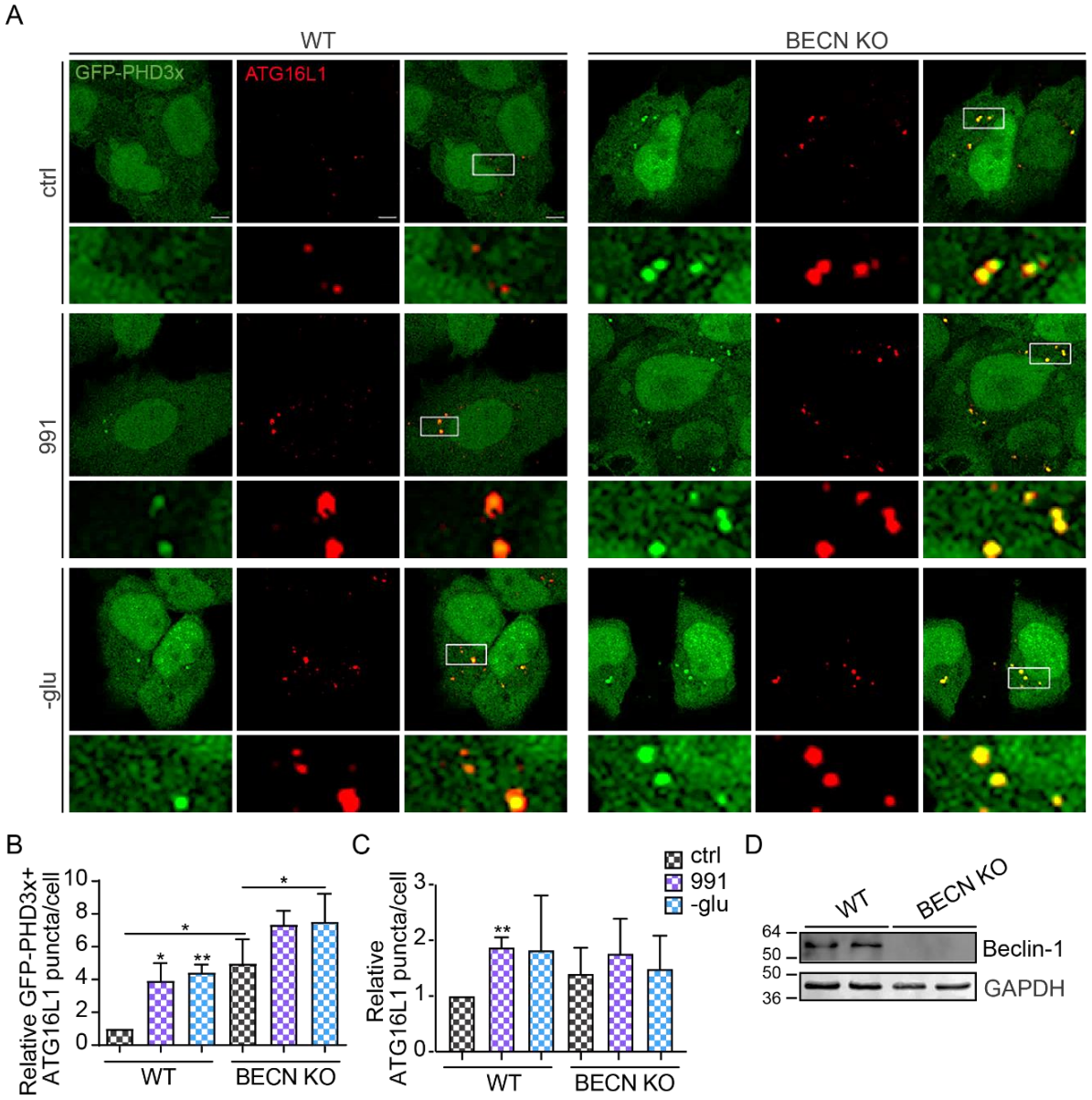

Figure 3.14 | Numbers of PI(5)P-containing phagophores increase following AMPK activation in BECN-null cells

(A) WT (TALEN) and BECN KO HeLa cells transfected with FLAG-LKB1, GFP-PHD3x and FLAG-ATG4B mutant treated with 991 (10 μM) or glucose-free media (-glu) for 1 hour were immunostained for ATG16L1 (Alexa 555: rabbit). DMSO was used as vehicle control. Representative micrographs shown. Scale bar, 5 μm. **(B)** Data show relative changes in GFP-PHD3x+ ATG16L1 puncta and **(C)** total ATG16L1 puncta for experiment in **(A)** normalised to control represented as mean ± SEM (n = 3, 20 cells/condition; **P < 0.01, *P < 0.05; ANOVA with Tukey's post hoc test).

3.3 PI(5)P-containing autophagosome biogenesis is regulated by the mTORC1 complex

In the conventional PI(3)P-dependent pathway, starvation-induced AMPK inhibits mTOR and the mTOR-mediated inactivation of ULK1 (Corradetti et al., 2004a; Gwinn et al., 2008b; Inoki et al., 2003b). Since AMPK also appears to be a key player in PI(5)P-dependent autophagy, I assessed the role of mTOR regulation in the formation of PI(5)P-containing autophagosome biogenesis.

3.3.1 mTORC1 activation prevents the increase in AMPK activation and glucose starvation-induced PI(5)P-containing phagophores

First, I transfected HeLa cells with the construct FLAG-Raptor-Rheb15 which activates the mTORC1 pathway upon transient expression (Sancak et al., 2011). I found that the activation of mTORC1 prevents the increase in PI(5)P-containing and total numbers of phagophores observed upon glucose starvation and AMPK activation **(Figure 3.15A-C)**. Accordingly, activation of mTORC1 impaired the increase in LC3 puncta mediated by glucose starvation and AMPK activation **(Figure 3.15D-E)**. The activation of mTORC1 was assessed by western blotting for the mTOR substrate the ribosomal S6 kinase 1 (S6K1), which becomes phosphorylated by mTOR on T389. Upon expression of FLAG-Raptor-Rheb15, the phosphorylation of S6K1 on T389 increased **(Figure 3.15F-G)**. This finding suggests that mTORC1 activation inhibits the formation of PI(5)P-containing phagophores.

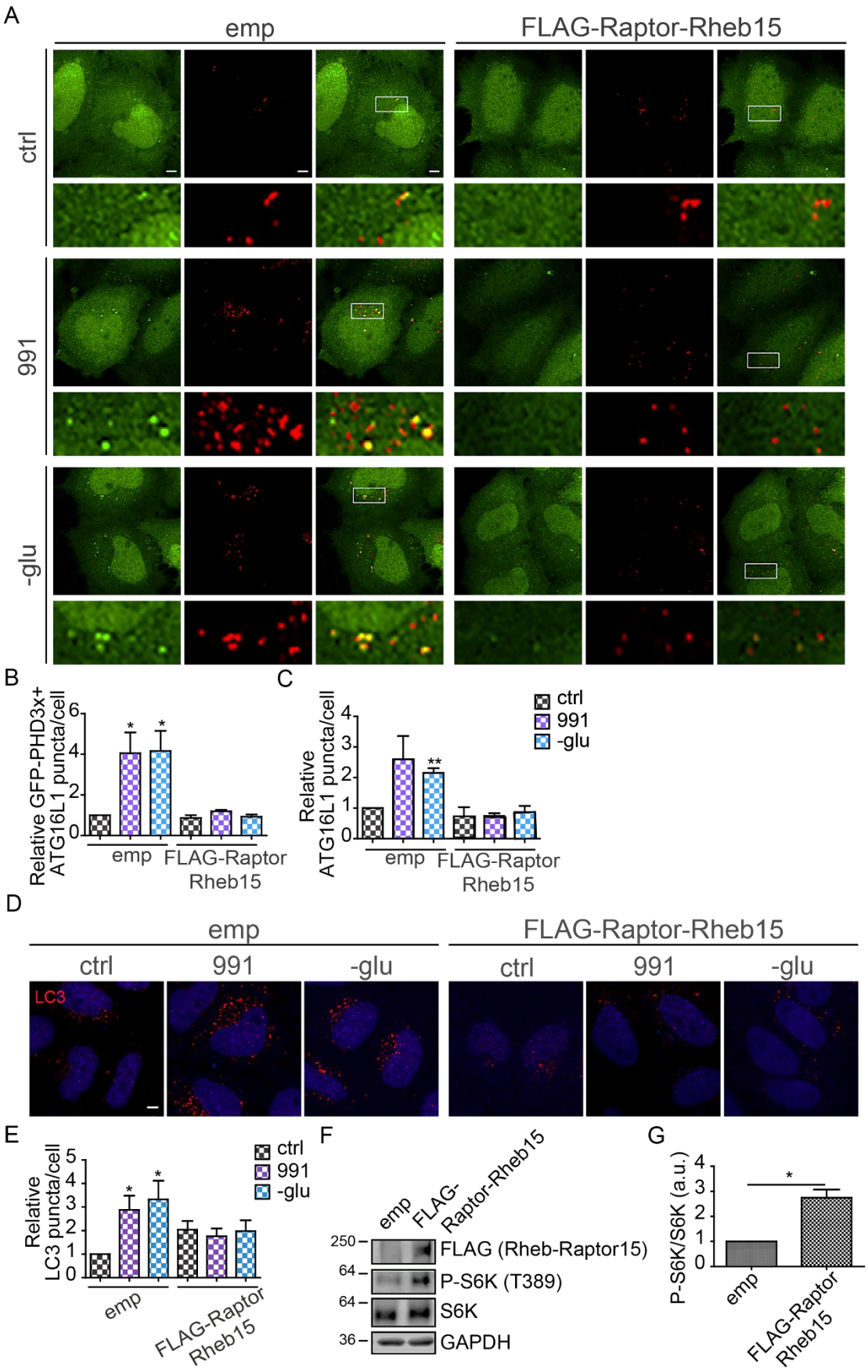
A
emp
FLAG-Raptor-Rheb15
ctrl
991
-glu
B
Relative GFP-PHD3x+ ATG16L1 puncta/cell
emp
FLAG-Raptor Rheb15
C
Relative ATG16L1 puncta/cell
ctrl
991
-glu
D
LC3
E
Relative LC3 puncta/cell
F
FLAG (Rheb-Raptor15)
P-S6K (T389)
S6K
GAPDH
G
P-S6K/S6K (a.u.)

Figure 3.15 | mTORC1 activation impairs formation of PI(5)P-containing phagophores

(A) HeLa cells transfected with FLAG-LKB1, GFP-PHD3x, FLAG-ATG4B mutant and FLAG-Raptor-Rheb15 treated with 991 (10 µM) or glucose-free media (-glu) for 1 hour were immunostained for ATG16L1 (Alexa 555: rabbit). DMSO was used as vehicle control. **(B)** Data show relative changes in GFP-PHD3x+ ATG16L1 puncta and **(C)** total ATG16L1 puncta for experiment in **(A)** normalised to empty control represented as mean ± SEM (n = 3, 20 cells/condition). **(D)** LC3 immunostaining (Alexa 555: rabbit) in HeLa cells with FLAG-LKB1, GFP-PHD3x, FLAG-ATG4B mutant and FLAG-Raptor-Rheb15 treated with 991 (10 µM) or glucose-free media (-glu) for 1 hour. **(E)** Data show relative changes in LC3 puncta/cell for experiment in **(D)** normalised to empty control (n = 4, ~30 cells/condition). **(F, G)** Total S6K1, P-S6K1 (T389) and FLAG immunoblots in HeLa cells transfected with empty vector or FLAG-Raptor-Rheb15. Data show relative changes in P-S6K1 (T389) normalised to total S6K1 (n = 3).
Empty vector was used as negative control. Representative micrographs shown. Scale bar, 5 µm. Data are represented as mean ± SEM (**P < 0.01; *P < 0.05; ANOVA with Tukey's post hoc test).

3.3.2 mTORC1 inhibition induces formation of PI(5)P-containing phagophores

Since mTORC1 activation prevented the formation of PI(5)P-containing phagohores, I hypothesized that mTOR inhibition with Torin1 treatment could induce formation of PI(5)P-containing phagophores. I treated WT and AMPK dKO MEFs with Torin1 and found that this increased the PI(5)P-containing and total numbers of phagophores in WT cells. This increase was not observed in AMPK dKO cells, which suggests that AMPK is required to induce formation of PI(5)P-containing phagophores **(Figure 3.16A-C)**. Accordingly, Torin1 treatment led to a significant increase in LC3 puncta in WT MEFs as expected **(Figure 3.16D-E)**. In both WT and AMPK dKO cells, Torin1 treatment effectively inhibited mTOR activity as detected by the phosphorylation of S6K1 **(Figure 3.16F-G)**.

These findings imply that mTOR regulates conventional PI(3)P-dependent autophagy and PI(5)P-dependent autophagy.

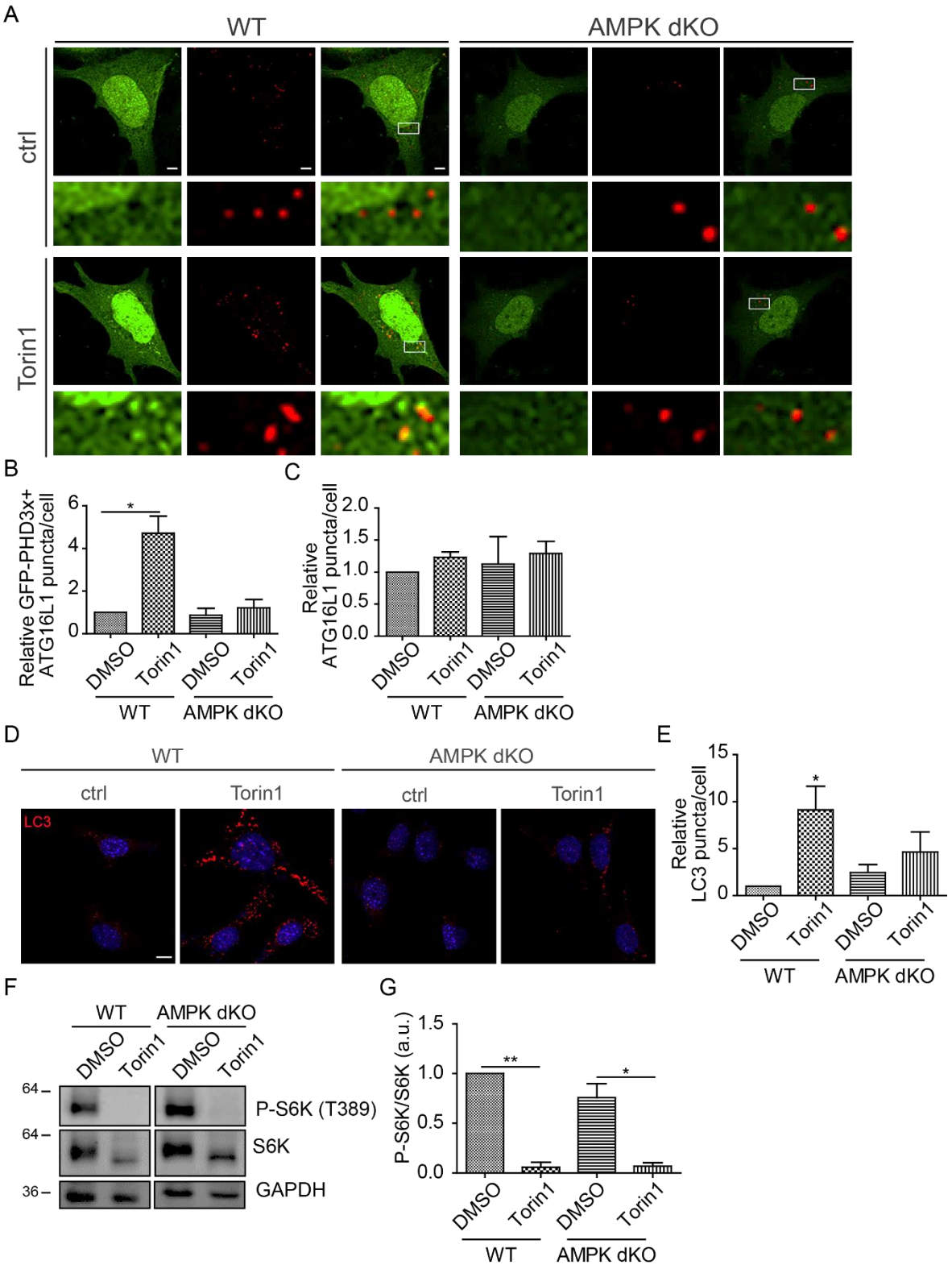

Figure 3.16 | mTOR inhibition induces PI(5)P-containing phagophore formation

(A) WT and AMPK dKO cells transfected with GFP-PHD3x and FLAG-ATG4B mutant were treated with Torin1 (1 µM, 4 hours) were immunostained for ATG16L1 (Alexa 555: rabbit). **(B)** Data show relative changes in GFP-PHD3x+ ATG16L1 puncta and **(C)** total ATG16L1 puncta for experiment in **(A)** normalised to DMSO WT represented

as mean ± SEM (n = 3, 10-20 cells/condition). **(D)** LC3 immunostaining (Alexa 555: rabbit) in WT and AMPK dKO cells treated with Torin1 (1 µM, 4 hours). **(E)** Data show relative changes in LC3 puncta/cell for experiment in **(D)** normalised to DMSO WT (n = 4, ~50 cells/condition). **(F, G)** Total S6K1 and P-S6K1 (T389) immunoblots in WT and AMPK dKO cells treated with Torin1 (1 µM, 4 hours). Data show relative changes in P-S6K1 (T389) normalised to total S6K1 (n = 3).
DMSO was used as vehicle control. Representative micrographs shown. Scale bar, 5 µm. Data are represented as mean ± SEM (**P < 0.01; *P < 0.05; ANOVA with Tukey's post hoc test).

3.4 PIKfyve activation is required for formation of PI(5)P-containing autophagosomes

Since PI(5)P can be generated by PIKfyve, I studied the role of PIKfyve in formation of PI(5)P-containing phagophores.

3.4.1 PIKfyve is localised on the recycling endosomes

Upon starvation with Earle's balanced salt solution (EBSS), PI(3)P-containing autophagosomes are formed on recycling endosomes from which membranes are sourced. WIPI2 is recruited by RAB11A, a core component of the recycling endosomes that serves as a direct platform for autophagosome assembly (Puri et al., 2018).

While PIKfyve is best known for its role in the maturation of early endosomes to late endosomes and reformation of lysosomes from endo-lysosomes (Bissig et al., 2017; Ikonomov et al., 2006; Sbrissa et al., 2007b), its relationship with the recycling endosome is unclear. I found that, GFP-PIKfyve interacts with the RAB11A-positive compartment in HeLa cells shown by confocal microscopy and with myc-tagged RAB11A proteins in immunoprecipitates from HEK 293T cells **(Figure 3.17)**. While this does not illuminate the activity of PIKfyve on the recycling endosomes, it links PIKfyve with the primary platform for autophagosome biogenesis.

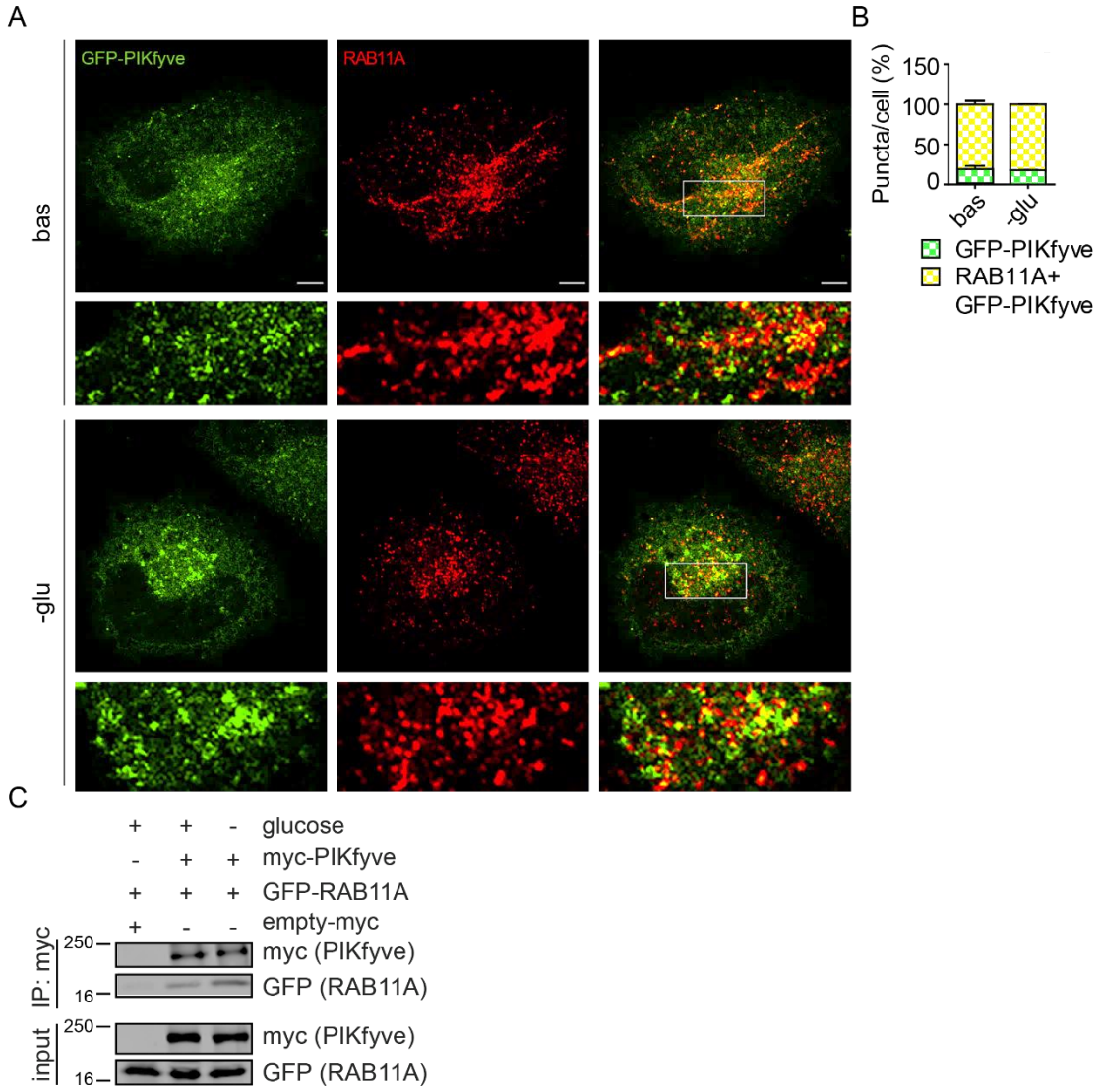

Figure 3.17 | PIKfyve is localised on the RAB11A-positive compartment

(A) HeLa cells transfected with GFP-PIKfyve incubated in basal or glucose-free media (-glu) for 1 hour were immunostained for RAB11A (Alexa 555: rabbit). Representative micrographs shown. Scale bar, 5 µm. **(B)** Data show percentage of RAB11A+ GFP-PIKfyve puncta for experiment in **(A)** normalised to total GFP-PIKfyve puncta represented as mean ± SEM (n = 3, 10 cells/condition, two-tailed, paired student's t-test). **(C)** HEK 293T cells were transfected with myc-PIKfyve and GFP-RAB11A and incubated in glucose-free media for 1 hour. myc-PIKfyve was immunoprecipitated with myc-trap beads. Empty vector was used as negative control (n = 2).

3.4.2 PI(5)P-containing phagophore formation is dependent on the chaperonin-like domain of PIKfyve

Next, I aimed to dissect the role of the PIKfyve activity in the formation of PI(5)P-containing phagophores.

First, I sought to determine the PIKfyve domain involved in the formation of PI(5)P-containing phagophores. I, therefore, overexpressed PIKfyve deletion mutants in cells **(Figure 3.18A-B**; Ikonomov et al., 2009**)** and examined their effects on the formation of PI(5)P-containing phagophores. I found that the conserved chaperonin-like (Cpn) domain was important for the increase in phagophores **(Figure 3.18C-E)** and the subsequent effect on LC3 levels **(Figure 3.18F-G)**. This domain was previously suggested to play a vital role in the formation of the PIKfyve complex on endosomes (Ikonomov et al., 2009). The authors found no vacuolar phenotype associated with reduced PI(3,5)P_2 synthesis when overexpressing the PIKfyve ΔCpn. Here, I found that this domain is important for formation of PI(5)P-containing phagophore and autophagy.

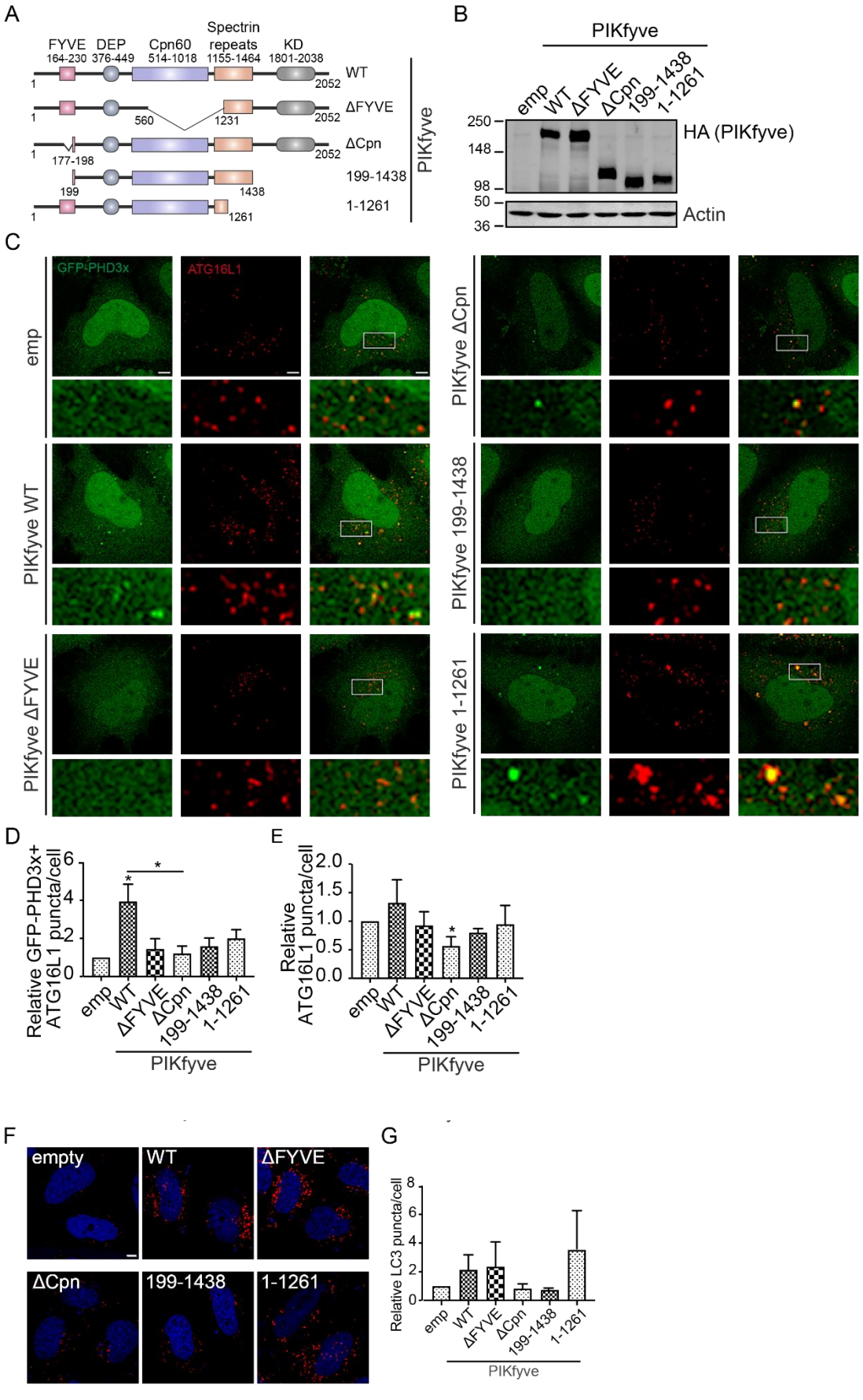
A
FYVE 164-230
DEP 376-449
Cpn60 514-1018
Spectrin repeats 1155-1464
KD 1801-2038
WT
ΔFYVE
ΔCpn
199-1438
1-1261
PIKfyve
B
PIKfyve
emp
WT
ΔFYVE
ΔCpn
199-1438
1-1261
HA (PIKfyve)
Actin
C
GFP-PHD3x
ATG16L1
emp
PIKfyve WT
PIKfyve ΔFYVE
PIKfyve ΔCpn
PIKfyve 199-1438
PIKfyve 1-1261
D
Relative GFP-PHD3x+ ATG16L1 puncta/cell
PIKfyve
E
Relative ATG16L1 puncta/cell
PIKfyve
F
empty
WT
ΔFYVE
ΔCpn
199-1438
1-1261
G
Relative LC3 puncta/cell
PIKfyve

Figure 3.18 | The chaperonin-like domain in PIKfyve is required for formation of PI(5)P-containing phagophores and LC3 puncta

(A) Schematic representation of the wildtype and mutant PIKfyve forms expressing residues 199-1438 or 1-1231 or mutant forms with deletions of the FYVE (ΔFYVE) or chaperonin-like (ΔCpn) domains. **(B)** Immunoblot probed with HA and actin antibodies showing expression of HA-tagged PIKfyve deletion mutants in HeLa cells. **(C)** HeLa cells transfected with FLAG-LKB1, GFP-PHD3x and FLAG-ATG4B mutant and PIKfyve deletion mutants were immunostained for ATG16L1 (Alexa 555: rabbit). **(D)** Data show relative changes in GFP-PHD3x+ ATG16L1 puncta and **(E)** total ATG16L1 puncta for experiment in **(C)** normalised to control. **(E, F)** LC3 immunostaining (Alexa 555: rabbit) in HeLa cells transfected with FLAG-LKB1 and PIKfyve deletion mutants. Data show relative changes in LC3 puncta/cell normalised to control.
Empty vector was used as negative control. Representative micrographs shown. Scale bar, 5 µm. Data are represented as mean ± SEM (n = 3, 20 cells/condition; *P < 0.05; ANOVA with Tukey's post hoc test).

3.4.3 PIKfyve inhibition abrogates formation of PI(5)P-containing phagophores

Next, I used the potent selective PIKfyve inhibitor YM201636 (YM) for one hour at 100 nM (Jefferies et al., 2008), which reduces PI(5)P levels (Sbrissa et al., 2012) and found that it abrogated the increase in PI(5)P-containing and total numbers of phagophores induced by glucose starvation as expected (Vicinanza et al., 2015) **(Figure 3.19A-C)**, as well as by 991 treatment **(Figure 3.19F-H)** and correlated with abrogation of the increased LC3 puncta observed upon glucose starvation and 991 treatment **(Figure 3.19D-E, I-J).**

To validate that the YM-mediated reduction of autophagy was not caused by a lysosomal defect, I measured changes in lysosome numbers using lysotracker and found that upon glucose starvation there was a tendency for lysosomes to increase. This increase was maintained when glucose starved cells were treated with YM **(Figure 3.20A-B)**. Additionally, I stained cells for the endosomal marker CD63 and found that the number of CD63-positive puncta did not change in glucose starved cells upon YM treatment **(Figure 3.20C-D)**. This indicates that the YM treatment conditions selected in this study do not interfere with the endocytic system. Studies that observe endosomal and lysosomal defects caused by YM treatment use this compound at concentrations ranging from 800 nM – 3 µM between 2 – 24 hours (Bissig et al., 2017; Compton et al., 2016; Sano et al., 2016; Schulze et al., 2017), while my experiments have used this drug for 1 hour at 100 nM .

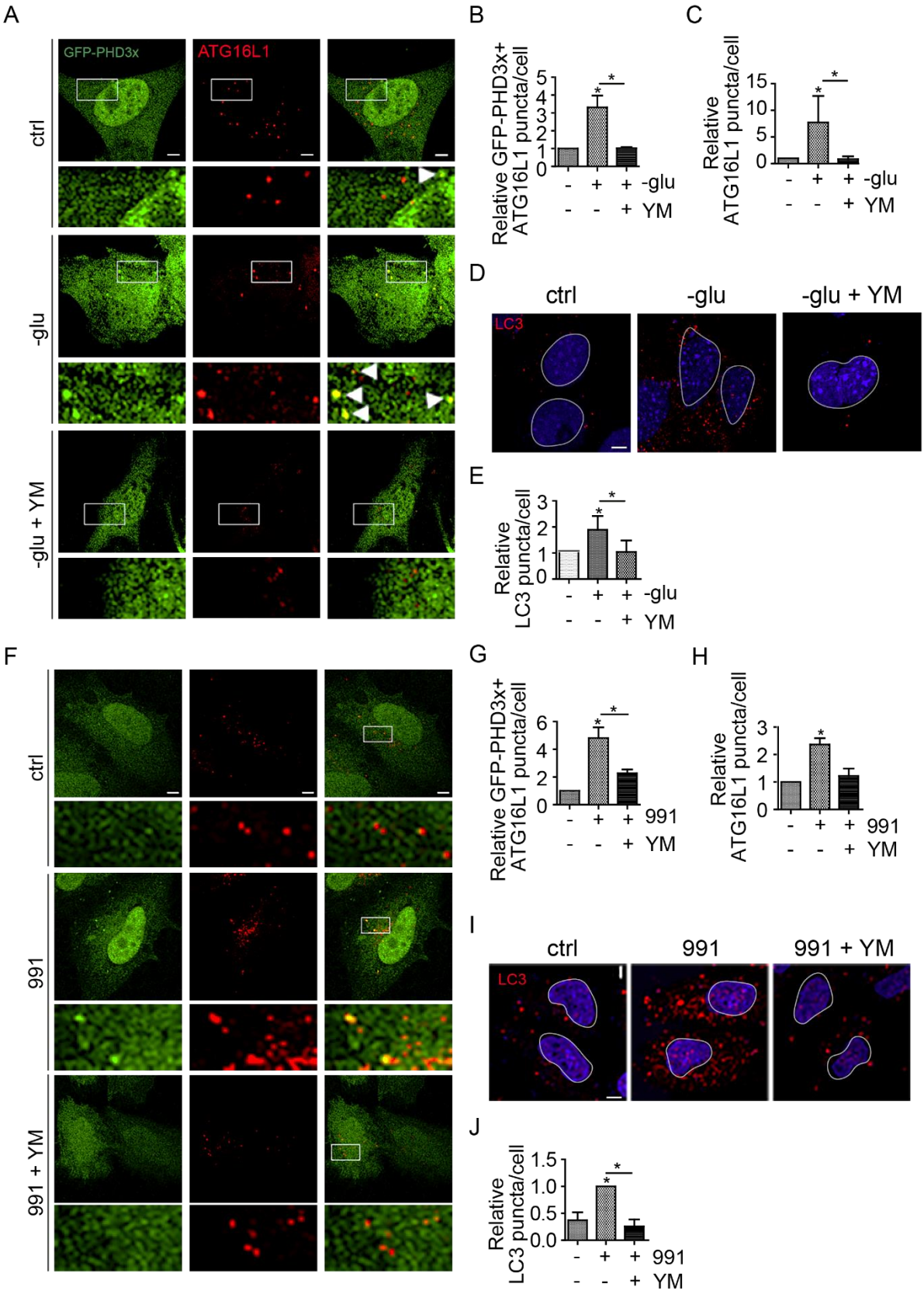
A
GFP-PHD3x
ATG16L1
ctrl
-glu
-glu + YM
B
Relative GFP-PHD3x+ ATG16L1 puncta/cell
-glu
YM
C
Relative ATG16L1 puncta/cell
D
ctrl
-glu
-glu + YM
LC3
E
Relative LC3 puncta/cell
F
991
991 + YM
G
Relative GFP-PHD3x+ ATG16L1 puncta/cell
H
Relative ATG16L1 puncta/cell
I
991
991 + YM
J
Relative LC3 puncta/cell

Figure 3.19 | PIKfyve inhibition is required for PI(5)P-containing phagophore upon AMPK activation

(A) SPCs transfected with GFP-PHD3x and FLAG-ATG4B mutant in glucose-free media (-glu) ± YM (100 nM) for 1 hour were immunostained for ATG16L1 (Alexa 555: rabbit). **(B)** Data show relative changes in GFP-PHD3x+ ATG16L1 and **(C)** total numbers of ATG16L1 puncta for experiment in **(A)** normalised to control (n = 3, 20 cells/condition). **(D)** LC3 immunostaining (Alexa 555: rabbit) in SPCs incubated in glucose-free media ± YM (100 nM, 1 hour). **(E)** Data show relative changes in LC3 puncta/cell for experiment in **(D)** normalised to control (n = 3, 30 cells/condition). **(F)** HeLa cells transfected with FLAG-LKB1, GFP-PHD3x and FLAG-ATG4B mutant were treated with 991 (10 µM) ± YM (100 nM) for 1 hour and immunostained for ATG16L1 (Alexa 555: rabbit). **(G)** Data show relative changes in GFP-PHD3x+ ATG16L1 and **(H)** total numbers of ATG16L1 puncta for experiment in **(F)** normalised to control (n = 3, 20 cells/condition). **(I)** LC3 immunostaining (Alexa 555: rabbit) in HeLa cells transfected with FLAG-LKB1 treated with 991 (10 µM) ± YM (100 nM) for 1 hour. **(J)** Data show relative changes in LC3 puncta/ for experiment in **(I)** normalised to control cell (n = 3, 30 cells/condition).
DMSO was used as vehicle control. Representative micrographs shown. Scale bar, 5 µm. Data are represented as mean ± SEM (n = 3, 20 cells/condition; *P < 0.05; ANOVA with Tukey's post hoc test).

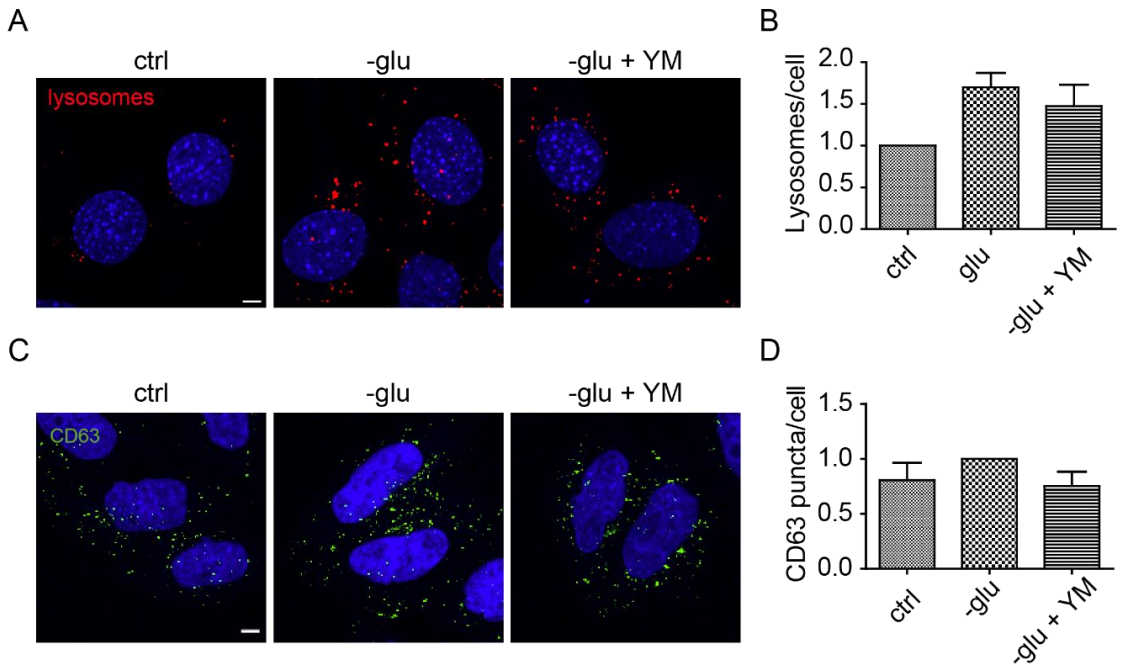

Figure 3.20 | The selected conditions for PIKfyve inhibition do not cause endo-lysosomal changes

(A) HeLa cells transfected with FLAG-LKB1 in glucose-free media (-glu) ± YM (100 nM) for 1 hour. LysoTracker Red was added to cells 5 minutes before fixation. **(B)** Data show relative changes in number of lysosomes for experiment in **(A)** normalised to control (n = 3, 30 cells/condition). **(C)** CD63 immunostaining (Alexa 488: mouse) in HeLa cells transfected with FLAG-LKB1 in glucose-free media (-glu) ± YM (100 nM) for 1 hour. **(D)** Data show relative changes in CD63 puncta/cell for experiment in **(C)** normalised to -glu (n = 3, 30 cells/condition). Representative micrographs shown. Scale bar, 5 µm. Data are represented as mean ± SEM (ANOVA with Tukey's post hoc test).

3.4.4 The kinase activity of PIKfyve is required to rescue the formation of PI(5)P-containing phagophores in AMPK dKO cells

Since our data suggested that the PIKfyve activity was required for the increase in PI(5)P-containing and total number of phagophores observed upon glucose starvation and AMPK activation, I further studied the role of the kinase activity of PIKfyve.

In 2002, Ikonomov et al. determined that the K2000 residue on PIKfyve was required for the PIKfyve-mediated synthesis of PI(5)P. They found that PI(5)P synthesis was reduced when overexpressing a mutant PIKfyve in which the lysine residue was exchanged with glutamate (K2000E) (Ikonomov et al., 2002).

I transfected HeLa cells with PIKfyve WT and K2000E and found that the increase in PI(5)P-containing phagophores observed upon glucose starvation and AMPK activation in cells overexpressing PIKfyve WT was abolished in cells transfected with PIKfyve K2000E **(Figure 3.21)**. Since other enzymes such as myotubularins have been proposed as modifiers of PI(5)P levels (Poli et al., 2019), this finding suggests that the main source of PI(5)P in glucose-starvation-induced, PI(5)P-dependent autophagy is PIKfyve.

Next, I transfected cells with a dominant-negative lipid kinase-deficient PIKfyve (K1831E) (Sbrissa et al., 2000) and found that this prevented the increase in PI(5)P-containing and total number of phagophores upon glucose starvation and 991 treatment in SPCs **(Figure 3.22A-C)** and in HeLa cells **(Figure 3.22D-G)**. Moreover, the biogenesis of PI(5)P-containing phagophores was abrogated in AMPK dKO cells reconstituted with AMPK α2 when treated with YM or upon expression of PIKfyve K1831E mutant **(Figure 3.23)**.

These findings suggest that the AMPK activity is required for the formation of PI(5)P-containing phagophores after glucose starvation and that PIKfyve is downstream of AMPK in this process.

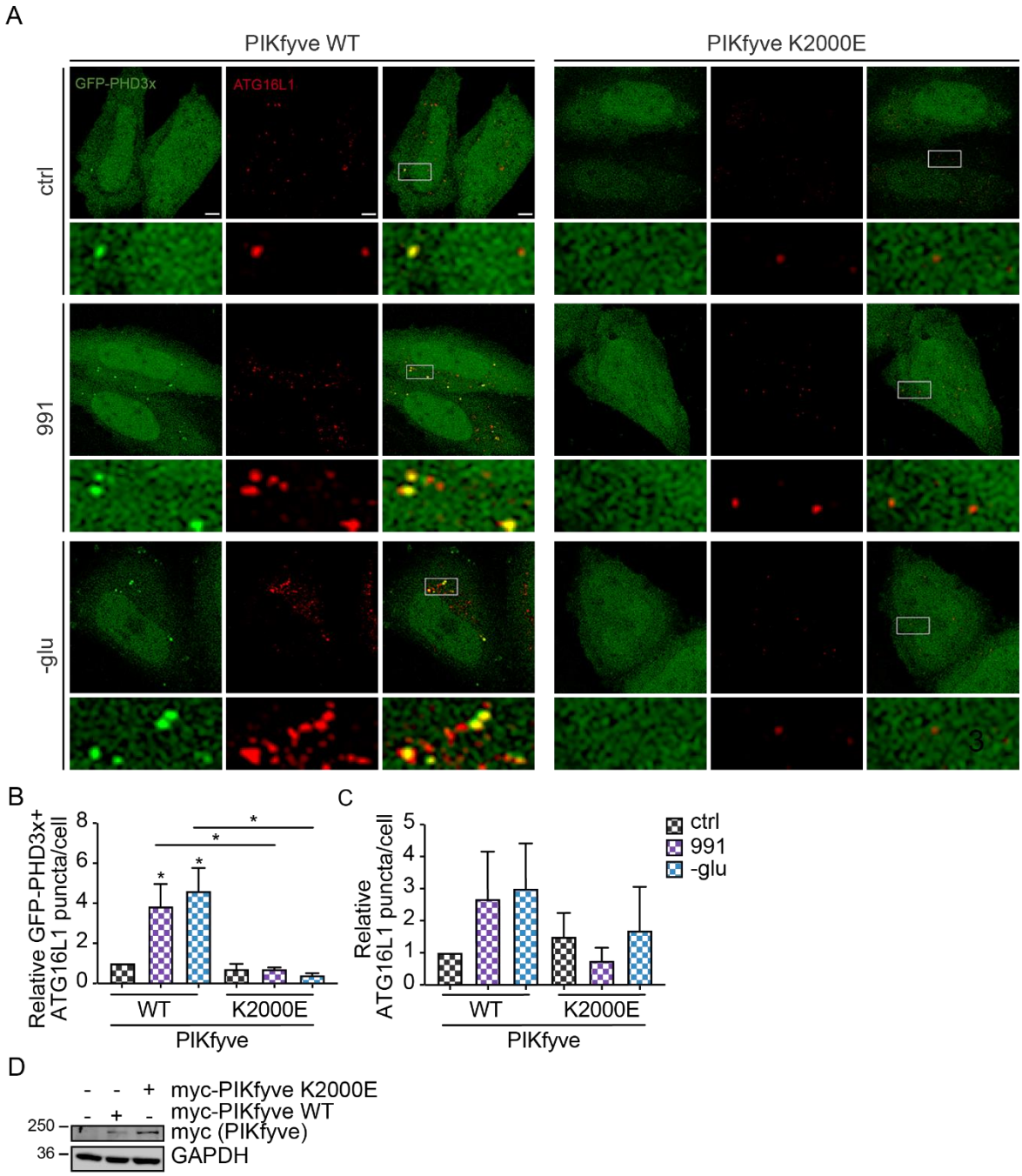

Figure 3.21 | Abrogated synthesis of PI(5)P prevents the increase in PI(5)P-containing phagophores upon glucose starvation and AMPK activation

(A) HeLa cells transfected with FLAG-LKB1, GFP-PHD3x, FLAG-ATG4B mutant and myc-PIKfyve WT or K2000E were treated with 991 (10 µM) or glucose-free media (-glu) for 1 hour. Cells were immunostained for ATG16L1 (Alexa 555: rabbit). DMSO was used as vehicle control. Representative micrographs shown. Scale bar, 5 µm. **(B)** Data show relative changes in GFP-PHD3x+ ATG16L1 puncta and **(C)** total ATG16L1 puncta for experiment in **(A)** normalised to control represented as mean ± SEM (n = 3, 20 cells/condition; *P < 0.05; ANOVA with Tukey's post hoc test). **(D)** Immunoblot probed with myc and GAPDH antibodies showing expression of myc-PIKfyve WT and K2000E mutant in HeLa cells.

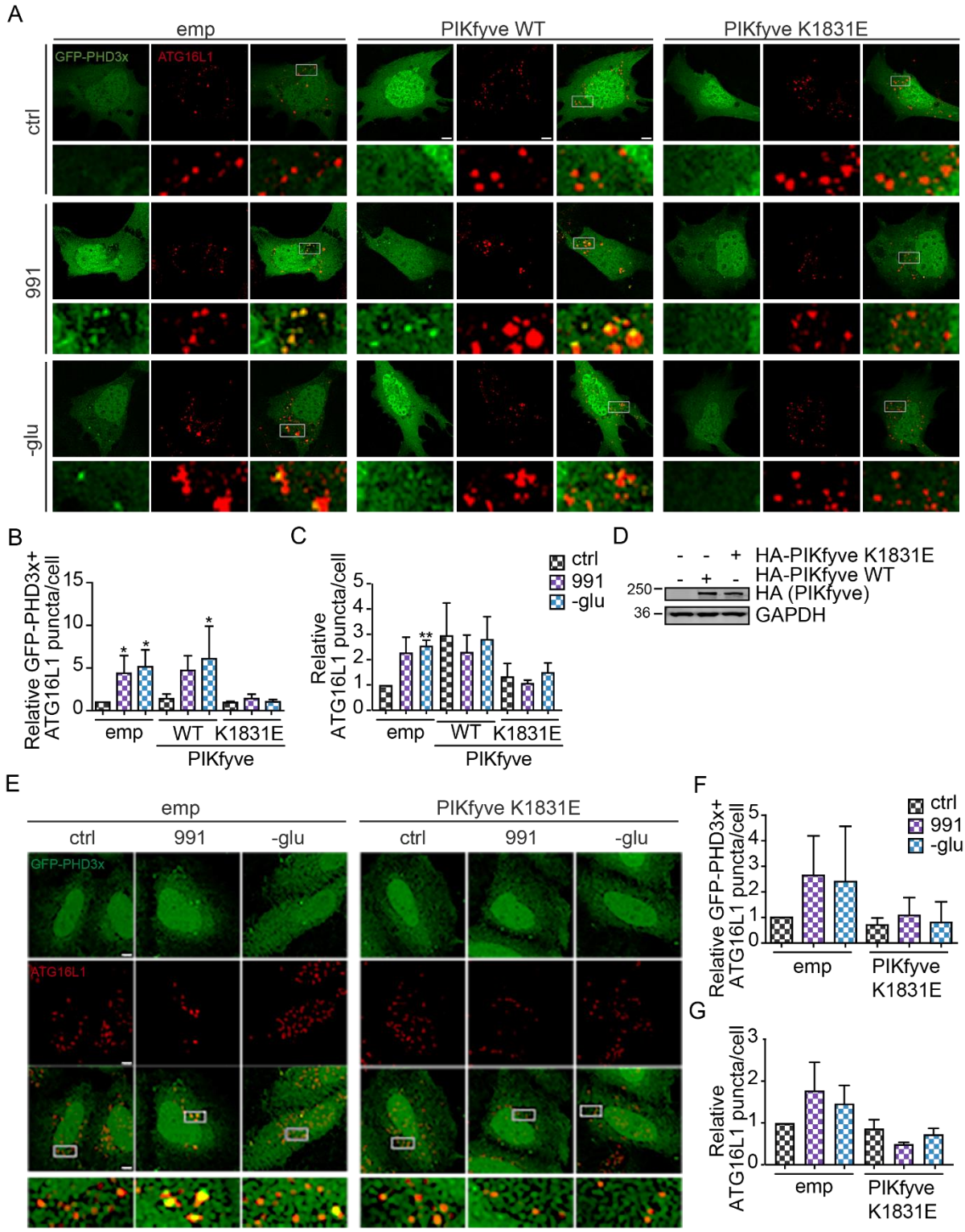

Figure 3.22 | Kinase-deficient PIKfyve prevents the increase in PI(5)P-containing phagophores upon glucose starvation and AMPK activation in HeLa cells

(A) SPCs transfected with GFP-PHD3x, FLAG-ATG4B mutant and empty myc (left panel), myc-PIKfyve WT (middle panel) or kinase-deficient dominant negative myc-PIKfyve K1831E (right panel) were treated with 991 (10 µM) or glucose-free media (-glu) for 1 hour and immunostained for ATG16L1 (Alexa 555: rabbit). **(B)** Data show

relative changes in GFP-PHD3x+ ATG16L1 puncta and **(C)** total ATG16L1 puncta for experiment in **(A)** normalised to empty control. **(D)** Immunoblot probed with HA and GAPDH antibodies showing expression of HA-PIKfyve WT and K1831E mutant in HeLa cells. **(E)** HeLa cells transfected with GFP-PHD3x, FLAG-ATG4B mutant and myc-PIKfyve WT or K1831E were treated with 991 (10 µM) or glucose-free media for 1 hour and immunostained for ATG16L1 (Alexa 555: rabbit). **(F)** Data show relative changes in GFP-PHD3x+ ATG16L1 puncta and **(G)** total ATG16L1 puncta for experiment in **(E)** normalised to empty control.
DMSO was used as vehicle control. Empty vector was used as negative control. Representative micrographs shown. Scale bar, 5 µm. Data are represented as mean ± SEM (n = 3, 20 cells/condition; **P < 0.01, *P < 0.05; ANOVA with Tukey's post hoc test).

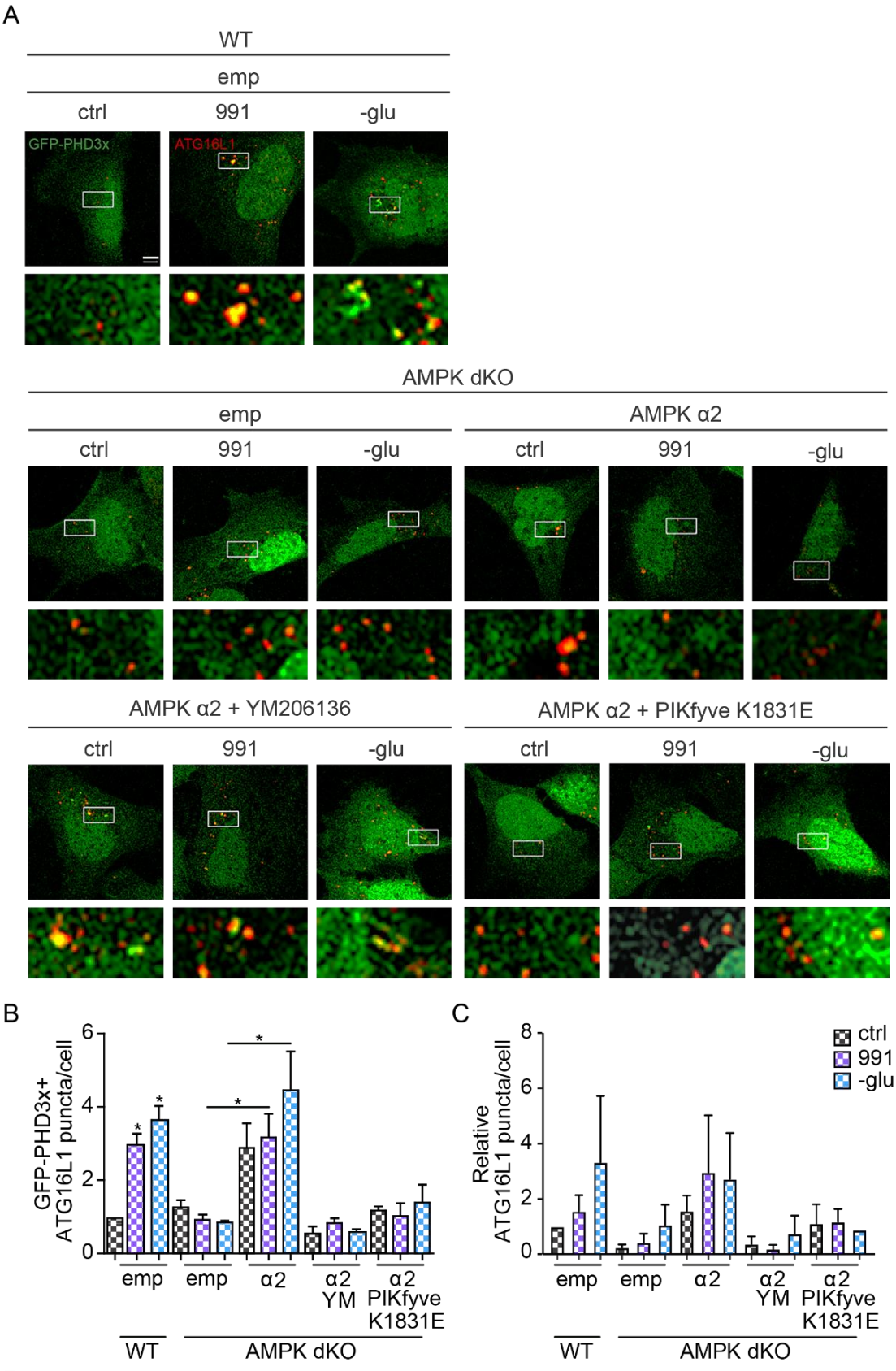
A
WT
emp
ctrl
991
-glu
GFP-PHD3x
ATG16L1
AMPK dKO
emp
AMPK α2
ctrl
991
-glu
ctrl
991
-glu
AMPK α2 + YM206136
AMPK α2 + PIKfyve K1831E
ctrl
991
-glu
ctrl
991
-glu
B
GFP-PHD3x+ ATG16L1 puncta/cell
0
2
4
6
*
*
*
*
emp
emp
α2
α2 YM
α2 PIKfyve K1831E
WT
AMPK dKO
C
Relative ATG16L1 puncta/cell
0
2
4
6
8
ctrl
991
-glu
emp
emp
α2
α2 YM
α2 PIKfyve K1831E
WT
AMPK dKO
D
- + HA-PIKfyve K1831E
250
HA (PIKfyve)
36
GAPDH

Figure 3.23 | Impaired PIKfyve activity prevents rescue of PI(5)P-containing phagophore levels in AMPK dKO cells following AMPK reconstitution

(A) WT and AMPK dKO cells were transfected with GFP-PHD3x and FLAG-ATG4B mutant. AMPK dKO cells were further transfected with myc-AMPK α2 co-transfected with PIKfyve K1831E or treated with YM (100 nM, 1 hour). Cells were immunostained for ATG16L1 (Alexa 555: rabbit). DMSO was used as vehicle control. Empty vector was used as negative control. Representative micrographs shown. Scale bar, 5 µm. **(B)** Data show relative changes in GFP-PHD3x+ ATG16L1 puncta and **(C)** total ATG16L1 puncta for experiment in **(A)** normalised to empty control represented as mean ± SEM (n = 3, 20 cells/condition; *P < 0.05; ANOVA with Tukey's post hoc test). **(D)** Immunoblot probed with HA and GAPDH antibodies showing expression of HA-PIKfyve K1831E in AMPK dKO cells.

3.5 Phosphorylation of PIKfyve S307 by AMPK does not affect the formation of PI(5)P-containing phagophores

AMPK interacts with and phosphorylates PIKfyve on S307 leading to increased PIKfyve activity and synthesis of $PI(3,5)P_2$ (Liu et al., 2013). I, therefore, validated the interaction by mass spectrometry (LS/MS/MS) of GFP-PIKfyve and subsequently by immunoprecipitation of GFP-PIKfyve and myc-AMPKα2 in HEK 293T cells **(Figure 3.24A)**. I also saw increased colocalization between PIKfyve and AMPK puncta following glucose starvation by immunofluorescence in HeLa cells **(Figure 3.24B-C)**. The interaction between PIKfyve and AMPK has been further corroborated by two recent studies, which were examining the role of AMPK, PIKfyve and $PI(3,5)P_2$ for lysosomal function (Fernandez-Mosquera et al., 2019; Yordanov et al., 2019). These findings raised the question of whether an AMPK-PIKfyve interaction plays a role in PI(5)P-dependent autophagy upregulation upon glucose starvation.

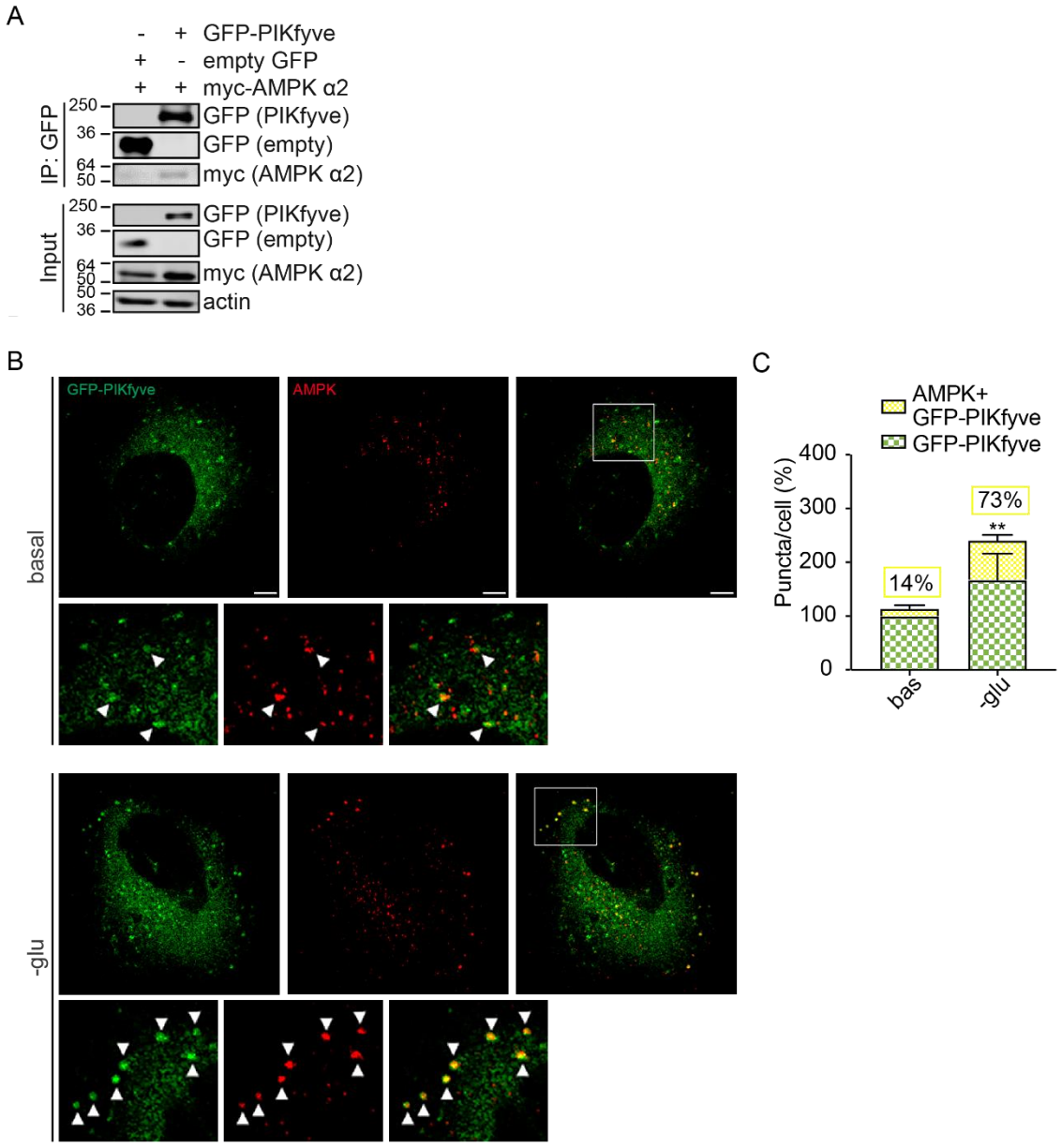

Figure 3.24 | PIKfyve and AMPK interacts in HEK 293T and HeLa cells

(A) HEK 293T cells were transfected with GFP-PIKfyve and myc-AMPK α2. GFP-PIKfyve was immunoprecipitated with GFP-trap beads. Empty vector was used as negative control (n = 3). **(B, C)** HeLa cells transfected with GFP-PIKfyve and incubated in basal or glucose-free media (-glu, 1 hour) were immunostained for AMPKα (Alexa 555: rabbit). Representative micrographs shown. Scale bar, 5 µm. Data show quantification of GFP-PIKfyve puncta (green) and GFP-PIKfyve puncta colocalized with AMPK (yellow) normalised to basal represented as mean ± SEM. The arrows indicate colocalization of GFP-PIKfyve and AMPK. The percentage of GFP-PIKfyve+, AMPK+ puncta is shown above the bar (n = 3, 10 cells/condition; **P < 0.01; two-tailed, paired student's t-test).

3.5.1 AMPK-mediated phosphorylation of PIKfyve on S307 increases PI(3,5)P_2 levels, but not PI(5)P levels.

Since the interaction between PIKfyve and AMPK was suggested to lead to PIKfyve phosphorylation on serine 307 (S307) resulting in increased PIKfyve activity and synthesis of PI(3,5)P_2 (Liu et al., 2013), I examined the effect of glucose starvation on AMPK-mediated PIKfyve phosphorylation on S307 by western blotting. I found that there was an increase in phosphorylation of PIKfyve S307 upon glucose starvation. AMPK inhibition with CC prevented the increase **(Figure 3.25A)**.

Although the AMPK-mediated phosphorylation of PIKfyve S307 appeared to have increased during glucose starvation, the phosphorylation of this residue was suggested to induce PI(3,5)P_2 synthesis. PI(3,5)P_2 is required for endosome to TGN (trans-Golgi network) retrograde trafficking (Rutherford et al., 2006) and for lysosome maturation (Bissig et al., 2017; Yordanov et al., 2019). Since it is uncertain whether this residue also plays a role in PI(5)P synthesis and phagophore formation, I overexpressed a phospho-mutant form of PIKfyve (S307A) in HeLa cells and assessed PI(5)P-containing structures as described above and PI(3,5)P_2-containing punctate structures by using a bio-probe that contains GFP bound to tandem repeats of MLN1, the cytosolic N-terminal polybasic domain of the mucolipin 1 (TRPML1) channel, which is known to be bound by PI(3,5)P_2 (Li et al., 2013). Since PI(3,5)P_2 is present on endosomes and lysosomes, I also stained cells for the endosomal marker CD63. I compared the effects of PIKfyve S307A overexpression with PIKfyve WT overexpression. While using various PIKfyve constructs in this study, I found that overexpression of PIKfyve WT leads to an increase in PI(5)P-containing and total numbers of phagophores compared to cells transfected with empty vectors **(Figure 3.18)**. This correlates with the observation made using a mass assay in HEK 293T cells stably expressing WT or K1831E PIKfyve displaying a 2-fold higher and 2-fold lower mass levels of PI(5)P, respectively, compared to the parental cell line (Sbrissa et al., 2002). This suggests that inducing PIKfyve activity leads to an increase in phagophore formation.

I found that while PIKfyve S307A reduced PI(3,5)P_2-containing puncta levels in a dominant-negative fashion, this mutation did not impede the increased formation of PI(5)P-containing phagophores observed with transfection of PIKfyve WT **(Figure**

3.25B-F). Thus, the observed effects of AMPK activation on increasing the formation of PI(5)P-containing phagophores is not mediated by an AMPK-mediated phosphorylation of PIKfyve on S307.

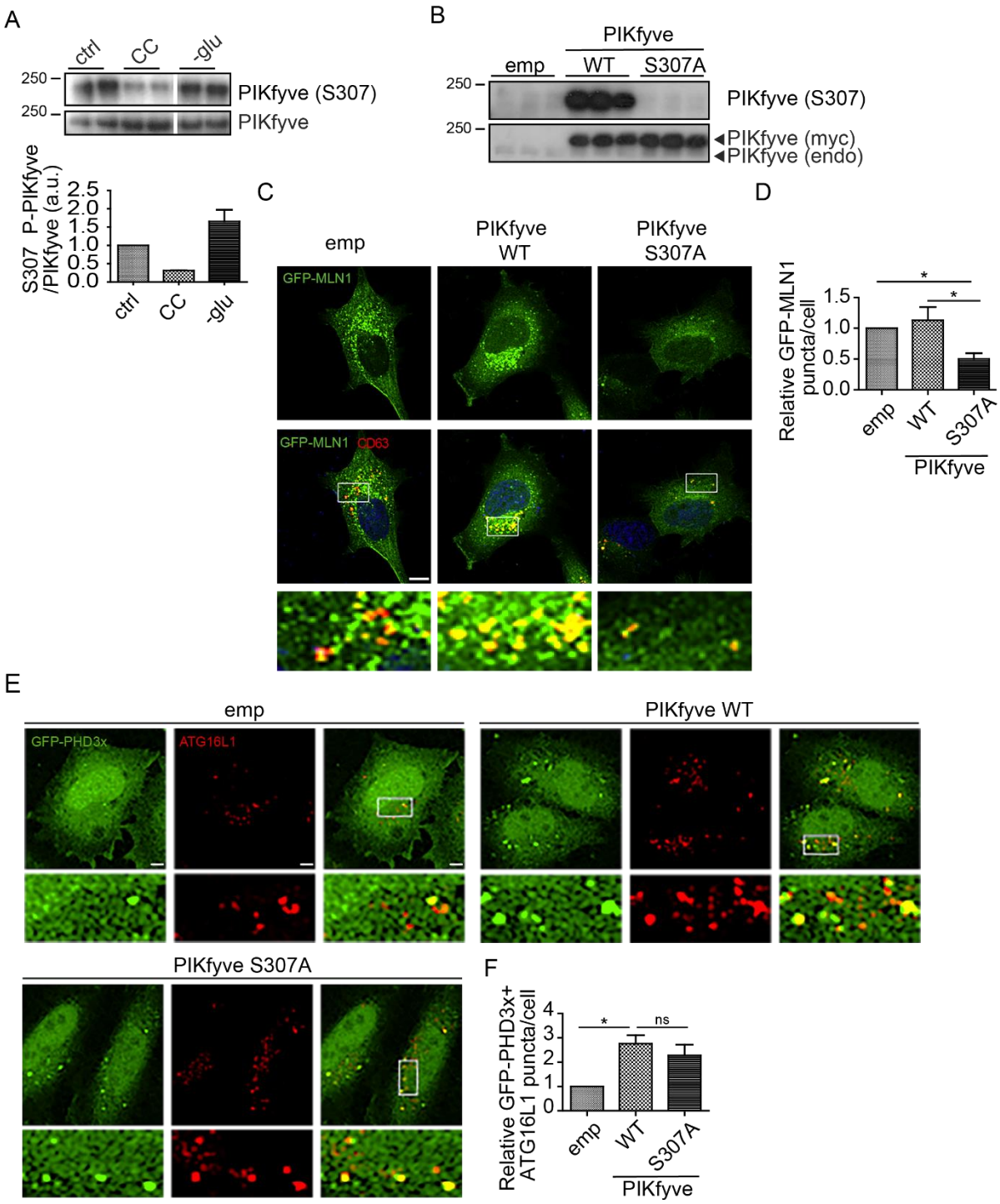

Figure 3.25 | Phosphorylation of PIKfyve on S307 upon glucose starvation does not affect PI(5)P-containing phagophore formation

(A) Immunoblots showing total PIKfyve and P-PIKfyve (S307) in SPCs treated with CC (60 µM, 6 hours), YM (100 nM, 1 hour) or glucose-free media (-glu, 1 hour). DMSO was used as vehicle control. Data show relative S307 P-PIKfyve normalised to total PIKfyve levels represented as mean ± SD (n = 3 for ctrl and -glu; n = 2 for CC). **(B)** Immunoblots showing total PIKfyve and P-PIKfyve (S307) in HeLa cells transfected with PIKfyve WT and phospho-mutant PIKfyve S307A. **(C, D)** HeLa cells transfected with GFP-MLN1, FLAG-LKB1 and PIKfyve WT or S307A were immunostained for

CD63 (Alexa 555: rabbit). Data show relative changes in GFP-MLN1+ puncta normalised to control. **(E, F)** HeLa cells transfected with FLAG-LKB1, GFP-PHD3x, FLAG-ATG4B mutant and PIKfyve WT or S307A were immunostained for ATG16L1 (Alexa 555: rabbit). Data show relative changes in GFP-PHD3x+ ATG16L1 puncta normalised to control.
Empty vector was used as negative control. Representative micrographs shown. Scale bar, 5 µm. Data are represented as mean ± SEM (n = 3, 20 cells/condition; *P < 0.05; ns – non-significant; ANOVA with Tukey's post hoc test).

3.6 Summary

In this chapter, I have shown that AMPK and PIKfyve are involved in PI(5)P-dependent autophagy upregulation. In summary, I have shown shown that:

1. Glucose starvation and AMPK activation cause an increase in autophagy.

2. Glucose starvation and AMPK activation increase PIKfyve activity leading to an increase in PI(5)P-containing phagophores in SPCs, MEFs and LKB1+ HeLa cells.

3. In the absence of AMPK, glucose starvation is unable to increase the PIKfyve-mediated formation of PI(5)P-containing phagophores.

4. mTORC1 activation inhibits the formation of PI(5)P-containing phagophores, while mTORC1 inhibition induces it.

Although I showed that AMPK is involved in PI(5)P-dependent autophagy upregulation, the exact mechanism behind this pathway remains unresolved and raises additional questions.

Since phosphorylation of PIKfyve on S307 by AMPK appears to have no role in the formation of PI(5)P-containing phagophores, I decided to assess whether AMPK phosphorylates other sites on PIKfyve given the role of AMPK in inducing PI(5)P-dependent autophagy in our study. I immunoprecipitated PIKfyve in presence and absence of CC, which were next subjected to a mass spectrometry analysis of phospho-enriched PIKfyve. A new phosphorylation site on PIKfyve was identified – serine 1862. This site is localised in the kinase domain of PIKfyve (Ikonomov et al., 2001). Upon exchange of the serine residue with an alanine to create a phospho-mutant form of this construct, I observed enlargement of vacuoles in HeLa cells

transfected with the S1862A mutant **(Figure 3.26)**. This phenotype is known to be caused by abrogated PI(3,5)P_2 synthesis as mentioned above. Interestingly, this mutant did not affect the ability of PIKfyve to synthesize PI(5)P and form PI(5)P-containing phagophores further corroborating the above-mentioned observations that AMPK phosphorylation of PIKfyve may be important for PI(3,5)P_2 synthesis.

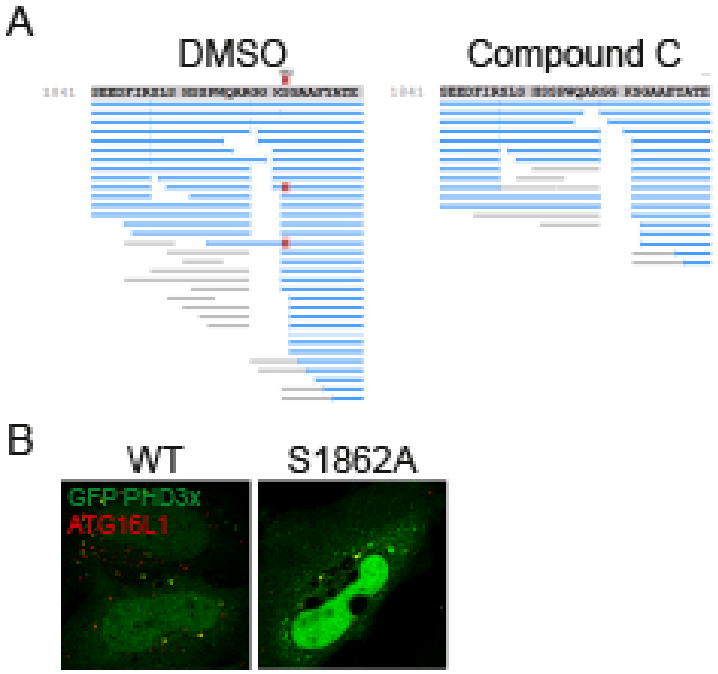

Figure 3.26 | Mutagenesis of novel AMPK phosphorylation site on PIKfyve leads to vacuolar enlargement

(A) HEK 293T cells were transfected with GFP-PIKfyve WT and treated with CC (60 µM, 4 hours) or DMSO. Cells were immunoprecipitated using GFP-trap beads. By LS/MS/MS analysis of the phospho-enriched PIKfyve peptides, AMPK phosphorylation sites on PIKfyve were identified. Each lane signifies a peptide. The red mark indicates the phosphorylation site (S1862). **(B)** HeLa cells transfected with FLAG-LKB1, GFP-PHD3x, FLAG-ATG4B mutant and myc-PIKfyve S1862A. Empty vector was used as negative control. Representative images shown. Scale bar, 5 µm.

These findings led us to believe that AMPK could have another effect on PIKfyve signalling in addition to those already reported:

- AMPK phosphorylation of an unknown kinase may increase PIKfyve activity leading to an increase in PI(5)P levels and PI(5)P-containing phagophore formation upon glucose starvation.

I, therefore, continued pursuing this hypothesis to understand the role of AMPK in PIKfyve-mediated autophagy upregulation and sought to identify the PIKfyve interactome involved in this.

4 AMPK-dependent PIKfyve activity is mediated through ULK1

In the present chapter, I sought to identify interactors involved in AMPK-mediated PI(5)P-dependent autophagy through activation of PIKfyve. Since our data is consistent with AMPK causing indirect activation of PIKfyve, I hypothesized that PIKfyve could be activated directly by another member of the AMPK interactome.

Another key kinase involved in the glucose starvation-induced autophagic pathway is ULK1, which is bound by AMPK on the P/S rich domain of ULK1. This interaction is required for ULK1-mediated autophagy upregulation (Lee et al., 2010b). AMPK phosphorylates ULK1 upon chemically-induced AMPK activation or glucose starvation (Egan et al., 2015; Kim et al., 2011b). I, therefore, studied the involvement of ULK1 in PI(5)P-dependent autophagy upregulation.

4.1 ULK1 activity is required for the increased PIKfyve activity observed upon glucose starvation and AMPK activation

It is well-established that canonical autophagy is initiated by inhibition of mTORC1 leading to the dephosphorylation of the ULK complex. ULK1 activates the VPS34 complex leading to synthesis of PI(3)P as previously described (Baskaran et al., 2014; Ganley et al., 2009; Hosokawa et al., 2009; Kim et al., 2011a).

Therefore, I was interested in examining whether ULK1 may also be involved in non-canonical PI(5)P-dependent autophagy signalling by activating PIKfyve.

4.1.1 ULK1 activity is required for the increased formation of PI(5)P-containing phagophores and LC3 puncta following glucose starvation and AMPK activation

I first tested whether inhibition of ULK1 would affect the formation of PI(5)P-containing phagophores observed upon glucose starvation and 991 treatment by using the selective ULK1 inhibitor SBI-0206965 (hereafter referred to as SBI). Treatment with this inhibitor was shown to abolish the increase in autophagy levels observed upon

treatment of A549 lung cancer cells with the mTORC1 inhibitor AZD8055 (Chresta et al., 2010).

I found that the increase in PI(5)P-containing and total numbers of phagophores observed upon glucose starvation and 991 treatment was mitigated when treating HeLa cells with SBI **(Figure 4.1)**. Consistently, treatment with SBI prevented the increase in LC3 puncta observed upon glucose starvation and 991 treatment **(Figure 4.2).**

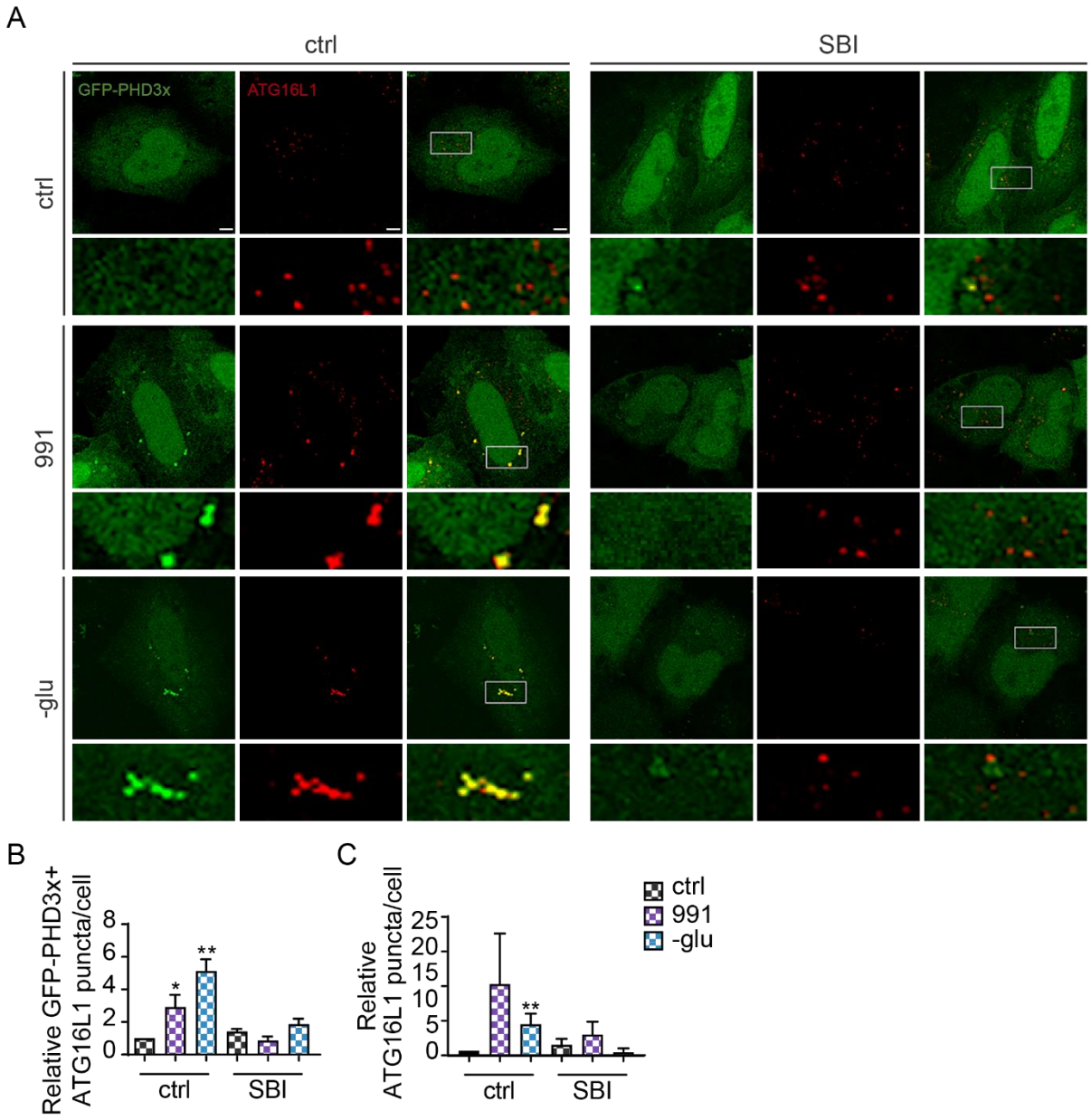

Figure 4.1 | ULK1 inhibition impairs the PI(5)P-containing phagophore increase upon glucose starvation and AMPK activation

(A) HeLa cells transfected with FLAG-LKB1, GFP-PHD3x and FLAG-ATG4B mutant were treated with the ULK1 inhibitor SBI-0206965 (SBI, 5 µM, 4 hours) and 991 (10 µM) or glucose-free media (-glu) for 1 hour. Cells were immunostained for ATG16L1 (Alexa 555: rabbit). DMSO was used as vehicle control. Representative micrographs shown. Scale bar, 5 µm. **(B)** Data show relative changes in GFP-PHD3x+ ATG16L1 puncta and **(C)** total ATG16L1 puncta for experiment in **(A)** normalised to control represented as mean ± SEM (n = 3, 20 cells/condition; (**P < 0.01, *P < 0.05; ANOVA with Tukey's post hoc test).

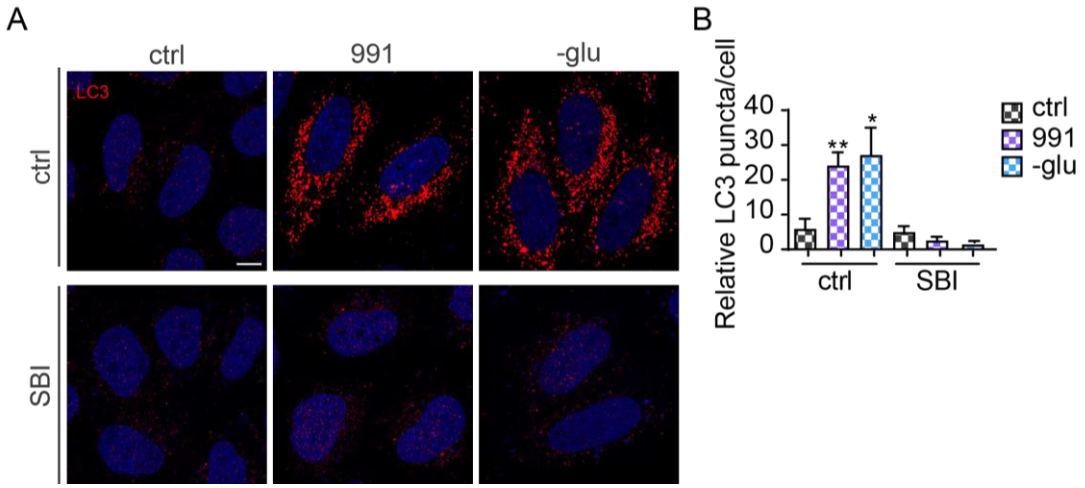

Figure 4.2 | ULK1 inhibitor impairs LC3 puncta increase upon glucose starvation and AMPK activation

(A) LC3 immunostaining (Alexa 555: rabbit) in HeLa cells transfected with FLAG-LKB1 and treated with SBI (5 μM, 4 hours) and 991 (10 μM) or glucose-free media (-glu) for 1 hour. DMSO was used as vehicle control. Representative micrographs shown. Scale bar, 5 μm. **(B)** Data show changes in LC3 puncta/cell for experiment in **(A)** normalised to control represented as mean ± SEM (n = 3, 30 cells/condition; **P < 0.01, *P < 0.05; ANOVA with Tukey's post hoc test).

4.1.2 The increase in PI(5)P-containing phagophore formation caused by PIKfyve overexpression is prevented by ULK1 inhibition

Since ULK1 inhibition appeared to abrogate formation of PI(5)P-containing phagophores, I treated cells transfected with PIKfyve with SBI to test whether ULK1 had a direct effect on PIKfyve activity. Inhibition of ULK1 mitigated the increase in PI(5)P-containing and total numbers of phagophores observed upon PIKfyve overexpression **(Figure 4.3)**, suggesting that ULK1 activity is required for the PIKfyve-mediated formation of PI(5)P-containing phagophores.

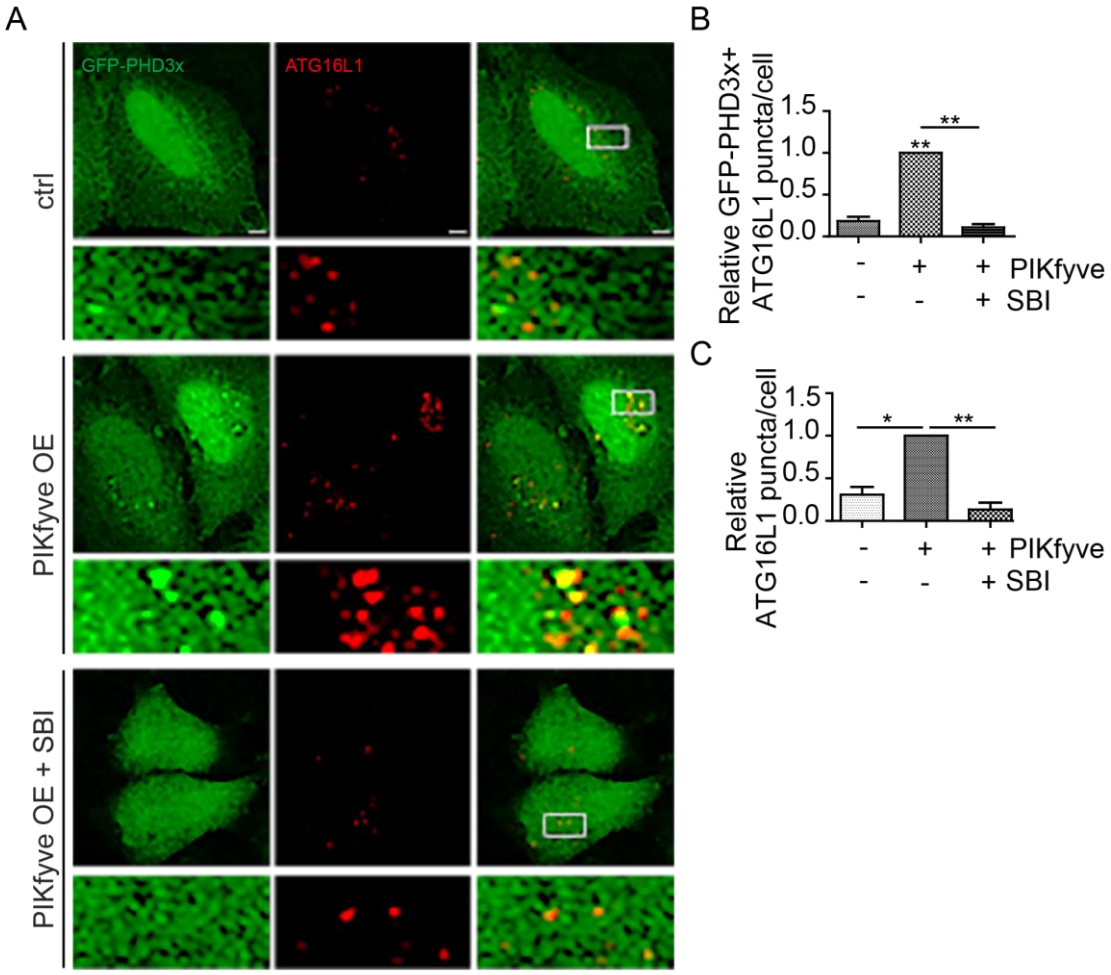

Figure 4.3 | ULK1 inhibition inactivates PIKfyve

(A) HeLa cells transfected with FLAG-LKB1, GFP-PHD3x, FLAG-ATG4B mutant and myc-PIKfyve were treated with SBI (5 µM, 4 hours) and immunostained for ATG16L1 (Alexa 555: rabbit). DMSO was used as vehicle control. Empty vector was used as negative control. Representative micrographs shown. Scale bar, 5 µm. **(B)** Data show relative changes in GFP-PHD3x+ ATG16L1 puncta and **(C)** total ATG16L1 puncta for experiment in **(A)** normalised to control represented as mean ± SEM (n = 3, 20 cells/condition; **P < 0.01, *P < 0.05; ANOVA with Tukey's post hoc test).

4.1.3 ULK1 increases PI(5)P-containing phagophores in basal conditions

Since ULK1 is constitutively active when overexpressed (Egan et al., 2015), I tested whether this would have an effect on formation of PI(5)P-containing phagophores. I found an increase in PI(5)P-containing phagophores upon ULK1 overexpression. This increase was abolished when treating with SBI **(Figure 4.4)** or YM **(Figure 4.5A-C)**. ULK1 overexpression led to an increase in autophagy flux, which was mitigated with YM treatment **(Figure 4.5D-E)** suggesting the existence of a relationship between the two kinases.

Additionally, ULK1 overexpression was found to increase PI(5)P-containing phagophores in AMPK dKO cells, indicating that a direct activation of PIKfyve in the context of PI(5)P and autophagy biogenesis is maintained by ULK1 and not AMPK **(Figure 4.6)**. ULK1 overexpression did, however, not increase the levels of $PI(3,5)P_2$ puncta that were visualised with the GFP-MLN1 bio-probe **(Figure 4.7)**. These findings suggest that the effects of AMPK activators and glucose starvation on the induction of PI(5)P-dependent autophagy is mediated through ULK1 and led to the hypothesis that AMPK indirectly activates PIKfyve via ULK1.

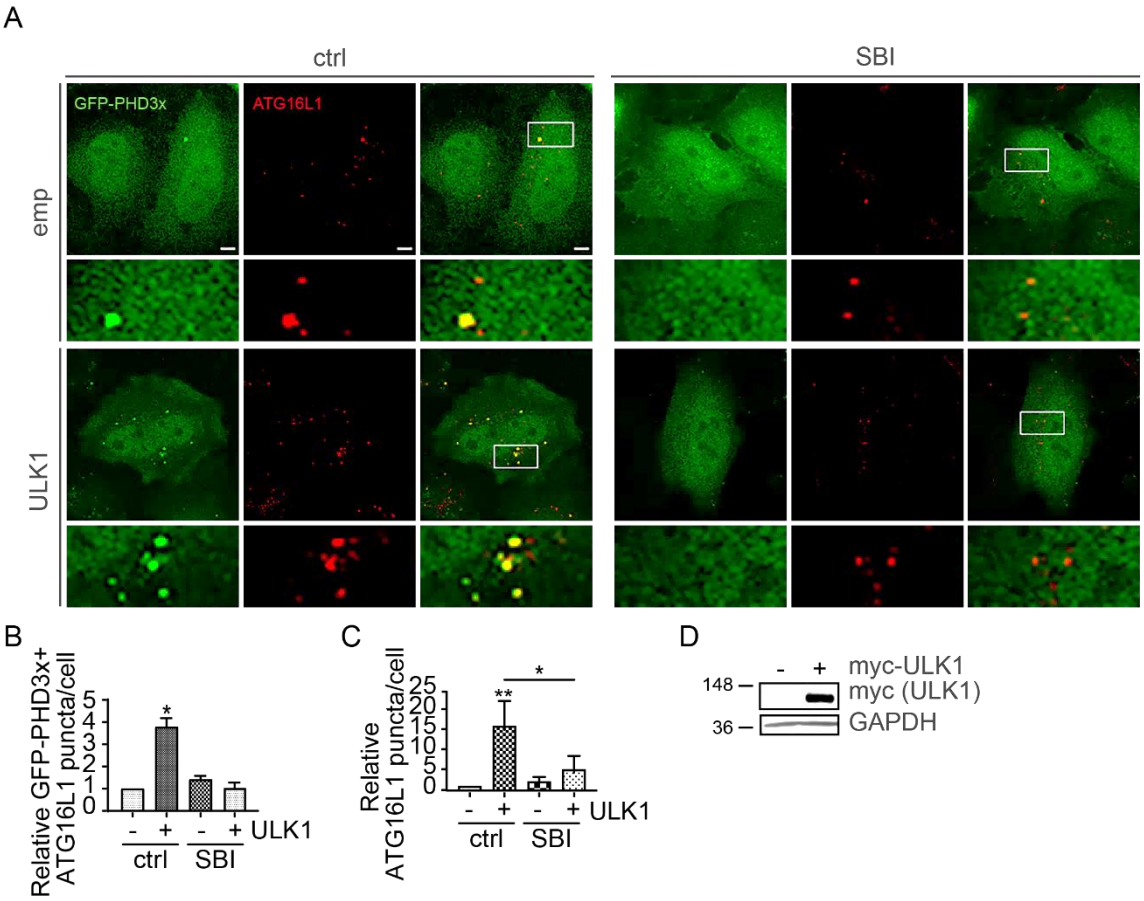

Figure 4.4 | ULK1 induces formation of PI(5)P-containing phagophores

(A) HeLa cells transfected with FLAG-LKB1, GFP-PHD3x, FLAG-ATG4B mutant and myc-ULK1 were treated with SBI (5 µM, 4 hours) and immunostained for ATG16L1 (Alexa 555: rabbit). DMSO was used as vehicle control. Empty vector was used as negative control. Representative micrographs shown. Scale bar, 5 µm. **(B)** Data show relative changes in GFP-PHD3x+ ATG16L1 puncta and **(C)** total ATG16L1 puncta for experiment in **(A)** normalised to control represented as mean ± SEM (n = 3, 20 cells/condition; **P < 0.01, *P < 0.05; ANOVA with Tukey's post hoc test). **(D)** Immunoblot probed with myc and GAPDH antibodies showing expression of myc-ULK1 in HeLa cells.

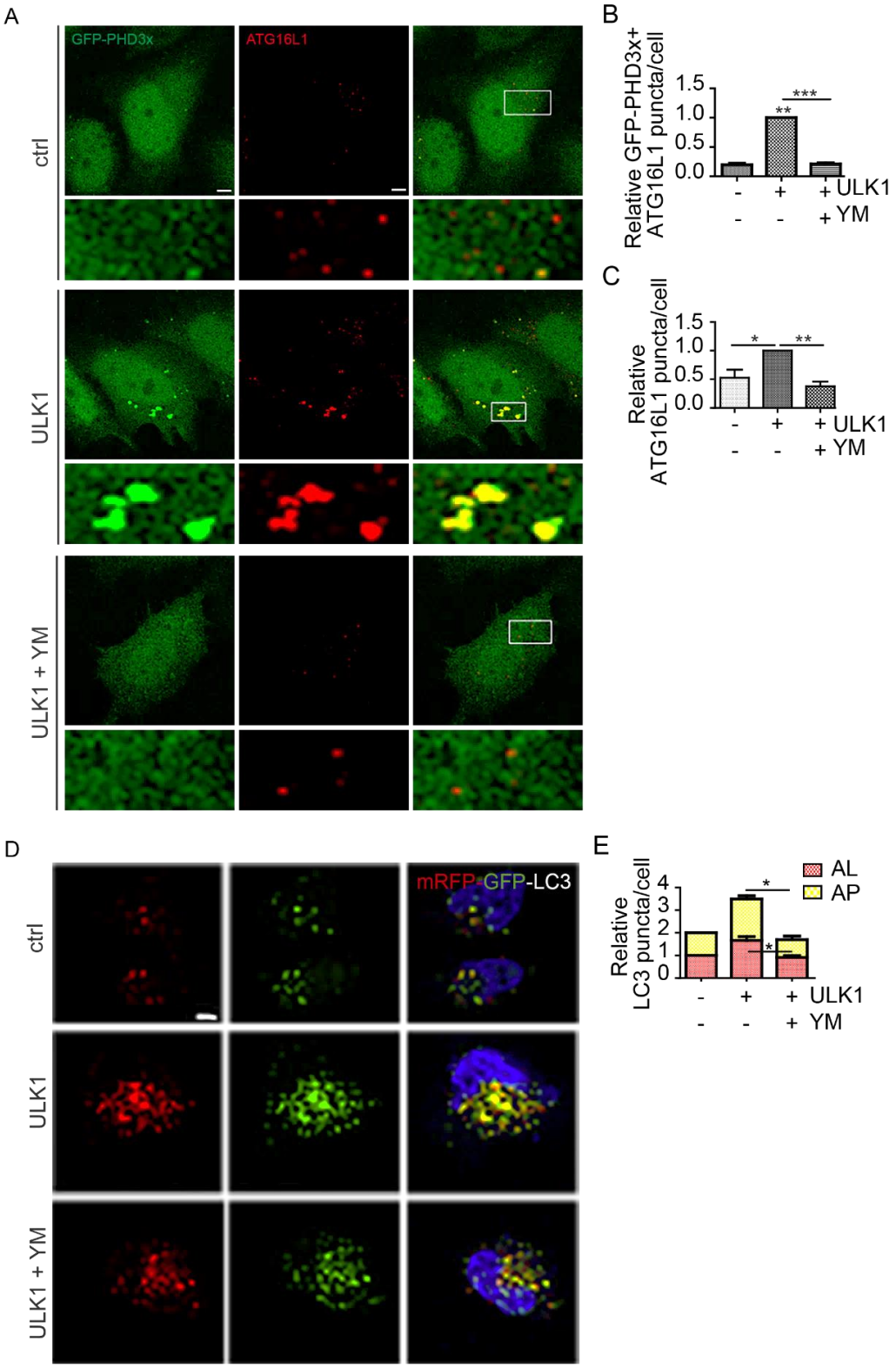

Figure 4.5 | ULK1 overexpression increases formation of PI(5)P-containing phagophores in basal conditions

(A) HeLa cells transfected with FLAG-LKB1, GFP-PHD3x, FLAG-ATG4B mutant and myc-ULK1 treated with YM (100 nM, 1 hour) were immunostained for ATG16L1 (Alexa

555: rabbit). **(B)** Data show relative changes in GFP-PHD3x+ ATG16L1 puncta and **(C)** total ATG16L1 puncta for experiment in **(A)** normalised to ULK1-transfected cells. **(D, E)** HeLa cells transfected with mRFP-GFP-LC3, FLAG-LKB1 and myc-ULK1 were treated with YM (100 nM, 1 hour). Data show relative changes in autophagosomes (yellow dots) and autolysosomes (red dots) normalised to control.
DMSO was used as vehicle control. Empty vector was used as negative control. Representative micrographs shown. Scale bar, 5 μm. Data are represented as mean ± SEM (n = 3, 20 cells/condition; ***P < 0.001, **P < 0.01, *P < 0.05; ANOVA with Tukey's post hoc test).

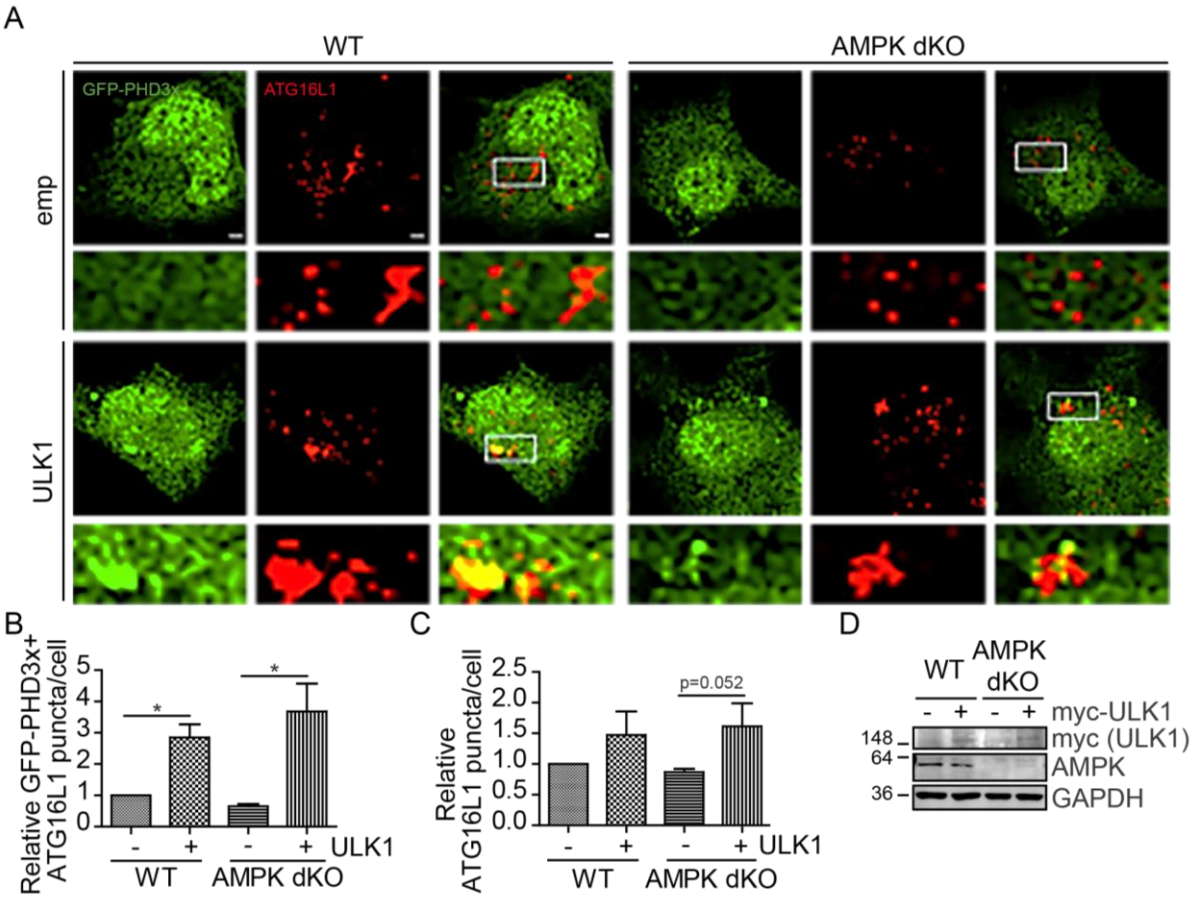

Figure 4.6 | Active ULK1 leads to an increase in PI(5)P-containing phagophores in the absence of AMPK

(A) WT and AMPK dKO cells transfected with GFP-PHD3x, FLAG-ATG4B mutant ± myc-ULK1 were immunostained for ATG16L1 (Alexa 555: rabbit). Empty vector was used as negative control. Representative micrographs shown. Scale bar, 5 µm. **(B)** Data show relative changes in GFP-PHD3x+ ATG16L1 puncta and **(C)** total ATG16L1 puncta for experiment in **(A)** normalised to empty control represented as mean ± SEM (n = 3, 20 cells/condition; *P < 0.05; ANOVA with Tukey's post hoc test). **(D)** Immunoblot probed with myc, AMPK and GAPDH antibodies showing expression of myc-ULK1 in WT and AMPK dKO cells.

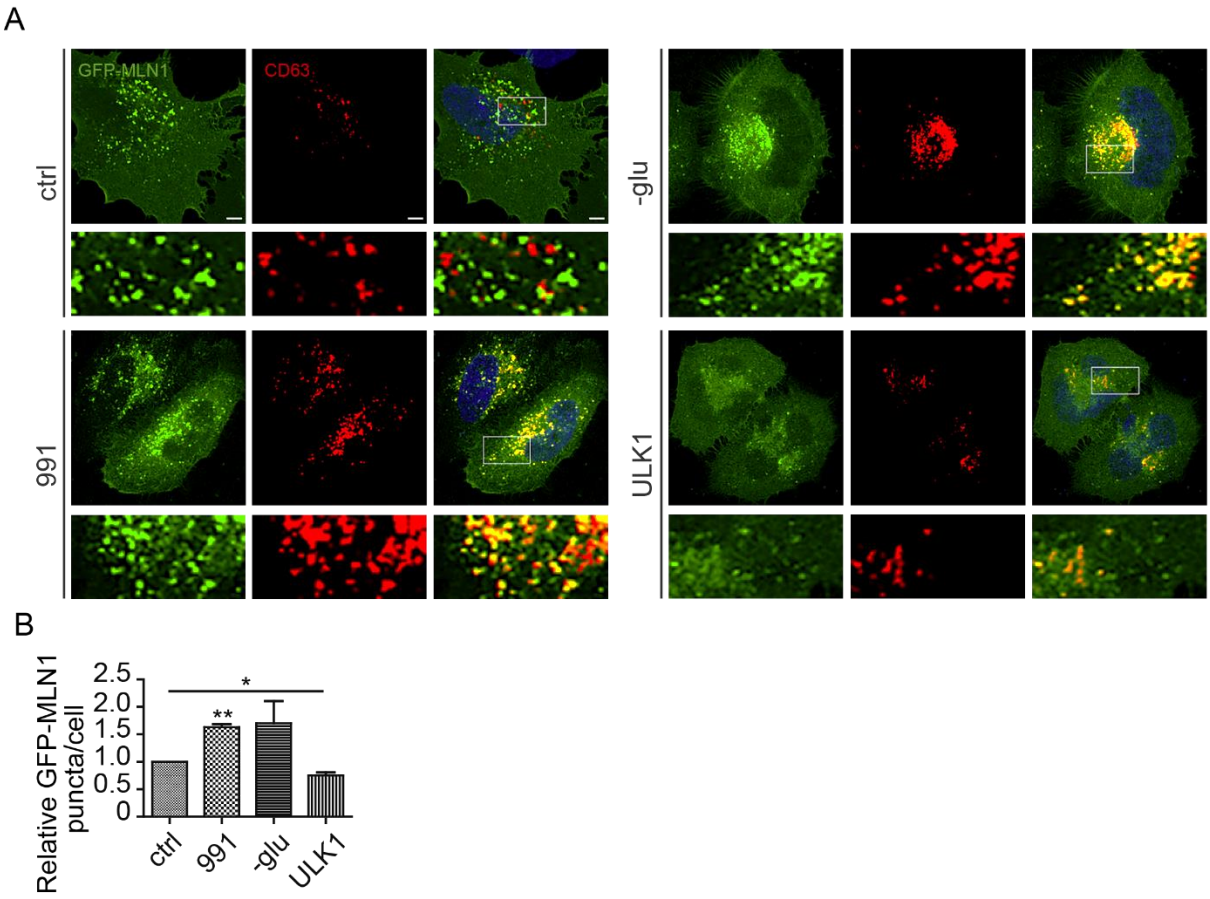

Figure 4.7 | ULK1 overexpression does not increase PI(3,5)P_2 puncta

(A) HeLa cells transfected with GFP-MLN1 and FLAG-LKB1 were treated with 991 (10 µM) or incubated in glucose-free media (-glu) for 1 hour or transfected with ULK1. DMSO was used as vehicle control. Empty vector was used as negative control. Representative micrographs shown. Scale bar, 5 µm. **(B)** Data show relative levels in GFP-MLN1+ puncta for experiment in **(A)** normalised to control represented as mean ± SEM (n = 3, 20 cells/condition; **P < 0.01, *P < 0.05; ANOVA with Tukey's post hoc test).

4.2 ULK1 is a newly identified PIKfyve interactor

Since the data suggests the existence of a link between ULK1 and PIKfyve, I sought to dissect this relationship by performing a range of immunoprecipitations and kinase assays.

4.2.1 PIKfyve and ULK1 interact

First, I analysed immunoprecipitates of endogenous PIKfyve in HEK 293T cells by western blotting and found that PIKfyve interacts with ULK1 **(Figure 4.8A)**. Consistently, immunoprecipitation of overexpressed myc-ULK1 showed an interaction with endogenous PIKfyve **(Figure 4.8B)**.

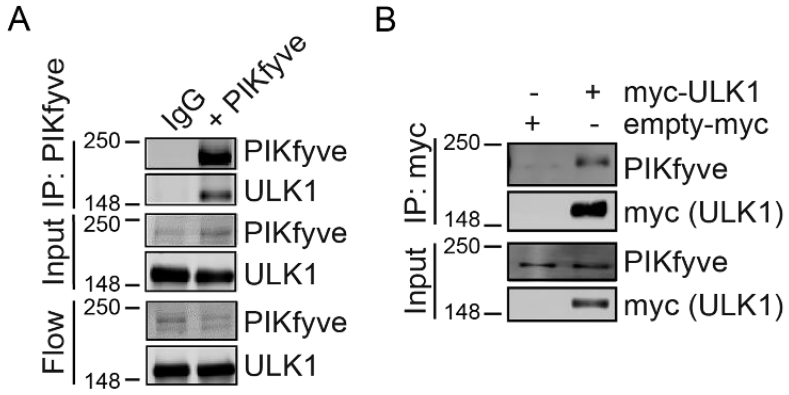

Figure 4.8 | PIKfyve immunoprecipitates with ULK1 in HEK 293T cells

(A) Immunoblots showing immunoprecipitation of endogenous PIKfyve in HEK 293T cells using anti-PIKfyve antibody. IgG antibody was used as negative control. Eluted proteins were visualised with PIKfyve and ULK1 antibodies (n = 3). **(B)** HEK 293T cells were transiently transfected with myc-ULK1. myc-ULK1 was immunoprecipitated with myc-trap beads. Empty vector was used as negative control. Eluted proteins were analysed by immunoblots with PIKfyve and myc antibodies (n = 2).

4.2.2 PIKfyve-ULK1 binding is independent of AMPK activity

Next, I considered whether the kinase activity of AMPK might be required for the binding between PIKfyve and ULK1. For instance, AMPK-mediated phosphorylation could cause a conformational change in PIKfyve that allows for its binding to ULK1 and results in its activation through phosphorylation by ULK1, a concept known as priming. To address this question, I transfected cells with GFP-PIKfyve WT and S307A and found that the inability of AMPK to phosphorylate PIKfyve on S307 did not affect the interaction between GFP-PIKfyve isolated by using GFP-trap beads and endogenous ULK1 **(Figure 4.9)**. Furthermore, transfection of cells with GFP-PIKfyve and dominant-negative catalytic-dead AMPK α2 K45R, did not affect the interaction between GFP-PIKfyve and ULK1 **(Figure 4.10)**. This suggests that the catalytic activity of AMPK does not impact PIKfyve-ULK1 binding (consistent with ULK1 overexpression inducing formation of PI(5)P-containing phagophores in AMPK dKO cells **(Figure 4.6)**).

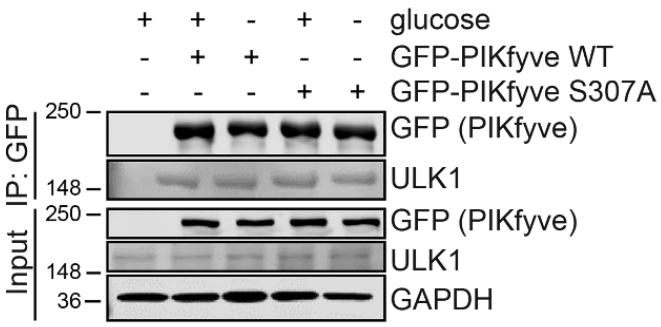

Figure 4.9 | Phospho-mutant PIKfyve immunoprecipitates with ULK1

HEK 293T cells transiently transfected with GFP-PIKfyve WT or phospho-mutant GFP-PIKfyve S307A were incubated in basal or glucose-free media (1 hour) and GFP-tagged proteins were immunoprecipitated with GFP-trap beads. Eluted proteins were analysed by immunoblots with GFP and ULK1 antibodies. Empty vector was used as negative control. GAPDH was used as a loading control (n = 2).

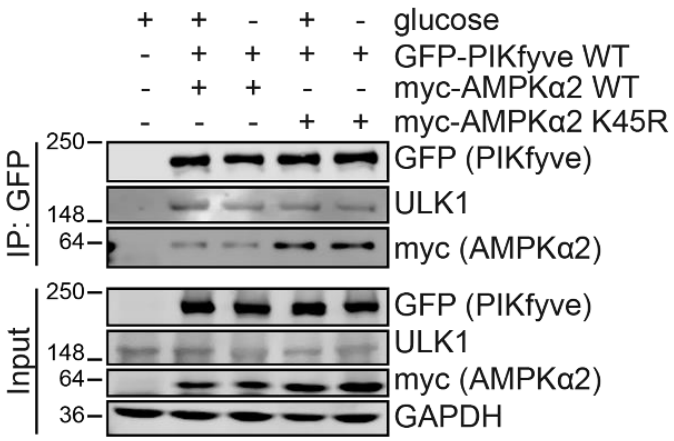

Figure 4.10 | Kinase-deficient AMPK overexpression does not impair PIKfyve-ULK1 immunoprecipitation

HEK 293T cells were transiently transfected with GFP-PIKfyve WT and myc-AMPK α2 WT or kinase-dead myc-AMPK α2 K45R and incubated in basal or glucose-free media (1 hour). GFP-PIKfyve was immunoprecipitated with GFP-trap beads. Eluted proteins were analysed by immunoblots with GFP, myc and ULK1 antibodies. Empty vector was used as negative control. GAPDH was used as a loading control (n = 2).

4.2.3 PIKfyve and ULK1 interaction increases following glucose starvation

Next, I tested the interaction between PIKfyve and ULK1 during glucose starvation and found that 30 minutes of glucose starvation increased endogenous ULK1-PIKfyve interaction in immunoprecipitates from HEK 293T cells **(Figure 4.11A-B)**. I also saw increased colocalization between PIKfyve and ULK1 by immunofluorescence following glucose starvation in HeLa cells **(Figure 4.11C-D)**.

The findings shown so far suggests that ULK1 plays an important role in the non-canonical signalling that leads to the formation of PI(5)P-containing autophagosomes upon glucose starvation.

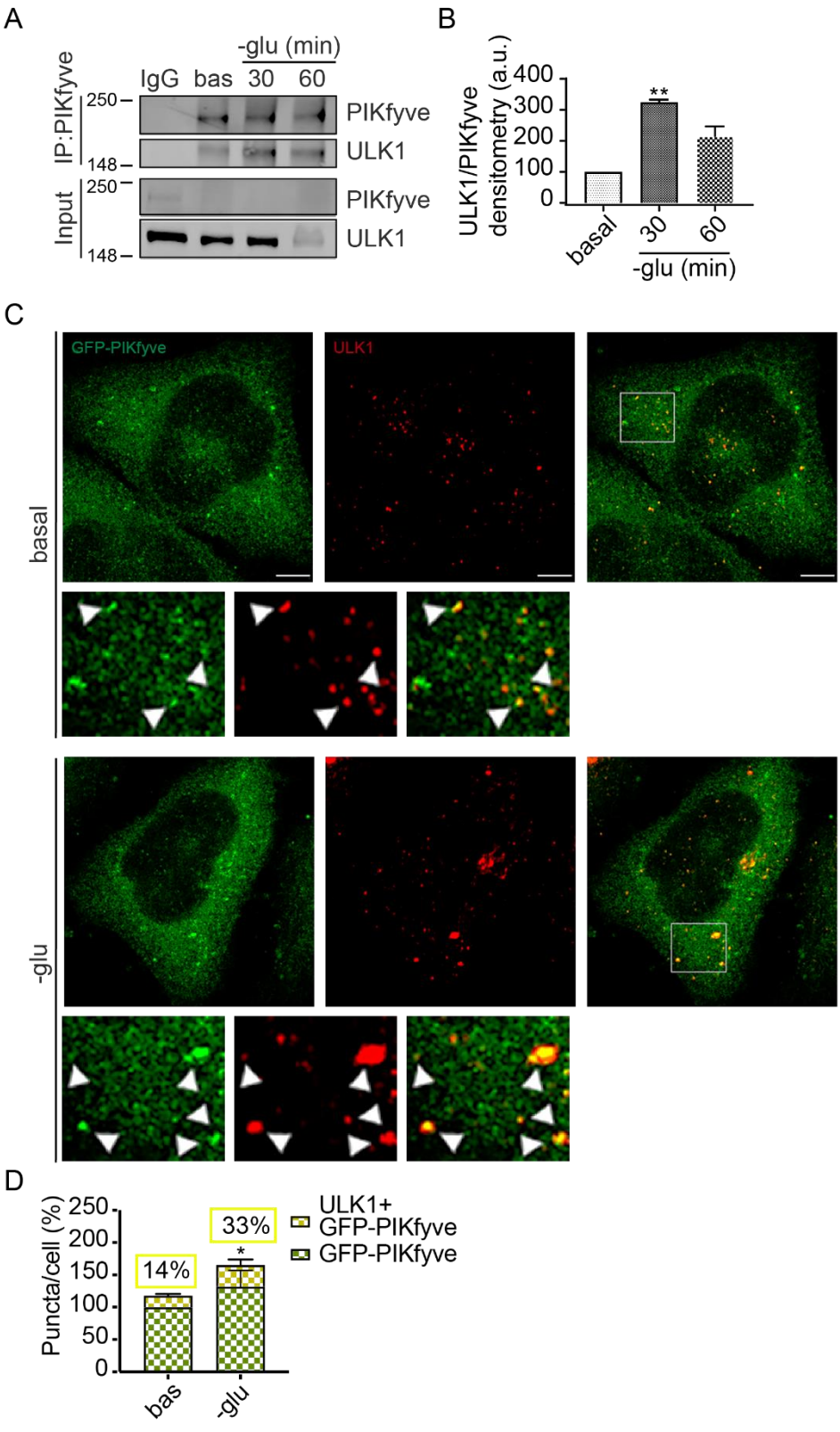

Figure 4.11 | Glucose starvation increases PIKfyve interaction with ULK1

(A, B) Immunoblots showing immunoprecipitation of endogenous PIKfyve in HEK 293T cells following glucose starvation (-glu) for 30 or 60 minutes using anti-PIKfyve antibody. IgG antibody was used as negative control. Eluted proteins were visualised with PIKfyve and ULK1 antibodies. Data show relative changes in ULK1/PIKfyve

binding normalised to basal (n = 3 for 30 minutes; n = 2 for 60 minutes). **(C, D)** HeLa cells transfected with GFP-PIKfyve were incubated in basal or glucose-free media (1 hour) and immunostained for ULK1 (Alexa 555: rabbit). Representative micrographs shown. Scale bar, 5 µm. Data show relative changes in GFP-PIKfyve puncta (green) and GFP-PIKfyve puncta colocalized with ULK1 (yellow). The arrows indicate colocalization of GFP-PIKfyve and ULK1. The percentage of GFP-PIKfyve+, ULK1+ puncta is shown above the bar (n = 3, 10 cells/condition).
Data are represented as mean ± SEM (**P < 0.01; two-tailed, paired student's t-test).

4.2.4 PIKfyve binds the kinase domain of ULK1

Since I found that ULK1 interacts with PIKfyve and causes an increase in PI(5)P-containing phagophore formation, I sought to identify the binding site of PIKfyve on ULK1.

To determine which region of ULK1 is required for its interaction with PIKfyve, I used a series of ULK1 deletion mutants (Lee et al., 2010b). Co-immunoprecipitation analyses revealed that PIKfyve binds to amino acids 1–278 within the kinase domain (KD) of ULK1 **(Figure 4.12A-B)**. Next, cells were transfected with GFP-PIKfyve and HA-ULK1 WT or a mutant HA-ULK1 with a deletion in the KD (ΔKD). Upon staining for HA, the inability of the mutant ULK1 to colocalise with PIKfyve was observed by immunofluorescence **(Figure 4.12C-D)**. As expected, when overexpressing a mutant ULK1 with a deletion in the KD (ΔKD) instead of ULK1 WT, the increase in PI(5)P-containing phagophores observed with ULK1 WT overexpression was abrogated **(Figure 4.13).**

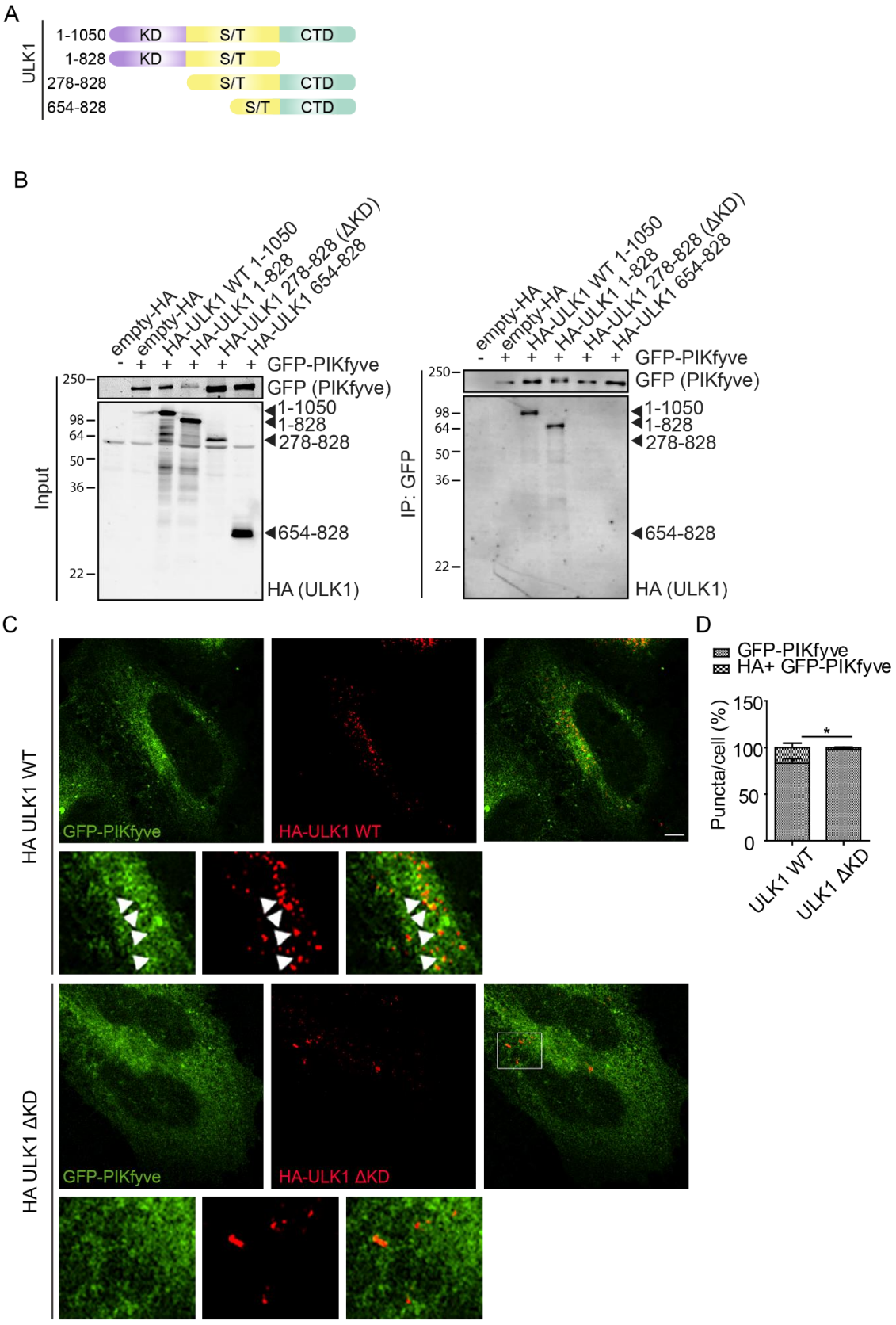
A
ULK1
1-1050
KD
S/T
CTD
1-828
KD
S/T
278-828
S/T
CTD
654-828
S/T
CTD
B
empty-HA
empty-HA
HA-ULK1 WT 1-1050
HA-ULK1 1-828
HA-ULK1 278-828 (ΔKD)
HA-ULK1 654-828
GFP-PIKfyve
GFP (PIKfyve)
Input
IP: GFP
250
98
64
50
36
22
1-1050
1-828
278-828
654-828
HA (ULK1)
C
HA ULK1 WT
HA ULK1 ΔKD
GFP-PIKfyve
HA-ULK1 WT
HA-ULK1 ΔKD
D
GFP-PIKfyve
HA+ GFP-PIKfyve
Puncta/cell (%)
150
100
50
0
*
ULK1 WT
ULK1 ΔKD

Figure 4.12 | PIKfyve binds the ULK1 kinase domain

(A) Schematic representation of ULK1 domain structure and deletion constructs used to map binding sites. The mouse ULK1 protein consists of an N-terminal kinase domain (KD; 1–278), serine/theonine-rich domain (S/T domain, 279–828), and C-terminal domain (CTD, 829–1051). **(B)** HEK 293T cells were transiently transfected with GFP-PIKfyve and the HA-tagged ULK1 deletion mutants. GFP-PIKfyve was precipitated using GFP-trap beads. Eluted proteins were analysed by immunoblots with GFP and HA antibodies. Empty vectors were used as negative controls (n = 3). **(C)** HeLa cells transfected with FLAG-LKB1, GFP-PIKfyve and HA-ULK1 WT or HA-ULK1 ΔKD were immunostained for HA (Alexa 555: mouse). Representative micrographs shown. Scale bar, 5 µm. **(D)** Data show the percentage of GFP-PIKfyve puncta colocalized with HA-ULK1 (yellow) (n = 3, 10 cells/condition) represented as mean ± SEM (*P < 0.05; two-tailed, paired student's t-test).

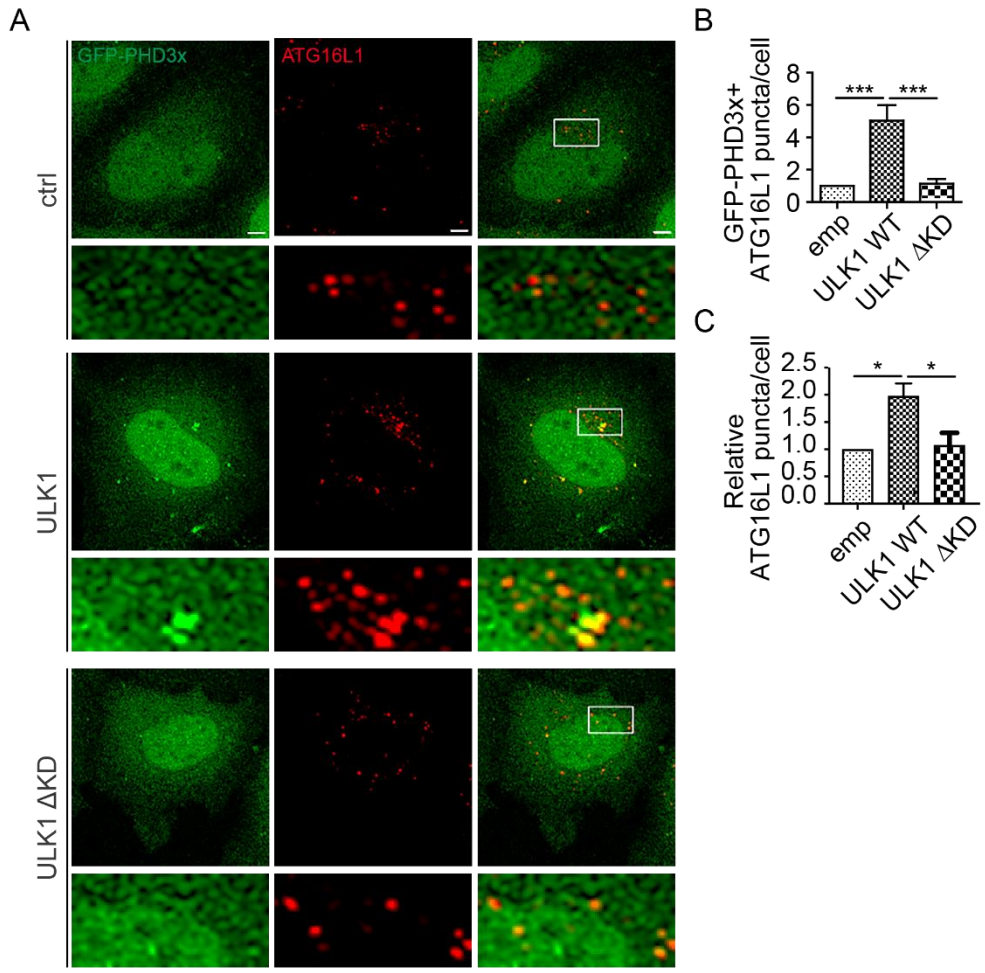

Figure 4.13 | The ULK1 kinase domain is required for ULK1-mediated increase in PI(5)P-containing phagophores

(A) HeLa cells transfected with FLAG-LKB1, GFP-PHD3x, FLAG-ATG4B mutant and HA-ULK1 WT or HA-ULK1 ΔKD were immunostained for ATG16L1 (Alexa 555: rabbit). Empty vector was used as negative control. Representative micrographs shown. Scale bar, 5 µm. **(B)** Data show relative changes in GFP-PHD3x+ ATG16L1 puncta and **(C)** total ATG16L1 puncta for experiment in **(C)** normalised to empty control are represented as mean ± SEM (n = 3, 20 cells/condition; ***P < 0.001; *P < 0.05; ANOVA with Tukey's post hoc test).

4.3 PIKfyve is phosphorylated by ULK1 in an AMPK-dependent manner

To examine the exact role of the ULK1 kinase activity for the upregulation of the PIKfyve lipid kinase function and the importance of AMPK in this regard, I performed a series of experiments to answer this question.

4.3.1 ULK1 overexpression causes a bandshift in GFP-PIKfyve caused by a phosphorylation event

Interestingly, when transfecting HEK 293T cells with GFP-PIKfyve and ULK1 (which is active when overexpressed), I found a mobility shift in PIKfyve. However, this mobility shift did not appear when cells where transfected with a kinase-dead form of ULK1 that contained a mutation in the ATP-binding pocket (M92A) (Jung et al., 2009). Likewise, when cells were treated with SBI, no mobility shift was observed **(Figure 4.14A)**, indicating that the mobility shift was directly caused by the ULK1 kinase activity. To test whether the mobility shift was caused by a phosphorylation event rather than a different post-translational modification, I treated immunoprecipitates with λ phosphatase *in vitro* before assessing mobility shift by western blotting and found that the shift was abolished **(Figure 4.14B)**. These findings suggest that ULK1 phosphorylates PIKfyve causing the mobility shift.

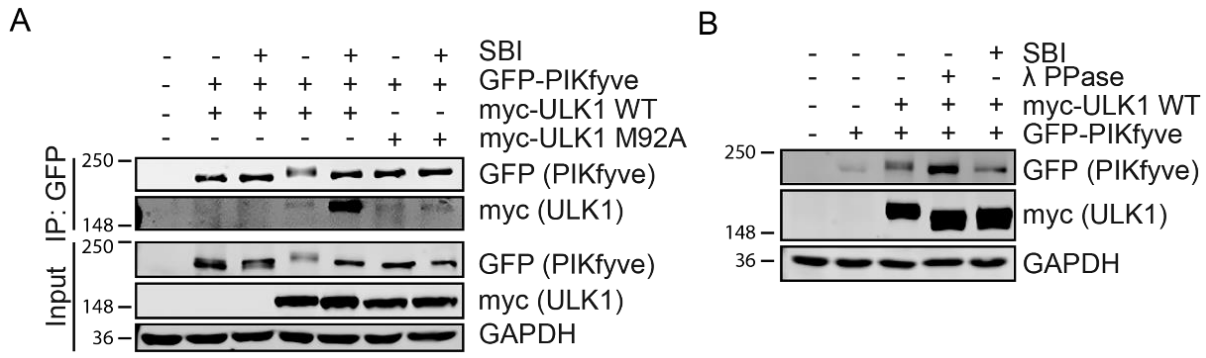

Figure 4.14 | ULK1 overexpression phosphorylates PIKfyve

(A) HEK 293T cells were transiently transfected with GFP-PIKfyve ± myc-ULK1 WT or kinase-dead M92A and treated with SBI (5 µM, 4 hours) as indicated. The PIKfyve mobility was visualised by immunoblotting for GFP (n = 3). **(B)** HEK 293T cells were transiently transfected with GFP-PIKfyve ± myc-ULK1 and treated with SBI (5 µM, 4 hours) or DMSO. Indicated immunoprecipitates were pre-treated with lambda phosphatase (λ PPase) for 1 hour. The PIKfyve mobility was visualised by immunoblotting for GFP. Empty vector was used as negative control. GAPDH was used as a loading control (n = 3).

4.3.2 ULK1 phosphorylates PIKfyve *in vitro*

To further validate that the observed effect of ULK1 on the PIKfyve mobility was caused by a phosphorylation, I purified HA-PIKfyve from HEK Expi293F cells with resin beads and incubated the resin-bound PIKfyve with recombinant ULK1 in an *in vitro* kinase assay using a fluorescence-based kit (R&D systems). This assay uses a phosphatase-coupled approach, in which the nucleotidase, CD39L2 is used to selectively release a phosphate from ADP. By subsequently using Malachite Green, the inorganic phosphate is detected by determining the optical density. This value was then correlated to a phosphate standard curve generated with serial dilutions of phosphate to determine the relative levels of phosphate released from ADP. A reaction mix that included a saturated concentration of ADP instead of ATP was used as a technical control in each experiment **(Figure 4.15A)**. The levels of released inorganic phosphate is a readout for phosphorylation.

I first sought to determine the concentration in which recombinant ULK1 is active and phosphorylates its substrates. Therefore, I incubated recombinant ULK1 with purified VPS34 since VPS34 is a known ULK1 substrate (Egan et al., 2015) and found a significant increase in inorganic phosphate release when treating VPS34 eluates with 10 ng ULK1 compared to samples in which ULK1 was not added. When ULK1 was pre-treated with SBI for 30 minutes, no increase in signal was observed compared with no kinase sample. Having determined the required concentration of ULK1, I incubated resin-bound PIKfyve with ULK1 for 10 or 20 minutes and found increased levels of phosphates, which were prevented by pre-treating ULK1 with SBI **(Figure 4.15).** These findings confirm that ULK1 phosphorylates PIKfyve.

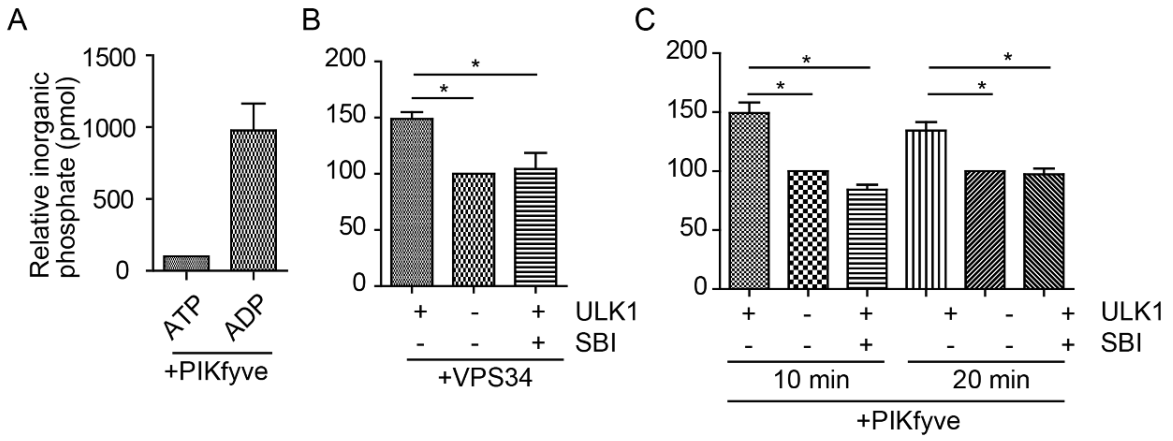

Figure 4.15 | ULK1 phosphorylates PIKfyve *in vitro*

(A) Resin-bound HA-PIKfyve precipitated from HEK Expi293F cells were incubated for 20 minutes with ULK1 (10 ng/µl), CD39L2 and either ATP or ADP as a technical control. **(B)** VPS34 eluate precipitated from HEK Expi293F cells were incubated for 20 minutes ± ULK1 (10 ng/µl) or ULK1 pre-treated with SBI for 30 minutes, in addition to ATP and CD39L2. **(C)** Resin-bound HA-PIKfyve precipitated from HEK Expi293F cells were incubated for 10 or 20 minutes ± ULK1 (10 ng/µl) or ULK1 pre-treated with SBI for 30 minutes, in addition to ATP and CD39L2. After incubating with Malachite green for 20 minutes, the optical density was determined using a spectrophotometer. The relative levels of released phosphate were determined by correcting to a phosphate standard curve (5000-0 pmol). Data are represented as mean ± SEM (n = 3, *P < 0.05; ANOVA with Tukey's post hoc test).

4.3.3 The band shift in PIKfyve caused by ULK1 overexpression is independent of AMPK phosphorylation of PIKfyve S307A

As a follow-up on my previous question about the role of AMPK in priming PIKfyve for ULK1-mediated activation, I wondered whether an AMPK-mediated phosphorylation of PIKfyve on S307 might be required for a second phosphorylation of PIKfyve by ULK1. I saw no difference in the mobility shift between GFP-PIKfyve WT and S307A transfected with ULK1 **(Figure 4.16)**.

Since I had already established that AMPK activity is involved in the formation of PI(5)P-containing phagophores upon glucose starvation, I tested whether this activity might be important for the ULK1-mediated PIKfyve phosphorylation, since it seems to be important for the ULK1-induced PI(5)P-containing phagophore formation. Upon treatment of cells transfected with GFP-PIKfyve and ULK1 with the AMPK inhibitor CC, I found that the mobility shift was abolished **(Figure 4.17)**. Although the phosphorylation of PIKfyve by AMPK appears to have no importance for ULK1 phosphorylation of PIKfyve, the catalytic activity of AMPK does play an overall role in this pathway.

AMPK activators such as phenformin and A769662 cause an AMPK-mediated phosphorylation of ULK1 (Bach et al., 2011; Egan et al., 2015). Our findings suggest that while ULK1 is active when overexpressed, this activity is not sustained when AMPK becomes inhibited and therefore places AMPK upstream of ULK1 in the AMPK-ULK1-PIKfyve axis, i.e. AMPK is required to activate ULK1 in order for ULK1 to phosphorylate PIKfyve. This suggests that the observed effects of AMPK activators on PI(5)P-containing phagophore formation could be due to an activation of ULK1 by AMPK, leading to phosphorylation of PIKfyve, thus resulting in increased synthesis of PI(5)P.

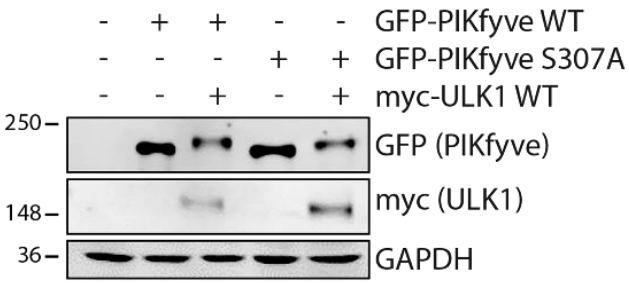

Figure 4.16 | The ULK1-mediated phosphorylation of PIKfyve is independent of AMPK phosphorylation of PIKfyve

HEK 293T cells were transiently transfected with GFP-PIKfyve WT or S307A and myc-ULK1 as indicated. PIKfyve mobility was visualised by western blotting for GFP. Empty vector was used as negative control. GAPDH was used as a loading control (n = 3).

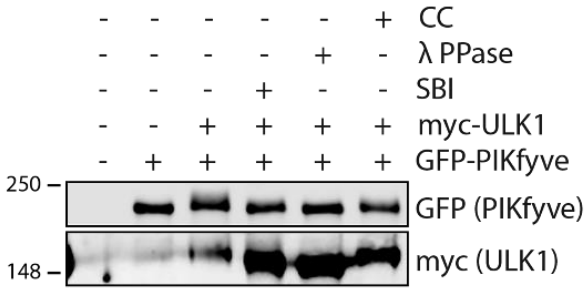

Figure 4.17 | The ULK1-mediated phosphorylation of PIKfyve is impaired by AMPK inhibition

HEK 293T cells were transiently transfected with GFP-PIKfyve WT ± myc-ULK1 WT and treated with SBI (5 µM, 4 hours), lambda phosphatase (λ ppase, 1 hour) or CC (60 µM, 6 hours) as indicated. PIKfyve mobility was visualised by western blotting. DMSO was used as vehicle control. Empty vector was used as negative control (n = 3).

4.3.4 ULK1 phosphorylation induces PIKfyve activity *in vitro*

I wondered whether the increase in ULK1 phosphorylation of PIKfyve leads to an increase in the PIKfyve lipid kinase activity, as my findings using the GFP-PHD3x bio-probe would suggest.

To this end, I developed a lipid-overlay assay to quantify PI(5)P levels using the approach described by Dowler et al., 2002. I performed an *in vitro* lipid kinase assay with myc-PIKfyve, recombinant ULK1, ATP and phosphoinositides (PI) using a method described by Sbrissa et al., 1999. The lipids were isolated and spotted on a nitrocellulose membrane. Additionally, serial dilutions of PI(5)P were spotted on the membrane. The membrane was next incubated with recombinant GST-tagged ING2, since the PHD domain of ING2 binds PI(5)P, thus allowing us to detect synthesis of PI(5)P in each reaction mix by immunostaining the membrane with anti-GST antibody. Using this method, I found an increase in ING2-bound PI(5)P in samples containing PIKfyve and ULK1 in presence of PI and ATP. A reduction in lipid kinase activity was observed when PIKfyve was pre-treated with the PIKfyve inhibitor YM for 30 minutes or when SBI was added to the reaction mixture to inhibit ULK1 **(Figure 4.18)**. In this assay, recombinant ING2 specifically recognised PI(5)P but not PI, PI(3)P or PI(3,5)P_2 **(Figure 4.18B)**. This finding also suggests that the bio-probe GFP-PHD3x is a reliable tool for PI(5)P visualisation in cells.

Together, these findings provide the first evidence that ULK1 phosphorylates PIKfyve and leads to an increase in the lipid kinase activity of PIKfyve *in vitro*, resulting in increased PI(5)P synthesis.

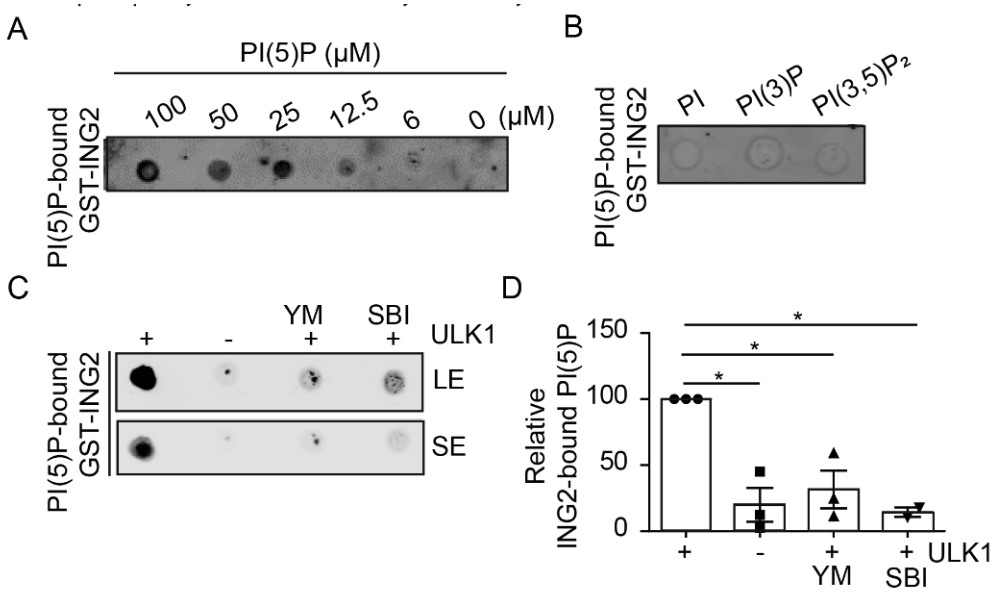

Figure 4.18 | ULK1 phosphorylation increases PIKfyve lipid kinase activity *in vitro*

(A) Six serial dilutions of PI(5)P (100-0 μM) were spotted on a nitrocellulose membrane and incubated with GST-ING2 recombinant protein. PI(5)P-bound GST-ING2 was visualised by blotting membranes with anti-GST antibody. A concentration curve was created by densitometric quantification of GST-ING2 bound to the serial dilutions of PI(5)P spotted on the membrane. **(B)** PI, PI(3)P and PI(3,5)P_2 lipids were spotted onto a nitrocellulose membrane and treated as in **(A)**. **(C)** HA-PIKfyve precipitated from HEK 293T using magnetic HA beads were incubated with PI and ATP ± recombinant ULK1 (15 minutes, 37 ºC) or following pre-treatment of HA-PIKfyve with YM (200 nM, 30 minutes) or the ULK1 recombinant protein (10 ng) with SBI (5 μM, 30 minutes). Lipids were extracted and spotted on a nitrocellulose membrane, which was treated as in **(A)**. DMSO was used as vehicle control. **(D)** Data show the relative levels of ING2-bound PI(5)P for experiment in **(C)** determined by using the standard curve in **(A)** represented as mean ± SEM (n = 3, *P < 0.05; ANOVA with Tukey's post hoc test). LE – long exposure; SE – short exposure.

4.4 ULK1 phosphorylation sites on PIKfyve were identified by mass spectrometry

Since the evidence suggests the existence of an ULK1-mediated phosphorylation of PIKfyve, I aimed to map the phosphorylation sites to further study the importance of this post-translational modification for PIKfyve activity and autophagosome biogenesis.

4.4.1 The effects of glucose starvation on PI(5)P-containing phagophore levels were abrogated when overexpressing phospho-mutant PIKfyve

To map ULK1-dependent phosphorylation events in PIKfyve, I co-expressed GFP-PIKfyve with myc-ULK1 treated with SBI or vehicle control. After isolating GFP-PIKfyve using GFP-trap beads, the core proteomics unit at Cambridge Institute for Medical Research ran a mass spectrometry analysis of phosphorylated peptides in the GFP-PIKfyve immunoprecipitates to map phosphorylation sites in PIKfyve under the three conditions. Four residues on PIKfyve (T309, S327, S710, S1548) were identified as ULK1 phosphorylation sites.

I made non-phosphorylatable forms of PIKfyve with a mutation in each of these four sites by exchanging the serine or threonine residues with alanine through site-directed mutagenesis and assessed the impact of each mutation on the formation of PI(5)P-containing phagophores in HeLa cells. I found that particularly overexpression of PIKfyve S1548A (human S1549) led to a reduction in levels of PI(5)P-containing phagophores compared with cells transfected with PIKfyve WT **(Figure 4.19)**.

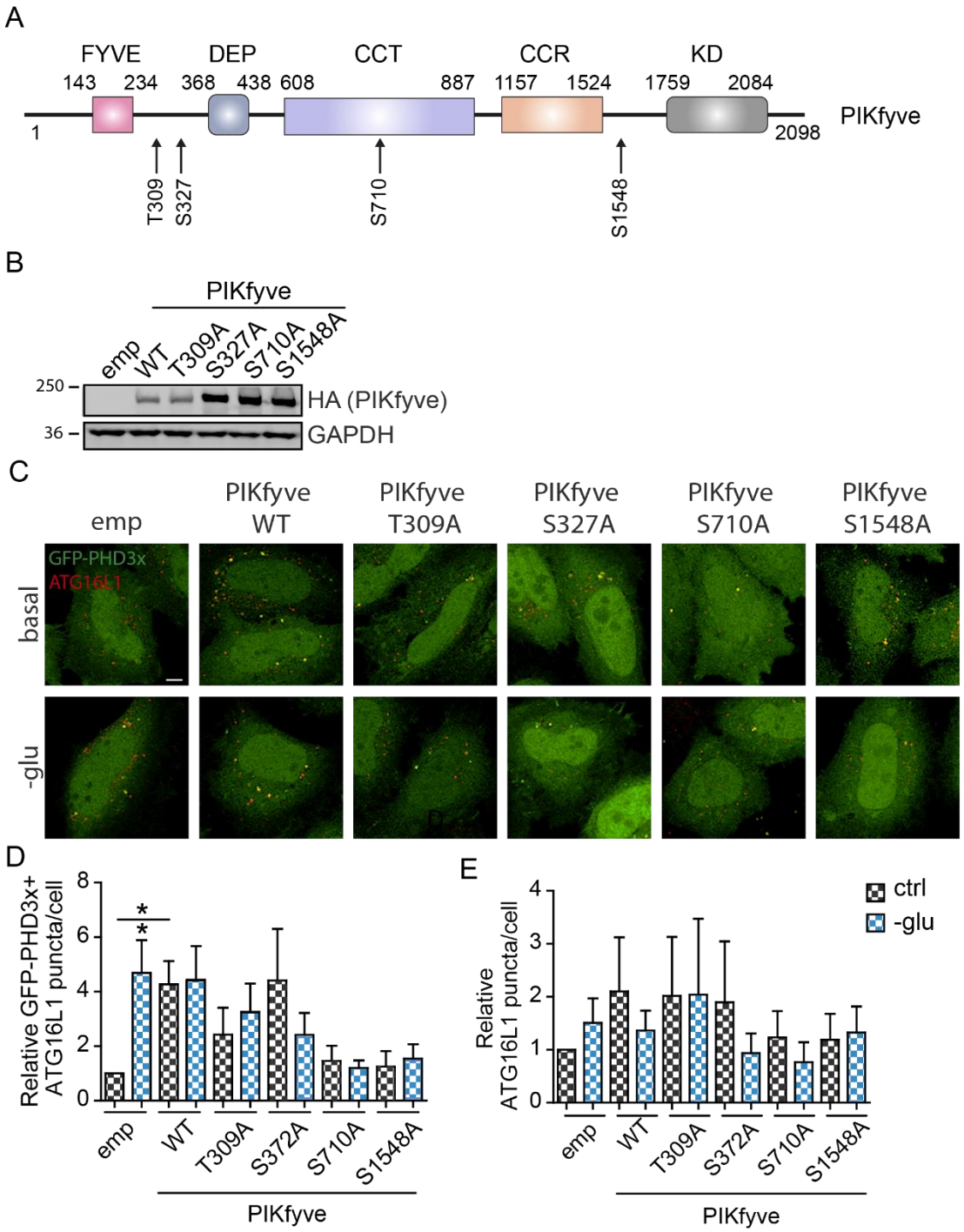

Figure 4.19 | PIKfyve residues phosphorylated by ULK1 were identified

(A) HEK 293T cells were transfected with GFP-PIKfyve WT ± myc-ULK1 WT treated with SBI (5 µM, 4 hours) or DMSO. Cells were immunoprecipitated using GFP-trap beads. By LS/MS/MS analysis of the phospho-enriched PIKfyve peptides, ULK1 phosphorylation sites on PIKfyve were identified. ULK1 phosphorylation of PIKfyve on amino acids T309, S327, S710 and S1548 are shown on the schematic representation of PIKfyve - FYVE: 143–234; DEP: 368–438; chaperone-containing TCP1 (CCT): 608–877; cysteine-rich (CCR) 1157–1524; kinase domain: 1759–2084. **(B)** Phosphorylation sites listed in **(A)** were mutated by site-directed mutagenesis into

alanine. Immunoblots probed with HA and GAPDH antibodies shows expression of HA-PIKfyve WT and phospho-mutants T309A, S327A, S710A and S1548A. **(C)** HeLa cells transfected with FLAG-LKB1, GFP-PHD3x, FLAG-ATG4B mutant and HA-tagged PIKfyve WT or phospho-mutant constructs were incubated in glucose-free media (-glu) for 1 hour and immunostained for ATG16L1 (Alexa 555: rabbit). Empty vector was used as negative control. Representative micrographs shown. Scale bar, 5 µm. **(D)** Data show relative changes in GFP-PHD3x+ ATG16L1 puncta and **(E)** total ATG16L1 puncta for experiment in **(C)** normalised to control represented as mean ± SEM (n = 3, 20 cells/condition; *P < 0.05; ANOVA with Tukey's post hoc test).

4.4.2 ULK1 phosphorylation of PIKfyve is required for PI(5)P synthesis *in vitro*

To further determine whether the ULK1 phosphorylation sites on PIKfyve identified by mass spectrometry were required for ULK1-mediated generation of PI(5)P, an *in vitro* lipid kinase assay was performed for PIKfyve WT and the non-phosphorylatable forms of PIKfyve with ULK1 as described above. I found that the PI(5)P synthesis resulting from incubation of PIKfyve with ULK1 was reduced in reactions with PIKfyve S1548A **(Figure 4.20)**, consistent with the effects observed when using the GFP-PHD3x bio-probe to assess PI(5)P-containing phagophores by microscopy in **Figure 4.19**, suggesting that this site is a major ULK1 phosphorylation site important for the PIKfyve-mediated increase in the formation of PI(5)P-containing phagophores.

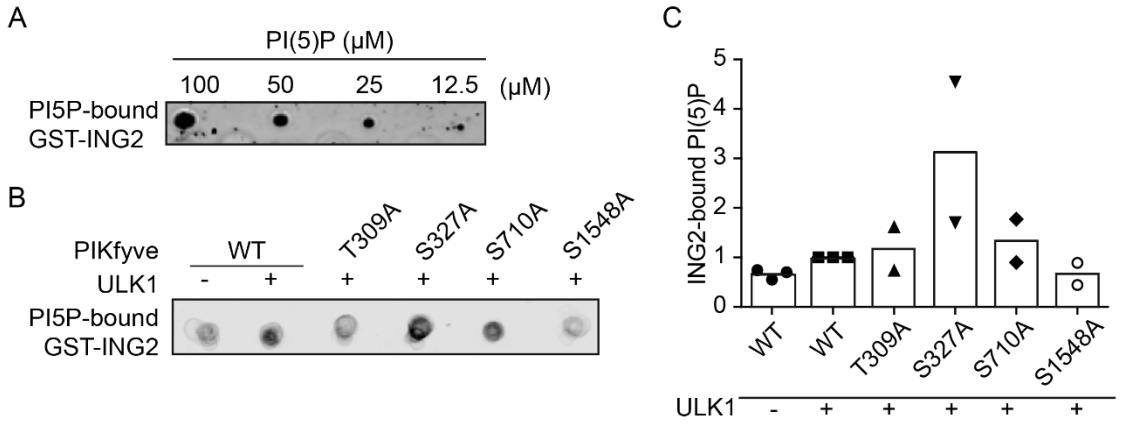

Figure 4.20 | ULK1 phosphorylation of S1548 is required for the increase in PI(5)P levels in vitro

(A) Serial dilutions of PI(5)P (100-12.5 μM) were spotted on a nitrocellulose membrane and incubated with GST-ING2 recombinant protein. The membrane was immunostained with anti-GST antibody. A concentration curve was created by densitometric quantification of GST-ING2 bound to the serial dilutions of PI(5)P spotted on the membrane. **(B, C)** HA-PIKfyve WT and phospho-mutants precipitated from HEK 293T using magnetic HA beads were incubated with PI and ATP ± recombinant ULK1 (15 minutes, 37 ºC). Lipids were extracted and spotted on a nitrocellulose membrane, which was treated as in **(A)**. Data show the relative levels of ING2-bound PI(5)P for experiment in **(B)** determined by using the standard curve in **(A)** normalised to WT represented as mean ± SEM (n = 3, n = 2 for PIKfyve mutants; *P < 0.05; ANOVA with Tukey's post hoc test).

4.5 ULK1 phosphorylation of PIKfyve S1548 is required for PIKfyve-mediated autophagy induction

Since glucose sensing is an evolutionarily conserved machinery, I wondered whether the PIKfyve S1548 amino acid was conserved across species. I, therefore, performed a multiple sequence alignment of PIKfyve orthologues from various species using the Clustal Omega tool and found that properties of the PIKfyve S1548 residue is strongly similar across species **(Figure 4.21B)**.

Since the preliminary experiments suggested that phosphorylation of PIKfyve on the S1548 residue is important for PI(5)P synthesis and biogenesis of PI(5)P-containing autophagosomes, I further studied the importance of this residue by using the phospho-mutant PIKfyve S1548A and by generating a phospho-mimic form of PIKfyve in which serine 1548 was exchanged with the negatively charged aspartate (S1548D) by site-directed mutagenesis, which thereby activates PIKfyve in the capacity achieved by phosphorylation of this residue.

4.5.1 ULK1 phosphorylation of PIKfyve S1548 increases formation of PI(5)P-containing phagophores

First, I transfected cells with the phospho-mimic and phospho-mutant forms of PIKfyve **(Figure 4.21C-D)** and consistently found that the overexpression of PIKfyve S1548A led to a reduction in levels of PI(5)P-containing phagophores compared to cells transfected with WT **(Figure 4.21E-G)**, as previously shown in **(Figure 4.19)**. The overexpression of phospho-mimic PIKfyve S1548D led to a similar increase in PI(5)P-containing as PIKfyve WT **(Figure 4.21E-G)**. Cells incubated in glucose-free media were added as a positive control to ensure the continuous sensitivity of this readout.

Interestingly, PIKfyve S1548A or S1548D did not change the increase in PI(3,5)P_2-positive puncta compared to PIKfyve WT determined by transfecting cells with GFP-MLN1 bio-probe **(Figure 4.22)**, indicating that ULK1 phosphorylation of PIKfyve specifically induces PI(5)P synthesis and not a general increase in the lipid kinase activity.

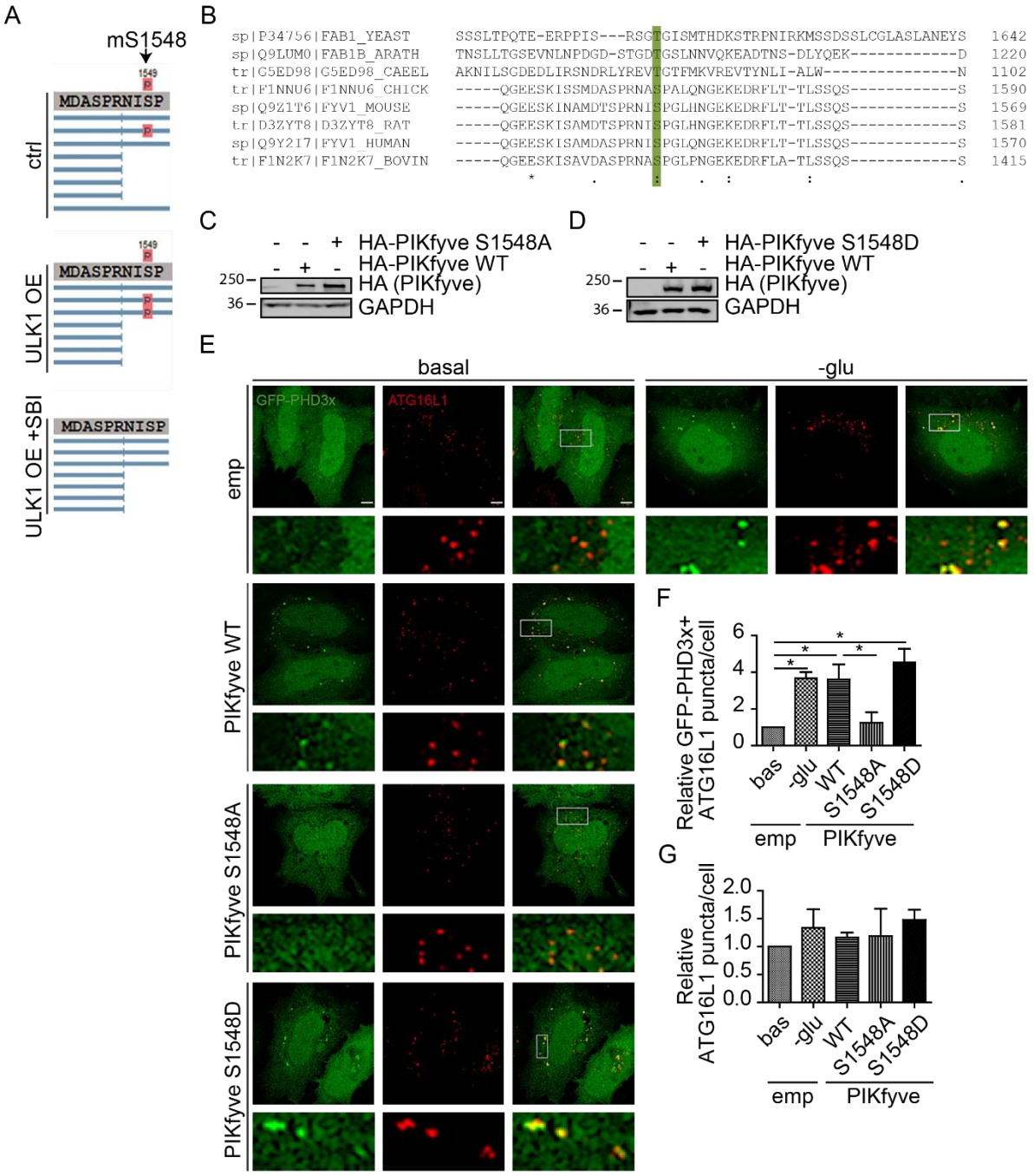

Figure 4.21 | ULK1-mediated phosphorylation of PIKfyve S1548 is required for formation of PI(5)P-containing phagophores

(A) LS/MS/MS analysis of phospho-enriched PIKfyve immunoprecipitated from HEK 293T cells transfected with GFP-PIKfyve ± myc-ULK1 WT treated with SBI (5 µM, 4 hours) or DMSO. ULK1 phosphorylation of PIKfyve on S1548 (S1549 in human) was identified. **(B)** Clustal Omega alignment of amino acid sequence of PIKfyve in *S. cerevisiae, A. thaliana, C. elegans*, chicken, mouse, rat, human and bovine. Green box, S1548; (*) indicates perfect alignment; (:) indicates a site belonging to group exhibiting strong similarity; (.) indicates a site belonging to a group exhibiting weak similarity. **(C)** Immunoblot probed with HA and actin antibodies showing expression of

HA-PIKfyve WT and S1548A in HeLa cells. **(D)** Phospho-mimic PIKfyve was generated by site-directed mutagenesis in which S1548 was exchanged with aspartate (S1548D). Immunoblot probed with HA and actin antibodies showing expression of HA-PIKfyve WT and S1548D in HeLa cells. **(E)** HeLa cells were transfected with FLAG-LKB1, GFP-PHD3x, FLAG-ATG4B mutant and HA-PIKfyve WT, S1548A and S1548D. Cells transfected with empty control were incubated in basal or glucose-free media (-glu, 1 hour). Cells were immunostained for ATG16L1 (Alexa 555: rabbit). Representative micrographs shown. Scale bar, 5 μm. **(F)** Data show relative changes in GFP-PHD3x+ ATG16L1 puncta and **(G)** total ATG16L1 puncta for experiment in **(E)** normalised to control represented as mean ± SEM (n = 3, 20 cells/condition; *P < 0.05; ANOVA with Tukey's post hoc test).

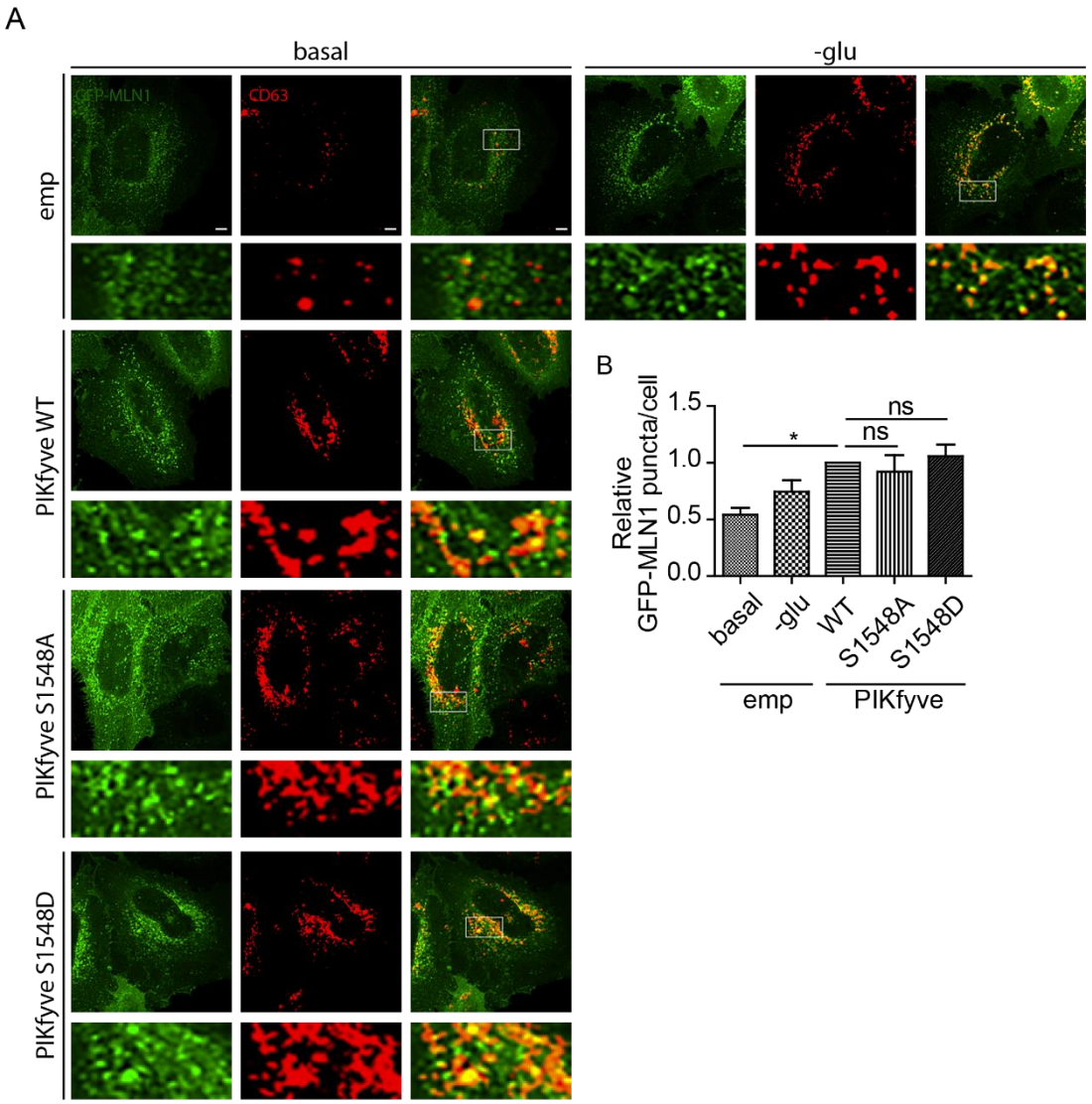

Figure 4.22 | ULK1-mediated phosphorylation of PIKfyve S1548 does not increase PI(3,5)P_2 formation

(A) HeLa cells were transfected with FLAG-LKB1, GFP-MLN1 and HA-PIKfyve WT, S1548A and S1548D. Cells transfected with empty control were incubated in glucose-free media (-glu, 1 hour) and immunostained for CD63 (Alexa 555: rabbit). Empty vector was used as negative control. Representative micrographs shown. Scale bar, 5 µm. **(B)** Data show relative changes in GFP-MLN1+ puncta for experiment in **(A)** normalised to WT control represented as mean ± SEM (*P < 0.05; ns – non-significant; ANOVA with Tukey's post hoc test).

4.5.2 ULK1 phosphorylation of PIKfyve on S1548 increases PI(5)P levels

Since the evidence suggests that ULK1 phosphorylation of PIKfyve on S1548 plays a role in the formation of PI(5)P-containing phagophores, I hypothesised that phosphorylation of this residue increases the lipid kinase activity of PIKfyve. An *in vitro* lipid kinase assay was performed showing that PIKfyve S1548A did not increase PI(5)P synthesis in the presence of ULK1, while PIKfyve S1548D increased PI(5)P levels in the absence of ULK1 **(Figure 4.23)**, confirming that phosphorylation of PIKfyve on S1548 increases the lipid kinase activity of PIKfyve.

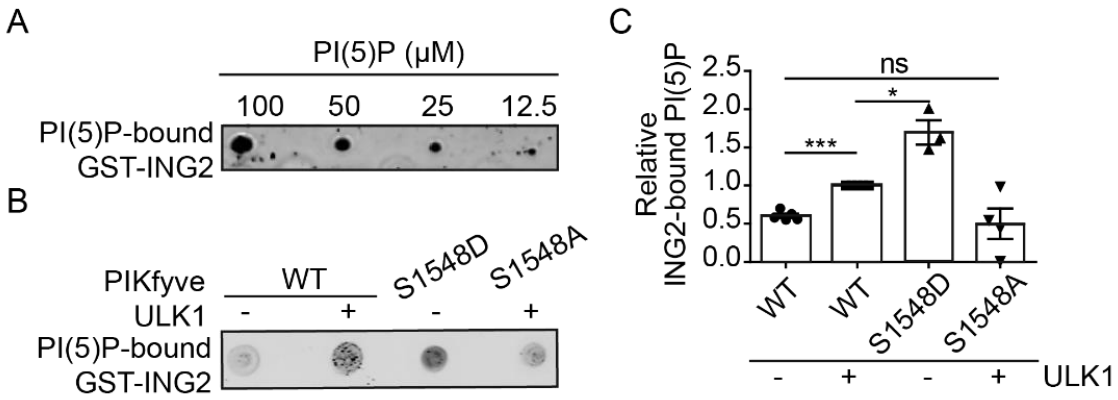

Figure 4.23 | PIKfyve S1548D increases PI(5)P levels in absence of ULK1 *in vitro*

(A) Serial dilutions of PI(5)P (100-12.5 μM) were spotted on a nitrocellulose membrane and incubated with GST-ING2 recombinant protein. The membrane was immunostained with anti-GST antibody. A concentration curve was created by densitometric quantification of GST-ING2 bound to the serial dilutions of PI(5)P spotted on the membrane. **(B, C)** HA-PIKfyve WT, S1548A and S1548D precipitated from HEK 293T using magnetic HA beads were incubated with PI and ATP ± recombinant ULK1 (15 minutes, 37 ºC). ULK1 was not added to the reaction with PIKfyve S1548D. Lipids were extracted and spotted on a nitrocellulose membrane, which was treated as in **(A)**. Data show relative levels of ING2-bound PI(5)P determined by using the standard curve based on PI(5)P standards in **(A)** normalised to WT represented as mean ± SEM (n = 3; ***P < 0.001; *P < 0.05; ns - non-significant; ANOVA with Tukey's post hoc test).

4.5.3 ULK1 phosphorylation of PIKfyve on S1548 increases autophagy flux

Next, I assessed whether the increased biogenesis of PI(5)P-containing phagophores caused by the ULK1-mediated phosphorylation of PIKfyve on S1548 resulted in increased autophagy flux. To answer this question, HeLa cells were transfected with PIKfyve WT, S1548A or S1548D with mRFP-GFP-LC3. Numbers of autophagosomes and autolysosomes were dramatically reduced in cells expressing PIKfyve S1548A in both basal conditions and upon glucose starvation, while cells expressing PIKfyve S1548D displayed a substantial increase in autophagy flux compared to WT **(Figure 4.24)**.

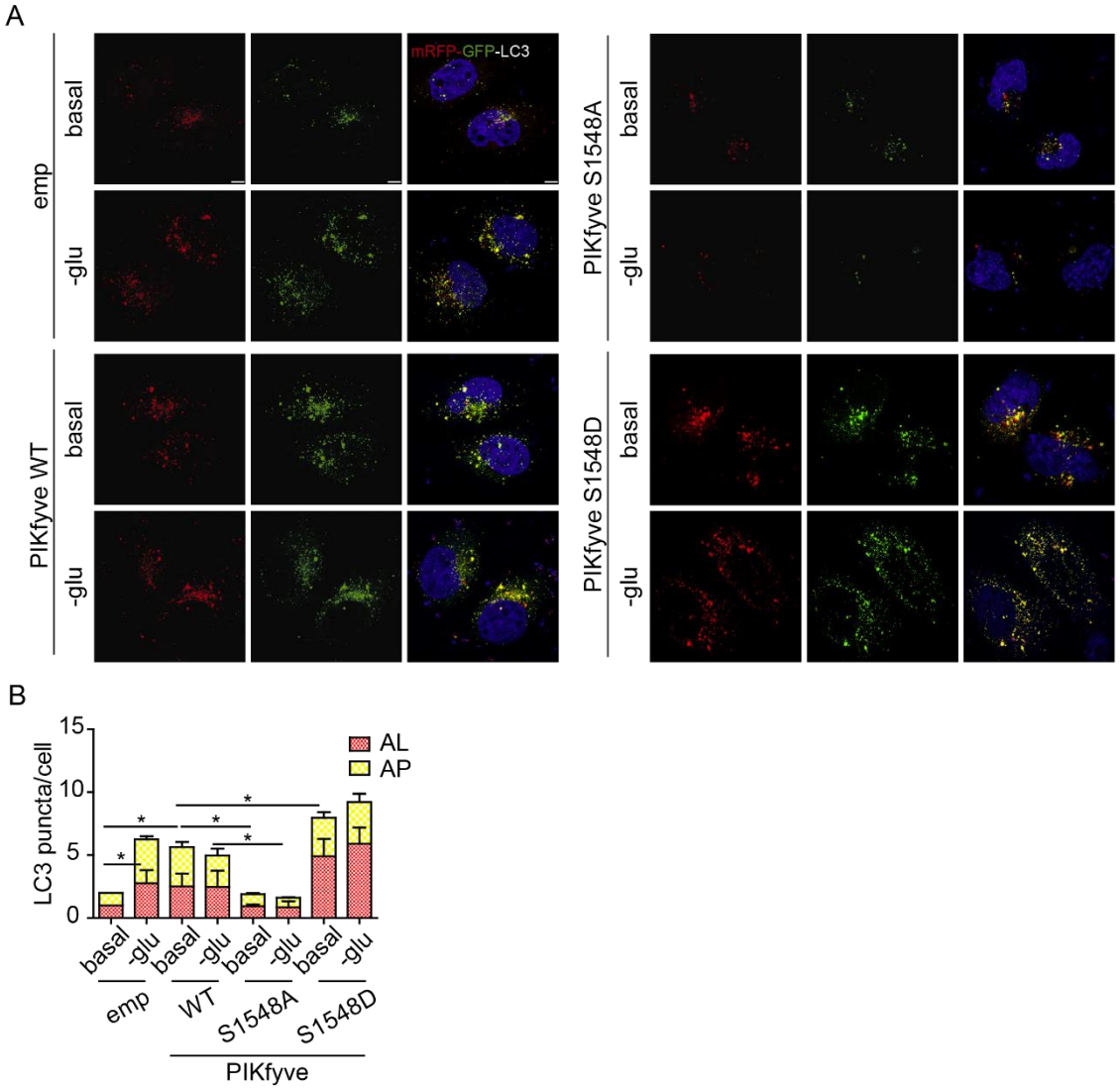

Figure 4.24 | ULK1 phosphorylation of S1548 is required for the increase in autophagy flux upon glucose starvation

(A) HeLa cells transiently transfected with mRFP-GFP-LC3, FLAG-LKB1 and HA-PIKfyve WT, S1548A or S1548D were incubated in basal or glucose-free media (-glu, 1 hour). Representative micrographs shown. Scale bar, 5 μm. **(B)** Data show relative levels of autophagosomes (yellow dots) and autolysosomes (red dots) for experiment in **(A)** normalised to empty control represented as mean ± SEM (n = 3, 10-20 cells/condition; *P < 0.05; ANOVA with Tukey's post hoc test).

4.6 Phospho-mimic PIKfyve S1548D induces autophagy and increases clearance of mutant huntingtin aggregates.

4.6.1 PIKfyve S1548D increases formation of PI(5)P-containing phagophores

Since our data suggests that phosphorylation of PIKfyve on S1548 can induce PI(5)P-containing autophagosome biogenesis, I further studied the phospho-mimic mutant PIKfyve S1548D in different conditions. Upon treatment of HeLa cells expressing PIKfyve S1548D with SBI, no effect was observed on the increase in PI(5)P-containing and total numbers of phagophores caused by PIKfyve S1548D overexpression **(Figure 4.25)**. Additionally, overexpression of PIKfyve S1548D in AMPK dKO cells led to an increase in PI(5)P-containing phagophores similar to the increase observed in WT MEFs **(Figure 4.26A)**. Finally, I transfected AMPK dKO cells with PIKfyve WT, S1548D or empty control and treated with SBI. Since PIKfyve WT is active when first transfected in cells, unlike PIKfyve S1548D, which appears to be constitutively active, both constructs increased PI(5)P-containing phagophores and total numbers of phagophores. Inhibition of ULK1 led to a decrease in PI(5)P-containing phagophores in cells transfected with the WT construct, while cells transfected with the S1548D mutant managed to sustain the biogenesis of PI(5)P-containing phagophores **(Figure 4.26B)**. Two observations can be made from these findings:

1. AMPK is not directly involved in the activation of PIKfyve that results in the formation of PI(5)P-containing phagophores.
2. ULK1 phosphorylation of PIKfyve on S1548 plays a pivotal role in the biogenesis of PI(5)P-containing autophagosomes.

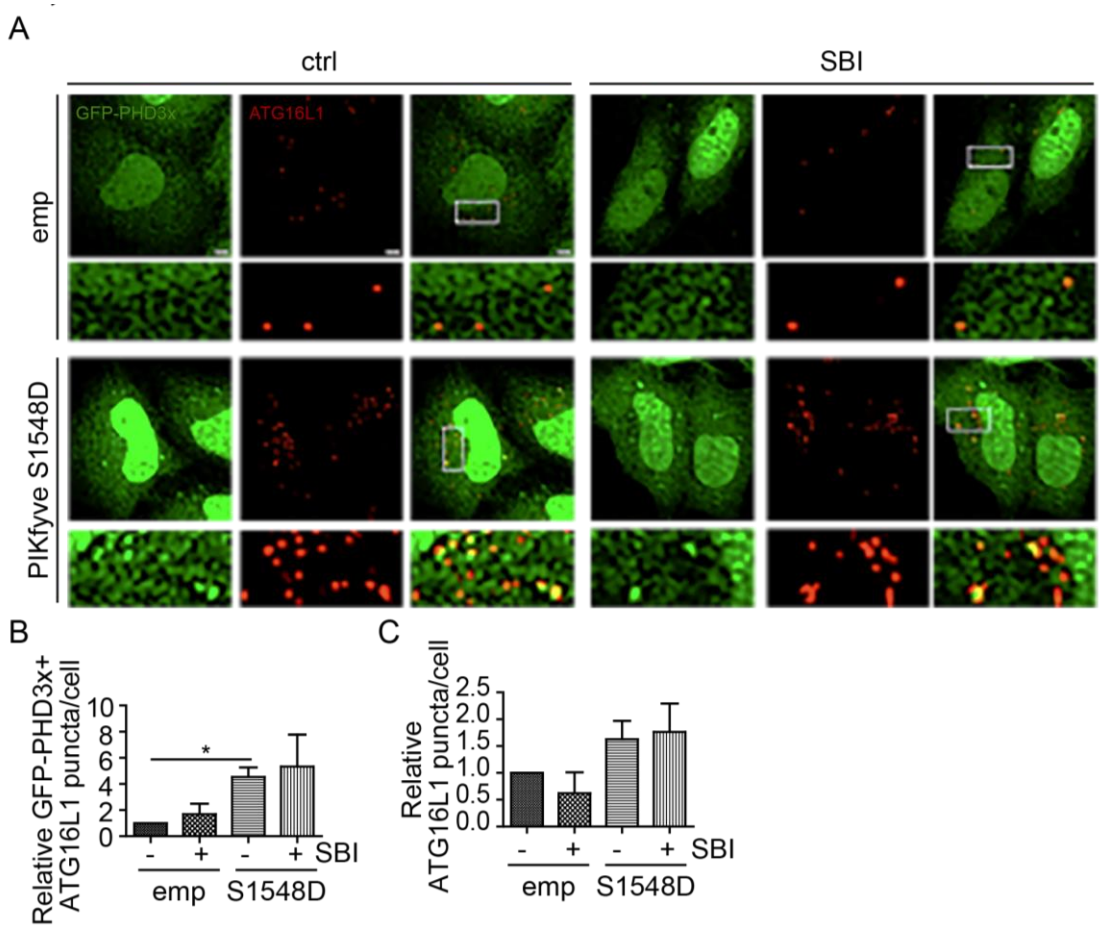

Figure 4.25 | ULK1 inhibition does not abrogate PI(5)P-containing phagophore formation in cells transfected with PIKfyve S1548D

(A) HeLa cells transfected with FLAG-LKB1, GFP-PHD3x, FLAG-ATG4B mutant ± HA-PIKfyve S1548D treated with SBI (5 μM, 4 hours) were immunostained for ATG16L1 (Alexa 555: rabbit). DMSO was used as vehicle control. Empty vector was used as negative control. Representative micrographs shown. Scale bar, 5 μm. **(B)** Data show relative changes in GFP-PHD3x+ ATG16L1 puncta and **(C)** total ATG16L1 puncta for experiment in **(A)** normalised to empty control represented as mean ± SEM (n = 3, 20 cells/condition; *P < 0.05; ANOVA with Tukey's post hoc test).

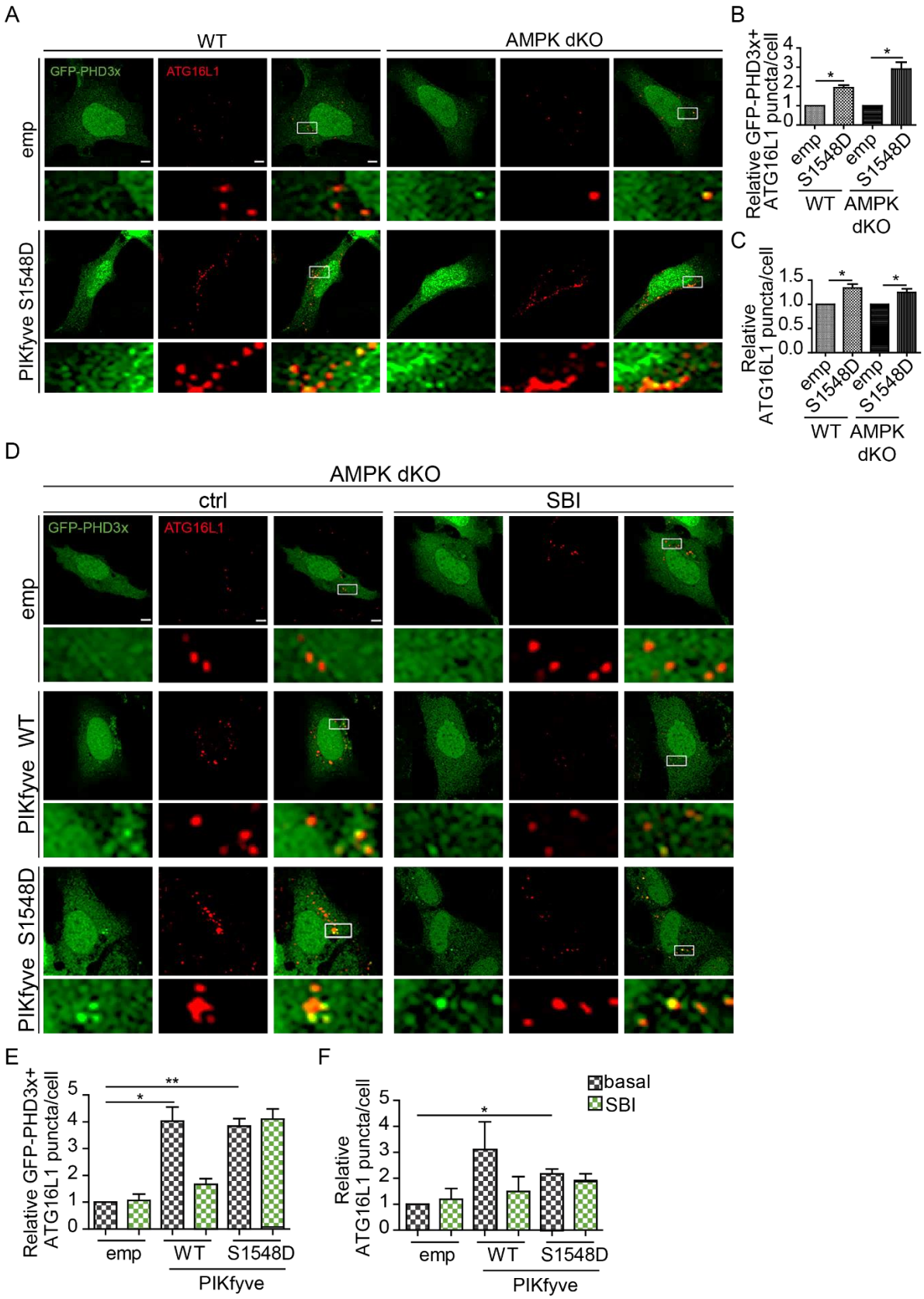
A
WT
AMPK dKO
GFP-PHD3x
ATG16L1
emp
PIKfyve S1548D
B
Relative GFP-PHD3x+ ATG16L1 puncta/cell
emp
S1548D
WT
AMPK dKO
C
Relative ATG16L1 puncta/cell
D
AMPK dKO
ctrl
SBI
PIKfyve WT
E
Relative GFP-PHD3x+ ATG16L1 puncta/cell
PIKfyve
F
basal
SBI
Relative ATG16L1 puncta/cell

Figure 4.26 | PIKfyve S1548D increases PI(5)P-containing phagophores in AMPK dKO cells

(A) WT and AMPK dKO cells transfected with GFP-PHD3x, FLAG-ATG4B mutant ± HA-PIKfyve S1548D were immunostained for ATG16L1 (Alexa 555: rabbit). **(B)** Data show relative changes in GFP-PHD3x+ ATG16L1 puncta and **(C)** total ATG16L1 puncta for experiment in **(A)** normalised to empty control (n = 4, 10 cells/condition). **(D)** AMPK dKO cells transfected with GFP-PHD3x, FLAG-ATG4B mutant and HA-PIKfyve WT or S1548D treated with SBI (5 μM, 4 hours) were immunostained for ATG16L1 (Alexa 555: rabbit). DMSO was used as vehicle control. **(E)** Data show relative changes in GFP-PHD3x+ ATG16L1 puncta and **(F)** total ATG16L1 puncta for experiment in **(D)** normalised to empty control (n = 3, 20 cells/condition).
Empty vector was used as negative control. Representative micrographs shown. Scale bar, 5 μm. Data are represented as mean ± SEM (**P < 0.01; *P < 0.05; ANOVA with Tukey's post hoc test).

4.6.2 PIKfyve S1548D increases autophagy flux

To further validate that the increased autophagosome biogenesis mediated by PIKfyve S1548D translated into an overall effect on autophagy flux, I transfected HeLa cells with PIKfyve WT and S1548D and mRFP-GFP-LC3. Upon inhibition of ULK1 with SBI, the increase in autophagy flux associated with PIKfyve S1548D expression was maintained **(Figure 4.27)**. Additionally, overexpression of PIKfyve S1548D in AMPK DKO had a similar effect on autophagy flux as it did in WT MEFs **(Figure 4.28A-B)**, suggesting that maintaining the PI(5)P-specific activity of PIKfyve can compensate for the lack of an upstream AMPK signal.

Consistently with the effects observed on formation of PI(5)P-containing phagophores, I found an increase in autophagy flux in AMPK dKO cells transfected with PIKfyve WT or S1548D, compared with empty control vector. Treatment with SBI abolished the increase autophagy flux in cells expressing PIKfyve WT, but not in cells expressing PIKfyve S1548D **(Figure 4.28C-D)**. These findings further confirm that ULK1 is directly involved in upregulating PI(5)P-containing phagophore formation through PIKfyve S1548 phosphorylation, resulting in increased autophagy flux.

Finally, I questioned whether the increased autophagy flux led to a reduction in autophagy substrates. To answer this question, I used a readout extensively employed by our lab to measure autophagic activity: EGFP-HTT (Q74) aggregate clearance (exon 1 of huntingtin with a 74-polyglutamine expansion fused to EGFP on its N terminal) (Ravikumar et al., 2002). Since mutant HTT is an autophagy substrate, transfection of cells with EGFP-HTT (Q74) leads to the accumulation of HTT aggregates. Induction of autophagy with known autophagy inducers such as rapamycin for 48 hours enhances the clearance of polyglutamine expansions (Berger et al., 2006), as shown in **Figure 4.29**. Using this rationale, I examined if phospho-mimic PIKfyve impacted the percentage of cells with huntingtin aggregates and found that overexpression of PIKfyve S1548D significantly decreased the number of cells with aggregates compared with control cells in a similar capacity as rapamycin treatment **(Figure 4.29)**.

These findings confirm that the ULK1-mediated phosphorylation of PIKfyve on S1548 causes an increase in autophagy flux resulting in increased autophagic clearance.

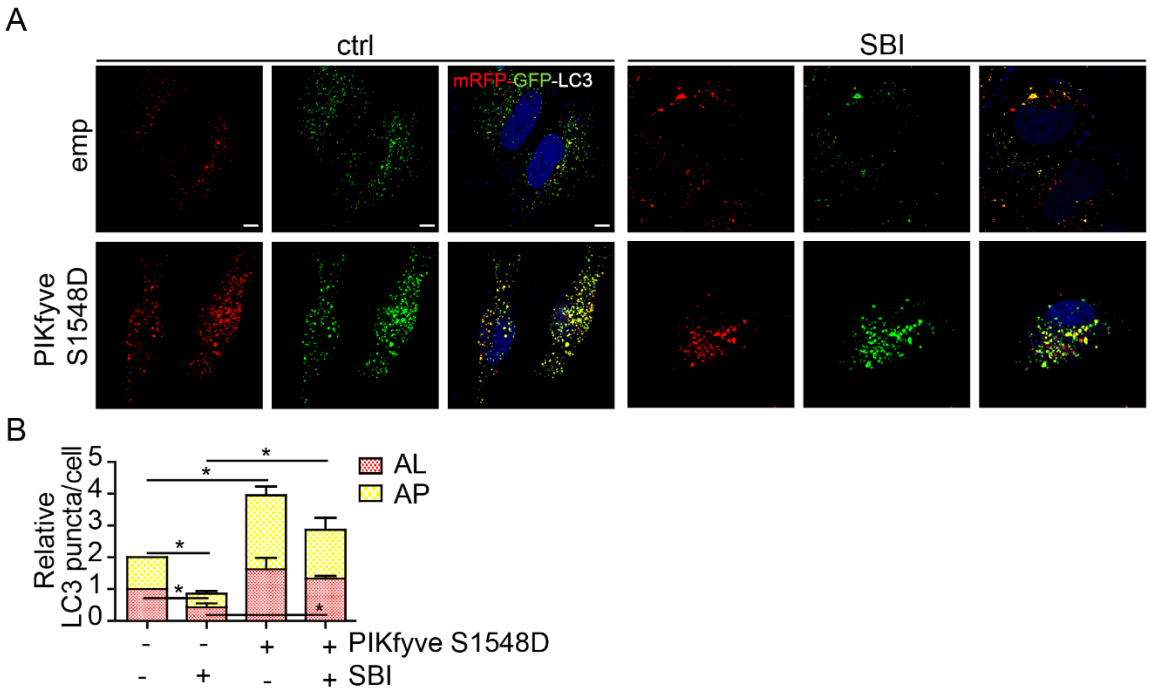

Figure 4.27 | ULK1 inhibition does not abrogate autophagy flux in cells transfected with PIKfyve S1548D

(A) HeLa cells transiently transfected with mRFP-GFP-LC3, FLAG-LKB1 and HA-PIKfyve S1548D were treated with SBI (5 µM, 4 hours). DMSO was used as vehicle control. Empty vector was used as negative control. Representative micrographs shown. Scale bar, 5 µm. **(B)** Data show relative levels of autophagosomes (yellow dots) and autolysosomes (red dots) for experiment in **(A)** normalised to AL in control represented as mean ± SEM (n = 3, 10 - 20 cells/condition; *P < 0.05; ANOVA with Tukey's post hoc test).

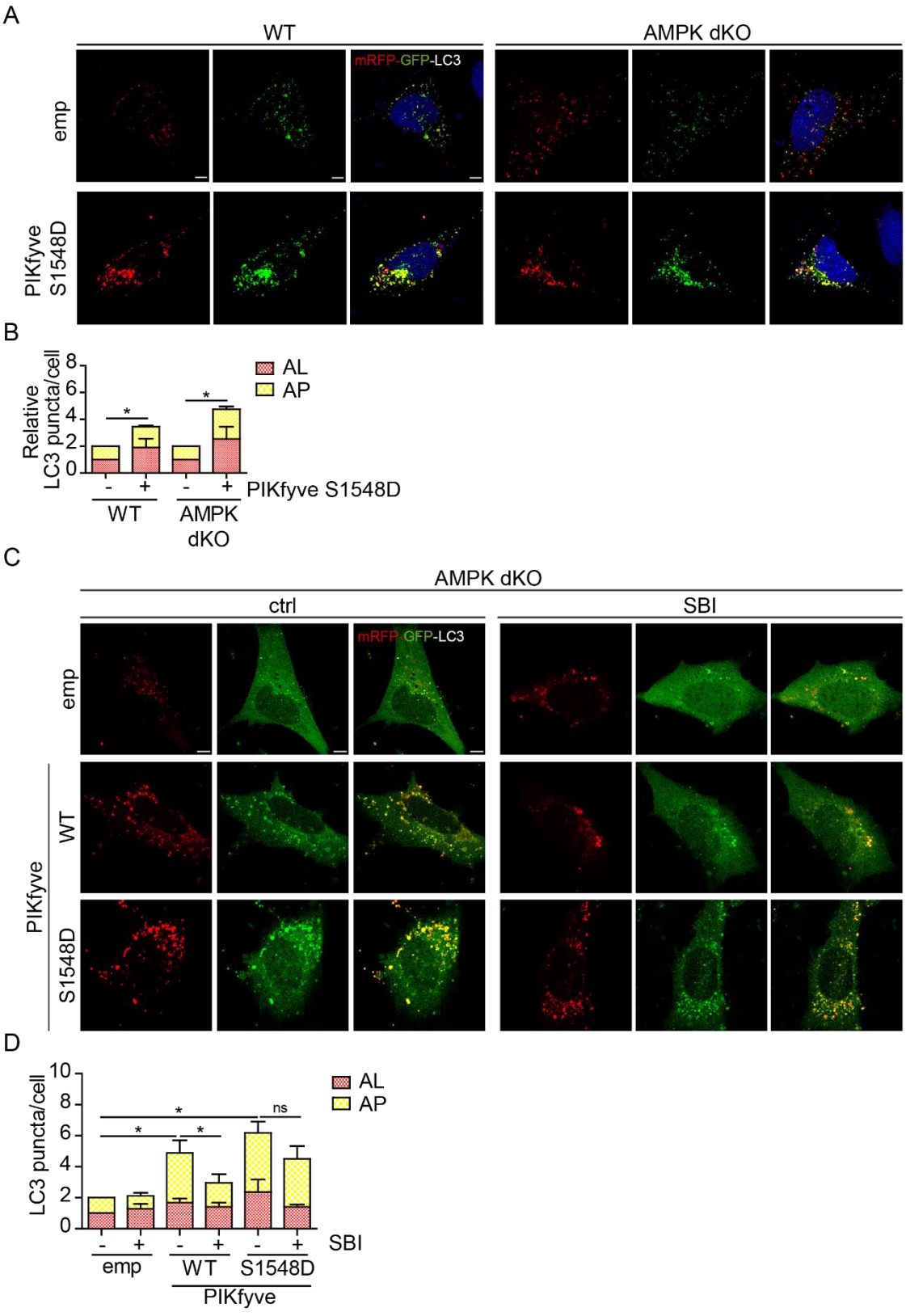

Figure 4.28 | PIKfyve S1548D increases autophagy flux in AMPK dKO cells

(A, B) WT and AMPK dKO cells transfected with mRFP-GFP-LC3 ± HA-PIKfyve S1548D. Data show relative levels of autophagosomes (yellow dots) and autolysosomes (red dots) normalised to AL in control. **(B, C)** AMPK dKO cells

transiently transfected with mRFP-GFP-LC3 and HA-PIKfyve WT or S1548D were treated with SBI (5 μM, 4 hours). DMSO was used as a vehicle control. Data show relative levels of autophagosomes (yellow dots) and autolysosomes (red dots) normalised to AL in control.
Empty vector was used as negative control. Representative micrographs shown. Scale bar, 5 μm. Data are represented as mean ± SEM (n = 3, 10 - 20 cells/condition; *P < 0.05; ns – non-significant; ANOVA with Tukey's post hoc test).

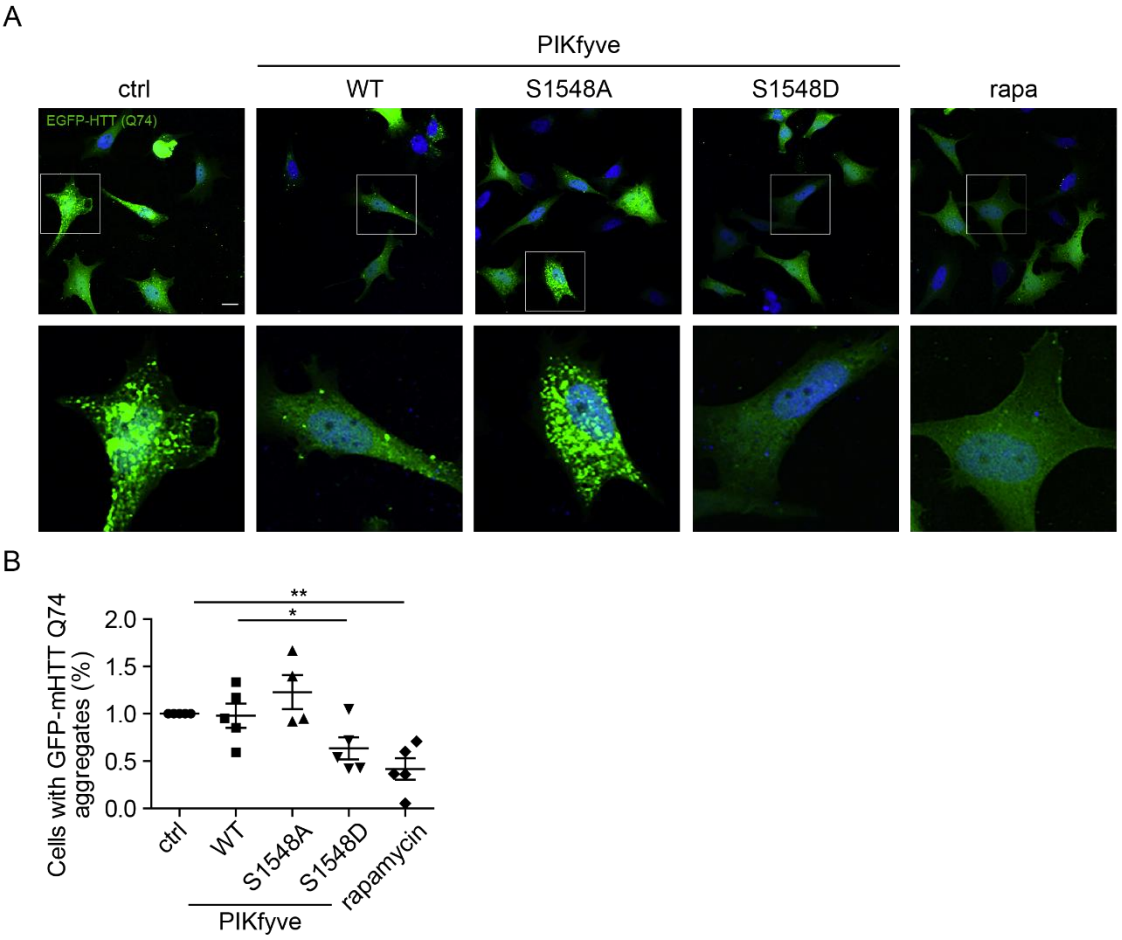

Figure 4.29 | PIKfyve S1548D reduces cells with mutant huntingtin aggregates

(A, B) HeLa cells were transiently transfected with EGFP-mHTT (Q74) in HeLa cells with HA-PIKfyve WT, S1548A or S1548D or empty vector for 48 hours before quantification. Cells transfected with empty vector were treated with rapamycin (rapa, 200 nM, 48 hours). DMSO was used as vehicle control. Representative micrographs shown. Scale bar, 5 μm. Data show percentages of GFP+ cells with aggregates normalised to empty control (n = 5 independent experiments, 200 - 300 cells/condition counted in triplicates; **P < 0.01, *P < 0.05; ANOVA with Tukey's post hoc test).

4.7 Summary

In this chapter, I have provided the first evidence of a relationship between ULK1 and PIKfyve and shown the importance of this interaction for PI(5)P-dependent autophagy upregulation upon glucose starvation.

In summary, I found that:

1. PIKfyve binds the kinase domain of ULK1. The interaction between PIKfyve and ULK1 increases upon glucose starvation.

2. Active ULK1 phosphorylates PIKfyve on S1548, thereby activating it leading to an increase in PI(5)P synthesis and formation of PI(5)P-containing phagophores, while not affecting the $PI(3,5)P_2$ levels.

3. ULK1-mediated phosphorylation of PIKfyve on S1548 induces autophagy, as autophagy flux is abrogated in cells expressing the non-phosphorylatable form of PIKfyve and results in increased autophagic clearance.

Additionally, the data presented in this chapter indicates that the increase in PI(5)P-containing phagophores observed upon AMPK activation is caused by an AMPK-mediated activation of ULK1, suggesting the presence of an AMPK-ULK1-PIKfyve axis involved in the upregulation of non-canonical autophagy.

Finally, the findings presented above suggest that AMPK induces a general increase in PIKfyve activity upon glucose starvation that appears to be required for lysosomal function and for activating ULK1, while ULK1 induces a refined, PI(5)P-specific increase in PIKfyve activity that leads to an increase in the biogenesis of PI(5)P-containing autophagosomes and therefore, PI(5)P-dependent autophagy.

5 Discussion and conclusions

In this chapter, I summarise the main findings presented above (see schematic in **Figure 5.1**) before highlighting several outstanding questions that remain to be addressed.

Results summary

In this study, I have described a mechanism by which non-canonical signalling leads to an increase in autophagy flux upon glucose starvation across multiple cell lines.

I have demonstrated that pharmacological activation of AMPK, primarily with the direct activator 991 leads to an increase in AMPK activity, formation of PI(5)P-containing autophagosomes and autophagy flux.

The initial hypothesis of this study was that the upregulation of PI(5)P-containing autophagosomes was achieved through a phosphorylation of PIKfyve on S307 by AMPK, a residue formerly shown to be phosphorylated by AMPK upon contraction in muscle cells (Liu et al., 2013). I corroborated that AMPK interacts with and phosphorylates PIKfyve on S307, leading to an increase in PI(3,5)P_2 synthesis (Liu et al., 2013), thus linking AMPK to lysosomal catabolism (Fernandez-Mosquera et al., 2019; Yordanov et al., 2019). I found that the phosphorylation of this residue is important for formation of PI(3,5)P_2 lipids as expected. However, AMPK-mediated phosphorylation of PIKfyve on S307 did not appear to play a role in the formation of PI(5)P-containing autophagosomes.

My findings using AMPK-null cells and AMPK activators would suggest that AMPK does play a role in PI(5)P-containing autophagosome biogenesis, albeit not through PIKfyve phosphorylation on S307. Additionally the AMPK-mediated effect on PI(5)P-containing autophagosomes was subject to regulation by mTORC1. I, therefore, studied other proteins in the AMPK interactome and identified ULK1 as a key player in the non-canonical signalling for PI(5)P-dependent autophagy.

I found that ULK1 inhibition abrogated this pathway, while ULK1 activation upregulated it. I provided evidence that PIKfyve binds ULK1 on its kinase domain and becomes phosphorylated by ULK1 on multiple amino acid residues. Of these sites, I found that the murine S1548 residue (S1549 in human) played an important regulatory role in the

formation of PI(5)P-containing autophagosomes. The phosphorylation of PIKfyve by ULK1 on S1548 led to an increase in PI(5)P lipids, PI(5)P-containing phagophores, autophagy flux and increased clearance of autophagy substrates.

While previously shown to be important for lysosomal metabolism, this study shows that PIKfyve is also directly involved in autophagosome biogenesis.

Additionally, this thesis shows that AMPK has a direct effect on PIKfyve for endolysosomal maturation and an indirect effect on PIKfyve through ULK1 on autophagosome biogenesis.

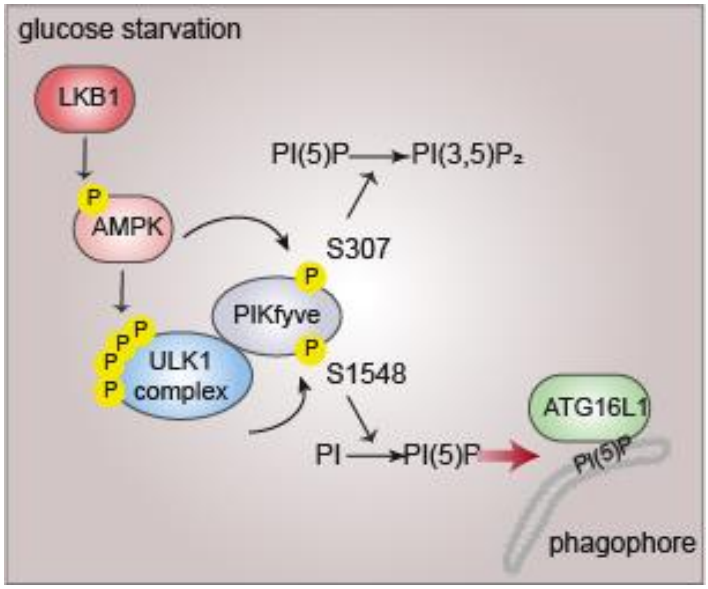

Figure 5.1 | Schematic overview of the ULK1-mediated PIKfyve activation

Upon glucose starvation, LKB1-mediated activation of AMPK leads to the activation of ULK1. ULK1 binds and phosphorylates PIKfyve on S1548, resulting in increased PI(5)P synthesis, formation of PI(5)P-containing autophagosomes and autophagy flux.

Outstanding questions

The findings highlighted above raise numerous questions that can be further addressed. These revolve around two main questions:

- **Who are the other players in the AMPK-ULK1-PIKfyve interactome?**
- **What is the physiological relevance of this pathway?**

i. What causes the differential ULK1-mediated activation of PIKfyve and VPS34?

ULK1 is a widely studied kinase whose effect on autophagy upregulation is well-established. While the general consensus is that starvation-induced AMPK-mediated activation of ULK1 leads to activation of VPS34, this thesis proposes a new mechanism for ULK1 upon glucose starvation showing that autophagy can be upregulated by ULK1 in a PIKfyve-dependent, VPS34-independent manner. ULK1/PIKfyve-mediated induction of autophagosome biogenesis could explain the presence of LC3-positive autophagosomes in VPS34-null sensory neurons (Zhou et al., 2010) and the PI(3)P-independent autophagy induced by glucose starvation (Mcalpine et al., 2013a).

It is possible that ULK1 differentially regulates autophagy based on the type of starvation method that has been used. Amino acid starvation leads to a direct ULK1-mediated activation of VPS34 (Russell et al., 2014). ULK1 can also activate the VPS34 complex by phosphorylating ATG14 on S29, a component of the VPS34 complex (Wold et al., 2016). Authors found this to be true upon mTOR inhibition with Torin1, in addition to amino acid starvation and serum starvation. Interestingly, this was not seen upon glucose starvation. An earlier study from our lab showed that starvation using HBSS (serum and amino acid starvation, low glucose levels) led to an increase in both PI(3)P and PI(5)P-containing autophagosomes (Vicinanza et al., 2015). Consistent with this, I found that mTOR inhibition with Torin1, which is known to induce an ULK1-mediated activation of the VPS34 complex (Wold et al., 2016), increased PI(5)P-containing autophagosomes, suggesting that it may be possible for ULK1 to activate both the VPS34 and PIKfyve complex simultaneously triggered by multiple forms of nutrient deprivation. To provide mechanistic insight into the differential functions of ULK1, future studies must consider the form of starvation used at various time points to dissect the exact contributions of ULK1 to amino acid and glucose starvation-induced autophagy, respectively. I showed in this study that the interaction between PIKfyve and ULK1 decreased already after 60 minutes of glucose starvation. It is possible upon prolonged glucose

starvation, that other proteins are involved in upregulating autophagy. Indeed, Kim et al., (2014) showed that AMPK directly activates VPS34 after three hours of glucose starvation. Interestingly, they also found that glucose starvation decreased overall PI(3)P production. Therefore, the AMPK-mediated activation of ULK1 and the ULK1-mediated activation of PIKfyve or VPS34, respectively in response to different types of starvation at various time points should be mapped.

Moreover, whether the upstream mechanism activates different residues on ULK1 depending on the type of deprivation remains to be resolved. As mentioned earlier, the starvation methods used to identify ULK1 phosphorylation residues in previous studies are significantly different from one another and has led to contentious results in the identified ULK1 phosphorylation sites. For example, AMPK phosphorylation of ULK1 on S317 and S777 was found after four hours of glucose starvation (Kim et al., 2011a). In another study, AMPK was found to phosphorylate ULK1 on S555 after 2 hours of starvation by incubating cells in Krebs–Ringer phosphate buffer (Bach et al., 2011). Therefore, the specific modifications that ULK1 undergoes upon different forms of starvation at various time point should be carefully described for this signalling pathway to become fully dissected.

ii. How is LKB1-mediated autophagy upregulation triggered?

I have shown that the presence of LKB1 is required for the effects of glucose starvation and AMPK activation on the formation of PI(5)P-containing phagophores. The exact mechanism by which LKB1 is activated under glucose starvation remains to be resolved.

LKB1 is predominantly activated through complex assembly (Boudeau et al., 2003). LKB1 forms a heterotrimeric complex with STRAD and MO25 (Baas et al., 2003; Boudeau et al., 2003). Binding of these two proteins to LKB1 promotes and stabilizes the activated conformation of LKB1 (Zeqiraj et al., 2009). How the LKB1-STRAD-MO25 complex is maintained remains unclear. A study showed that K63-linked LKB1 polyubiquitination by Skp2-SCF ubiquitin ligase is critical for LKB1 activation and for LKB1-mediated

AMPK activation (Lee et al., 2015). These findings were made in a study on cancer cell survival. Whether an ubiquitination or another post-translational modification is involved in LKB1 activation in the context of glucose starvation-induced autophagy is not yet clear.

Additionally, while AMPK specifically senses AMP levels in the cells, it is unclear what LKB1 senses causing it to phosphorylate AMPK on Thr172 and to subsequently terminate the AMPK activation. It is very likely that a feedback mechanism exists between LKB1 and some of the kinases involved in this pathway to cease the signal for autophagy induction. Since K63-linked ubiquitination is required for its activation, it is also possible that a yet unknown deubiqutinase may be involved in disassembling the LKB1-STRAD-MO25 complex.

iii. What is the interplay between mTORC1 and the AMPK-ULK1-PIKfyve pathway?

An elusive piece in the AMPK-ULK-PIKfyve interactome is the mTORC1 complex. Each of these players have been shown to interact with mTORC1 in different studies and contexts. In energy-replete condition, mTORC1 phosphorylates ULK1 on Ser757, thus disrupting the interaction between ULK1 and AMPK (Kim et al., 2011a). mTORC1 also hyperphosphorylates ATG13, thereby preventing its binding to ULK1 (Kamada et al., 2010). Upon starvation, AMPK inhibits mTOR (Corradetti et al., 2004a; Gwinn et al., 2008b; Inoki et al., 2003b). This event has been proposed to take place via an LKB1-mediated process on the lysosomal surface where mTORC1 is localised (Zhang et al., 2014). In this thesis, I found that formation of PI(5)P-containing autophagosomes were subject to mTORC1 regulation similar to canonical autophagy. However, there are still many unanswered questions regarding the relationship between mTOR and PIKfyve.

While multiple studies have implicated a link between AMPK and PIKfyve in the context of lysosomal maturation, PIKfyve has also in recent years been proposed to have a role in mTORC1 activity and in TFEB regulation via its synthesis of $PI(3,5)P_2$ lipids. A PIKfyve-mediated increase in $PI(3,5)P_2$

caused activation of TFEB in the context of xenophagy (Sharma et al., 2020). Conversely, in another study PIKfyve appeared to cause activation of mTORC1 in energy-replete condition via $PI(3,5)P_2$ synthesis (Bridges et al., 2012). More work is required to fully understand the contribution of PIKfyve to mTORC1 or TFEB activation.

Additionally, it appears that PIKfyve plays both a role in autophagosome formation via its interactions with AMPK and ULK1 and synthesis of PI(5)P and a role in autophagosome-lysosome fusion through its role in lysosomal function and synthesis of $PI(3,5)P_2$. While the findings in this thesis showed that ULK1 specifically led to an increase in the PI(5)P-related function of PIKfyve, glucose starvation did, however, appear to increase $PI(3,5)P_2$ through an AMPK-mediated activation. Whether the $PI(3,5)P_2$ involved in mTORC1 activation is sourced from a different pool and separate mechanism than the $PI(3,5)P_2$ involved in lysosomal function remains unclear.

To define the contribution of PIKfyve to mTORC1 inhibition/TFEB activation or mTORC1 activation, one could introduce point mutations in PIKfyve that abrogate either its synthesis of PI(5)P or $PI(3,5)P_2$ (Ikonomov et al., 2002) and study their effects on mTORC1 activity and TFEB nuclear translocation upon autophagy induction.

The PIKfyve-mediated induction of autophagy may be terminated via its interactions with the mTORC1 complex. Interestingly, the ULK1 kinase domain, which I found PIKfyve to be binding in this study, is also the site for mTORC1 binding (Kim et al., 2011b), suggesting that PIKfyve and mTORC1 may be competing for the same binding site on ULK1. How this competition is resolved and whether PIKfyve may have a differential effect on cellular metabolism and a capacity to shift the cell from anabolism to catabolism remains unknown. Further studies are required to dissect the interactions and hierarchies between these four kinases during starvation.

iv. How do PI(3)P and PI(5)P-containing autophagosomes differ?

A previous study from our lab showed that during starvation with HBSS both PI(3)P and PI(5)P-containing autophagosomes were formed. The shift towards PI(5)P-containing autophagosomes were found upon VPS34 inhibition with wortmannin (Vicinanza et al., 2015). The PI(5)P-containing autophagosomes recruit WIPI2 and DFCP1 similar to PI(3)P-containing autophagosomes (Vicinanza et al., 2015). We have yet to establish differences in the autophagosomes other than the signalling molecules involved in their formation. In the canonical pathway, PI(3)P-containing autophagosomes are formed on the RAB11A compartment of the recycling endosome (Puri et al., 2018). I found that PIKfyve is localised on RAB11A structures during both basal and glucose-deprived conditions and I showed that PIKfyve immunoprecipitates with RAB11A proteins. Additionally, our lab showed that PI(5)P-containing autophagosomes were found on the RAB11A structures (Karabiyik et al., Dev Cell, in revision). Further studies are required to determine whether the PI(5)P-containing autophagosomes on the RAB11A compartment are sourced from the recycling endosomes. Many sources have been proposed to contribute to autophagosomal membranes, including the endoplasmic reticulum (ER), Golgi, plasma membrane and others (Ravikumar et al., 2010a). It is possible that PI(5)P-containing autophagosomes are sourced from other membranes. To resolve this question, one could map the binding between PIKfyve and RAB11A and determine whether disruption of this binding could interfere with the formation of PI(5)P-containing autophagosomes. Ideally, both PI(3)P and PI(5)P-containing autophagosomes should be isolated and their compositions described to ascertain their exact identities.

v. What is the structural importance of PIKfyve S1548 phosphorylation?

I showed that ULK1 phosphorylates PIKfyve on S1548. In accordance with this, a recent study showed that this residue was phosphorylated in the PIKfyve complex in human PIKfyve although the source and function of this phosphorylation remained unknown (Lees et al., 2020). Its source and function is described in this thesis, as phosphorylation of PIKfyve on S1548

results in an increase in PI(5)P synthesis and the formation of PI(5)P-containing autophagosomes.

While we show the physiological importance of the phosphorylation of S1548, the structural importance remains unknown. This residue lies immediately downstream of the conserved cysteine-rich (CCR, amino acids 1157–1524). The CCR domain interacts with other PIKfyve domains and inhibits the lipid kinase activity of PIKfyve (Lang et al., 2017). It is possible that the phosphorylation of S1548 causes a conformational change that affects the interaction of the CCR domain with other components of the PIKfyve complex and leads to an increase in its lipid kinase activity. Due to its size (~230 kDa), the entire protein has yet to be structurally resolved. Further studies are required to study the structural importance of phosphorylation of PIKfyve on S1548.

vi. Are other components of the PIKfyve complex regulated upon autophagy induction?

PIKfyve forms a complex with the adaptor protein ArPIKfyve, which is critical for complex formation (Bonangelino et al., 2002; Sbrissa et al., 2004) and the lipid 5-phosphatase Fig4, which specifically dephosphorylates $PI(3,5)P_2$. ArPIKfyve depletion leads to a decrease in both $PI(3,5)P_2$ and PI(5)P levels, while overexpression of ArPIKfyve leads to an increase in said lipids (Sbrissa et al., 2004). Formation of the ternary complex PIKfyve-ArPIKfyve-Fig4 is required for PIKfyve activation (Sbrissa et al., 2008). A recent study showed that an intact complex comprises one copy of PIKfyve and Fig4 and a pentameric Vac14 scaffold (Lees et al., 2020). This is the same study that found that PIKfyve was phosphorylated on S1548. They showed, however, that this was only the case when the complex was assembled. Since Fig4 regulates PIKfyve activity (Hasegawa et al., 2017), it would be valuable studying the contribution of each component of the PIKfyve complex to autophagy induction.

As mentioned earlier, specific Fig4 mutations cause neurodegeneration in humans including CMT4J and ALS (Chow et al., 2007, 2009). In fibroblasts

derived from a cohort of CMT4J patients an extensive lipid profiling revealed substantial decreases in steady-state levels of both $PI(3,5)P_2$ and PI(5)P levels in CMT4J patient cells (Shisheva et al., 2019). Defects in autophagic degradation in CMT4J has been suggested by multiple studies (Ferguson et al., 2010; Vaccari et al., 2015) based on an increase in LC3-II, LAMP1 and the autophagy substrate p62 in brains of Fig4-mutant mice. While these findings do suggest a lysosomal defect caused by reduced $PI(3,5)P_2$ lipids, it is possible that the reduction in PI(5)P may contribute to disease pathology by causing reduced autophagosome biogenesis.

vii. Do any known autophagy modulators increase PIKfyve S1548 phosphorylation?

Many autophagy modulators have been studied for their therapeutic potential for the treatment of neurodegenerative diseases (Fleming et al., 2011). While generally categorised as either mTOR-dependent compounds, including rapamycin and its analogues or mTOR-independent compounds, including the disaccharide trehalose, their role in the signalling mechanisms causing autophagy induction is not yet fully elucidated.

Trehalose has been found to improve motor dysfunction and extend lifespan in a transgenic mouse model of Huntington disease (Tanaka et al., 2004); enhanced autophagic clearance of tau aggregates and increased neuronal survival in an AD mouse model (Schaeffer et al., 2012) and in a mouse model of tau overexpression with Parkinsonism (Rodríguez-Navarro et al., 2010); enhanced clearance of α-syn both *in vitro* (Sarkar et al., 2007b) and *in vivo* (Tanji et al., 2015).

Multiple studies show that trehalose induces autophagy in a mTOR-independent manner through activation of AMPK (Mizunoe et al., 2018; Rodríguez-Navarro et al., 2010; Sarkar et al., 2007b). Interestingly, a recent study showed that treatment of infected macrophages with trehalose caused a PIKfyve-mediated increase in $PI(3,5)P_2$, which led to Ca^{2+} release from the lysosomal lumen, resulting in TFEB activation and increased xenophagy (Sharma et al., 2020). These findings suggest that trehalose

causes an AMPK-mediated activation of PIKfyve. Whether trehalose also causes activation of PIKfyve via ULK1 is unclear.

Whether any autophagy modulators induce PI(5)P-dependent autophagy has yet to be assessed and could provide valuable insight into the physiological importance of non-canonical autophagy induction.

viii. Does this pathway have therapeutic potential?

I found that the ULK1-mediated activation of PIKfyve led to an increased clearance of mutant huntingtin. This experiment was both a verification that the increased autophagy flux caused by PIKfyve S1548 phosphorylaton did indeed increase clearance of autophagy substrates, but also an indication that this pathway may have clinical potential. This finding may have therapeutic value particularly in situations where Beclin-1/VPS34-dependent autophagy signalling dysfunction occurs, like in some neurodegenerative diseases, including Huntington's disease (Ashkenazi et al., 2017; Mealer et al., 2014; Pickford et al., 2008).

As described earlier, many AMPK activators have been studied in animal models of neurodegeneration. While the AMP analogue AICAR was shown to reduce Aβ levels in cellular and animal models of AD (Cai et al., 2012b; Li et al., 2018; Won et al., 2010) and tau phosphorylation in cellular models of AD (Greco et al., 2009), the direct AMPK activator A769662 reduced mHTT-containing aggregates in SPCs (Walter et al., 2016). I have shown that both compounds increased PI(5)P-containing phagophores in cells. The therapeutic potential of 991, which was shown in this thesis to have a profound effect on PI(5)P-dependent autophagy, has yet to be studied in the context of neurodegeneration.

The strategy of using AMPK activators for mitigating the pathology associated with neurodegenerative disease appears to be promising. Therefore, characterising the mechanism by which these activators induce autophagy and reduce protein aggregates would provide valuable insight.

Although I observed an increase in PI(5)P-dependent autophagy upon treatment of cells with AMPK activators, whether these modulators cause an increased phosphorylation of PIKfyve on S1548 remains to be shown. Additionally, the physiological importance of this pathway will be more evident once the phosphorylation of this residue is shown *in vivo.*

Concluding remarks

The identification of PIKfyve as a direct target of ULK1 and the involvement of AMPK in the ULK1-mediated induction of PI(5)P-dependent autophagy is a significant step towards the dissection of the complex cellular nutrient regulation system that leads to the activation of the autophagy machinery as a response to glucose starvation.

6 References

Adams, J., Chen, Z., Denderen, B.J.W.V.A.N., Morton, C.J., Parker, M.W., Witters, L.E.E.A., Stapleton, D., and Kemp, B.E. (2004). Intrasteric control of AMPK via the C1 subunit AMP allosteric regulatory site. Protein Sci. *13*, 155–165.

Akutsu, M., Dikic, I., and Bremm, A. (2016). Ubiquitin chain diversity at a glance. J. Cell Sci. *129*, 875–880.

Alison Goate, Marie-Christine, Chartier-Harlin, Mullan, M., Brown, J., Crawford, F., Fidani, L., Giuffrat, L., Haynes, A., Irving, N., et al. (1991). Segregation of a missense mutation in the amyloid β-protein precursor gene with familial Alzheimer's disease. Nature *349*, 704–706.

Ando, K., Brion, J.P., Stygelbout, V., Suain, V., Authelet, M., Dedecker, R., Chanut, A., Lacor, P., Lavaur, J., Sazdovitch, V., et al. (2013). Clathrin adaptor CALM/PICALM is associated with neurofibrillary tangles and is cleaved in Alzheimer's brains. Acta Neuropathol. *125*, 861–878.

Arnoux, I., Willam, M., Griesche, N., Krummeich, J., Watari, H., Offermann, N., Weber, S., Dey, P.N., Chen, C., Monteiro, O., et al. (2018). Metformin reverses early cortical network dysfunction and behavior changes in Huntington's disease. Elife *7*, 1–32.

Ashkenazi, A., Bento, C.F., Ricketts, T., Vicinanza, M., Pavel, M., Squitieri, F., Hardenberg, M.C., Imarisio, S., Menzies, F.M., and Rubinsztein, D.C. (2017). Polyglutamine tracts regulate beclin 1-dependent autophagy. Nature *545*, 108–111.

Aspernig, H., Heimbucher, T., Qi, W., Gangurde, D., Curic, S., Yan, Y., Donner von Gromoff, E., Baumeister, R., and Thien, A. (2019). Mitochondrial Perturbations Couple mTORC2 to Autophagy in C. elegans. Cell Rep. *29*, 1399-1409.e5.

Axe, E.L., Walker, S.A., Manifava, M., Chandra, P., Roderick, H.L., Habermann, A., Griffi, G., and Ktistakis, N.T. (2008). Autophagosome formation from membrane compartments enriched in phosphatidylinositol 3-phosphate and dynamically connected to the endoplasmic reticulum. J. Cell Biol. *182*, 685–701.

Baas, A.F., Boudeau, J., Sapkota, G.P., Smit, L., Medema, R., Morrice, N.A., Alessi, D.R., and Clevers, H.C. (2003). Activation of the tumour suppressor kinase LKB1 by the STE20-like pseudokinase STRAD. EMBO J. *22*, 3062–3072.

Bach, M., Larance, M., James, D.E., and Ramm, G. (2011). The serine/threonine kinase ULK1 is a target of multiple phosphorylation events. Biochem. J. *440*, 283–291.

Backer, J.M. (2008). The regulation and function of Class III PI3Ks: novel roles for Vps34. Biochem J *410*, 1–17.

Bai, H., Kang, P., Hernandez, A.M., and Tatar, M. (2013). Activin Signaling Targeted by Insulin/dFOXO Regulates Aging and Muscle Proteostasis in Drosophila. PLoS Genet. *9*.

Bar-Peled, L., Schweitzer, L.D., Zoncu, R., and Sabatini, D.M. (2012). Ragulator is a GEF for the rag GTPases that signal amino acid levels to mTORC1. Cell *150*, 1196–1208.

Baskaran, S., Carlson, L.A., Stjepanovic, G., Young, L.N., Kim, D.J. i., Grob, P., Stanley, R.E., Nogales, E., and Hurley, J.H. (2014). Architecture and dynamics of the autophagic phosphatidylinositol 3-kinase complex. Elife *3*, 1–19.

Behrends, C., Sowa, M.E., Gygi, S.P., and Harper, J.W. (2010). Network organization of the human autophagy system. Nature *466*, 68–76.

Bento, C.F., Ashkenazi, A., Jimenez-sanchez, M., and Rubinsztein, D.C. (2016). The Parkinson's disease-associated genes ATP13A2 and SYT11 regulate autophagy via a common pathway. Nat. Commun. *7*, 1–16.

Ber, Y., Shiloh, R., Gilad, Y., Degani, N., Bialik, S., and Kimchi, A. (2015). DAPK2 is a novel regulator of mTORC1 activity and autophagy. Cell Death Differ. *22*, 465–475.

Berger, Z., Ravikumar, B., Menzies, F.M., Oroz, L.G., Underwood, B.R., Pangalos, M.N., Schmitt, I., Wullner, U., Evert, B.O., Kane, C.J.O., et al. (2006). Rapamycin alleviates toxicity of different aggregate-prone proteins. Hum. Mol. Genet. *15*, 433–442.

Berwick, D.C., Dell, G.C., Welsh, G.I., Heesom, K.J., Hers, I., Fletcher, L.M., Cooke, F.T., and Tavaré, J.M. (2004). Protein kinase B phosphorylation of PIKfyve regulates the trafficking of GLUT4 vesicles. J. Cell Sci. *117*, 5985–5993.

Birk, J.B., and Wojtaszewski, J.F.P. (2006). Predominant α2/β2/γ3 AMPK activation during exercise in human skeletal muscle. J. Physiol. *577*, 1021–1032.

Bissig, C., Hurbain, I., Raposo, G., and van Niel, G. (2017). PIKfyve activity regulates reformation of terminal storage lysosomes from endolysosomes. Traffic 747–757.

Boisset, G., Polok, B.K., and Schorderet, D.F. (2008). Characterization of pip5k3 fleck corneal dystrophy-linked gene in zebrafish. Gene Expr. Patterns *8*, 404–410.

Boland, B., Kumar, A., Lee, S., Platt, F.M., Wegiel, J., Yu, W.H., and Nixon, R.A. (2008). Autophagy induction and autophagosome clearance in neurons: Relationship to autophagic pathology in Alzheimer's disease. J. Neurosci. *28*, 6926–6937.

Bonangelino, C.J., Nau, J.J., Duex, J.E., Brinkman, M., Wurmser, A.E., Gary, J.D., Emr, S.D., and Weisman, L.S. (2002). Osmotic stress-induced increase of phosphatidylinositol 3,5-bisphosphate requires Vac14p, an activator of the lipid kinase Fab1p. J. Cell Biol. *156*, 1015–1028.

Boudeau, J., Baas, A.F., Deak, M., Morrice, N.A., Kieloch, A., Schutkowski, M., Prescott, A.R., Clevers, H.C., and Alessi, D.R. (2003). MO25α/β interact with STRADα/β enhancing their ability to bind, activate and localize LKB1 in the cytoplasm. EMBO J. *22*, 5102–5114.

Boya, P., Gonzalez-Polo, Rosa-Ana Casares, N., Perfettini, J.-L., Dessen, P.,

Larochette, N., Métivier, D., Meley, D., Souquere, S., Yoshimori, T., Pierron, G., et al. (2005). Inhibition of Macroautophagy Triggers Apoptosis. Mol. Cell. Biol. *25*, 1025–1040.

Bridges, D., Ma, J.T., Park, S., Inoki, K., Weisman, L.S., and Saltiel, A.R. (2012). Phosphatidylinositol 3,5-bisphosphate plays a role in the activation and subcellular localization of mechanistic target of rapamycin 1. Mol. Biol. Cell *23*, 2955–2962.

Bua, D.J., Martin, G.M., Binda, O., and Gozani, O. (2013). Nuclear phosphatidylinositol-5-phosphate regulates ING2 stability at discrete chromatin targets in response to DNA damage. Sci. Rep. *3*.

Caccamo, A., Majumder, S., Richardson, A., Strong, R., and Oddo, S. (2010). Molecular interplay between mammalian target of rapamycin (mTOR), amyloid-β, and Tau: Effects on cognitive impairments. J. Biol. Chem. *285*, 13107–13120.

Cadwell, K., Liu, J.Y., Brown, S.L., Miyoshi, H., Loh, J., Lennerz, J.K., Kishi, C., Kc, W., Carrero, J.A., Hunt, S., et al. (2008). A key role for autophagy and the autophagy gene Atg16l1 in mouse and human intestinal Paneth cells. Nature *456*, 259–263.

Cai, Z., Zhao, B., Li, K., Zhang, L., Li, C., Quazi, S.H., and Tan, Y. (2012a). Mammalian target of rapamycin: A valid therapeutic target through the autophagy pathway for alzheimer's disease? J. Neurosci. Res. *90*, 1105–1118.

Cai, Z., Li, B., Li, K., and Zhao, B. (2012b). Down-Regulation of Amyloid-B Through AMPK Activation by Inhibitors of GSK-3B in SH-SY5Y and SH-SY5Y-ABPP695 Cells. J. Alzheimer's Dis. *29*, 89–98.

Carnio, S., LoVerso, F., Baraibar, M.A., Longa, E., Khan, M.M., Maffei, M., Reischl, M., Canepari, M., Loefler, S., Kern, H., et al. (2014). Autophagy Impairment in Muscle Induces Neuromuscular Junction Degeneration and Precocious Aging. Cell Rep. *8*, 1509–1521.

Cavallini, G., Donati, A., Gori, Z., Pollera, M., and Bergamini, E. (2001). The protection of rat liver autophagic proteolysis from the age-related decline co-varies with the duration of anti-ageing food restriction. Exp. Gerontol. *36*, 497–506.

Chang, J.T., Kumsta, C., Hellman, A.B., Adams, L.M., and Hansen, M. (2017). Spatiotemporal regulation of autophagy during Caenorhabditis elegans aging. Elife *6*, 1–23.

Chantranupong, L., Wolfson, R.L., Orozco, J.M., Saxton, R.A., Scaria, S.M., Bar-Peled, L., Spooner, E., Isasa, M., Gygi, S.P., and Sabatini, D.M. (2014). The sestrins interact with gator2 to negatively regulate the amino-acid-sensing pathway upstream of mTORC1. Cell Rep. *9*, 1–8.

Chen, J.L., Luo, C., Pu, D., Zhang, G.Q., Zhao, Y.X., Sun, Y., Zhao, K.X., Liao, Z.Y., Lv, A.K., Zhu, S.Y., et al. (2019). Metformin attenuates diabetes-induced tau hyperphosphorylation in vitro and in vivo by enhancing autophagic clearance. Exp. Neurol. *311*, 44–56.

Chi, H.C., Chen, S.L., Tsai, C.Y., Chuang, W.Y., Huang, Y.H., Tsai, M.M., Wu, S.M.,

Sun, C.P., Yeh, C.T., and Lin, K.H. (2016). Thyroid hormone suppresses hepatocarcinogenesis via DAPK2 and SQSTM1-dependent selective autophagy. Autophagy *12*, 2271–2285.

Chiang, M.C., Cheng, Y.C., Chen, S.J., Yen, C.H., and Huang, R.N. (2016). Metformin activation of AMPK-dependent pathways is neuroprotective in human neural stem cells against Amyloid-beta-induced mitochondrial dysfunction. Exp. Cell Res. *347*, 322–331.

Chow, C.Y., Zhang, Y., Dowling, J.J., Jin, N., Adamska, M., Shiga, K., Szigeti, K., Shy, M.E., Li, J., Zhang, X., et al. (2007). Mutation of FIG4 causes neurodegeneration in the pale tremor mouse and patients with CMT4J. Nature *448*, 68–72.

Chow, C.Y., Landers, J.E., Bergren, S.K., Sapp, P.C., Grant, A.E., Jones, J.M., Everett, L., Lenk, G.M., McKenna-Yasek, D.M., Weisman, L.S., et al. (2009). Deleterious Variants of FIG4, a Phosphoinositide Phosphatase, in Patients with ALS. Am. J. Hum. Genet. *84*, 85–88.

Chresta, C.M., Davies, B.R., Hickson, I., Harding, T., Cosulich, S., Critchlow, S.E., Vincent, J.P., Ellston, R., Jones, D., Sini, P., et al. (2010). AZD8055 is a potent, selective, and orally bioavailable ATP-competitive mammalian target of rapamycin kinase inhibitor with in vitro and in vivo antitumor activity. Cancer Res. *70*, 288–298.

Ciechanover, A. (2017). Intracellular protein degradation: From a vague idea thru the lysosome and the ubiquitin-proteasome system and onto human diseases and drug targeting. Best Pract. Res. Clin. Haematol. *30*, 341–355.

Claret, M., Smith, M.A., Batterham, R.L., Selman, C., Choudhury, A.I., Fryer, L.G.D., Clements, M., Al-Qassab, H., Heffron, H., Xu, A.W., et al. (2007). AMPK is essential for energy homeostasis regulation and glucose sensing by POMC and AgRP neurons. J. Clin. Invest. *117*, 2325–2336.

Clarke, J.H., Wang, M., and Irvine, R.F. (2010). Localization, regulation and function of Type II phosphatidylinositol 5-phosphate 4-kinases. Adv. Enzyme Regul. *50*, 12–18.

Clarke, J.H., Giudici, M.L., Burke, J.E., Williams, R.L., Maloney, D.J., Marugan, J., and Irvine, R.F. (2015). The function of phosphatidylinositol 5-phosphate 4-kinase γ (Pi5p4Kγ) explored using a specific inhibitor that targets the PI5P-binding site. Biochem. J. *466*, 359–367.

Codogno, P., Mehrpour, M., and Proikas-cezanne, T. (2011). Canonical and non-canonical autophagy: variations on a common theme of self-eating? Nat. Publ. Gr. *13*, 7–12.

Coffey, E.E., Beckel, J.M., Laties, A.M., and Mitchell, C.H. (2014). Lysosomal alkalization and dysfunction in human fibroblasts with the alzheimer's disease-linked presenilin 1 A246E mutation can be reversed with cAMP. Neuroscience *263*, 111–124.

Collodet, C., Foretz, M., Deak, M., Bultot, L., Metairon, S., Viollet, B., Lefebvre, G.,

Raymond, F., Parisi, A., Civiletto, G., et al. (2019). AMPK promotes induction of the tumor suppressor FLCN through activation of TFEB independently of mTOR. FASEB J. *33*, 12374–12391.

Compton, L.M., Ikonomov, O.C., Sbrissa, D., Garg, P., and Shisheva, A. (2016). Active vacuolar H+ atpase and functional cycle of rab5 are required for the vacuolation defect triggered by ptdins(3,5)p2 loss under PIKfyve or Vps34 deficiency. Am. J. Physiol. - Cell Physiol. *311*, C366–C377.

Cook, K.L., Soto-Pantoja, D.R., Abu-Asab, M., Clarke, P.A.G., Roberts, D.D., and Clarke, R. (2014). Mitochondria directly donate their membrane to form autophagosomes during a novel mechanism of parkin-associated mitophagy. Cell Biosci. *4*, 1–9.

Corradetti, M.N., Inoki, K., Bardeesy, N., Depinho, R.A., and Guan, K. (2004a). Regulation of the TSC pathway by LKB1: evidence of a molecular link between tuberous sclerosis complex and Peutz-Jeghers syndrome. Genes Dev. *18*, 1533–1538.

Corradetti, M.N., Inoki, K., Bardeesy, N., DePinho, R.A., and Guan, K.L. (2004b). Regulation of the TSC pathway by LKB1: Evidence of a molecular link between tuberous sclerosis complex and Peutz-Jeghers syndrome. Genes Dev. *18*, 1533–1538.

Crews, L., Spencer, B., Desplats, P., Patrick, C., Paulino, A., Rockenstein, E., Hansen, L., Adame, A., Galasko, D., and Masliah, E. (2010). Selective Molecular Alterations in the Autophagy Pathway in Patients with Lewy Body Disease and in Models of a -Synucleinopathy. PLoS One *5*.

Cuervo, A.M. (2009). Autophagy and aging. Trends Genet *24*, 604–612.

Cuervo, A.M., and Dice, J.F. (2000). Age-related decline in chaperone-mediated autophagy. J. Biol. Chem. *275*, 31505–31513.

Currinn, H., Guscott, B., Balklava, Z., Rothnie, A., and Wassmer, T. (2016). APP controls the formation of PI(3,5)P2 vesicles through its binding of the PIKfyve complex. Cell. Mol. Life Sci. *73*, 393–408.

Davies, S.P., Helps, N.R., Cohen, P.T.W., and Hardie, D.G. (1995). 5′-AMP inhibits dephosphorylation, as well as promoting phosphorylation, of the AMP-activated protein kinase. Studies using bacterially expressed human protein phosphatase-2Cα and native bovine protein phosphatase-2Ac. FEBS Lett. *377*, 421–425.

Davies, S.W., Turmaine, M., Cozens, B.A., DiFiglia, M., Scherzinger, E., Sharp, A.H., Ross, C.A., Wanker, E.E., Mangiarini, L., and Bates, G.P. (1997). Formation of neuronal intranuclear inclusions underlies the neurological dysfunction in mice transgenic for the HD mutation. Cell *90*, 537–548.

Demetriades, C., Plescher, M., and Teleman, A.A. (2016). Lysosomal recruitment of TSC2 is a universal response to cellular stress. Nat. Commun. *7*.

Demontis, F., and Perrimon, N. (2010). FOXO/4E-BP signaling in Drosophila

muscles regulates organism-wide proteostasis during aging. Cell *143*, 813–825.

Devereaux, K., Dall'Armi, C., Alcazar-Roman, A., Ogasawara, Y., Zhou, X., Wang, F., Yamamoto, A., de Camilli, P., and Di Paolo, G. (2013). Regulation of Mammalian Autophagy by Class II and III PI 3-Kinases through PI3P Synthesis. PLoS One *8*, 10–12.

Diao, J., Liu, R., Rong, Y., Zhao, M., Zhang, J., Lai, Y., Zhou, Q., Wilz, L.M., Li, J., Vivona, S., et al. (2015). ATG14 promotes membrane tethering and fusion of autophagosomes to endolysosomes. *520*, 563–566.

Dite, T.A., Ling, N.X.Y., Scott, J.W., Hoque, A., Galic, S., Parker, B.L., Ngoei, K.R.W., Langendorf, C.G., O'Brien, M.T., Kundu, M., et al. (2017). The autophagy initiator ULK1 sensitizes AMPK to allosteric drugs. Nat. Commun. *8*, 1–13.

Dodson, M.W., Zhang, T., Jiang, C., Chen, S., and Guo, M. (2012). Roles of the Drosophila LRRK2 homolog in Rab7-dependent lysosomal positioning. Hum. Mol. Genet. *21*, 1350–1363.

Donati, A. (2006). The involvement of macroautophagy in aging and anti-aging interventions. *27*, 455–470.

Dooley, H.C., Razi, M., Polson, H.E.J., Girardin, S.E., Wilson, M.I., and Tooze, S.A. (2014). WIPI2 Links LC3 Conjugation with PI3P, Autophagosome Formation, and Pathogen Clearance by Recruiting Atg12–5-16L1. Mol. Cell *55*, 238–252.

Dorsey, F.C., Rose, K.L., Coenen, S., Prater, S.M., Cavett, V., Cleveland, J.L., and Caldwell-Busby, J. (2009). Mapping the phosphorylation sites of Ulk1. J. Proteome Res. *8*, 5253–5263.

Dowler, S., Kular, G., and Alessi, D.R. (2002). Protein lipid overlay assay. Sci. STKE *2002*, 1–11.

Duncan, L.M., Piper, S., Dodd, R.B., Saville, M.K., Sanderson, C.M., Luzio, J.P., and Lehner, P.J. (2006). Lysine-63-linked ubiquitination is required for endolysosomal degradation of class I molecules. EMBO J. *25*, 1635–1645.

Dunlop, E.A., Hunt, D.K., Acosta-Jaquez, H.A., Fingar, D.C., and Tee, A.R. (2011). ULK1 inhibits mTORC1 signaling, promotes multisite Raptor phosphorylation and hinders substrate binding. Autophagy *7*, 737–747.

Duve, C. de, and Wattiaux, R. (1965). FUNCTIONS OF LYSOSOMES.

Egan, D.F., Shackelford, D.B., Mihaylova, M.M., Gelino, S.R., Rebecca, A., Mair, W., Vasquez, D.S., Joshi, A., Gwinn, D.M., Asara, J.M., et al. (2011). Phosphorylation of ULK1 (hATG1) by AMP-activated protein kinase connects energy sensing to mitophagy. Science (80-.). *331*, 456–461.

Egan, D.F., Chun, M.G.H., Vamos, M., Zou, H., Rong, J., Miller, C.J., Lou, H.J., Raveendra-Panickar, D., Yang, C.C., Sheffler, D.J., et al. (2015). Small Molecule Inhibition of the Autophagy Kinase ULK1 and Identification of ULK1 Substrates. Mol. Cell *59*, 285–297.

Elobeid, A., Libard, S., Leino, M., and Popova, S.N. (2016). Altered Proteins in the Aging Brain. J. Neuropathol Exp Neurol *75*, 316–325.

Endo, H., Owada, S., Inagaki, Y., Shida, Y., and Tatemichi, M. (2018). Glucose starvation induces LKB1-AMPK-mediated MMP-9 expression in cancer cells. Sci. Rep. *8*, 1–16.

Er, E., Mendoza, M., Mackey, A., Rameh, L., and Blenis, J. (2014). AKT Facilitates EGFR Trafficking and Degradation by Phosphorylating and Activating PIKfyve. Sci Signal *6*, 1–28.

Fan, W., Nassiri, A., and Zhong, Q. (2011). Autophagosome targeting and membrane curvature sensing by Barkor/Atg14(L). Proc. Natl. Acad. Sci. U. S. A. *108*, 7769–7774.

Ferguson, C.J., Lenk, G.M., and Meisler, M.H. (2010). PtdIns(3,5)P2 and autophagy in mouse models of neurodegeneration. Autophagy *6*, 170–171.

Fernandez-Mosquera, L., Yambire, K.F., Couto, R., Pereyra, L., Pabis, K., Ponsford, A.H., Diogo, C. V., Stagi, M., Milosevic, I., and Raimundo, N. (2019). Mitochondrial respiratory chain deficiency inhibits lysosomal hydrolysis. Autophagy *15*, 1572–1591.

Filimonenko, M., Stuffers, S., Raiborg, C., Yamamoto, A., Malerød, L., Fisher, E.M.C., Isaacs, A., Brech, A., Stenmark, H., and Simonsen, A. (2007). Functional multivesicular bodies are required for autophagic clearance of protein aggregates associated with neurodegenerative disease. J. Cell Biol. *179*, 485–500.

Fleming, A., Noda, T., Yoshimori, T., and Rubinsztein, D.C. (2011). Chemical modulators of autophagy as biological probes and potential therapeutics. Nat. Chem. Biol. *7*, 9–17.

Fogarty, S., Ross, F.A., Ciruelos, D.V., Gray, A., and Gowans, G.J. (2016). AMPK Causes Cell Cycle Arrest in LKB1-deficient Cells via Activation of CAMKK2. Mol Cancer Res *14*, 683–695.

Fujita, N., Itoh, T., Omori, H., Fukuda, M., Noda, T., and Yoshimori, T. (2008a). The Atg16L Complex Specifies the Site of LC3 Lipidation for Membrane Biogenesis in Autophagy. Mol. Biol. Cell *19*, 2092–2100.

Fujita, N., Hayashi-Nishino, M., Fukumoto, H., Omori, H., Yamamoto, A., Noda, T., and Yoshimori, T. (2008b). An Atg4B Mutant Hampers the Lipidation of LC3 Paralogues and Causes Defects in Autophagosome Closure. Mol. Biol. Cell *19*, 4651–4659.

Gadalla, A.E., Pearson, T., Currie, A.J., Dale, N., Hawley, S.A., Sheehan, M., Hirst, W., Michel, A.D., Randall, A., Hardie, D.G., et al. (2004). AICA riboside both activates AMP-activated protein kinase and competes with adenosine for the nucleoside transporter in the CA1 region of the rat hippocampus. J. Neurochem. *88*, 1272–1282.

Ganley, I.G., Lam, D.H., Wang, J., Ding, X., Chen, S., and Jiang, X. (2009). ULK1-ATG13-FIP200 Complex Mediates mTOR Signaling and Is Essential for Autophagy.

J. Biol. Chem. *284*, 12297–12305.

Gayle, S., Landrette, S., Beeharry, N., Conrad, C., Hernandez, M., Beckett, P., Ferguson, S.M., Xu, T., Rothberg, J., and Lichenstein, H. (2017). B-cell non-Hodgkin lymphoma: Selective vulnerability to PIKFYVE inhibition. Autophagy *13*, 1082–1083.

Ge, L., Melville, D., Zhang, M., and Schekman, R. (2013). The ER–Golgi intermediate compartment is a key membrane source for the LC3 lipidation step of autophagosome biogenesis. Elife *2*, 1–23.

Göransson, O., McBride, A., Hawley, S.A., Ross, F.A., Shpiro, N., Foretz, M., Viollet, B., Hardie, D.G., and Sakamoto, K. (2007). Mechanism of action of A-769662, a valuable tool for activation of AMP-activated protein kinase. J. Biol. Chem. *282*, 32549–32560.

Gowans, G.J., Hawley, S.A., Ross, F.A., and Hardie, D.G. (2013). AMP is a true physiological regulator of amp-activated protein kinase by both allosteric activation and enhancing net phosphorylation. Cell Metab. *18*, 556–566.

Gozani, O., Karuman, P., Jones, D.R., Ivanov, D., Cha, J., Lugovskoy, A.A., Baird, C.L., Zhu, H., Field, S.J., Lessnick, S.L., et al. (2003). The PHD finger of the chromatin-associated protein ING2 functions as a nuclear phosphoinositide receptor. Cell *114*, 99–111.

Greco, S.J., Sarkar, S., Casadesus, G., Johnston, X.Z.M.A.S.J.W.A.J.M., and Tezapsidis, N. (2009). Leptin Inhibits Glycogen Synthase Kinase-3β to Prevent Tau Phosphorylation in Neuronal Cells. Neurosci. Lett. *455*, 1–7.

Grice, G.L., and Nathan, J.A. (2016). The recognition of ubiquitinated proteins by the proteasome. Cell. Mol. Life Sci. *73*, 3497–3506.

Gunawardena, S., Her, L.S., Brusch, R.G., Laymon, R.A., Niesman, I.R., Gordesky-Gold, B., Sintasath, L., Bonini, N.M., and Goldstein, L.S.B. (2003). Disruption of axonal transport by loss of huntingtin or expression of pathogenic polyQ proteins in Drosophila. Neuron *40*, 25–40.

Gupta, A., Bisht, B., and Dey, C.S. (2011). Peripheral insulin-sensitizer drug metformin ameliorates neuronal insulin resistance and Alzheimer's-like changes. Neuropharmacology *60*, 910–920.

Gwinn, D.M., Shackelford, D.B., and Egan, D.F. (2008a). AMPK phosphorylation of raptor mediates a metabolic checkpoint. Mol. Cell *30*, 214–226.

Gwinn, D.M., Shackelford, D.B., Egan, D.F., Mihaylova, M.M., Mery, A., Vasquez, D.S., Turk, B.E., and Shaw, R.J. (2008b). AMPK Phosphorylation of Raptor Mediates a Metabolic Checkpoint. Mol. Cell *30*, 214–226.

Ha, J., Guan, K.L., and Kim, J. (2015). AMPK and autophagy in glucose/glycogen metabolism. Mol. Aspects Med. *46*, 46–62.

Haar, E. Vander, Lee, S., Bandhakavi, S., Griffin, T.J., and Kim, D. (2007). Insulin signalling to mTOR mediated by the Akt / PKB substrate PRAS40. *9*.

Han, J.M., Jeong, S.J., Park, M.C., Kim, G., Kwon, N.H., Kim, H.K., Ha, S.H., Ryu, S.H., and Kim, S. (2012). Leucyl-tRNA synthetase is an intracellular leucine sensor for the mTORC1-signaling pathway. Cell *149*, 410–424.

Hanada, T., Noda, N.N., Satomi, Y., Ichimura, Y., Fujioka, Y., Takao, T., Inagaki, F., and Ohsumi, Y. (2007). The Atg12-Atg5 Conjugate Has a Novel E3-like Activity for Protein Lipidation in Autophagy. J. Biol. Chem. *282*, 37298–37302.

Hansen, M., Chandra, A., Mitic, L.L., Onken, B., Driscoll, M., and Kenyon, C. (2008). A Role for Autophagy in the Extension of Lifespan by Dietary Restriction in C . elegans. *4*.

Hansen, M., Rubinsztein, D.C., and Walker, D.W. (2018). Autophagy as a promoter of longevity: insights from model organisms. Nat. Rev. Mol. Cell Biol. *19*, 611.

Hara, T., Nakamura, K., Matsui, M., Yamamoto, A., Nakahara, Y., Suzuki-migishima, R., Yokoyama, M., Mishima, K., Saito, I., and Okano, H. (2006). Suppression of basal autophagy in neural cells causes neurodegenerative disease in mice. Nat. Publ. Gr. *441*, 885–889.

Hardie, D.G. (2007). AMP-activated/SNF1 protein kinases: Conserved guardians of cellular energy. Nat. Rev. Mol. Cell Biol. *8*, 774–785.

Hardie, D.G. (2011). AMPK and autophagy get connected. EMBO J. *30*, 634–635.

Harold, D., Abraham, R., Hollingworth, P., Sims, R., Gerrish, A., Hamshere, M.L., Pahwa, J.S., Moskvina, V., Dowzell, K., Williams, A., et al. (2009). Genome-wide association study identifies variants at CLU and PICALM associated with Alzheimer's disease. Nat. Genet. *41*, 1088–1093.

Hasegawa, J., StrunkL, B.S., and Weisman, L.S. (2017). PI5P and PI(3,5)P2 : Minor, but Essential Phosphoinositides. Cell Struct Funct. *42*, 49–60.

Haung Yu, W., Cuervo, A.M., Kumar, A., Peterhoff, C.M., Schmidt, S.D., Lee, J.H., Mohan, P.S., Mercken, M., Farmery, M.R., Tjernberg, L.O., et al. (2005). Macroautophagy - A novel β-amyloid peptide-generating pathway activated in Alzheimer's disease. J. Cell Biol. *171*, 87–98.

Hawley, S.A., Boudeau, J., Reid, J.L., Mustard, K.J., Udd, L., Mäkelä, T.P., Alessi, D.R., and Hardie, D.G. (2003). Complexes between the LKB1 tumor suppressor, STRADα/β and MO25α/β are upstream kinases in the AMP-activated protein kinase cascade. J. Biol. *2*, 1–16.

Hawley, S.A., Pan, D.A., Mustard, K.J., Ross, L., Bain, J., Edelman, A.M., Frenguelli, B.G., and Hardie, D.G. (2005). Calmodulin-dependent protein kinase kinase-β is an alternative upstream kinase for AMP-activated protein kinase. Cell Metab. *2*, 9–19.

Hawley, S.A., Ross, F.A., Chevtzoff, C., Green, K.A., Evans, A., Fogarty, S., Towler, M.C., Brown, L.J., Ogunbayo, O.A., Evans, A.M., et al. (2010). Use of cells expressing γ subunit variants to identify diverse mechanisms of AMPK activation. Cell Metab. *11*, 554–565.

Hawley, S.A., Ross, F.A., Gowans, G.J., Tibarewal, P., Leslie, N.R., and Hardie, D.G. (2014). Phosphorylation by Akt within the ST loop of AMPK-α1 down-regulates its activation in tumour cells. Biochem. J. *459*, 275–287.

Hayashi-Nishino, M., Fujita, N., Noda, T., Yamaguchi, A., Yoshimori, T., and Yamamoto, A. (2009). A subdomain of the endoplasmic reticulum forms a cradle for autophagosome formation. Nat. Cell Biol. *11*, 1433–1437.

He, R., Peng, J., Yuan, P., Xu, F., and Wei, W. (2015). Divergent roles of BECN1 in LC3 lipidation and autophagosomal function. Autophagy *11*, 740–747.

He, X. Di, Gong, W., Zhang, J.N., Nie, J., Yao, C.F., Guo, F.S., Lin, Y., Wu, X.H., Li, F., Li, J., et al. (2018). Sensing and Transmitting Intracellular Amino Acid Signals through Reversible Lysine Aminoacylations. Cell Metab. *27*, 151-166.e6.

Hemelaar, J., Lelyveld, V.S., Kessler, B.M., and Ploegh, H.L. (2003). A Single Protease, Apg4B, Is Specific for the Autophagy-related Ubiquitin-like Proteins GATE-16, MAP1-LC3, GABARAP, and Apg8L. J. Biol. Chem. *278*, 51841–51850.

Hemesath, T.J., Steingrímsson, E., McGill, G., Hansen, M.J., Vaught, J., Hodgkinson, C.A., Arnheiter, H., Copeland, N.G., Jenkins, N.A., and Fisher, D.E. (1994). microphthalmia, A critical factor in melanocyte development, defines a discrete transcription factor family. Genes Dev. *8*, 2770–2780.

Heng, M.Y., Duong, D.K., Albin, R.L., Tallaksen-Greene, S.J., Hunter, J.M., Lesort, M.J., Osmand, A., Paulson, H.L., and Detloff, P.J. (2010). Early autophagic response in a novel knock-in model of Huntington disease. Hum. Mol. Genet. *19*, 3702–3720.

Hershko, A., Heller, H., Elias, S., and Ciechanover, A. (1983). Components of Ubiquitin-Protein Ligase System. J. Biol. Chem. *258*, 8206–8214.

Hill, E. V, Hudson, C.A., Vertommen, D., Rider, M.H., and Tavaré, J.M. (2010). Biochemical and Biophysical Research Communications Regulation of PIKfyve phosphorylation by insulin and osmotic stress. Biochem. Biophys. Res. Commun. *397*, 650–655.

Hofmann, R.M., and Pickart, C.M. (1999). Noncanonical MMS2-Encoded Ubiquitin-Conjugating Enzyme Functions in Assembly of Novel Polyubiquitin Chains for DNA Repair. Cell *96*, 645–653.

Hosokawa, N., Hara, T., Kaizuka, T., Kishi, C., Takamura, A., Miura, Y., Iemura, S., Natsume, T., Takehana, K., Yamada, N., et al. (2009). Nutrient-dependent mTORC1 Association with the ULK1–Atg13–FIP200 Complex Required for Autophagy. Mol. Biol. Cell *20*, 1981–1991.

Huang, J., and Manning, B.D. (2009). A complex interplay between Akt, TSC2, and the two mTOR complexes. Biochem Soc Trans *37*, 217–222.

Hudson, E.R., Pan, D.A., James, J., Lucocq, J.M., Hawley, S.A., Green, K.A., Baba, O., Terashima, T., and Hardie, D.G. (2003). A novel domain in AMP-activated protein kinase causes glycogen storage bodies similar to those seen in hereditary cardiac arrhythmias. Curr. Biol. *13*, 861–866.

Hurley, R.L., Anderson, K.A., Franzone, J.M., Kemp, B.E., Means, A.R., and Witters, L.A. (2005). The Ca2+/calmodulin-dependent protein kinase kinases are AMP-activated protein kinase kinases. J. Biol. Chem. *280*, 29060–29066.

Hwa Jung, C., Bong Jun, C., Ro, S.-H., Kim, Y.-M., Michael Otto, N., Cao, J., Kundu, M., Kim, D.-H., and Schmid, S.L. (2009). ULK-Atg13-FIP200 Complexes Mediate mTOR Signaling to the Autophagy Machinery. Mol. Biol. Cell *20*, 1992–2003.

Ichimura, Y., Kirisako, T., Takao, T., Satomi, Y., Shimonishi, Y., Ishihara, N., Mizushima, N., Tanida, I., Kominami, E., Ohsumi, M., et al. (2000). A ubiquitin-like system mediates protein lipidation. Nature *408*, 488–492.

Ikonomov, O.C., Sbrissa, D., and Shisheva, A. (2001). Mammalian Cell Morphology and Endocytic Membrane Homeostasis Require Enzymatically Active Phosphoinositide 5-Kinase PIKfyve. J. Biol. Chem. *276*, 26141–26147.

Ikonomov, O.C., Sbrissa, D., Mlak, K., Kanzaki, M., Pessin, J., and Shisheva, A. (2002). Functional dissection of lipid and protein kinase signals of PIKfyve reveals the role of PtdIns 3,5-P2production for endomembrane integrity. J. Biol. Chem. *277*, 9206–9211.

Ikonomov, O.C., Sbrissa, D., and Shisheva, A. (2006). Localized PtdIns 3,5-P2 synthesis to regulate early endosome dynamics and fusion. Am. J. Physiol. - Cell Physiol. *291*, 393–404.

Ikonomov, O.C., Sbrissa, D., Fenner, H., and Shisheva, A. (2009). PIKfyve-ArPIKfyve-Sac3 core complex: Contact sites and their consequence for Sac3 phosphatase activity and endocytic membrane homeostasis. J. Biol. Chem. *284*, 35794–35806.

Ikonomov, O.C., Sbrissa, D., Delvecchio, K., Xie, Y., Jin, J.P., Rappolee, D., and Shisheva, A. (2011). The phosphoinositide kinase PIKfyve is vital in early embryonic development: Preimplantation lethality of PIKfyve-/- embryos but normality of PIKfyve+/- mice. J. Biol. Chem. *286*, 13404–13413.

Ikonomov, O.C., Sbrissa, D., Delvecchio, K., Feng, H.Z., Cartee, G.D., Jin, J.P., and Shisheva, A. (2013). Muscle-specific Pikfyve gene disruption causes glucose intolerance, insulin resistance, adiposity, and hyperinsulinemia but not muscle fiber-type switching. Am. J. Physiol. - Endocrinol. Metab. *305*, 119–131.

Inoki, K., Li, Y., Zhu, T., Wu, J., and Guan, K.L. (2002). TSC2 is phosphorylated and inhibited by Akt and suppresses mTOR signalling. Nat. Cell Biol. *4*, 648–657.

Inoki, K., Li, Y., Xu, T., and Guan, K.L. (2003a). Rheb GTpase is a direct target of TSC2 GAP activity and regulates mTOR signaling. Genes Dev. *17*, 1829–1834.

Inoki, K., Zhu, T., Guan, K., and Arbor, A. (2003b). TSC2 Mediates Cellular Energy Response to Control Cell Growth and Survival. Cell *115*, 577–590.

Isobe, Y., Nigorikawa, K., Tsurumi, G., Takemasu, S., Takasuga, S., Kofuji, S., and Hazeki, K. (2018). PIKfyve accelerates phagosome acidification through activation of TRPML1 while arrests aberrant vacuolation independent of the Ca2+ channel. J.

Biochem.

Itakura, E., and Mizushima, N. (2010). Characterization of autophagosome formation site by a hierarchical analysis of mammalian Atg proteins. Autophagy *6*, 764–776.

Itakura, E., Kishi, C., Inoue, K., and Mizushima, N. (2008). Beclin 1 Forms Two Distinct Phosphatidylinositol 3-Kinase Complexes with Mammalian Atg14 and UVRAG. Mol. Biol. Cell *19*, 5360–5372.

Jahreiss, L., Menzies, F.M., and Rubinsztein, D.C. (2008). The itinerary of autophagosomes: From peripheral formation to kiss-and-run fusion with lysosomes. Traffic *9*, 574–587.

Jefferies, H.B.J., Cooke, F.T., Jat, P., Boucheron, C., Koizumi, T., Hayakawa, M., Kaizawa, H., Ohishi, T., Workman, P., Waterfield, M.D., et al. (2008). A selective PIKfyve inhibitor blocks PtdIns(3,5)P2 production and disrupts endomembrane transport and retroviral budding. EMBO Rep. *9*, 164–170.

Jewell, J.L., Russell, R.C., and Guan, K.L. (2013). Amino acid signalling upstream of mTOR. Nat. Rev. Mol. Cell Biol. *14*, 133–139.

Jia, J., Abudu, Y.P., Claude-Taupin, A., Gu, Y., Kumar, S., Choi, S.W., Peters, R., Mudd, M., Allers, L., Salemi, M., et al. (2018). Galectins control mTOR in response to endomembrane damage. Mol Cell *70*, 120–135.

Jia, J., Bissa, B., Brecht, L., Allers, L., Choi, S.W., Gu, Y., Zbinden, M., Burge, M.R., Timmins, G., Hallows, K., et al. (2020). AMPK, a Regulator of Metabolism and Autophagy, Is Activated by Lysosomal Damage via a Novel Galectin-Directed Ubiquitin Signal Transduction System. Mol. Cell 1–19.

Jiang, P., Nishimura, T., Sakamaki, Y., Itakura, E., Hatta, T., Natsume, T., and Mizushima, N. (2014a). The HOPS complex mediates autophagosome-lysosome fusion through interaction with syntaxin 17. Mol. Biol. Cell *25*, 1327–1337.

Jiang, T., Yu, J.T., Zhu, X.C., Zhang, Q.Q., Cao, L., Wang, H.F., Tan, M.S., Gao, Q., Qin, H., Zhang, Y.D., et al. (2014b). Temsirolimus attenuates tauopathy in vitro and in vivo by targeting tau hyperphosphorylation and autophagic clearance. Neuropharmacology *85*, 121–130.

Juhász, G., Érdi, B., Sass, M., and Neufeld, T.P. (2007). Atg7-dependent autophagy promotes neuronal health, stress tolerance, and longevity but is dispensable for metamorphosis in Drosophila. Genes Dev. 3061–3066.

Jung, C.H., Jun, C.B., Ro, S.-H., Kim, Y.-M., Otto, N.M., Cao, J., Kundu, M., and Kim, D.-H. (2009). ULK-Atg13-FIP200 Complexes Mediate mTOR Signaling to the Autophagy Machinery. Mol. Biol. Cell *20*, 1992–2003.

Kabeya, Y., Mizushima, N., Ueno, T., Yamamoto, A., Kirisako, T., Noda, T., Kominami, E., Ohsumi, Y., and Yoshimori, T. (2000). LC3, a mammalian homolog of yeast Apg8p, is localized in autophagosome membranes after processing. EMBO J. *19*, 5720–5728.

Kamada, Y., Yoshino, K. -i., Kondo, C., Kawamata, T., Oshiro, N., Yonezawa, K., and Ohsumi, Y. (2010). Tor Directly Controls the Atg1 Kinase Complex To Regulate Autophagy. Mol. Cell. Biol. *30*, 1049–1058.

Karabiyik, C., Lee, M.J., and Rubinsztein, D.C. (2017). Autophagy impairment in Parkinson's disease. Essays Biochem. *61*.

Kaushik, S., Arias, E., Kwon, H., Lopez, N.M., Athonvarangkul, D., Sahu, S., Schwartz, G.J., Pessin, J.E., and Singh, R. (2012). Loss of autophagy in hypothalamic POMC neurons impairs lipolysis. EMBO Rep. *13*, 258–265.

Kim, J., Kundu, M., Viollet, B., and Guan, K. (2011a). AMPK and mTOR regulate autophagy through direct phosphorylation of Ulk1. Nat. Cell Biol. *13*, 132–141.

Kim, J., Kundu, M., Viollet, B., and Guan, K. (2011b). AMPK and mTOR regulate autophagy through direct phosphorylation of Ulk1. Nat Cell Biol *13*, 132–141.

Kim, J., Kim, Y.C., Fang, C., Russell, R.C., Kim, J.H., Fan, W., Liu, R., Zhong, Q., and Guan, K.L. (2013). Differential regulation of distinct Vps34 complexes by AMPK in nutrient stress and autophagy. Cell *152*, 290–303.

Kimura, S., Noda, T., and Yoshimori, T. (2007). Dissection of the autophagosome maturation process by a novel reporter protein, tandem fluorescent-tagged LC3. Autophagy *3*, 452–460.

Kimura, S., Noda, T., and Yoshimori, T. (2008). Dynein-dependent movement of autophagosomes mediates efficient encounters with lysosomes. Cell Struct. Funct. *33*, 109–122.

Klionsky, D.J., Abdelmohsen, K., Abe, A., Abedin, J., Abeliovich, H., Bartolom, A., Beckham, J.D., Bertolotti, A., Bess, A.S., and Bozhkov, P. V (2016). Guidelines for the use and interpretation of assays for monitoring autophagy (3rd edition). Autophagy *12*, 1–222.

Knaevelsrud, H., Carlsson, S.R., and Simonsen, A. (2013). SNX18 tubulates recycling endosomes for autophagosome biogenesis. Autophagy *9*, 1639–1641.

Knorr, R.L., Lipowsky, R., and Dimova, R. (2015). Autophagosome closure requires membrane scission. Autophagy *11*, 2134–2137.

Komatsu, M., Waguri, S., Chiba, T., Murata, S., Iwata, J., Tanida, I., Ueno, T., Koike, M., Uchiyama, Y., Kominami, E., et al. (2006). Loss of autophagy in the central nervous system causes neurodegeneration in mice. Nature *441*, 880–884.

Korolchuk, V.I., Saiki, S., Lichtenberg, M., Siddiqi, F.H., Roberts, E.A., Imarisio, S., Jahreiss, L., Sarkar, S., Futter, M., Menzies, F.M., et al. (2011). Lysosomal positioning coordinates cellular nutrient responses. Nat. Cell Biol. *13*, 453–462.

Kraft, C., and Martens, S. (2012). Mechanisms and regulation of autophagosome formation. Curr. Opin. Cell Biol. *24*, 496–501.

Krüger, U., Wang, Y., Kumar, S., and Mandelkow, E.M. (2012). Autophagic

degradation of tau in primary neurons and its enhancement by trehalose. Neurobiol. Aging *33*, 2291–2305.

Laderoute, K.R., Amin, K., Calaoagan, J.M., Knapp, M., Le, T., Orduna, J., Foretz, M., and Viollet, B. (2006). 5′-AMP-Activated Protein Kinase (AMPK) Is Induced by Low-Oxygen and Glucose Deprivation Conditions Found in Solid-Tumor Microenvironments. Mol. Cell. Biol. *26*, 5336–5347.

Laker, R.C., Drake, J.C., Wilson, R.J., Lira, V.A., Lewellen, B.M., Ryall, K.A., Fisher, C.C., Zhang, M., Saucerman, J.J., Goodyear, L.J., et al. (2017). Ampk phosphorylation of Ulk1 is required for targeting of mitochondria to lysosomes in exercise-induced mitophagy. Nat. Commun. *8*.

Lang, M.J., Strunk, B.S., Azad, N., Petersen, J.L., and Weisman, L.S. (2017). An intramolecular interaction within the lipid kinase Fab1 regulates cellular phosphatidylinositol 3,5-bisphosphate lipid levels. Mol. Biol. Cell *28*, 858–864.

Langendorf, C.G., and Kemp, B.E. (2015). Choreography of AMPK activation. Nat. Publ. Gr.

Lapierre, L.R., De Magalhaes Filho, C.D., McQuary, P.R., Chu, C.C., Visvikis, O., Chang, J.T., Gelino, S., Ong, B., Davis, A.E., Irazoqui, J.E., et al. (2013). The TFEB orthologue HLH-30 regulates autophagy and modulates longevity in Caenorhabditis elegans. Nat. Commun. *4*.

Laplante, M., and Sabatini, D.M. (2012). mTOR signaling in growth control and disease. Cell *149*, 274–293.

de Lartigue, J., Polson, H., Feldman, M., Shokat, K., Tooze, S.A., Urbé, S., and Clague, M.J. (2009). PIKfyve regulation of endosome-linked pathways. Traffic *10*, 883–893.

Lee, H.N., Zarza, X., Kim, J.H., Yoon, M.J., Kim, S.H., Lee, J.H., Paris, N., Munnik, T., Otegui, M.S., and Chung, T. (2018). Vacuolar trafficking protein VPS38 is dispensable for autophagy. Plant Physiol. *176*, 1559–1572.

Lee, J.A., Beigneux, A., Ahmad, S.T., Young, S.G., and Gao, F.B. (2007). ESCRT-III Dysfunction Causes Autophagosome Accumulation and Neurodegeneration. Curr. Biol. *17*, 1561–1567.

Lee, J.H., Yu, W.H., Kumar, A., Lee, S., Mohan, P.S., Peterhoff, C.M., Wolfe, D.M., Martinez-Vicente, M., Massey, A.C., Sovak, G., et al. (2010a). Lysosomal proteolysis and autophagy require presenilin 1 and are disrupted by Alzheimer-related PS1 mutations. Cell *141*, 1146–1158.

Lee, J.W., Park, S., Takahashi, Y., and Wang, H.G. (2010b). The association of AMPK with ULK1 regulates autophagy. PLoS One *5*, 1–9.

Lee, S.-W., Li, C.-F., Jin, G., Cai, Z., Han, F., Chan, C.-H., Yang, W.-L., Li, B.-K., Rezaeian, A.H., Li, H.-Y., et al. (2015). Skp2-dependent Ubiquitination and Activation of LKB1 Is Essential for Cancer Cell Survival under Energy Stress. Mol Cell *57*, 1022–1033.

Lees, J.A., Li, P., Kumar, N., Weisman, L.S., Reinisch, K.M., Lees, J.A., Li, P., Kumar, N., Weisman, L.S., and Reinisch, K.M. (2020). Insights into Lysosomal PI (3 , 5) P 2 Homeostasis from a Structural-Biochemical Analysis of the PIKfyve Lipid Kinase Complex. Mol. Cell 1–8.

Leibson, C.L., Rocca, W.A., Hanson, V.A., Cha, R., Kokmen, E., O'Brien, P.C., and Palumbo, P.J. (1997). Risk of dementia among persons with diabetes mellitus: A population- based cohort study. Am. J. Epidemiol. *145*, 301–308.

Li, H., Wu, J., Zhu, L., Sha, L., Yang, S., Wei, J., Ji, L., Tang, X., Mao, K., Cao, L., et al. (2018). Insulin degrading enzyme contributes to the pathology in a mixed model of Type 2 diabetes and Alzheimer's disease: possible mechanisms of IDE in T2D and AD. Biosci. Rep. *38*, 1–10.

Li, J., Deng, J., Sheng, W., and Zuo, Z. (2012). Metformin attenuates Alzheimer's disease-like neuropathology in obese, leptin-resistant mice. Pharmacol. Biochem. Behav. *101*, 564–574.

Li, S., Tiab, L., Jiao, X., Munier, F.L., Zografos, L., Frueh, B.E., Sergeev, Y., Smith, J., Rubin, B., Meallet, M.A., et al. (2005). Mutations in PIP5K3 are associated with François-Neetens mouchetée fleck corneal dystrophy. Am. J. Hum. Genet. *77*, 54–63.

Li, X., Wang, X., Zhang, X., Zhao, M., Tsang, W.L., Zhang, Y., Yau, R.G.W., Weisman, L.S., and Xu, H. (2013). Genetically encoded fluorescent probe to visualize intracellular phosphatidylinositol 3,5-bisphosphate localization and dynamics. Proc. Natl. Acad. Sci. U. S. A. *110*, 21165–21170.

Li, X., Wang, L., Zhou, X.E., Ke, J., De Waal, P.W., Gu, X., Tan, M.H.E., Wang, D., Wu, D., Xu, H.E., et al. (2015). Structural basis of AMPK regulation by adenine nucleotides and glycogen. Cell Res. *25*, 50–66.

Liang, C., Feng, P., Ku, B., Dotan, I., Canaani, D., Oh, B.H., and Jung, J.U. (2006). Autophagic and tumour suppressor activity of a novel Beclin1-binding protein UVRAG. Nat. Cell Biol. *8*, 688–698.

Liang, C., Lee, J., Inn, K., Gack, M.U., Li, Q., Roberts, E.A., Vergne, I., Deretic, V., Feng, P., Akazawa, C., et al. (2008). Beclin1-binding UVRAG targets the class C Vps complex to coordinate autophagosome maturation and endocytic trafficking. Nat Cell Biol *10*, 776–787.

Lin, S.C., and Hardie, D.G. (2018). AMPK: Sensing Glucose as well as Cellular Energy Status. Cell Metab. *27*, 299–313.

Liu, R., Barkhordarian, H., Emadi, S., Chan, B.P., and Sierks, M.R. (2005). Trehalose differentially inhibits aggregation and neurotoxicity of beta-amyloid 40 and 42. Neurobiol. Dis. *20*, 74–81.

Liu, X., Chhipa, R.R., Pooya, S., Wortman, M., Yachyshin, S., Chow, L.M.L., Kumar, A., Zhou, X., Sun, Y., Quinn, B., et al. (2014a). Discrete mechanisms of mTOR and cell cycle regulation by AMPK agonists independent of AMPK. Proc. Natl. Acad. Sci. U. S. A. *111*, 435–444.

Liu, X., Chhipa, R.R., Nakano, I., and Dasgupta, B. (2014b). The AMPK inhibitor Compound C is a potent AMPK-independent anti-glioma agent. Mol Cancer Ther *13*, 596–605.

Liu, Y., Lai, Y.-C., Hill, E. V, Tyteca, D., Carpentier, S., Ingvaldsen, A., Vertommen, D., Lantier, L., Foretz, M., Dequiedt, F., et al. (2013). Phosphatidylinositol 3-phosphate 5-kinase (PIKfyve) is an AMPK target participating in contraction-stimulated glucose uptake in skeletal muscle. Biochem. J. *455*, 195–206.

Livneh, I., Cohen-Kaplan, V., Cohen-Rosenzweig, C., Avni, N., and Ciechanover, A. (2016). The life cycle of the 26S proteasome: From birth, through regulation and function, and onto its death. Cell Res. *26*, 869–885.

Löffler, A.S., Alers, S., Dieterle, A.M., Keppeler, H., Franz-Wachtel, M., Kundu, M., Campbell, D.G., Wesselborg, S., Alessi, D.R., and Stork, B. (2011). Ulk1-mediated phosphorylation of AMPK constitutes a negative regulatory feedback loop. Autophagy *7*, 696–706.

Lonskaya, I., Hebron, M.L., Desforges, N.M., and Schachter, J.B. (2014). Nilotinib-induced autophagic changes increase endogenous parkin level and ubiquitination, leading to amyloid clearance Charbel E-H Moussa. J Mol Med *92*, 373–386.

Lonskaya, I., Hebron, M.L., Selby, S.T., Turner, R.S., and Moussa, C.E.H. (2015). Nilotinib and bosutinib modulate pre-plaque alterations of blood immune markers and neuro-inflammation in Alzheimer's disease models. Neuroscience *304*, 316–327.

Lopez, A., Lee, S.E., Wojta, K., Ramos, E.M., Klein, E., Chen, J., Boxer, A.L., Gorno-Tempini, M.L., Geschwind, D.H., Schlotawa, L., et al. (2017). A152T tau allele causes neurodegeneration that can be ameliorated in a zebrafish model by autophagy induction. Brain *140*, 1128–1146.

Luo, S., and Rubinsztein, D.C. (2010). Apoptosis blocks Beclin 1-dependent autophagosome synthesis: An effect rescued by Bcl-xL. Cell Death Differ. *17*, 268–277.

Luzio, J.P., Pryor, P.R., and Bright, N.A. (2007). Lysosomes: fusion and function. Nat. Publ. Gr. *8*, 622–632.

Ma, L., Chen, Z., Erdjument-Bromage, H., Tempst, P., and Pandolfi, P.P. (2005). Phosphorylation and functional inactivation of TSC2 by Erk: Implications for tuberous sclerosis and cancer pathogenesis. Cell *121*, 179–193.

Ma, Q., Qiang, J., Gu, P., Wang, Y., Geng, Y., and Wang, M. (2011). Age-related autophagy alterations in the brain of senescence accelerated mouse prone 8 (SAMP8) mice. EXG *46*, 533–541.

MacDonald, M.E., Ambrose, C.M., Duyao, M.P., Myers, R.H., Lin, C., Srinidhi, L., Barnes, G., Taylor, S.A., James, M., Groot, N., et al. (1993). A novel gene containing a trinucleotide repeat that is expanded and unstable on Huntington's disease chromosomes. Cell *72*, 971–983.

Maeda, S., Otomo, C., and Otomo, T. (2019). The autophagic membrane tether

ATG2A transfers lipids between membranes. Elife *8*, 1–24.

Malagelada, C., Jin, Z.H., Jackson-lewis, V., Przedborski, S., and Greene, L.A. (2010). Rapamycin Protects against Neuron Death in In Vitro and In Vivo Models of Parkinson's Disease. J. Neurosci. *30*, 1166–1175.

Martin, S., Harper, C.B., May, L.M., Coulson, E.J., Meunier, F.A., and Osborne, S.L. (2013). Inhibition of PIKfyve by YM-201636 Dysregulates Autophagy and Leads to Apoptosis-Independent Neuronal Cell Death. PLoS One *8*.

Martina, J.A., Diab, H.I., Lishu, L., Jeong-A, L., Patange, S., Raben, N., and Puertollano, R. (2014). The nutrient-responsive transcription factor TFE3 promotes autophagy, lysosomal biogenesis, and clearance of cellular debris. Sci. Signal. *7*, 1–16.

Maruyama, R., Goto, K., Takemura, G., Ono, K., Nagao, K., Horie, T., Tsujimoto, A., Kanamori, H., Miyata, S., Ushikoshi, H., et al. (2008). Morphological and biochemical characterization of basal and starvation-induced autophagy in isolated adult rat cardiomyocytes. Am. J. Physiol. - Hear. Circ. Physiol. *295*, 1599–1607.

Matsunaga, K., Saitoh, T., Tabata, K., Omori, H., Satoh, T., Kurotori, N., Maejima, I., Shirahama-Noda, K., Ichimura, T., Isobe, T., et al. (2009). Two Beclin 1-binding proteins, Atg14L and Rubicon, reciprocally regulate autophagy at different stages. Nat. Cell Biol. *11*, 385–396.

Mauthe, M., Jacob, A., Freiberger, S., Hentschel, K., Stierhof, Y.D., Codogno, P., and Proikas-Cezanne, T. (2011). Resveratrol-mediated autophagy requires WIPI-1-regulated LC3 lipidation in the absence of induced phagophore formation. Autophagy *7*, 1448–1461.

Mcalpine, F., Williamson, L.E., Tooze, S.A., and Chan, E.Y.W. (2013a). Regulation of nutrient-sensitive autophagy by uncoordinated 51-like kinases 1 and 2. Autophagy *9*, 361–373.

Mcalpine, F., Williamson, L.E., Tooze, S.A., and Chan, E.Y.W. (2013b). Regulation of nutrient-sensitive autophagy by uncoordinated 51-like kinases 1 and 2. Autophagy *9*, 361–373.

Mealer, R.G., Murray, A.J., Shahani, N., Subramaniam, S., and Snyder, S.H. (2014). Rhes, a Striatal-selective Protein Implicated in Huntington Disease, Binds Beclin-1 and activates autophagy. J. Biol. Chem. *289*, 3547–3554.

Medina, D.L., Paola, S. Di, Peluso, I., Armani, A., Stefani, D. De, Venditti, R., Montefusco, S., Scotto-rosato, A., Prezioso, C., Settembre, C., et al. (2016). Lysosomal calcium signaling regulates autophagy via calcineurin and TFEB. J. Cell Biol. *17*, 288–299.

Meléndez, A., Talloczy, Z., Matthew, Eskelinen, E., Hall, D.H., and Levine, B. (2003). Autophagy Genes Are Essential for Dauer Development and Life-Span Extension in C . elegans. Science (80-.). *301*, 1387–1392.

Meley, D., Bauvy, C., Houben-weerts, J.H.P.M., Dubbelhuis, P.F., Helmond, M.T.J.,

Codogno, P., and Meijer, A.J. (2006). AMP-activated Protein Kinase and the Regulation of Autophagic Proteolysis. J. Biol. Chem. *281*, 34870–34879.

Menzies, F.M., Moreau, K., and Rubinsztein, D.C. (2011). Protein misfolding disorders and macroautophagy. Curr. Opin. Cell Biol. *23*, 190–197.

Menzies, F.M., Fleming, A., and Rubinsztein, D.C. (2015). Compromised autophagy and neurodegenerative diseases. Nat. Publ. Gr. *16*, 345–357.

Menzies, F.M., Fleming, A., Caricasole, A., Bento, C.F., Andrews, S.P., Ashkenazi, A., Füllgrabe, J., Jackson, A., Jimenez Sanchez, M., Karabiyik, C., et al. (2017a). Autophagy and Neurodegeneration: Pathogenic Mechanisms and Therapeutic Opportunities. Neuron *93*.

Menzies, F.M., Fleming, A., Caricasole, A., Bento, C.F., Andrews, S.P., Jackson, A., Sanchez, M.J., Karabiyik, C., Ashkenazi, A., Jens, F., et al. (2017b). Autophagy and Neurodegeneration : Pathogenic Mechanisms and Therapeutic Opportunities. Neuron *93*, 1015–1034.

Metlagel, Z., Otomo, C., Takaesu, G., and Otomo, T. (2013). Structural basis of ATG3 recognition by the autophagic ubiquitin-like protein ATG12. Proc. Natl. Acad. Sci. U. S. A. *110*, 18844–18849.

Michell, R.H., Heath, V.L., Lemmon, M.A., and Dove, S.K. (2006). Phosphatidylinositol 3,5-bisphosphate: Metabolism and cellular functions. Trends Biochem. Sci. *31*, 52–63.

Min, S.H., Suzuki, A., Stalker, T.J., Zhao, L., Wang, Y., McKennan, C., Riese, M.J., Guzman, J.F., Zhang, S., Lian, L., et al. (2015). Loss of PIKfyve in platelets causes a lysosomal disease leading to inflammation and thrombosis in mice. Nat Commun *5*, 1–28.

Mitchelhill, K.I., Michell, B.J., House, C.M., Stapleton, D., Dyck, J., Gamble, J., Ullrich, C., Witters, L.A., and Kemp, B.E. (1997). Posttranslational modifications of the 5'-AMP-activated protein kinase β1 subunit. J. Biol. Chem. *272*, 24475–24479.

Mizunoe, Y., Kobayashi, M., Sudo, Y., Watanabe, S., Yasukawa, H., Natori, D., Hoshino, A., Negishi, A., Okita, N., Komatsu, M., et al. (2018). Trehalose protects against oxidative stress by regulating the Keap1–Nrf2 and autophagy pathways. Redox Biol. *15*, 115–124.

Mizunuma, M., Neumann-Haefelin, E., Moroz, N., Li, Y., and Blackwell, T.K. (2014). mTORC2-SGK-1 acts in two environmentally responsive pathways with opposing effects on longevity. Aging Cell *13*, 869–878.

Mizushima, N., Sugita, H., Yoshimori, T., and Ohsumi, Y. (1998). A new protein conjugation system in human. T. J. Biol. Chem. *273*, 33889–33893.

Mizushima, N., Yamamoto, A., Hatano, M., Kobayashi, Y., Kabey, Y., Suzuki, K., Tokuhis, T., Ohsumi, Y., and Yoshimori, T. (2001). Dissection of autophagosome formation using Apg5-deficient mouse embryonic stem cells. J. Cell Biol. *152*, 657–667.

Moreau, K., Fleming, A., Imarisio, S., Lopez Ramirez, A., Mercer, J.L., Jimenez-Sanchez, M., Bento, C.F., Puri, C., Zavodszky, E., Siddiqi, F., et al. (2014). PICALM modulates autophagy activity and tau accumulation. Nat. Commun. *5*.

Mu, J., Brozinick, J.T., Valladares, O., Bucan, M., and Birnbaum, M.J. (2001). A role for AMP-activated protein kinase in contraction- and hypoxia-regulated glucose transport in skeletal muscle. Mol. Cell *7*, 1085–1094.

Munoz, C., Almilaji, A., Setiawan, I., Föller, M., and Lang, F. (2013). Up-regulation of the inwardly rectifying K+ channel Kir2.1 (KCNJ2) by protein kinase B (PKB/Akt) and PIKfyve. J. Membr. Biol. *246*, 189–197.

Musi, N., Hirshman, M.F., Nygren, J., Svanfeldt, M., Bavenholm, P., Rooyackers, O., Zhou, G., Williamson, J.M., Ljunqvist, O., Efendic, S., et al. (2002). Metformin Increases AMP-Activated Protein Kinase Activity in Skeletal Muscle of Subjects With Type 2 Diabetes. Diabetes *51*, 2074–2081.

Nathan, J.A., Tae Kim, H., Ting, L., Gygi, S.P., and Goldberg, A.L. (2013). Why do cellular proteins linked to K63-polyubiquitin chains not associate with proteasomes? EMBO J. *32*, 552–565.

Nemoto, T., Tanida, I., Tanida-Miyake, E., Minematsu-Ikeguchi, N., Yokota, M., Ohsumi, M., Ueno, T., and Kominami, E. (2003). The mouse APG10 homologue, an E2-like enzyme for Apg12p conjugation, facilitates MAP-LC3 modification. J. Biol. Chem. *278*, 39517–39526.

Nguyen, T.N., Padman, B.S., Usher, J., Oorschot, V., Ramm, G., and Lazarou, M. (2016). Atg8 family LC3 / GAB ARAP proteins are crucial for autophagosome – lysosome fusion but not autophagosome formation during PINK1 / Parkin mitophagy and starvation.

Nicot, A.-S., Fares, H., Payrastre, B., Chisholm, A.D., Labouesse, M., and Laporte, J. (2006). The Phosphoinositide Kinase PIKfyve/Fab1p Regulates Terminal Lysosome Maturation in Caenorhabditis elegans. Mol. Biol. Cell *17*, 3062–3074.

Noda, N.N., Fujioka, Y., Hanada, T., Ohsumi, Y., and Inagaki, F. (2013). Structure of the Atg12-Atg5 conjugate reveals a platform for stimulating Atg8-PE conjugation. EMBO Rep. *14*, 206–211.

Noda, T., Kim, J., Huang, W.P., Baba, M., Tokunaga, C., Ohsumi, Y., and Klionsky, D.J. (2000). Apg9p/Cvt7p is an integral membrane protein required for transport vesicle formation in the Cvt and autophagy pathways. J. Cell Biol. *148*, 465–479.

Noda, T., Fujita, N., and Yoshimori, T. (2009). The late stages of autophagy: How does the end begin? Cell Death Differ. *16*, 984–990.

Nwadike, C., Williamson, L.E., Gallagher, L.E., Guan, J., and Chan, E.Y.W. (2018). AMPK Inhibits ULK1-Dependent Autophagosome Formation. Mol. Cell. Biol. *38*, 1–22.

Oakhill, J.S., Chen, Z.P., Scott, J.W., Steel, R., Castelli, L.A., Linga, N., Macaulay, S.L., and Kemp, B.E. (2010). β-Subunit myristoylation is the gatekeeper for initiating

metabolic stress sensing by AMP-activated protein kinase (AMPK). Proc. Natl. Acad. Sci. U. S. A. *107*, 19237–19241.

Oakhill, J.S., Steel, R., Chen, Z.P., Scott, J.W., Ling, N., Tam, S., and Kemp, B.E. (2011). AMPK is a direct adenylate charge-regulated protein kinase. Science (80-.). *332*, 1433–1435.

Ohashi, Y., and Munro, S. (2010). Membrane Delivery to the Yeast Autophagosome from the Golgi–Endosomal System. Mol. Biol. Cell *21*, 4325–4337.

Osawa, T., Kotani, T., Kawaoka, T., Hirata, E., Suzuki, K., Nakatogawa, H., Ohsumi, Y., and Noda, N.N. (2019). Atg2 mediates direct lipid transfer between membranes for autophagosome formation. Nat. Struct. Mol. Biol. *26*, 281–288.

Ou, Z., Kong, X., Sun, X., He, X., Zhang, L., Gong, Z., Huang, J., Xu, B., Long, D., Li, J., et al. (2018). Metformin treatment prevents amyloid plaque deposition and memory impairment in APP/PS1 mice. Brain. Behav. Immun. *69*, 351–363.

Ozcelik, S., Fraser, G., Castets, P., Schaeffer, V., Skachokova, Z., Breu, K., Clavaguera, F., Sinnreich, M., Kappos, L., Goedert, M., et al. (2013). Rapamycin Attenuates the Progression of Tau Pathology in P301S Tau Transgenic Mice. PLoS One *8*, 2–8.

Palmieri, M., Impey, S., Kang, H., Ronza, A., Pelz, C., and Sardiello, M. (2011). Characterization of the CLEAR network reveals an integrated control of cellular clearance pathways. Hum. Mol. Genet. *20*, 3852–3866.

Pankiv, S., Alemu, E.A., Brech, A., Bruun, J.A., Lamark, T., Øvervatn, A., Bjørkøy, G., and Johansen, T. (2010). FYCO1 is a Rab7 effector that binds to LC3 and PI3P to mediate microtubule plus end - Directed vesicle transport. J. Cell Biol. *188*, 253–269.

Park, S.Y., Lee, H.R., Lee, W.S., Shin, H.K., Kim, H.Y., Hong, K.W., and Kim, C.D. (2016). Cilostazol Modulates Autophagic Degradation of β-Amyloid Peptide via SIRT1-Coupled LKB1/AMPKα Signaling in Neuronal Cells. PLoS One *11*, e0160620.

Parker, J.A., Arango, M., Abderrahmane, S., Lambert, E., Tourette, C., Catoire, H., and Néri, C. (2005). Resveratrol rescues mutant polyglutamine cytotoxicity in nematode and mammalian neurons. Nat. Genet. *37*, 349–350.

Parmigiani, A., Nourbakhsh, A., Ding, B., Wang, W., Kim, Y.C., Akopiants, K., Guan, K.L., Karin, M., and Budanov, A. V. (2014). Sestrins Inhibit mTORC1 Kinase Activation through the GATOR Complex. Cell Rep. *9*, 1281–1291.

Pavel, M., Imarisio, S., Menzies, F.M., Jimenez-sanchez, M., Siddiqi, F.H., Wu, X., Renna, M., Kane, C.J.O., Crowther, D.C., and Rubinsztein, D.C. (2016). CCT complex restricts neuropathogenic protein aggregation via autophagy. Nat. Commun. *7*.

Pickart, C.M. (2001). Mechanisms nderlying biquitination. Annu. Rev. Biochem. *70*, 503–533.

Pickford, F., Masliah, E., Britschgi, M., Lucin, K., Narasimhan, R., Jaeger, P.A., Small, S., Spencer, B., Rockenstein, E., Levine, B., et al. (2008). The autophagy-related protein beclin 1 shows reduced expression in early Alzheimer disease and regulates amyloid β accumulation in mice. J. Clin. Invest. *118*, 2190–2199.

Ploper, D., Taelman, V.F., Robert, L., Perez, B.S., Titz, B., Chen, H.W., Graeber, T.G., Von Euw, E., Ribas, A., and De Robertis, E.M. (2015). MITF drives endolysosomal biogenesis and potentiates Wnt signaling in melanoma cells. Proc. Natl. Acad. Sci. U. S. A. *112*, E420–E429.

Polekhina, G., Gupta, A., Michell, B.J., Van Denderen, B., Murthy, S., Feil, S.C., Jennings, I.G., Campbell, D.J., Witters, L.A., Parker, M.W., et al. (2003). AMPK β subunit targets metabolic stress sensing to glycogen. Curr. Biol. *13*, 867–871.

Poli, A., Zaurito, A.E., Abdul-Hamid, S., Fiume, R., Faenza, I., and Divecha, N. (2019). Phosphatidylinositol 5 phosphate (Pi5p): From behind the scenes to the front (nuclear) stage. Int. J. Mol. Sci. *20*, 1–17.

Proikas-Cezanne, T., Waddell, S., Gaugel, A., Frickey, T., Lupas, A., and Nordheim, A. (2004). WIPI-1α (WIPI49), a member of the novel 7-bladed WIPI protein family, is aberrantly expressed in human cancer and is linked to starvation-induced autophagy. Oncogene *23*, 9314–9325.

Proikas-Cezanne, T., Ruckerbauer, S., Stierhof, Y.D., Berg, C., and Nordheim, A. (2007). Human WIPI-1 puncta-formation: A novel assay to assess mammalian autophagy. FEBS Lett. *581*, 3396–3404.

Puri, C., Renna, M., Bento, C.F., Moreau, K., and Rubinsztein, D.C. (2013). Diverse autophagosome membrane sources coalesce in recycling endosomes. Cell *154*, 1285–1299.

Puri, C., Vicinanza, M., Ashkenazi, A., Gratian, M.J., Zhang, Q., Bento, C.F., Renna, M., Menzies, F.M., and Rubinsztein, D.C. (2018). The RAB11A-Positive Compartment Is a Primary Platform for Autophagosome Assembly Mediated by WIPI2 Recognition of PI3P-RAB11A. Dev. Cell *45*, 114-131.e8.

Pyo, J.O., Yoo, S.M., Ahn, H.H., Nah, J., Hong, S.H., Kam, T.I., Jung, S., and Jung, Y.K. (2013). Overexpression of Atg5 in mice activates autophagy and extends lifespan. Nat. Commun. *4*, 1–9.

Qiao, L., Hamamichi, S., Caldwell, K.A., Caldwell, G.A., Yacoubian, T.A., Wilson, S., Xie, Z., Speake, L.D., Parks, R., Crabtree, D., et al. (2008). Lysosomal enzyme cathepsin D protects against alpha-synuclein aggregation and toxicity. Mol. Brain *1*, 1–18.

Rabanal-Ruiz, Y., and Korolchuk, V.I. (2018). mTORC1 and nutrient homeostasis: The central role of the lysosome. Int. J. Mol. Sci. *19*.

Rajeshwary Ghosh, Vishaka Vinod, J.D.S. and S.B. (2020). Mechanisms and Cardiac Aging.

Rameh, L.E., Tolias, K.F., Duckworth, B.C., and Cantley, L.C. (1997). A new

pathway for synthesis of phosphatidylinositol-4,5-bisphosphate. Nature *390*, 192–196.

Ravikumar, B., Duden, R., and Rubinsztein, D.C. (2002). Aggregate-prone proteins with polyglutamine and polyalanine expansions are degraded by autophagy. Hum. Mol. Genet. *11*, 1107–1117.

Ravikumar, B., Vacher, C., Berger, Z., Davies, J.E., Luo, S., Oroz, L.G., Scaravilli, F., Easton, D.F., Duden, R., O'Kane, C.J., et al. (2004). Inhibition of mTOR induces autophagy and reduces toxicity of polyglutamine expansions in fly and mouse models of Huntington disease. Nat. Genet. *36*, 585–595.

Ravikumar, B., Acevedo-Arozena, A., Imarisio, S., Berger, Z., Vacher, C., O'Kane, C.J., Brown, S.D.M., and Rubinsztein, D.C. (2005). Dynein mutations impair autophagic clearance of aggregate-prone proteins. Nat. Genet. *37*, 771–776.

Ravikumar, B., Sarkar, S., Davies, J.E., Futter, M., Garcia-Arencibia, M., Green-Thompson, Z.W., Jimenez-Sanchez, M., Korolchuk, V.I., Lichtenberg, M., Luo, S., et al. (2010a). Regulation of mammalian autophagy in physiology and pathophysiology. Physiol. Rev. *90*, 1383–1435.

Ravikumar, B., Moreau, K., Jahreiss, L., Puri, C., and Rubinsztein, D.C. (2010b). Plasma membrane contributes to the formation of pre-autophagosomal structures. Nat. Cell Biol. *12*, 747–757.

Razi, M., Chan, E.Y.W., and Tooze, S.A. (2009). Early endosomes and endosomal coatomer are required for Autophagy. J. Cell Biol. *185*, 305–321.

Renna, M., Jimenez-sanchez, M., Sarkar, S., and Rubinsztein, D.C. (2010). Chemical Inducers of Autophagy That Enhance the Clearance of Mutant Proteins in Neurodegenerative Diseases. J. Biol. Chem. *285*, 11061–11067.

Renna, M., Bento, C.F., Fleming, A., Menzies, F.M., Siddiqi, F.H., Ravikumar, B., Puri, C., Garcia-Arencibia, M., Sadiq, O., Corrochano, S., et al. (2013). IGF-1 receptor antagonism inhibits autophagy. Hum. Mol. Genet. *22*, 4528–4544.

Roczniak-Ferguson, A., Petit, C.S., Froehlich, F., Qian, S., Ky, J., Angarola, B., Walther, T.C., and Ferguson, S.M. (2012). The Transcription Factor TFEB Links mTORC1 Signaling to Transcriptional Control of Lysosome Homeostasis. Sci Signal *5*.

Rodríguez-Navarro, J.A., Rodríguez, L., Casarejos, M.J., Solano, R.M., Gómez, A., Perucho, J., Cuervo, A.M., García de Yébenes, J., and Mena, M.A. (2010). Trehalose ameliorates dopaminergic and tau pathology in parkin deleted/tau overexpressing mice through autophagy activation. Neurobiol. Dis. *39*, 423–438.

Rohn, T.T., Wirawan, E., Brown, R.J., Harris, J.R., Masliah, E., and Vandenabeele, P. (2011). Depletion of Beclin-1 due to proteolytic cleavage by caspases in the Alzheimer's disease brain. Neurobiol. Dis. *43*, 68–78.

Rose, C., Menzies, F.M., Renna, M., Acevedo-arozena, A., Corrochano, S., Sadiq, O., Brown, S.D., and Rubinsztein, D.C. (2010). Rilmenidine attenuates toxicity of

polyglutamine expansions in a mouse model of Huntington ' s disease. *19*, 2144–2153.

Del Roso, A., Vittorini, S., Cavallini, G., Donati, A., Gori, Z., Masini, M., Pollera, M., and Bergamini, E. (2003). Ageing-related changes in the in vivo function of rat liver macroautophagy and proteolysis. Exp. Gerontol. *38*, 519–527.

Ross, F.A., Jensen, T.E., and Hardie, D.G. (2016). Differential regulation by AMP and ADP of AMPK complexes containing different γ subunit isoforms. Biochem. J. *473*, 189–199.

Ross, O.A., Braithwaite, A.T., Skipper, L.M., Kachergus, J., Hulihan, M.M., Middleton, F.A., Nishioka, K., Fuchs, J., Gasser, T., Maraganore, D.M., et al. (1998). Genomic investigation of α-Synuclein multiplication and parkinsonism. J. Natl. Cancer Inst. *90*, 1894–1900.

Rubinsztein, D.C., Marino, G., and Kroemer, G. (2010). Autophagy and Aging. Cell.

Russell, R.C., Tian, Y., Yuan, H., Park, H.W., Chang, Y., Kim, H., Neufeld, T.P., Dillin, A., and Guan, K. (2014). ULK1 induces autophagy by phosphorylating Beclin-1 and activating Vps34 lipid kinase. Nat. Cell Biol. *15*, 741–750.

Rusten, T.E., Vaccari, T., Lindmo, K., Rodahl, L.M.W., Nezis, I.P., Sem-Jacobsen, C., Wendler, F., Vincent, J.P., Brech, A., Bilder, D., et al. (2007a). ESCRTs and Fab1 Regulate Distinct Steps of Autophagy. Curr. Biol. *17*, 1817–1825.

Rusten, T.E., Rodahl, L.M.W., Pattni, K., Englund, C., Samakovlis, C., Dove, S., Brech, A., and Stenmark, H. (2007b). Fab1 Phosphatidylinositol 3-Phosphate 5-Kinase Controls Trafficking but Not Silencing of Endocytosed Receptors. Mol. Biol. Cell *18*, 986–994.

Rutherford, A.C., Traer, C., Wassmer, T., Pattni, K., Bujny, M. V., Carlton, J.G., Stenmark, H., and Cullen, P.J. (2006). The mammalian phosphatidylinositol 3-phosphate 5-kinase (PIKfyve) regulates endosome-to-TGN retrograde transport. J. Cell Sci. *119*, 3944–3957.

Sabatini, D.M., Erdjument-Bromage, H., Lui, M., Tempst, P., and Snyder, S.H. (1994). RAFT1: A mammalian protein that binds to FKBP12 in a rapamycin-dependent fashion and is homologous to yeast TORs. Cell *78*, 35–43.

Samari, H.R., and Seglen, P.O. (1998). Inhibition of hepatocytic autophagy by adenosine, aminoimidazole-4- carboxamide riboside, and N6-mercaptopurine riboside. Evidence for involvement of AMP-activated protein kinase. J. Biol. Chem. *273*, 23758–23763.

Sancak, Y., Thoreen, C.C., Peterson, T.R., Lindquist, R.A., Kang, S.A., Spooner, E., Carr, S.A., and Sabatini, D.M. (2007). PRAS40 Is an Insulin-Regulated Inhibitor of the mTORC1 Protein Kinase. Mol. Cell *25*, 903–915.

Sancak, Y., Bar-Peled, L., Zoncu, R., Markhard, A.L., Nada, S., and Sabatini, D.M. (2008). Ragulator-rag complex targets mTORC1 to the lysosomal surface and is necessary for its activation by amino acids. Cell *141*, 290–303.

Sancak, Y., Bar-Peled, L., Zoncu, R., Markhard, A.L.S.N., and Sabatini, D.M. (2011). Ragulator-Rag complex targets mTORC1 to the lysosomal surface and is necessary for its activation by amino acids. *141*, 290–303.

Sanchez, A.M.J., Csibi, A., Raibon, A., Cornille, K., Gay, S., Bernardi, H., and Candau, R. (2012). AMPK promotes skeletal muscle autophagy through activation of forkhead FoxO3a and interaction with Ulk1. J. Cell. Biochem. *113*, 695–710.

Sanders, M.J., Ali, Z.S., Hegarty, B.D., Heath, R., Snowden, M.A., and Carling, D. (2007). Defining the mechanism of activation of AMP-activated protein kinase by the small molecule A-769662, a member of the thienopyridone family. J. Biol. Chem. *282*, 32539–32548.

Sano, O., Kazetani, K., Funata, M., Fukuda, Y., Matsui, J., and Iwata, H. (2016). Vacuolin-1 inhibits autophagy by impairing lysosomal maturation via PIKfyve inhibition. FEBS Lett. *590*, 1576–1585.

Sapp, E., Schwarz, C., Chase, K., Bhide, P.G., Young, A.B., Penney, J., Vonsattel, J.P., Aronin, N., and DiFiglia, M. (1997). Huntingtin localization in brains of normal and Huntington's disease patients. Ann. Neurol. *42*, 604–612.

Sarbassov, D.D., Ali, S.M., Sengupta, S., Sheen, J.H., Hsu, P.P., Bagley, A.F., Markhard, A.L., and Sabatini, D.M. (2006). Prolonged Rapamycin Treatment Inhibits mTORC2 Assembly and Akt/PKB. Mol. Cell *22*, 159–168.

Sardiello, M., Palmieri, M., Ronza, A. di, Medina, D.L., Valenza, M., Gennarino, V.A., Malta, C. Di, Donaudy, F., Embrione, V., Polishchuk, R.S., et al. (2009). A Gene Network Regulating Lysosomal Biogenesis and Function. Science (80-.). *325*, 473–476.

Sarkar, S., Floto, R.A., Berger, Z., Imarisio, S., Cordenier, A., Pasco, M., Cook, L.J., and Rubinsztein, D.C. (2005). Lithium induces autophagy by inhibiting inositol monophosphatase. J. Cell Biol. *170*, 1101–1111.

Sarkar, S., Perlstein, E.O., Imarisio, S., Pineau, S., Cordenier, A., Maglathlin, R.L., Webster, J.A., Lewis, T.A., O'Kane, C.J., Schreiber, S.L., et al. (2007a). Small molecules enhance autophagy and reduce toxicity in Huntington's disease models. Nat. Chem. Biol. *3*, 331–338.

Sarkar, S., Davies, J.E., Huang, Z., Tunnacliffe, A., and Rubinsztein, D.C. (2007b). Trehalose, a Novel mTOR-independent Autophagy Enhancer, Accelerates the Clearance of Mutant Huntingtin. J. Biol. Chem. *282*, 5641–5652.

Sarkis, G.J., Ashcom, J.D., Hawdon, J.M., and Jacobson, L.A. (1988). Decline in protease activities with age in the nematode caenorhabditis elegans. Mech. Ageing Dev. *45*, 191–201.

Saxton, R.A., Knockenhauer, K.E., Wolfson, R.L., Chantranupong, L., Pacold, M.E., Wang, T., Schwartz, T.U., and Sabatini, D.M. (2016). Structural basis for leucine sensing by the Sestrin2-mTORC1 pathway. Science (80-.). *351*, 53–58.

Sbrissa, D., and Shisheva, A. (2005). Acquisition of unprecedented

phosphatidylinositol 3,5-bisphosphate rise in hyperosmotically stressed 3T3-L1 adipocytes, mediated by ArPIKfyve-PIKfyve pathway. J. Biol. Chem. *280*, 7883–7889.

Sbrissa, D., Ikonomov, O.C., and Shisheva, A. (1999a). PIKfyve, a Mammalian Ortholog of Yeast Fab1p Lipid Kinase, Synthesizes 5-Phosphoinositides. J. Biol. Chem. *274*, 21589–21597.

Sbrissa, D., Ikonomov, O.C., and Shisheva, A. (1999b). PIKfyve, a mammalian ortholog of yeast Fab1p lipid kinase, synthesizes 5-phosphoinositides. Effect of insulin. J. Biol. Chem. *274*, 21589–21597.

Sbrissa, D., Ikonomov, O.C., and Shisheva, A. (2000). PIKfyve lipid kinase is a protein kinase: Downregulation of 5′-phosphoinositide product formation by autophosphorylation. Biochemistry *39*, 15980–15989.

Sbrissa, D., Ikonomov, O.C., Deeb, R., and Shisheva, A. (2002). Phosphatidylinositol 5-phosphate biosynthesis is linked to PIKfyve and is involved in osmotic response pathway in mammalian cells. J. Biol. Chem. *277*, 47276–47284.

Sbrissa, D., Ikonomov, O.C., Strakova, J., Dondapati, R., Mlak, K., Deeb, R., Silver, R., and Shisheva, A. (2004). A mammalian ortholog of Saccharomyces cerevisiae Vac14 that associates with and up-regulates PIKfyve phosphoinositide 5-kinase activity. Mol. Cell. Biol. *24*, 10437–10447.

Sbrissa, D., Ikonomov, O.C., Fu, Z., Ijuin, T., Gruenberg, J., Takenawa, T., and Shisheva, A. (2007a). Core protein machinery for mammalian phosphatidylinositol 3,5-bisphosphate synthesis and turnover that regulates the progression of endosomal transport: Novel Sac phosphatase joins the ArPIKfyve-PIKfyve complex. J. Biol. Chem. *282*, 23878–23891.

Sbrissa, D., Ikonomov, O.C., Fu, Z., Ijuin, T., Gruenberg, J., Takenawa, T., and Shisheva, A. (2007b). Core protein machinery for mammalian phosphatidylinositol 3,5-bisphosphate synthesis and turnover that regulates the progression of endosomal transport: Novel Sac phosphatase joins the ArPIKfyve-PIKfyve complex. J. Biol. Chem. *282*, 23878–23891.

Sbrissa, D., Ikonomov, O.C., Fenner, H., and Shisheva, A. (2008). ArPIKfyve Homomeric and Heteromeric Interactions Scaffold PIKfyve and Sac3 in a Complex to Promote PIKfyve Activity and Functionality. J. Mol. Biol. *384*, 766–779.

Sbrissa, D., Ikonomov, O.C., Filios, C., Delvecchio, K., and Shisheva, A. (2012). Functional dissociation between PIKfyve-synthesized PtdIns5P and PtdIns(3,5)P 2 by means of the PIKfyve inhibitor YM201636. Am. J. Physiol. - Cell Physiol. *303*, 436–446.

Scarlatti, F., Maffei, R., Beau, I., Codogno, P., and Ghidoni, R. (2008). Role of non-canonical Beclin 1-independent autophagy in cell death induced by resveratrol in human breast cancer cells. Cell Death Differ. *15*, 1318–1329.

Schaeffer, V., Lavenir, I., Ozcelik, S., Tolnay, M., Winkler, D.T., and Goedert, M. (2012). Stimulation of autophagy reduces neurodegeneration in a mouse model of

human tauopathy. Brain *135*, 2169–2177.

Schöndorf, D.C., Aureli, M., Mcallister, F.E., Hindley, C.J., Mayer, F., Scho, D.C., Schmid, B., Sardi, S.P., Valsecchi, M., Hoffmann, S., et al. (2014). iPSC-derived neurons from GBA1-associated Parkinson's disease patients show autophagic defects and impaired calcium homeostasis. Nat Commun *5*, 1–17.

Schulze, U., Vollenbröker, B., Kühnl, A., Granado, D., Bayraktar, S., Rescher, U., Pavenstädt, H., and Weide, T. (2017). Cellular vacuolization caused by overexpression of the PIKfyve-binding deficient Vac14L156R is rescued by starvation and inhibition of vacuolar-ATPase. Biochim. Biophys. Acta - Mol. Cell Res. *1864*, 749–759.

Scott, J.W., Ling, N., Issa, S.M.A., Dite, T.A., O'Brien, M.T., Chen, Z.P., Galic, S., Langendorf, C.G., Steinberg, G.R., Kemp, B.E., et al. (2014). Small molecule drug A-769662 and AMP synergistically activate naive AMPK independent of upstream kinase signaling. Chem. Biol. *21*, 619–627.

Shaltiel, G., Shamir, A., Shapiro, J., Ding, D., Dalton, E., Bialer, M., Harwood, A.J., Belmaker, R.H., Greenberg, M.L., and Agam, G. (2004). Valproate decreases inositol biosynthesis. Biol. Psychiatry *56*, 868–874.

Shang, L., Chen, S., Du, F., Li, S., Zhao, L., and Wang, X. (2011). Nutrient starvation elicits an acute autophagic response mediated by Ulk1 dephosphorylation and its subsequent dissociation from AMPK. Proc. Natl. Acad. Sci. U. S. A. *108*, 4788–4793.

Sharma, V., Makhdoomi, M., Singh, L., Kumar, P., Khan, N., Singh, S., Verma, H.N., Luthra, K., Sarkar, S., and Kumar, D. (2020). Trehalose limits opportunistic mycobacterial survival during HIV co-infection by reversing HIV-mediated autophagy block. Autophagy *00*, 1–20.

Shaw, R.J., Kosmatka, M., Bardeesy, N., Hurley, R.L., Witters, L.A., DePinho, R.A., and Cantley, L.C. (2004). The tumor suppressor LKB1 kinase directly activates AMP-activated kinase and regulates apoptosis in response to energy stress. Proc. Natl. Acad. Sci. U. S. A. *101*, 3329–3335.

Shibata, M., Lu, T., Furuya, T., Degterev, A., Mizushima, N., Yoshimori, T., Macdonald, M., Yankner, B., and Yuan, J. (2006). Regulation of Intracellular Accumulation of Mutant Huntingtin by Beclin 1 *. *281*, 14474–14485.

Shiloh, R., Gilad, Y., Ber, Y., Eisenstein, M., Aweida, D., Bialik, S., Cohen, S., and Kimchi, A. (2018). Non-canonical activation of DAPK2 by AMPK constitutes a new pathway linking metabolic stress to autophagy. Nat. Commun. *9*.

Shisheva, A. (2001). PIKfyve: The road to PtdIns 5-P and PtdIns 3,5-P2. Cell Biol. Int. *25*, 1201–1206.

Shisheva, A., Sbrissa, D., and Ikonomov, O. (1999). Cloning, Characterization, and Expression of a Novel Zn 2+-Binding FYVE Finger-Containing Phosphoinositide Kinase in Insulin-Sensitive Cells. Mol. Cell. Biol. *19*, 623–634.

Shisheva, A., Sbrissa, D., Hu, B., and Li, J. (2019). Severe Consequences of

SAC3/FIG4 Phosphatase Deficiency to Phosphoinositides in Patients with Charcot-Marie-Tooth Disease Type-4J. Mol. Neurobiol.

Siddiqi, F.H., Menzies, F.M., Lopez, A., Stamatakou, E., Karabiyik, C., Ureshino, R., Ricketts, T., Jimenez-Sanchez, M., Esteban, M.A., Lai, L., et al. (2019a). Author Correction: Felodipine induces autophagy in mouse brains with pharmacokinetics amenable to repurposing (Nature Communications, (2019), 10, 1, (1817), 10.1038/s41467-019-09494-2). Nat. Commun. *10*.

Siddiqi, F.H., Menzies, F.M., Lopez, A., Stamatakou, E., Karabiyik, C., Ureshino, R., Ricketts, T., Jimenez-Sanchez, M., Esteban, M.A., Lai, L., et al. (2019b). Felodipine induces autophagy in mouse brains with pharmacokinetics amenable to repurposing. Nat. Commun. *10*, 1–14.

Simonsen, A., Cumming, R.C., Brech, A., Isakson, P., Schubert, D.R., and Finley, K.D. (2008a). Promoting basal levels of autophagy in the nervous system enhances longevity and oxidant resistance in adult Drosophila. Autophagy *4*, 176–184.

Simonsen, A., Cumming, R.C., Brech, A., Isakson, P., Schubert, D.R., and Finley, K.D. (2008b). Promoting basal levels of autophagy in the nervous system enhances longevity and oxidant resistance in adult Drosophila. Autophagy *4*, 176–184.

Singh, P., Ravanan, P., and Talwar, P. (2016). Death associated protein kinase 1 (DAPK1): A regulator of apoptosis and autophagy. Front. Mol. Neurosci. *9*, 1–11.

Sinha, R.A., Singh, B.K., Zhou, J., Wu, Y., Farah, B.L., Ohba, K., Lesmana, R., Gooding, J., Bay, B.H., and Yen, P.M. (2015). Thyroid hormone induction of mitochondrial activity is coupled to mitophagy via ROS-AMPKULK1 signaling. Autophagy *11*, 1341–1357.

Smith, E.M., Finn, S.G., Tee, A.R., Brownei, G.J., and Proud, C.G. (2005). The tuberous sclerosis protein TSC2 is not required for the regulation of the mammalian target of rapamycin by amino acids and certain cellular stresses. J. Biol. Chem. *280*, 18717–18727.

Son, S.M., Park, S.J., Lee, H., Siddiqi, F., Lee, J.E., Menzies, F.M., and Rubinsztein, D.C. (2019). Leucine Signals to mTORC1 via Its Metabolite Acetyl-Coenzyme A. Cell Metab. *29*, 192-201.e7.

Sou, Y., Waguri, S., Iwata, J., Ueno, T., Fujimura, T., Taichi Hara, N.S., Yamada, A., Mizushima, N., Uchiyama, Y., Kominami, E., et al. (2018). The Atg8 Conjugation System Is Indispensable for Proper Development of Autophagic Isolation Membranes in Mice. Mol. Biol. Cell *19*, 4762–4775.

Soussi, H., Reggio, S., Alili, R., Prado, C., Mutel, S., Pini, M., Rouault, C., Clément, K., and Dugail, I. (2015). DAPK2 downregulation associates with attenuated adipocyte autophagic clearance in human obesity. Diabetes *64*, 3452–3463.

Spencer, B., Potkar, R., Trejo, M., Rockenstein, E., Gindi, R., Adame, A., Wyss-coray, T., and Masliah, E. (2010). Beclin 1 Gene Transfer Activates Autophagy and Ameliorates the Neurodegenerative Pathology in α-Synuclein Model of Parkinson's and Lewy Body Disease. J Neurosci *29*, 13578–13588.

Spillantini, M., Schmidt, M., Lee, V., Trojanowski, J., Jakes, R., and Goedert, M. (1997). α-Synuclein in Lewy bodies. Nature *388*, 839–840.

Stanga, D., Zhao, Q., Milev, M.P., Saint-Dic, D., Jimenez-Mallebrera, C., and Sacher, M. (2019). TRAPPC11 functions in autophagy by recruiting ATG2B-WIPI4/WDR45 to preautophagosomal membranes. Traffic *20*, 325–345.

Stein, S.C., Woods, A., Jones, N.A., Davison, M.D., and Carling, D. (2000). The regulation of AMP-activated protein kinase by phosphorylation. Biochem. J. *345 Pt 3*, 437–443.

Stolz, A., Ernst, A., and Dikic, I. (2014). Cargo recognition and trafficking in selective autophagy. Nat. Cell Biol. *16*, 495–501.

Sultana, F., Morse, L.R., Picotto, G., Liu, W., Jha, P.K., Odgren, P.R., and Battaglino, R.A. (2019). Snx10 and PIKfyve are required for lysosome formation in osteoclasts. J. Cell. Biochem. 2927–2937.

Suzuki, K., Kirisako, T., Kamada, Y., Mizushima, N., Noda, T., and Ohsumi, Y. (2001). The pre-autophagosomal structure organized by concerted functions of APG genes is essential for autophagosome formation. EMBO J. *20*, 5971–5981.

Takahashi, Y., Coppola, D., Matsushita, N., Cualing, H.D., Sato, Y., Liang, C., Jung, J.U., Cheng, J.Q., Mulé, J.J., Jack, W., et al. (2007). Bif-1 interacts with Beclin 1 through UVRAG and regulates autophagy and tumorigenesis. Nat Cell Biol *9*, 1142–1151.

Tanaka, M., Machida, Y., Niu, S., Ikeda, T., Jana, N.R., Doi, H., Kurosawa, M., Nekooki, M., and Nukina, N. (2004). Trehalose alleviates polyglutamine-mediated pathology in a mouse model of Huntington disease. Nat. Med. *10*, 148–154.

Tang, Q., Zheng, G., Feng, Z., Chen, Y., Lou, Y., Wang, C., Zhang, X., Zhang, Y., Xu, H., Shang, P., et al. (2017). Trehalose ameliorates oxidative stress-mediated mitochondrial dysfunction and ER stress via selective autophagy stimulation and autophagic flux restoration in osteoarthritis development. Cell Death Dis. *8*, e3081.

Tanida, I., Sou, Y.S., Ezaki, J., Minematsu-Ikeguchi, N., Ueno, T., and Kominami, E. (2004a). HsAtg4B/HsApg4B/autophagin-1 cleaves the carboxyl termini of three human Atg8 homologues and delipidates microtubule-associated protein light chain 3- and GABAA receptor-associated protein-phospholipid conjugates. J. Biol. Chem. *279*, 36268–36276.

Tanida, I., Ueno, T., and Kominami, E. (2004b). LC3 conjugation system in mammalian autophagy. Int. J. Biochem. Cell Biol. *36*, 2503–2518.

Tanida, I., Minematsu-Ikeguchi, N., Ueno, T., and Kominami, E. (2005). Lysosomal Turnover, but Not a Cellular Level, of Endogenous LC3 is a Marker for Autophagy. Autophagy *1*, 84–91.

Tanik, S.A., Schultheiss, C.E., Volpicelli-daley, L.A., Brunden, K.R., and Lee, V.M.Y. (2013). Lewy Body-like α-Synuclein Aggregates Resist Degradation and Impair Macroautophagy. J. Biol. Chem. *288*, 15194–15210.

Tanji, K., Miki, Y., Maruyama, A., Mimura, J., Matsumiya, T., Mori, F., Imaizumi, T., and Itoh, K. (2015). Biochemical and Biophysical Research Communications Trehalose intake induces chaperone molecules along with autophagy in a mouse model of Lewy body disease. Biochem. Biophys. Res. Commun. *465*, 746–752.

Tian, W., Li, W., Chen, Y., Yan, Z., Huang, X., Zhuang, H., Zhong, W., Chen, Y., Wu, W., Lin, C., et al. (2015). Phosphorylation of ULK1 by AMPK regulates translocation of ULK1 to mitochondria and mitophagy. FEBS Lett. *589*, 1847–1854.

Trettel, F., Rigamonti, D., Hilditch-Maguire, P., Wheeler, V.C., Shar, A.H., Persichetti, F., Cattaneo, E., and MacDonald, M.E. (2000). Dominant phenotypes produced by the HD mutation in STHdhQ111 striatal cells. Hum. Mol. Genet. *9*, 2799–2809.

Tsuboyama, K., Koyama-Honda, I., Sakamaki, Y., Koike, M., Morishita, H., and Mizushima, N. (2016). The ATG conjugation systems are important for degradation of the inner autophagosomal membrane. Science (80-.). *354*, 1036–1041.

Tsukada, M., and Ohsumi, Y. (1993). Isofation and characterization of autophagy-defective mutants of Saccharomyces Cerevisiae. Febs Lett. *333*, 6.

Vaccari, I., Carbone, A., Previtali, S.C., Mironova, Y.A., Alberizzi, V., Noseda, R., Rivellini, C., Bianchi, F., Del Carro, U., D'Antonio, M., et al. (2015). Loss of Fig4 in both Schwann cells and motor neurons contributes to CMT4J neuropathy. Hum. Mol. Genet. *24*, 383–396.

Valverde, D.P., Yu, S., Boggavarapu, V., Kumar, N., Lees, J.A., Walz, T., Reinisch, K.M., and Melia, T.J. (2019). ATG2 transports lipids to promote autophagosome biogenesis. J. Cell Biol. *218*, 1787–1798.

Velikkakath, A.K.G., Nishimura, T., Oita, E., Ishihara, N., and Mizushima, N. (2012). Mammalian Atg2 proteins are essential for autophagosome formation and important for regulation of size and distribution of lipid droplets. Mol. Biol. Cell *23*, 896–909.

Viana, R., Aguado, C., Esteban, I., Moreno, D., Viollet, B., Knecht, E., and Sanz, P. (2008). Role of AMP-activated protein kinase in autophagy and proteasome function. Biochem. Biophys. Res. Commun. *369*, 964–968.

Viaud, J., Boal, F., Tronchère, H., Gaits-Iacovoni, F., and Payrastre, B. (2014). Phosphatidylinositol 5-phosphate: A nuclear stress lipid and a tuner of membranes and cytoskeleton dynamics. BioEssays *36*, 260–272.

Vicente, M.M., Talloczy, Z., Wong, E., Tang, G., Koga, H., Kaushik, S., Arias, E., Harris, S., Sulzer, D., and Cuervo, a M. (2010). Inefficient Autophagy in Huntington's Disease. Nat. Neurosci. *13*, 567–576.

Vicinanza, M., Korolchuk, V.I., Ashkenazi, A., Puri, C., Menzies, F.M., Clarke, J.H., and Rubinsztein, D.C. (2015). PI(5)P Regulates Autophagosome Biogenesis Graphical. Mol. Cell *57*, 219–234.

Vingtdeux, V., Giliberto, L., Zhao, H., Chandakkar, P., Wu, Q., Simon, J.E., Janle, E.M., Lobo, J., Ferruzzi, M.G., Davies, P., et al. (2010). AMP-activated protein

kinase signaling activation by resveratrol modulates amyloid-β peptide metabolism. J. Biol. Chem. *285*, 9100–9113.

Vingtdeux, V., Chandakkar, P., Zhao, H., d'Abramo, C., Davies, P., and Marambaud, P. (2011). Novel synthetic small-molecule activators of AMPK as enhancers of autophagy and amyloid-β peptide degradation. FASEB J. *25*, 219–231.

Viollet, B., Andreelli, F., Jørgensen, S.B., Perrin, C., Geloen, A., Flamez, D., Mu, J., Lenzner, C., Baud, O., Bennoun, M., et al. (2003). The AMP-activated protein kinase α2 catalytic subunit controls whole-body insulin sensitivity. J. Clin. Invest. *111*, 91–98.

Walker, D.M., Urbe, S., Dove, S.K., Tenza, D., Raposo, G., and Clague, M.J. (2001). Characterization of MTMR3 : an inositol lipid 3-phosphatase with novel substrate specificity. Curr. Biol. *11*, 1600–1605.

Walter, C., Clemens, L.E., Müller, A.J., Fallier-Becker, P., Proikas-Cezanne, T., Riess, O., Metzger, S., and Nguyen, H.P. (2016). Activation of AMPK-induced autophagy ameliorates Huntington disease pathology in vitro. Neuropharmacology *108*, 24–38.

Wang, R.C., Wei, Y., An, Z., Zou, Z., Xiao, G., Bhagat, G., White, M., Reichelt, J., and Levine, B. (2012). Akt-Mediated Regulation of Autophagy and Tumorigenesis Through Beclin 1 Phosphorylation. Science (80-.). *338*, 956–959.

Wang, W., Gao, Q., Yang, M., Zhang, X., Yu, L., Lawas, M., Li, X., Bryant-Genevier, M., Southall, N.T., Marugan, J., et al. (2015). Up-regulation of lysosomal TRPML1 channels is essential for lysosomal adaptation to nutrient starvation. Proc. Natl. Acad. Sci. U. S. A. *112*, E1373–E1381.

Webb, J.L., Ravikumar, B., Atkins, J., Skepper, J.N., and Rubinsztein, D.C. (2003). α-Synuclein Is Degraded by Both Autophagy and the Proteasome. J. Biol. Chem. *278*, 25009–25013.

Weerasekara, V.K., Panek, D.J., Broadbent, D.G., Mortenson, J.B., Mathis, A.D., Logan, G.N., Prince, J.T., Thomson, D.M., Thompson, J.W., and Andersen, J.L. (2014). Metabolic-stress-induced rearrangement of the 14-3-3ζ interactome promotes autophagy via a ULK1- and AMPK-regulated 14-3-3ζ interaction with phosphorylated Atg9. Mol. Cell. Biol. *34*, 4379–4388.

Wheeler, V.C., White, J.K., Gutekunst, C.-A., Vrbanac, V., Weaver, M., Xiao-Jiang, Li, S.-H., Yi, H., Vonsattel, J.-P., Gusella, J.F., et al. (2000). Long glutamine tracts cause nuclear localization of a novel form of huntingtin in medium spiny striatal neurons in HdhQ92 and HdhQ111 knock-in mice. Hum. Mol. Genet. *9*, 503–513.

Williams, A., Sarkar, S., Cuddon, P., Ttofi, E.K., Saiki, S., Siddiqi, F.H., Jahreiss, L., Fleming, A., Pask, D., Goldsmith, P., et al. (2008). Novel targets for Huntington's disease in an mTOR-independent autophagy pathway. Nat Chem Biol *4*, 295–305.

Williams, R.S.B., Cheng, L., Mudge, A.W., and Harwood, A.J. (2002). A common mechanism of action for three mood-stabilizing drugs. Nature *417*, 292–295.

Williams, T., Forsberg, L.J., Viollet, B., and Brenman, J.E. (2009). Basal autophagy induction without AMP-activated protein kinase under low glucose conditions. Autophagy *5*, 1155–1165.

Willows, R., Sanders, M.J., Xiao, B., Patel, B.R., Martin, S.R., Read, J., Wilson, J.R., Hubbard, J., Gamblin, S.J., and Carling, D. (2017). Phosphorylation of AMPK by upstream kinases is required for activity in mammalian cells. Biochem. J. *474*, 3059–3073.

Winslow, A.R., Chen, C.W., Corrochano, S., Acevedo-Arozena, A., Gordon, D.E., Peden, A.A., Lichtenberg, M., Menzies, F.M., Ravikumar, B., Imarisio, S., et al. (2010). α-Synuclein impairs macroautophagy: Implications for Parkinson's disease. J. Cell Biol. *190*, 1023–1037.

Wold, M.S., Lim, J., Lachance, V., Deng, Z., and Yue, Z. (2016). ULK1-mediated phosphorylation of ATG14 promotes autophagy and is impaired in Huntington's disease models. Mol. Neurodegener. *11*, 1–13.

Wolfe, D.M., Lee, J. hyun, Kumar, A., Lee, S., Orenstein, S.J., and Nixon, R.A. (2013). Autophagy failure in Alzheimer's disease and the role of defective lysosomal acidification. Eur. J. Neurosci. *37*, 1949–1961.

Won, J.S., Im, Y. Bin, Kim, J., Singh, A.K., and Singh, I. (2010). Involvement of AMP-activated-protein-kinase (AMPK) in neuronal amyloidogenesis. Biochem. Biophys. Res. Commun. *399*, 487–491.

Woods, A., Johnstone, S.R., Dickerson, K., Leiper, F.C., Fryer, L.G.D., Neumann, D., Schlattner, U., Wallimann, T., Carlson, M., and Carling, D. (2003). LKB1 Is the Upstream Kinase in the AMP-Activated Protein Kinase Cascade. Curr. Biol. *13*, 2004–2008.

Woods, A., Dickerson, K., Heath, R., Hong, S.P., Momcilovic, M., Johnstone, S.R., Carlson, M., and Carling, D. (2005). Ca2+/calmodulin-dependent protein kinase kinase-β acts upstream of AMP-activated protein kinase in mammalian cells. Cell Metab. *2*, 21–33.

Wu, S., He, Y., Qiu, X., Yang, W., Liu, W., Li, X., Li, Y., Shen, H.M., Wang, R., Yue, Z., et al. (2018). Targeting the potent Beclin 1-UVRAG coiled-coil interaction with designed peptides enhances autophagy and endolysosomal trafficking. Proc. Natl. Acad. Sci. U. S. A. *115*, E5669–E5678.

Xiao, B., Sanders, M.J., Carmena, D., Bright, N.J., Haire, L.F., Underwood, E., Patel, B.R., Heath, R.B., Walker, P.A., Hallen, S., et al. (2013). Structural basis of AMPK regulation by small molecule activators. Nat. Commun. *4*, 1–10.

Xinxin Song, S.Z., Chen, P., Hou, W., Wen, Q., Liu, J., Xie, Y., Liu, J., Klionsky, D.J., Kroemer, G., Lotze, M.T., et al. (2018). AMPK-mediated BECN1 phosphorylation Promotes Ferroptosis by Directly Blocking System Xc − Activity. Curr. Biol. *28*, 2388–2399.

Xu, D., Wang, Z., Wang, C., Zhang, D., Wan, H., Zhao, Z., Gu, J., Zhang, Y., Li, Z., Man, K., et al. (2016). PAQR 3 controls autophagy by integrating AMPK signaling to

enhance ATG 14L- associated PI 3K activity . EMBO J. *35*, 496–514.

Xu, P., Duong, D.M., Seyfried, N.T., Cheng, D., Xie, Y., Robert, J., Rush, J., Hochstrasser, M., Finley, D., and Peng, J. (2009). Quantitative Proteomics Reveals the Function of Unconventional Ubiquitin Chains in Proteasomal Degradation. Cell *137*, 133–145.

Ylä-Anttila, P., Vihinen, H., Jokitalo, E., and Eskelinen, E.L. (2009). 3D tomography reveals connections between the phagophore and endoplasmic reticulum. Autophagy *5*, 1180–1185.

Yordanov, T.E., Hipolito, V.E.B., Liebscher, G., Vogel, G.F., Stasyk, T., Herrmann, C., Geley, S., Teis, D., Botelho, R.J., Hess, M.W., et al. (2019). BORC regulates late endosomal/lysosomal size through PIKfyve- dependent phosphatidylinositol- 3,5-bisphosphate. Traffic 674–696.

Yoshimori, T., Yamamoto, A., Moriyama, Y., Futai, M., and Tashiro, Y. (1991). Bafilomycin-a1, a Specific Inhibitor of Vacuolar-Type H-Atpase, Inhibits Acidification and Protein-Degradation in Lysosomes of Cultured-Cells. J. Biol. Chem. *266*, 17707–17712.

Young, N.P., Kamireddy, A., Van Nostrand, J.L., Eichner, L.J., Shokhirev, M.N., Dayn, Y., and Shaw, R.J. (2016). AMPK governs lineage specification through Tfeb-dependent regulation of lysosomes. Genes Dev. *30*, 535–552.

Yu, H.C., Lin, C.S., Tai, W.T., Liu, C.Y., Shiau, C.W., and Chen, K.F. (2013). Nilotinib induces autophagy in hepatocellular carcinoma through AMPK activation. J. Biol. Chem. *288*, 18249–18259.

Yu, Y., Yoo, S.-O., Poulogiannis, G., Yang, Q., Ma, X.M., Villén, J., Kubica, N., Hoffman, G.R., Cantley, L.C., Gygi, S.P., et al. (2011). Quantitative Phosphoproteomic Analysis Identifies the Adaptor Protein Grb10 as an mTORC1 Substrate that Negatively Regulates Insulin Signaling. Science (80-.). *332*, 1322–1326.

Zavodszky, E., Seaman, M.N., Moreau, K., Jimenez-Sanchez, M., Breusegem, S.Y., Harbour, M.E., and Rubinsztein, D.C. (2014). Mutation in VPS35 associated with Parkinson's disease impairs WASH complex association and inhibits autophagy. Nat Commun *5*, 1–16.

Zeqiraj, E., Filippi, B.M., Deak, M., Alessi, D.R., and Van Aalten, D.M.F. (2009). Structure of the LKB1-STRAD-MO25 complex reveals an allosteric mechanism of kinase activation. Science (80-.). *326*, 1707–1711.

Zhang, C.S., Jiang, B., Li, M., Zhu, M., Peng, Y., Zhang, Y.L., Wu, Y.Q., Li, T.Y., Liang, Y., Lu, Z., et al. (2014). The lysosomal v-ATPase-ragulator complex is a common activator for AMPK and mTORC1, acting as a switch between catabolism and anabolism. Cell Metab. *20*, 526–540.

Zhang, C.S., Hawley, S.A., Zong, Y., Li, M., Wang, Z., Gray, A., Ma, T., Cui, J., Feng, J.W., Zhu, M., et al. (2017). Fructose-1,6-bisphosphate and aldolase mediate glucose sensing by AMPK. Nature *548*, 112–116.

Zhang, D., Wang, W., Sun, X., Xu, D., Wang, C., Zhang, Q., Wang, H., Luo, W., Chen, Y., Chen, H., et al. (2016). AMPK regulates autophagy by phosphorylating BECN1 at threonine 388. Autophagy *12*, 1447–1459.

Zhang, Y., Zolov, S.N., Chow, C.Y., Slutsky, S.G., Richardson, S.C., Piper, R.C., Yang, B., Nau, J.J., Westrick, R.J., Morrison, S.J., et al. (2007). Loss of Vac14, a regulator of the signaling lipid phosphatidylinositol 3,5-bisphosphate, results in neurodegeneration in mice. Proc. Natl. Acad. Sci. U. S. A. *104*, 17518–17523.

Zhou, F., Wu, Z., Zhao, M., Murtazina, R., Cai, J., Zhang, A., Li, R., Sun, D., Li, W., Zhao, L., et al. (2019). Rab5-dependent autophagosome closure by ESCRT. J. Cell Biol. *218*, 1908–1927.

Zhou, X., Wang, L., Hasegawa, H., Amin, P., Han, B., Kaneko, S., and He, Y. (2010). Deletion of PIK3C3 / Vps34 in sensory neurons causes rapid neurodegeneration by disrupting the endosomal but not the autophagic pathway. Proc. Natl. Acad. Sci. U. S. A. *107*, 9424–9429.

Zhuang, X., Chung, K.P., Cui, Y., Lin, W., Gao, C., Kang, B.H., Jiang, L., and Bassham, D.C. (2017). ATG9 regulates autophagosome progression from the endoplasmic reticulum in Arabidopsis. Proc. Natl. Acad. Sci. U. S. A. *114*, E426–E435.

Zolov, S.N., Bridges, D., Zhang, Y., Lee, W.W., Riehle, E., Verma, R., Lenk, G.M., Converso-Baran, K., Weide, T., Albin, R.L., et al. (2012). In vivo, Pikfyve generates PI(3,5)P2, which serves as both a signaling lipid and the major precursor for PI5P. Proc. Natl. Acad. Sci. U. S. A. *109*, 17472–17477.

Zong, Y., Zhang, C.S., Li, M., Wang, W., Wang, Z., Hawley, S.A., Ma, T., Feng, J.W., Tian, X., Qi, Q., et al. (2019). Hierarchical activation of compartmentalized pools of AMPK depends on severity of nutrient or energy stress. Cell Res. *29*, 460–473.

7 Appendix

7.1 Abbreviations

Aβ	amyloid-β
Acetyl-CoA	acetyl-coenzyme A
ACC	Acetyl-CoA carboxylase
AD	Alzheimer's disease
ADaM	allosteric drug and metabolite
ADP	adenosine diphosphate
AICAR	5-aminoimidazole-4-carboxamide ribonucleoside
AL	autolysosomes
ALS	Amyotrophic Lateral Sclerosis
AMP	adenosine monophosphate
AMPK	AMP-activated protein kinase
ANOVA	analysis of variance
AP	autophagosomes
APP	amyloid precursor protein
ATG	autophagy-related genes
ATP	adenosine triphosphate
AXIN1	Axis inhibition protein 1
BafA1	Bafilomycin A1
β-CBM	carbohydrate-binding module
β-CTD	C-terminal domain
BECN1	Beclin-1
BLOC-1	biogenesis of lysosome-related organelles complex 1
BSA	bovine serum albumin
CaMKKs	calmodulin-dependent kinase kinases

cAMP	cyclic AMP
CBS	cystathionine-β-synthase
CC	Compound C
CCR	conserved cysteine-rich
C. elegans	*Caenorhabditis elegans*
CFD	corneal fleck dystrophy
CMA	chaperone-mediated autophagy
CMT4J	Charcot-Marie-Tooth syndrome type 4J
co-IP	co-immunoprecipitation
Cpn	chaperonin-like
DAG	diacylglycerol
DAPI	4,6-diamidino-2-phenylindole
DAPK2	death-associated protein kinase 2
DEPTOR	DEP domain containing mTOR-interacting protein
DFCP1	FYVE-containing protein 1
DIV	days *in vitro*
dKO	double knock-out
DMEM	Dulbecco's Modified Eagles Medium
DMSO	dimethyl sulfoxide
DTT	dithiothreitol
EBSS	Earle's balanced salt solution
ECL	electrochemical luminescence
EGFP-HTT(Q74)	huntingtin exon 1 with 74 glutamine repeats
ER	endoplasmic reticulum
ERAD	endoplasmic reticulum-associated degradation
ESCRT	endosomal sorting complex required for transport

FAD	familial Alzheimer disease
FBS	fetal bovine serum
FIP200	focal adhesion kinase family interacting protein of 200 kDa
FKBP12	intracellular 12-kDa FK506-binding protein
FYCO1	FYVE and coiled-coil domain-containing protein 1
Gal9	galectin 9
GAP	GTPase-activation protein
GAPDH	glyceraldehyde 3-phosphate dehydrogenase
GβL	protein β-subunit like protein
GFP	green fluorescent protein
glu	glucose
HBSS	Hanks Balanced Salt Solution
HD	Huntington’s disease
HEK 293T	human embryonic kidney 293
HeLa	human epithelial cervical cancer cells
HEPES	4-(2-Hydroxyethyl)piperazine-1-ethanesulfonic acid
HOPS	homotypic fusion and protein sorting
Htt	huntingtin
I1R	imidazoline-1 receptor
IgG	immunoglobulin G
IGF-1	insulin-like growth factor
IP	immunoprecipitation
IP_3	inositol 1,4,5-trisphosphate
iPSC	induced pluripotent stem cells
KD	kinase domain

kDa	kilo Dalton
KO	knockout
LAMP	lysosomal-associated membrane glycoprotein
LE	long exposure
LKB1	liver kinase B1
MAP1-LC3/LC3	microtubule-associated protein 1 light chain3
MCOLN1	mucolipin 1
MEFs	mouse embryonic fibroblasts
mHTT	mutant HTT
MiT/TFE	microphthalmia/transcription factor E
mRFP	monomeric red fluorescent protein
MTOC	microtubule organizing center
mTOR	mammalian target of rapamycin
mTORC	mTOR complex
MVBs	multivesicular bodies
p70 S6K1	ribosomal protein S6 kinase, 70 kDa, polypeptide 1
PAS	pre-autophagosomal structure
PBS	phosphate buffered saline
PD	Parkinson’s disease
PE	phosphatidylethanolamine
PFA	paraformaldehyde
PHD	plant homeodomain
PI	phosphoinositide
PI3K	phosphatidylinositol 3-kinase
PI(3)P	phosphatidylinositol 3-phosphate
$PI(3,5)P_2$	phosphatidylinositol 3,5-phosphate

PI(5)P	phosphatidylinositol 5-phosphate
PIP4K2	phosphatidylinositol 5-phosphate 4-kinase
PICALM	phosphatidylinositol-binding clathrin assembly protein
PKB	protein kinase B
PKC	protein kinase C
PRAS40	proline-rich Akt substrate 40 kDa
PS1	presenilin 1
Protor	protein observed with rictor 1 and 2
RAB11A	Ras-associated protein 11A
Raptor	regulatory-associated protein of mammalian target of rapamycin
Rheb	Ras homolog enriched in brain
rictor	rapamycin-insensitive companion of mTOR
SD	standard deviation
SDS-PAGE	sodium dodecyl sulphate-polyacrylamide gel electrophoresis
SE	short exposure
SEM	standard error of mean
SGK-1	serum- and glucocorticoid-inducible kinase 1
siRNA	short interfering RNA
SPC	striatal progenitor cell
TFEB	transcription factor EB
TSC1	tuberous sclerosis 1
Ub	ubiquitin
ULK1/2	unc-51-like autophagy activating kinase 1/2
UPS	ubiquitin-proteasome system
UVRAG	UV radiation resistance associated gene

v-ATPase	vacuolar [H^+] ATPase
VPS	vacuolar protein sorting
WIPI	WD repeat domain phosphoinositide-interacting
WT	wildtype
YM	YM201636